

**KINETICS, TECHNOLOGY &
CHARACTERISATION OF IMPURITY-FREE
VACANCY DISORDERING FOR PHOTONIC
DEVICES IN GaAs-AlGaAs**

A Thesis submitted to the Department of Electronics & Electrical Engineering for
the degree of Doctor of Philosophy.

November, 1998.

©Amr Saher Helmy, 1998.

ProQuest Number: 13818668

All rights reserved

INFORMATION TO ALL USERS

The quality of this reproduction is dependent upon the quality of the copy submitted.

In the unlikely event that the author did not send a complete manuscript and there are missing pages, these will be noted. Also, if material had to be removed, a note will indicate the deletion.



ProQuest 13818668

Published by ProQuest LLC (2018). Copyright of the Dissertation is held by the Author.

All rights reserved.

This work is protected against unauthorized copying under Title 17, United States Code
Microform Edition © ProQuest LLC.

ProQuest LLC.
789 East Eisenhower Parkway
P.O. Box 1346
Ann Arbor, MI 48106 – 1346

GLASGOW
UNIVERSITY
LIBRARY

11550 (copy 1)

ABSTRACT

The work presented in this thesis studies the kinetics, technology, and characterisation methods used for the impurity-free vacancy disordering process using dielectric cap annealing technique.

- Statistical models for defect diffusion have successfully described the kinetics of compositional intermixing in GaAs. Order of magnitude agreement between the predicted and experimentally measured PL shifts was obtained.
- Various dielectric caps have been investigated when studying the technology of dielectric cap annealing induced intermixing, of which SrF₂, SiO₂, SiO₂:P are most important. A selective intermixing process using only SiO₂ was also developed, by processing the caps in Oxygen plasma to suppress intermixing. Differential shifts in excess of 100 meV at anneal temperature of 925 °C were achieved with a 10 meV shift underneath the un-intermixed regions.
- Characterisation of the intermixing process was carried out using:
 - PLE measurements indicated a non-square QW profile as-grown samples. As-grown QWs were best fitted with a symmetric exponential profile.
 - DLTS detected the deep level traps, EL2, EL16 and E5A after annealing MOVPE and MBE grown structures. The concentration of the EL2 trap, as the defect responsible for intermixing, matched those predicted from the model.
 - SIMS measurements of Ga and As diffusion during annealing showed excessive Ga out-diffusion into the dielectric caps when enhancement of intermixing is observed.
 - Spatially and temporally resolved PL showed that the resolution of intermixing process is better than 3 μm for MQW stack 1 μm below the surface. Due to the defects associated with intermixing carrier lifetime was reduced by a factor 3, where enhanced intermixing was observed.
 - Spatially and spectrally resolved PL showed that 1:1 gratings fabricated using IFVD, with periods less than 10 μm, are a very efficient means of suppressing intermixing.
 - Spatially resolved intermixed patterns were also identified using Raman spectroscopy by studying the position and line width of different Raman peaks. PL shifts ≥ 6 nm were detected from grating periods ≥ 4 μm.

TABLE OF CONTENTS

Abstract	ii
Table of Contents	iii
Acknowledgement	vi
Refereed Publications	vii
Conference Contributions	viii
List of Tables	x
List of Figures	xii
1. Introduction	1
I. Rationale	2
II. Basic Principles	3
II.A. Native Defects in GaAs and Related Compounds	3
II.B. Quantum Well Intermixing	5
II.B.1 Effect of QWI on the Electronic and Optical Properties	6
II.B.2. Impurity-Free Vacancy Disordering	9
III. Thesis Outline	9
IV. References	11
2. Review of Techniques and Advances	13
I. Introduction	14
II. Intermixing Techniques	14
II.A. Impurity Induced Disordering	15
II.B. Irradiation Induced Disordering	17
II.B.1. Implantation & Focused Ion Beam Induced Disordering	17
II.B.2. Plasma Induced Defect Layer Disordering	22
II.B.3. Laser Induced Disordering	24
II.C. Impurity Free Vacancy Induced Disordering	26
II.C.1. Dielectric Cap Annealing Induced Disordering	27
II.C.2. Other IFVD Techniques	29
III. Summary	31
IV. References	33

3. Quantifying Intermixing Kinetics	40
I. Introduction	41
II. Intermixing Mechanisms	41
III. Elements Of The Model	42
IV. Modelling The Kinetics Of Different Processes	47
IV.A. Kinetics Of Plasma Induced Defect Layer Intermixing	47
IV.B. Kinetics Of Impurity Free Vacancy Disordering	53
V. Summary	56
VI. References	58
4. Technology of Dielectric-Cap-Annealing Induced Intermixing	60
I. Introduction	61
II. Investigation of Dielectric Caps for IFVD	61
II.A. Silica; SiO ₂	62
II.B. Silicon Nitride; Si ₃ N ₄	62
II.C. Strontium Fluoride; SrF ₂	63
II.D. Phosphorus-doped Silica; SiO ₂ :P	65
II.E. Fluorine-doped Silica; SiO ₂ :F	67
II.F. Surface Effects	68
III. Discussion	69
IV. Plasma Treatment of SiO ₂ Films: A Means of Inhibiting QWI	70
IV.A. Single Cap IFVD	73
V. Summary	74
VI. References	76
5. Characterisation using Optical Techniques	80
I. Introduction	81
II. Photoluminescence Spectroscopy	82
II.A. Studying the Extent of Quantum Well Intermixing using a Photoluminescence Micro-Probe	85
II.B. Spectrally Resolved Photoluminescence Micro-Probe Measurements	90
III. Raman Spectroscopy	93
III.A. Studying the Extent of Quantum Well Intermixing using Raman Backscattering Measurements	95
III.A.1. p-i-n Laser Structure	97

III.A.2. Undoped Waveguide Structure	99
III.A.3. Undoped Waveguide Structure After Etching the Contact Layer	102
III.B. Summary of Raman Measurements	105
III.C. Studying the Spatial Localisation of Quantum Well Intermixing using a Raman Micro-Probe	105
III.C.1. Raman Micro-Probe of Intermixed Waveguide Structures	106
IV. Photoluminescence Excitation Spectroscopy	108
IV.A. Studying Quantum Well Intermixing Profiles using Photoluminescence Excitation	110
V. Summary	114
VI. References	116
6. Characterisation of Lattice Constituents and Defect Diffusion	119
I. Introduction	120
II Defect characterisation	122
IIA. Studying Vacancy Diffusion using DLTS	124
IIB. The EL2 Defect and More DLTS Experiments	127
III. Out-Diffusion of Lattice Constituents	128
III.A. Studying Out-Diffusion in Dielectric Caps using SIMS	130
IV. Summary	135
V. References	136
7. Conclusions and Future work	139
I. Conclusions	140
II. Future work	143
8. Appendices	
Appendix 1; Wafer Structures	145
Appendix 2; Experimental Design Techniques	149
I. Using Statistical Design Methods for Process Optimisation	150
II. Process Optimisation Using Factorial Design	152
III. References	157

ACKNOWLEDGEMENT

The privilege of carrying out my Ph.D. research in the department was granted to me thanks to S. Aitchison, J. Marsh, and also to the heads of department Professors P. Laybourn and S. Beaumont. My supervisors, John and Stewart, gave more than the opportunity of being part of the optoelectronics research group, I am indebted to their support, guidance, and enduring my English writing.

In the optoelectronics group, I am very grateful to A. C. Bryce, R. M. De La Rue, C. D. W. Wilkinson, J. Arnold, M. Rahman, B. S. Ooi, K. McIlvaney, E. Avrutin, D. Hutchings, N. Johnson, F. Camacho, C. Hamilton, A. McLaughlin, M. Street, S. McDougall, and the rest of the research team for providing me with the encouragement, advice, fun and sarcasm necessary for carrying out this work. The optoelectronics and nanoelectronics technical staff are real heroes and deserve many sincere thanks for the patient, and pleasant training they have given me over the years.

I also must confess that I am very glad to have passed through almost two years of amateur Scottish football without injuries.

On the scientific front I would like to thank my collaborators, at Renishaw Transducers, Defence Evaluation and Research Agency, University of Laval for fruitful collaborations.

I would have never made it without my family in Glasgow, Hany, Veronique, Ahmed, Marie-Peirre, Rosaria, Nicolas, Jenny and the rest of the gang who made Glasgow home very quickly.

Last but not least, my Mum, Dad, Sherief, Family and Friends back home, to whom I dedicate this work. Nothing said or done will be equivalent to the support I have been given despite of the distance. Thank you!

REFEREED PUBLICATIONS

A. Saher Helmy, A. C. Bryce, C. N. Ironside, J. S. Aitchison, J.H. Marsh, " Size-Dependent Quantum Well Intermixing in GaAs/AlGaAs Heterostructures; Evidence of the Role of Stress in Impurity-Free Vacancy Disordering," *Appl. Phys. Lett.*, to be Submitted.

A. Saher Helmy, A. C. Bryce, C. N. Ironside, J. S. Aitchison, J.H. Marsh, " Raman Spectroscopy for Characterising Compositional Intermixing in GaAs/AlGaAs Heterostructures," *Appl. Phys. Lett.*, vol. 74, 1999.

G. Li, S. J. Chua, J. H. Tang, , A. Saher Helmy, J.H. Marsh, "Controlling Bandgap Shifts in Impurity Free Vacancy Disordering of Al_{0.3}Ga_{0.7}As/GaAs using Native Surface Oxide and an Al layer," *Appl. Phys. Lett.*, Submitted.

A. Saher Helmy, S. K. Murad, A. C. Bryce, J. S. Aitchison, J.H. Marsh, S. K. Hicks, C. D. W. Wilkinson, "Control of silica cap properties by oxygen plasma treatment for single-cap selective impurity free vacancy disordering," *Appl. Phys. Lett.*, vol. 74, P 732, 1999.

G. Li, S. J. Chua, S. J. Xu, X. C. Wang, A. Saher Helmy, M. L. Ke, J.H. Marsh, "Silica capping for Al_{0.3}Ga_{0.7}As/GaAs and In_{0.2}Ga_{0.8}As/GaAs quantum well intermixing," *Appl. Phys. Lett.*, vol. 73, P 3393, 1998.

A. Saher Helmy, J. S. Aitchison, and J. H. Marsh, "Quantitative model for the kinetics of compositional intermixing in GaAs/AlGaAs quantum confined heterostructures," *IEEE J. Selected Topics in Quantum Electronics*, vol. 4, P 653, 1998.

A. Saher Helmy, N. P. Johnson, M. L. Ke, A. C. Bryce, J. S. Aitchison, J.H. Marsh, I. Gontijo, G. S. Buller, J. Davidson, P. Dawson, "A study of impurity-free vacancy disordering in GaAs/AlGaAs for improved modelling," *IEEE J. Selected Topics in Quantum Electronics*, vol. 4, P 661, 1998.

P. Dumais, A. Villeneuve, A. Saher Helmy, J. S. Aitchison, "Soliton-emitting AlGaAs waveguide," *Optics Express*, Vol. 2, P 455, 1998.

M. Ke, A. Saher Helmy, A. C. Bryce, J. S. Aitchison, J.H. Marsh, J. Davidson, P. Dawson, "The electronic structure and optical properties of intermixed GaAs/AlGaAs double quantum wells," *J Appl. Phys.*, vol. 84 P 2855, 1998.

B.S. Ooi, Y.S. Tang, A. Saher Helmy, A.C. Bryce, J.H. Marsh, M. Paquette, J. Beauvais, "Optical characterisation of GaAs/AlGaAs quantum well wires fabricated using arsenic implantation induced intermixing," *J. Appl. Phys.*, Vol. 83, P 4526, 1998.

A. Saher Helmy, J. S. Aitchison, and J. H. Marsh, "The kinetics intermixing in GaAs/AlGaAs quantum confined heterostructures," *Appl. Phys. Lett.*, Vol. 71, P 2998, 1997.

B. S. Ooi, K. McIlvaney, A. Saher Helmy, S. G. Ayling, A. C. Bryce, J. H. Marsh, "Selective quantum well intermixing in GaAs/AlGaAs structures using impurity free vacancy disordering," *IEEE Journal of Quantum Electronics*, Vol. 33, P 1784 , 1997.

F. Camacho, E. A. Avrutin, P. Cusumano, A. Saher Helmy, A. C. Bryce, J. H. Marsh, "Improvements in mode-locked semiconductor diode lasers using monolithic integrated

passive waveguides made by quantum well intermixing," *IEEE Photonics Technology Letters*, Vol. 9, P 1208, 1997.

P. Cusumano, B. S. Ooi, A. Saher Helmy, S. G. Ayling, A. C. Bryce, J. H. Marsh, B. Voegele, M. J. Rose, "Suppression of quantum well intermixing in GaAs/AlGaAs laser structures using phosphorous-doped SiO₂ encapsulant layer," *Journal of Applied Physics*, Vol. 81, P 2445, 1997.

CONFERENCE CONTRIBUTIONS

A. Saher Helmy, A. C. Bryce, C. N. Ironside, J. S. Aitchison, J.H. Marsh, " Characterising Compositional Intermixing in GaAs/AlGaAs Heterostructures using Raman Spectroscopy," *CLEO 99*, Submitted.

A. Saher Helmy, A. C. Bryce, C. N. Ironside, J. S. Aitchison, and J. H. Marsh, I. Gontijo, G. S. Buller, S. Karlin, I. Wilcock, "Characterisation of the Resolution of Impurity Free Vacancy Disordering in GaAs/AlGaAs using Raman and Photoluminescence Correlation Measurements," *LEOS Annual Meeting, 1998*.

N. P. Johnson, A. Saher Helmy, A. C. Bryce, J.H. Marsh, "Deep levels induced by impurity free vacancy disordering," *CLEO Europe 98*.

B. S. Ooi, A. Saher Helmy, Y.S. Tang, A. C. Bryce, J.H. Marsh, M. Paquette, J. Beauvais, "Quantum well wires using As implantation induced intermixing in GaAs/AlGaAs," *CLEO Europe 98*.

A. Saher Helmy, B. S. Ooi, F. Camacho, A. C. Bryce, J. S. Aitchison, R. M. De La Rue, J. H. Marsh, "Mach-Zehnder modulators monolithically integrated with Fabry-Perot laser diodes in GaAs/AlGaAs using impurity-free vacancy disordering," *CLEO Europe 98*.

M. Ke, A. Saher Helmy, A. C. Bryce, J.H. Marsh, J. Davidson, P. Dawson, "The effect of non-abrupt initial interface on the electronic structure of the intermixed QWs," *CLEO Europe 98*.

A. Saher Helmy, J. S. Aitchison, J. H. Marsh, "Kinetics of Impurity Free Vacancy Disordering in GaAs/AlGaAs," *IEEE/LEOS Fall meeting, 1997*.

A. Saher Helmy, B. S. Ooi, F. Camacho, A. C. Bryce, J. S. Aitchison, R. M. De La Rue, J. H. Marsh, " Mach-Zehnder modulators in GaAs/AlGaAs double quantum well structures: A regrowth-free approach for monolithic integration," *IEE Proc. Optoelectronics Integration and Switching, 1997*.

P. Dumais, A. Villeneuve, A. Saher Helmy, C. Hamilton, J. S. Aitchison, "Soliton emission from an AlGaAs waveguide," *Quantum Electronics and Laser Science 97*, P 166, 1997.

A. Saher Helmy, J. S. Aitchison, and J. H. Marsh, "Quantifying Intermixing of GaAs/AlGaAs Quantum Confined Heterostructures," *Quantum Electronics 13*, Cardiff-UK, 1997.

A. Saher Helmy, B. S. Ooi, A. C. Bryce, J. S. Aitchison, R. M. DeLaRue, J.H.Marsh, "Mach-Zehnder modulators in GaAs/AlGaAs double quantum well structures: A regrowth-free approach for monolithic integration," *Semiconductor Integrated OptoElectronics 97*, Cardiff-UK.

P. Cusumano, *A. Saher Helmy*, B. S. Ooi, S. G. Ayling, A. C. Bryce, J. H. Marsh, B. Voegelé, M. J. Rose, "Suppression of quantum well intermixing in GaAs/AlGaAs laser structures using phosphorous-doped SiO₂ encapsulant layer," *Mat. Res. Soc. Symp. Proc.*, Vol.450 , P 419, 1996.

A. Saher Helmy, B. S. Ooi, J. H. Marsh, "Investigation of the resolution limit of the hydrogen Plasma Induced Defect Layer Intermixing Process," *Integrated Photonics Research 96*, Boston-USA, 1996.

LIST OF TABLES

Table 4.1 Parameters of the set of experiments carried out using to investigate the effects of oxide growth on the QWI using IFVD.

Table 4.2 Properties of the Silica caps before and after exposure to 70 minutes of Oxygen plasma with a flow rate of 5 sccm, at a pressure of 10 mTorr, and a power of 275 W.

Table 5.1 Observed and reported Raman peaks for the 4QW GaAs/AlGaAs p-i-n structure. The reported peaks are after Abstriter *et al.*

Table 5.2 Observed and reported Raman peaks for the MQW GaAs/AlGaAs undoped structure. The reported peaks are after Abstriter *et al.*

Table 5.3. Experimentally observed transition energies for a non-intermixed reference sample (column 2). The calculated results from both a square well (column 3) and an exponential well profile (column 4) are also included.

Table 5.4. Experimentally observed transition energies for an intermixed sample (column 2), which was annealed at 925 °C for 60 s. The calculated results for the diffusion of both an initial abrupt well (column 3) and an exponential well profile (column 4) are also included.

Table 6.1 Penetration depth of various probe particles.

Table 6.2 Experimental conditions for both ion species used in the SIMS experiments.

Table A3.1 An example set of experiments for a 2 level $2^{(4-1)}$ fractional factorial experiment design.

Table A3.2 A set of experiments designed using 1/2 fractional design. Also shown are the PL shifts measured after annealing the samples at 925 °C for 60 s.

Table A3.3 The set of experiment parameters and their combinations to show the interactions.

Table A3.4 The coefficients of the equation generated using the experiments parameters and their combinations to show the interactions.

Table A3.5 Results obtained from the model generated for the experiment predicting a decrease intermixing as time of exposure is increased, agreeing with experiment.

LIST OF FIGURES

Fig. 1.1 A schematic representation of a GaAs/Al_{0.5}Ga_{0.5}As heterostructure before and after intermixing. Also shown is a schematic, for the conduction and valence bands before and after intermixing.

Fig. 1.2 A schematic representation of a IFVD processing of a GaAs/Al_{0.5}Ga_{0.5}As heterostructure. The dielectric caps used during annealing in this example are SiO₂, and SiO₂:P

Fig. 2.1 Auger depth profiles of Ga in a superlattice doped with Be and Si, with profile as shown on the top of the graph. As grown profile is shown in (a), while (b) shows the profile after a 2 hr. furnace anneal at 780 °C. After Kobayashi *et al.*

Fig 2.2 5 K photoluminescence spectra from (a) as-grown, (b) homogeneous implanted, and the wire samples of widths from 150 nm (c) to 35 nm (g). The samples were implanted with arsenic dose of $1 \times 10^{13} \text{ cm}^{-2}$, at 45 keV and annealed at 875 °C for 30 s. After Ooi *et al.*

Fig 2.3 Transition energies from PR spectra. The equal energy separation of transitions from the heavy hole related transitions indicate harmonic potential confinements in the wires. In wires smaller than about 100 nm, the relatively flat trend of light hole transitions suggest that the light hole wavefunction is spread everywhere across the gratings with no effective hole confinement taking place. This can be ascribed to the significant effect of both the strong inter-wire coupling and the light hole effective mass. After Ooi *et al.*

Fig 2.4 A schematic diagram for the gratings used to measure the resolution limit of the PIDLI process. Their effect on the quantum well energy gap is expressed in the width of the line representing them, a) shows partially intermixed region and b) shows fully intermixed region.

Fig 2.5 Photoluminescence spectra of different grating periods. In (a) the two peaks resembling the two bandgaps in the grating are marked by arrows, while (b) focuses on the smaller peak.

Fig. 2.6 SEMs from different GaAs/AlAs superlattice samples after laser processing. In (a) the as-grown sample is shown, (b) shows the sample after annealing with Si₃N₄ cap, and (c) shows a sample after annealing with SiO₂ cap. The damage of the lattice is apparent in the SEMs.

Fig. 3.1 Schematic diagram of the lattice hops comprised in Ga out-diffusion from the quantum wells, and the quantum well interface crossings carried out by group three vacancies during the random walks associated with their diffusion.

Fig. 3.2 Schematic of the group III GaAs/AlGaAs sublattice showing the different steps of vacancy diffusion across the QW/barrier interface for the initial stage of a AlAs/GaAs heterostructure, and after a long diffusion time, where there is a finite amount intermixing on the group III sublattice. At the early stages of diffusion, all the vacancy interface crossings, N_{QW} , will result in Ga, Al interdiffusion from the QW, barrier respectively. However after some time, the probability that a Ga atom diffuses out of the well, when a V_{III} moves in is finite, and is equal to C_{Ga}^{QW} / C_o . Similarly the probability that an Al atom diffuses into the well, when a V_{III} moves out is finite, and is equal to $C_{Al}^{barrier} / C_o$. That is why the total number of lattice hops result in interdiffusion should have a factor to account for the initial and time induced change in the Ga/Al concentration in the QW/barrier respectively. The coefficient should be the product of the probabilities that the transported across the interface is the one required (i.e. Ga out of the QW, and Al into the QW).

Fig. 3.3 Group three vacancy concentration in the GaAs/AlGaAs single quantum well structure for different annealing time spans for the PIDLI process. The surface recombination velocity of group three vacancies used in the calculations is $0.1 \text{ cm}\cdot\text{s}^{-1}$.

Fig. 3.4 Plot for the PL shift versus the corresponding diffusion length for an asymmetric quantum well. The inset shows the QW composition.

Fig. 3.5 Plot for the square of the diffusion length and the anneal time for the both the PIDLI and IFVD processes. The slope of the line passing through the measured points is approximately constant giving a value of D_{QW} equal to $3 \times 10^{-17} \text{ cm}^2\cdot\text{s}^{-1}$ for the PIDLI process, and equal to $3.22 \times 10^{-15} \text{ cm}^2\cdot\text{s}^{-1}$ for the IFVD process.

Fig. 3.6 Measured and calculated PL shifts resulting from the PIDLI process in a shallow single quantum well for different values of D_{vac} .

Fig. 3.7 Measured and calculated PL shifts resulting from the PIDLI process in a shallow single quantum well for different values of D_{vac} .

Fig. 3.8 Plot for the Ga profile in a 200 nm SiO_2 film, and the resulting group III vacancy profile in the semiconductor for different annealing times at $950 \text{ }^\circ\text{C}$.

Fig. 3.9 Plot for the PL shift versus the corresponding diffusion length for a double quantum well. The inset shows the QW composition.

Fig. 3.10 Plot for measured and calculated PL shifts resulting from the IFVD process in a double quantum well for different values of D_{vac} .

Fig. 4.1 Plot for the bandgap shifts as a function of anneal temperature for samples capped with SrF_2 and SiO_2 and annealed for 30 s with 15 s rise time.

Fig. 4.2 Plot for the bandgap shifts as a function of anneal time for samples capped with SrF_2 and SiO_2 and annealed at $925 \text{ }^\circ\text{C}$ with 15 s rise time.

Fig. 4.3 Plot for the bandgap shifts as a function of anneal temperature for *n-i-p* DQW samples capped with SiO₂:P and SiO₂. Samples were then annealed for 30 s with 15 s rise time.

Fig. 4.4 Plot for the bandgap shifts as a function of anneal temperature for *n-i-p* DQW samples capped with SiO₂:P and SiO₂. Samples were then annealed for 30 s with 15 s rise time.

Fig. 4.5 Plot for the bandgap shifts as a function of fluorine content for different anneal temperature for DQW samples capped with SiO₂:F. Samples were annealed for 60 s with 15 s rise time.

Fig. 4.6 Plot for the bandgap shifts as a function of fluorine content for different anneal temperature for DQW samples capped with SiO₂:F. Samples were annealed for 60 seconds with 15 s rise time.

Fig. 4.7 Plot for the bandgap shifts as a function of anneal temperature for DQW samples capped with E-gun deposited SiO₂ and exposed to oxygen plasma for 30 mins. Samples were annealed for 60 seconds at 925 °C with 15 s rise time.

Fig. 4.8 Plot for the bandgap shifts as a function of anneal temperature for MQW samples capped with E-gun deposited SiO₂ exposed to oxygen plasma for 30 mins. Samples were annealed for 60 seconds at 925 °C with 15 s rise time.

Fig. 4.10 Plot for the bandgap shifts as a function of exposure time for DQW samples capped with E-gun deposited SiO₂ exposed to oxygen plasma for different times. Samples were annealed for 60 s at 925 °C with 15 s rise time.

Fig. 4.11 Plot for the bandgap shifts as a function of Fluorine content for DQW samples capped with SiO₂:F. Two sets of samples are shown, exposed and unexposed to oxygen plasma for 30 mins. Samples were annealed for 60 s at 925 °C with 15 s rise time.

Fig. 4.12 Plot for the bandgap shifts as a function of exposure time for DQW samples capped with sputter deposited SiO₂ exposed to oxygen plasma for different times. Samples were annealed for 60 seconds at 925 °C with 15 s rise time.

Fig. 4.13 Change in bandgap emission wavelength as a function of temperature for p-i-n doped DQW samples annealed for 60 s with 350 nm of evaporated SiO₂ cap

Fig. 5.1 A schematic for the PL set-up used at Glasgow University.

Fig. 5.2 A schematic for the photogenerated carriers in a bandgap grating induced by IFVD using SiO₂:P/ SiO₂ caps. The significance of the carrier diffusion depends on both, the spot size of the excitation laser beam, and the period of the bandgap grating.

Fig. 5.3 A schematic of the setup used for spatially and temporally resolved PL measurements.

Fig. 5.4. Scan across a grating sample with a period of $16\ \mu\text{m}$ for (a) the PL signal at the un-intermixed wavelength peak, and (b) the photogenerated carrier lifetime. Also shown are (c) the PL signals from the intermixed and un-intermixed parts of the sample.

Fig. 5.5. Scan across a grating sample with a period of $16\ \mu\text{m}$ for the photogenerated carrier lifetime. The dielectric cap grating used for intermixing and the resulting bandgap grating are also shown.

Fig. 5.6 A schematic diagram for the Raman microprobe instrument, from Renishaw, used to acquire the measurements presented in this work.

Fig. 5.7 Line scans for the PL shift along two periods of (a) $4\ \mu\text{m}$ and (b) $12\ \mu\text{m}$ 1:1 gratings in a 4QW sample.

Fig. 5.8 PL wavelength shift as a function of the grating period obtained from (error bars) large area PL system as shown in Fig. 5.1, and (points) PL obtained from the spectrally and spatially resolved PL. The blue horizontal lines indicate the lower and upper limits in annealing with large area caps

Fig. 5.9 Raman spectra from the as-grown 4QW sample. The Raman spectrum is shown (a) before and (b) after removing the photoluminescence background line. The GaAs-like and AlAs-like Raman spectra are indicated.

Fig. 5.10 PL wavelength shift for the 2 sets of samples used in the Raman measurements. One set of DQW samples and two other of MQW samples.

Fig. 5.11 The change in the FWHM and energy shift the peaks detected in the 4QW samples as a function of the PL wavelength shift are shown in (a) and (b) respectively. No consistent trend can be seen in the change of both parameters as a function of the amount of intermixing.

Fig. 5.12 Raman spectra from the as-grown MQW sample with a top GaAs layer. The Raman spectrum were induced using a HeNe laser and are shown after removing the photoluminescence background line. Also shown are the two groups of the Raman spectra belonging to the GaAs-like and the AlAs-like modes. The change in the FWHM and the energy shift all the peaks as a function of the PL wavelength shift is shown in (b) and (c) respectively.

Fig. 5.13 Raman spectra from the MQW as-grown with the top GaAs contact layer removed. The Raman spectrum is shown (a) before and (b) after removing the photoluminescence background line. The GaAs-like and AlAs-like Raman spectra are indicated.

Fig. 5.14 The change in (a) the FWHM and (b) the energy shift for all the Raman peaks detected as a function of the PL wavelength shift.

Fig. 5.15 Raman spectra from the MQW sample annealed with E-gun deposited SiO₂ caps at 960 °C for 60 s. The Raman spectrum is shown (a) before and (b) after removing the photoluminescence background line. The GaAs-like and AlAs-like Raman spectra are indicated.

Fig. 5.16 Line scans for the PL shift across two periods of an intermixed grating of a MQW sample without the GaAs layer annealed for 60 s at 950 °C with SiO₂/SiO₂:P caps are shown in (e) and (f). The scan of the (a) FWHM and the (b) position of the LO GaAs like Raman peak of the Al_{0.4}Ga_{0.6}As cladding layer, and another scan of the (c) FWHM and the (d) TO GaAs like Raman peak of the Al_{0.4}Ga_{0.6}As cladding layer are also shown.

Fig. 5.17 As-grown wafer and waveguide schematics.

Fig. 5.18 Mode profiles for a 7 μm wide waveguide. The outputs in the TE guided mode and the TM slab mode cases are shown.

Fig. 5.19 Line scans for the PL shift across two waveguides of an intermixed MQW waveguide sample, with the GaAs layer and intermixed using sputtered silica technique, are shown in (g) and (h). The scan of the (a) FWHM and the (b) position of the LO GaAs like Raman peak of the GaAs layer, and another scan of the (c) FWHM and the (d) TO GaAs like Raman peak of the Al_{0.4}Ga_{0.6}As cladding layer are also shown.

Fig. 5.20. Plot of PL spectra of the samples used in the PLE experiment, and typical PLE spectra obtained from the samples.

Fig. 5.21. Plot of the measured e₁→lh₁, and e₂→hh₂ transitions obtained from PLE measurements. Transitions fitted for an initial square, exponential, and single sided exponential QW profiles are also plotted and represented by the dashed, solid, and dashed-dotted lines respectively.

Fig. 6.1 Plot of the DLTS signal of a sample annealed at 925 °C for 120 s.

Fig. 6.2 Arrhenius plot of the signature of deep level traps identified in the various samples tested using DLTS.

Fig. 6.3 Comparison of the number of point defects obtained from the DLTS measurements and those calculated from the model for the same annealing parameters.

Fig. 6.4 SIMS profile of various GaAs and SiO₂:F constituents in the semiconductor with different depth resolutions.

Fig. 6.5 SIMS profile of various GaAs and SiO₂:P constituents (a) in the semiconductor, and (b) in the SiO₂:Pcap.

Fig. 6.6 SIMS profile of various GaAs and SiO₂ constituents in the SiO₂ cap.

Fig. A3.1 The effect of various parameters on the process response. Figures (a), (b), and (c), show the response for different parameter for given settings.

INTRODUCTION

Following the invention of the semiconductor laser diode in the early 60's, optoelectronic technologies were considered a solution to the inherent limitations of electronic devices. Despite the growing advances in optoelectronic technologies driven by the semiconductor industry, the anticipated replacement of electronic devices by optoelectronics has not been achieved. That is ascribed to the slow progress in optoelectronic technology when compared to the rapid advances achieved in electronic device functionality as well as circuit integration technologies. To improve upon electronic devices, the optoelectronics industry-driven-research will have to offer superior functionality and similar, if not more competitive, economics of fabrication. There is also a time limit on achieving such goals, since markets use any technology, which can satisfy its goals first.

I. RATIONALE

A revolution in semiconductor electronics technology did not take place until integrated circuits came about. The performance of the basic discrete electron device, namely the transistor, drastically improved when integrated with other components. It was not only the improved device performance, but also the functionality and economics of integrated circuits that allowed semiconductors to occupy the position they currently hold. Even now, advances in semiconductor electronics are far from saturation. Epitaxial growth of compound semiconductors allowed quantum confined heterostructures to be realised, which gave the physics of electron devices extra degrees of freedom and novel functionality. Epitaxial growth also allow Si/SiGe heterostructures to be realised, which allowed the economics of integrating novel electron devices, based on quantum effects, to be profitable since they are grown on Si substrates. These advantages, together with the shrinking minimum-feature-size achievable using optical lithography, make the competition with electronic integrated circuits not a trivial matter.

On the other hand there are many benefits to be gained when using photons to realise a given device functionality rather than electrons. Photons (bosons) have different properties from electrons (fermions). However, optoelectronic devices are large in size, partially because of the wavelength of photons in comparison to electrons, but also because of the utilisation of quantum effects in electronic devices, whereas quantum effects are not fully utilised yet in the optical domain. The sizes of current optoelectronic devices make their demand of real estate (i.e. foot-print or area) on semiconductor wafers quite large, so increasing their fabrication cost, whether discrete, or integrated. It is now obvious that optoelectronics research should be made on two main fronts, the first being the utilisation of quantum effects to provide new device functionality, increased efficiency, and reduced device size. The other is to improve optoelectronic device integration technologies to be able to integrate many different, reasonably sized, devices on the same semiconductor structure.

If, however, optoelectronics fail to deliver a medium term alternative to electron-devices, advances in many of the crucial applications of semiconductors will be driven and limited by the capabilities and progress in the electron device performance at that time. Applications such as switching in telecommunication networks will continue to be a bottleneck, limiting the system throughput. The input/output data buses of large processing modules will also continue to be limited by the speed of the electronic data buses and the associated crosstalk. Electron device switching times will always limit circuit bandwidth; also the frequency and the pulse widths of electromagnetic waves will be limited by the inherent

limitations of electron devices, including electron mobility, capacitance induced by the space charge of p - n junction, etc.

Due to the nature of the optoelectronic devices currently in use, the need for different epitaxial structures can be a detrimental obstacle in the route to integration. Some of the solutions currently used are to change the operating principles of the devices, e.g. by electrically pumping all the regions of the device to overcome absorption. However, this solution introduces excessive spontaneous noise, and has a high power consumption. Other approaches include regrowth after selectively etching various areas of the wafer. This approach is associated with very high growth demands, and hence increased costs. It also has a very low device yield, a detrimental factor when realising such devices in an industrial fashion. Another favoured approach is the use of post-growth bandgap tuning of quantum-confined heterostructures. This technique is very attractive because of its simplicity and suitability for the mass production of devices. It is particularly suitable for Aluminium containing semiconductors because of the severe limitations posed by Al oxidation when the etch-and-regrowth processes are used. Therefore, by careful design of the semiconductor wafer, quantum well intermixing (QWI) can be used to tailor the electronic, and optical properties, of such structures to facilitate the integration of active and passive optoelectronic and photonic devices on the same chip.

II. BASIC PRINCIPLES

To develop processes for integrated device fabrication using QWI, a detailed understanding of the semiconductor material is necessary. This is due to the dependence of the QWI technology on process thermodynamics, optical properties of quantum confined heterostructures, semiconductor fabrication technologies, etc. Before going into the details of modelling intermixing kinetics, development and characterisation of intermixing processes and device fabrication using QWI, some light ought to be shed on the basic sciences used within the course of work in this thesis.

II.A. Native Defects in GaAs and related compounds

The native defects in GaAs and related compounds are group III and V antisites, vacancies, and interstitials. In GaAs they read, Ga_{As} , As_{Ga} , V_{Ga} , V_{As} , I_{Ga} , I_{As} , respectively. There has been increasing interest in characterising native point defects in III-V compound semiconductors because of their profound influence on device characteristics. They play an important role as device sizes shrink down to the nanometer regime. Point defects are of particular importance when studying QWI because they facilitate interdiffusion. The nature and concentration of such defects in a semiconductor lattice depends on the history of

treatment the lattice has undergone, and the method of growth.¹ Although they are the simplest defects, native point defects exhibit behaviour which depends on their charged state, and whether they have a metastable, or bistable state (metastable is having two different lattice configurations for the same charged state, while bistable is having two different lattice configurations for two different charged states).² Probing their influence on the lattice properties can however indirectly help identify native point defects. Positron annihilation, deep level transient spectroscopy, and many other techniques have been successfully used to detect such defects. For a review of these techniques and defect properties see ref. 2. It is of great importance to note that the presence of extended defects, in the vicinity of point defects acts as a sink for such defects, because of the annihilation of point defects at boundaries. So, from the perspective of introducing damage for QWI, it is clear that there is an optimum concentration of defects, after which extended defects will form and alleviate the effect of the existing point defects on interdiffusion. This phenomenon has been reported for various implantation induced intermixing processes.^{3,4}

Out of the six native point defects in the GaAs lattice, only group III vacancies and antisites, V_{III} , and Ga_{As} or Al_{As} , are expected to have an acceptor-like energy state in the crystal, with varying number of charged states. The rest of the defects are expected to have a donor like energy states, with varying number of charged states.⁵ The solubility, diffusion, and interactions of point defects within crystals are topics of current research interest. Careful experiments with precise control of the sample environment are needed for accurate characterisation of point defects.⁶ The equilibrium concentration of charged point defects, taking V_{III} as an example, in an extrinsic medium can be written as,

$$[V_{III}^{-\beta}] \propto [V_{III}^0] \sigma^\beta \propto P_{As_4}^{1/4} \sigma^\beta = k(T) \sigma^\beta, \quad (1.1)$$

where β is the charge number of the defect, σ is the carrier concentration (n or p), $k(T)$ is a temperature dependent coefficient. The vapour pressure of the As tetramer, $P_{As_4}^{1/4}$ is approximately equal to P_{As} , the total As vapour pressure, at high As over-pressure.⁶ Determination of non-equilibrium, or dynamically changing, defect concentration is even more complex to characterise. It is still an open question and has attracted some work in recent years with success limited by the control one has on the experimental environment.⁶ It should be noted that the equilibrium concentration depends on the carrier type and concentration, which directly indicates that potential barriers such as p - n junctions can play a significant role in determining the equilibrium concentrations of defects and hence their diffusion. Because V_{III} is the defect of prime importance in the process of interdiffusion in GaAs,⁵ it was used when presenting relation 1.1. However similar relations hold for all other defects.⁶ It should be noted that, although initial work suggested that it was the triply charged

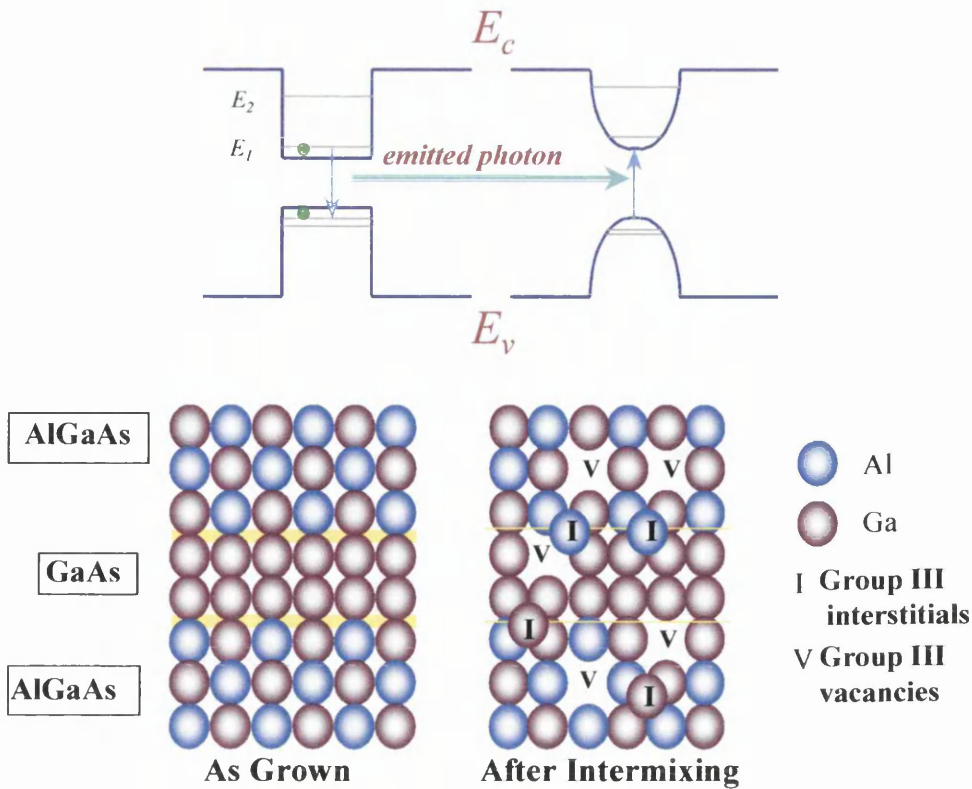


Fig. 1.1 A schematic representation of a GaAs/Al_{0.5}Ga_{0.5}As heterostructure before and after intermixing. Also shown is a schematic for the conduction and valence bands before and after intermixing.

V_{III}^{-3} which was responsible for interdiffusion in GaAs/AlGaAs heterostructures, recent experiments have shown that it is the singly charged V_{III}^{-} , which makes the main contribution to interdiffusion.⁶

II.B. Quantum Well Intermixing

Quantum Well Intermixing is a technique by which one can alter the band gap of quantum confined heterostructures. The characteristics of quantum confined heterostructures chiefly lie in their electronic properties and hence bandgap energy. Hence post-growth control of the semiconductor bandgap can enable the properties of semiconductors to be modified after growth, selectively across the wafer. As can be seen in Fig. 1.1, the bandgap of GaAs/AlGaAs heterostructures can be increased by initiating interdiffusion on the group III sublattice. As the Ga and Al of the QW and cladding are allowed to interdiffuse, Al will cross the QW boundaries, as can be seen in Fig. 1.1. This will lead to grading of the QW/barrier interface. The interface grading together with the presence of Al in the middle of the QW will cause an increase in the ground state energy.

The bandgap energy as a function of Al content, at the edge of the intermixed QWs can be expressed as,⁷

$$E_g = 1.424 + 1.247x_{Al}, \quad (1.2)$$

where x_{Al} is the Al content of the group III sub-lattice, and E_g is the bandgap energy. The width reduction of the QW and the increase of the QW Al composition, increases the energies of the bound states in the conduction and the valence bands. Accordingly the energy of a photon emitted from the bound states, and especially the ground state e1-lh1, will increase. Hence, the optical losses due to bandedge absorption will be reduced for a wavelength emitted from the non-intermixed region. Also the compositional change causes a change in refractive index. At 850 nm it takes of the form,⁷

$$n(x_{Al}) = 3.59 - 0.71x_{Al} + 0.091x_{Al}^2, \quad (1.3)$$

However, due to the small overlap of the optical field with the intermixed regions, in the case of 2 QWs, the effect of refractive index change is negligible. On the other hand, if the QWI takes place in a superlattice or a region packed with heterostructure interfaces, the refractive index change can be considerable. Change of up to 5 % in the refractive index was reported in MQW waveguides.⁸ The main criterion for QWI methods to be useful is to be able to cause controlled intermixing at temperatures less than those required for thermal interdiffusion.

II.B.1. Effect of QWI on the Electronic and Optical Properties

Electronic states in QW structures are governed by the Schrödinger wave equation, with the potential function being the potential of the as-grown quantum well structures.⁹ For a QW, the equation describing the wavefunction and the energy for the bound states in the conduction band would then read,

$$\left(-\frac{\hbar^2}{2m^*(z)} \frac{\partial^2}{\partial z^2} + V_c(z) \right) \psi_n(z) = E_n \psi_n(z), \quad (1.4)$$

$$\begin{aligned} V_c(z) &= 0 & 0 < z_{QW} < L_z, \\ V_c(z) &= V_{barrier} & 0 > z_{QW} > L_z. \end{aligned} \quad (1.5)$$

where L_z is the quantum well thickness, \hbar is the reduced Planck's constant, $V_c(z)$ is the potential function of the conduction band, which defines the heterostructure and is considered a square function for as-grown QWs as seen in equation (1.5) and Fig. 1.1. The confined energy states are denoted by E_n , where n defines the energy level number, $\psi_n(z)$ is the envelop wavefunction of the confined state and $m^*(z)$ is the effective electron mass.⁹ As the interdiffusion between the QW and the barrier takes place, the QW shape is modified from the square profile to an *erf* profile assuming that diffusion obeys Fick's law. The QW alloy profile for single and double wells then take respectively the form,¹⁰

$$C_{QW}(z,t) = \frac{C_o}{2} \left[\operatorname{erf} \left[\frac{L_z - z}{2\sqrt{D_{QW}t}} \right] + \operatorname{erf} \left[\frac{z}{2\sqrt{D_{QW}t}} \right] \right], \quad (1.6)$$

$$C_{QW}(z,t) = \frac{C_o}{2} \left[2 - \operatorname{erf} \left[\frac{z}{2\sqrt{D_{QW}t}} \right] - \operatorname{erf} \left[\frac{3L_z - z}{2\sqrt{D_{QW}t}} \right] + \operatorname{erf} \left[\frac{2L_z - z}{2\sqrt{D_{QW}t}} \right] + \operatorname{erf} \left[\frac{z - L_z}{2\sqrt{D_{QW}t}} \right] \right], \quad (1.7)$$

where C_{QW} and D_{QW} are the concentration and the diffusion coefficient of Ga atoms from the quantum well respectively, $C_o = C_{Ga} - C_{Al}$ is the initial concentration in the wells, L_z is the quantum well thickness, and z is the spatial depth parameter. In equations (1.6) and (1.7) the origin of the z co-ordinate is taken at the left barrier of the wells. Numerical solutions are needed to find bound state for the diffused QW profile, and have been reported for QWs in many material systems.¹¹ The corresponding change in the absorption, which is chiefly governed by excitonic effects in the vicinity of the bandgap energy, can be calculated through an evaluation of the optical matrix elements and summation over all the bound energy transitions.¹² The expression governing absorption in QWs cannot, however, be properly explained without an involved description of the bound states and the optical matrix, which is beyond the scope of this introduction. Empirical expressions representing QW absorption were reported before and are therefore used here to describe absorption in QWs. One expression takes the form,¹³

$$\alpha(\hbar\omega, F) = \alpha_p(F) \operatorname{sech} \left[1.317 \frac{\hbar\omega - E_{exc}(F)}{\beta(F)} \right], \quad (1.8)$$

where $\hbar\omega$ is the photon energy, F is the electric field applied to the structure, E_{exc} is the field dependent exciton binding energy, α_p is the field dependent peak absorption, β is the field dependent half width half maximum of the exciton peak. The parameters E_{exc} , α_p , and β all have a quadratic dependence on the applied field F , and are reported for GaAs/AlGaAs MQWs.¹³ The change in absorption will subsequently induce a change in the refractive index of the heterostructure, since both are related by the Kramers-Krönig relation. The change in refractive index due to a change in absorption can therefore be expressed as,¹⁴

$$\Delta n(\lambda) = \frac{\lambda^2}{2\pi^2} P \int_0^\infty \frac{\Delta\alpha(\lambda')}{(\lambda')^2 - (\lambda)^2} d(\lambda'), \quad (1.9)$$

where λ is the photon wavelength at which Δn is calculated, $\Delta\alpha$ is the change in the absorption coefficient, and P is the Cauchy principal value of the following integral, which takes the form,

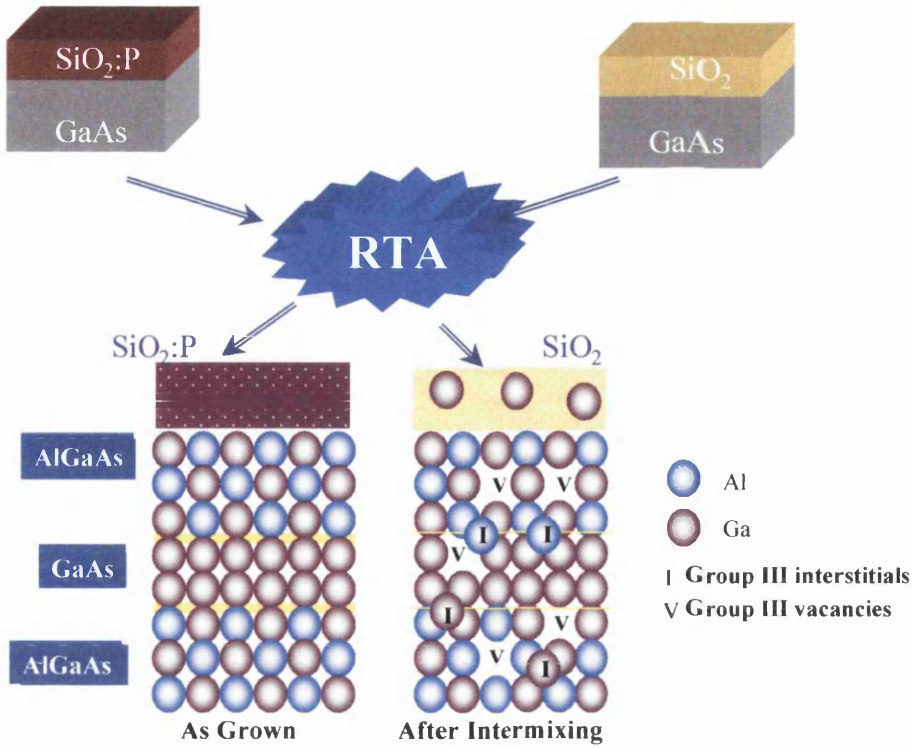


Fig. 1.2 A schematic representation of a IFVD processing of a GaAs/Al_{0.5}Ga_{0.5}As heterostructure. The dielectric caps used during annealing in this example are SiO₂, and SiO₂:P

$$P \int_{\mathbb{J}}^{\infty} = \lim_{\delta \rightarrow 0} \left(\int_{\mathbb{J}}^{\lambda - \delta} + \int_{\lambda + \delta}^{\infty} \right). \quad (1.10)$$

The change in the bandgap also changes the non-linear properties of the semiconductor, such as changing the $\chi^{(3)}$ in GaAs/AlGaAs MQWs.¹⁵ It can also change the $\chi^{(2)}$ introduced within GaAs/AlGaAs asymmetric MQWs¹⁶ and, when applied periodically, can induce domain disordering to obtain quasi phase matching.¹⁷

It should be noted that the change in the optical properties mentioned here would have to be scaled with the overlap integral between the semiconductor layers involved and the mode of the optical field. Such an overlap integral can be expressed as,¹⁸

$$\Gamma = \int_{QWs} |E_{opt}|^2 dz / \int_{-\infty}^{\infty} |E_{opt}|^2 dz, \quad (1.11)$$

This implies that, to maximise the effect of a given number of QWs within a heterostructure on the optical field, the mode should be highly confined within the QW region.

Because of the graded well profile induced by the intermixing of the QWs, it has been also reported that, by intermixing InP-based QWs, the polarisation sensitivity of the optical properties of QWs can be eliminated,¹⁹ and the quantum confined stark effect can be enhanced.²⁰

II.B.2. Impurity-Free Vacancy Disordering

Impurity free vacancy disordering (IFVD) is a widely used QWI technique due to its simplicity, the low optical losses of disordered material and low residual damage.²¹ IFVD makes use of the diffusion of point defects, namely group three vacancies and interstitials, created by thermal treatment in a rapid thermal annealer (RTA). Samples are usually capped with dielectric layers, which either promote, or impede, the diffusion of Ga out from the semiconductor, and hence enhance or suppress QWI respectively. Various dielectric caps have been studied for optimum intermixing performance.^{22,23,24} A schematic explanation of the process stages is shown in Fig. 1.2. SiO₂ is the most widely used, due to the early studies which used such caps for GaAs integrated circuit processing.^{25,26} As the temperature of capped samples is raised above a certain threshold, Ga and As start to out-diffuse into the cap from the semiconductor. The out-diffused Ga and As leave native point defects in the lattice. At the annealing temperatures, the native point defects have large kinetic energies allowing them to diffuse down towards the heterostructures in the lattice, thus promoting interdiffusion. The properties of the films as well as the dielectric/semiconductor interface are thought to be the main factors that control the amount of Ga out-diffusion, as will be seen later within the thesis. Therefore characterisation and control of the properties of dielectric films involved in the IFVD process are vital for achieving a reliable and reproducible process.

III. THESIS OUTLINE

In the second chapter an overview of the main intermixing techniques currently available is presented. The basic mechanisms, properties, merits, drawbacks, and applications of each intermixing technique are introduced. This gives us the insights needed to carry out the research and decide on the process to investigate for a generic intermixing technology independent of the intended application. In chapter 3, an atomic-scale model for the kinetics of intermixing of GaAs/AlGaAs quantum confined heterostructures is developed. The model hypothesis has been validated by successfully predicting the amounts of quantum well intermixing induced by the processes of hydrogen plasma induced defect layer intermixing and impurity free vacancy disordering, two different techniques for quantum well intermixing. In chapter 4, the process of dielectric-cap-induced intermixing is studied. The performance of various dielectric caps in IFVD was investigated, by studying the bandgap shifts produced by each dielectric cap after annealing at elevated temperatures. A discussion is then presented, to assist in obtaining an optimum combination of caps for IFVD. An optimum process is then developed and its performance is characterised. In the following chapter, various aspects of the process of IFVD are characterised. Parameters regarding technological, as well as the

theoretical aspects, of disordering are investigated. Temporally resolved PL is used to investigate the effect of intermixing on the photogenerated carrier lifetimes in intermixed lattice. A PL micro-probe is used to carry out spatially resolved measurements, by which the variation in the PL energy along gratings with alternating intermixed and unintermixed regions can be investigated. Also a Raman micro-probe is used to carry out a spatially resolve investigation of the change in the Raman mode properties as a function of intermixing. While the techniques mentioned so far study parameters that are mostly related to the IFVD technology, PLE was also used to investigate the QW shapes prior to, and after annealing. In chapter 6 deep level transient spectroscopy measurements were used to characterise the nature, profiles, and diffusion of defects, and deep level traps associated with IFVD. Finally secondary ion mass spectroscopy profiles were measured for IFVD samples processed with various dielectric caps to reveal some of the mechanisms associated with Ga out-diffusion during annealing. The device chosen to demonstrate IFVD for integrated optoelectronics is a DBR laser with an integrated Mach-Zehnder modulator. Measurements and characterisation of discrete modulator devices, as well as modulators integrated with DBR lasers are presented in chapter 6. Technological aspects of the fabrication and the effect of intermixing on the performance of the integrated device are also presented in this chapter.

IV. REFERENCES

- ¹ C. Kittel, "Introduction to solid state physics," Academic Press, sixth edition, 1986.
- ² J. C. Bourgoin, H. J. von bardeleben, D. Stievenard, *J. Appl. Phys.*, vol. 64, P R65, 1988.
- ³ T. Venkatesan, S. A. Schwartz, D. M. Hawng, R. Bhat, M. Koza, H. W. Yoon, P. Mei, Y. Arakawa, and A. Yariv, *Appl. Phys. Lett.*, vol. 49, P 701, 1986.
- ⁴ S. A. Schwartz, T. Venkatesan, D. M. Hawng, H. W. Yoon, R. Bhat, Y. Arakawa, *Appl. Phys. Lett.*, vol. 50, P 281, 1987.
- ⁵ D. G. Deppe, N. Holonyak, Jr., *J. Appl. Phys.*, vol. 64, P R93, 1988.
- ⁶ R. M. Cohen, *Mat. Sci. Eng. R*, vol. R20, P 167, 1997.
- ⁷ K. Iga, S. Kinoshita, "Process Technology for Semiconductor Lasers," Springer-Verlag, 1995.
- ⁸ S. I. Hansen, J. H. Marsh, J. S. Roberts, R. Gwilliam, *Appl. Phys. Lett.*, vol. 58, P 1398, 1991.
- ⁹ C. D. Weisbuch, B. Vinter, "Quantum Semiconductor structures, Fundamentals and Applications," Academic Press, 1991.
- ¹⁰ I. Gontijo, T. Krauss, J.H. Marsh, and R. M. De La Rue, *IEEE J. Quantum Electron.*, vol. 30, P 1189, 1994.
- ¹¹ E. H. Li, editor, "Selected Papers on Quantum Well Intermixing," *SPIE Optical Engineering Press*, 1998.
- ¹² I Galbraith, *Phys. Rev. B*, vol. 48, P 5105, 1993.
- ¹³ D. T. Nelson, *IEEE J. Quant. Electron.*, vol. 33, P 1094, 1997.
- ¹⁴ C. Thirstrup, *Appl. Phys. Lett.* vol. 61, P 2641, 1992.
- ¹⁵ C. J. Hamilton, J. H. Marsh, D. C. Hutchings, J. S. Aitchison, G. T. Kennedy and W. Sibbett, *Appl. Phys. Lett.*, vol. 68, P 3078, 1996.
- ¹⁶ M. W. Street, N. D. Whitbread, D. C. Hutchings, J. M. Arnold, J. H. Marsh, J. S. Aitchison, G. T. Kennedy and W. Sibbett, *Optics Lett.*, vol. 22, P 1600, 1997.
- ¹⁷ M. W. Street, N. D. Whitbread, C. J. Hamilton, B. Vogeles, C. R. Stanley, D. C. Hutchings, J. H. Marsh, J. S. Aitchison, G. T. Kennedy and W. Sibbett, *Appl. Phys. Lett.*, vol. 70, P 2804, 1997.
- ¹⁸ A. Yariv, "Optical Electronics," Academic Press, Fourth edition, 1994.
- ¹⁹ W. C. Choy, E. H. Li, J. Micallef, *IEEE J. Quant. Electron.*, vol. 33, P 1316, 1997.
- ²⁰ E. S. Koteles, *Private Communication*.
- ²¹ J. H. Marsh, P. Cusumano, A. C. Bryce, B. S. Ooi, and S. G. Ayling, *Proc. SPIE*, vol. 74, P 2401, 1995.

- ²² W. J. Choi, S. Lee, S. K. Kim, J. I. Lee, K. N. Kang, N. Park, H. L. Park, and K. Cho, *J. Mat. Sci. Lett.*, vol. 14, P 1433 1995.
- ²³ P. Cusumano, B. S. Ooi, A. Saher Helmy, S. G. Ayling, A.C. Bryce, J. H. Marsh, B. Voegelé, and M. J. Rose, *J. Appl. Phys.*, vol. 81, P 2445, 1997.
- ²⁴ B. S. Ooi, K. McIlvaney, M. W. Street, A. Saher Helmy, S. G. Ayling, A.C. Bryce, J. H. Marsh, and J. S. Roberts, *IEEE J. Quant. Electron.*, vol. 33, P 1784, 1997.
- ²⁵ J. Gyulai, J. W. Mayer, I.V. Mitchell, and V. Rodriguez, *Appl. Phys. Lett.*, vol. 17, P 332, 1970.
- ²⁶ D. G. Deppe, L. J. Guido, N. Holonyak, Jr., K. C. Hsieh, R. D. Burnham, R. L. Thorton, and T. L. Paoli, *Appl. Phys. Lett.* 49, 510 (1986).

REVIEW OF TECHNIQUES AND ADVANCES

Intermixing of quantum confined heterostructures was initially studied in the GaAs/AlGaAs system as an undesirable phenomenon occurring during the heat treatment of wafers. Later intermixing was found to be useful, especially for optoelectronics applications. Because intermixing takes place through native point defects, it is necessary to have an understanding the behaviour of such defects in order to control the process. Such an understanding requires a large parameter space to be quantitatively characterised. In brief, the techniques and advances in compositional disordering in GaAs/AlGaAs material system predominantly lie in the control of point defect generation and manipulation within the lattice. Different techniques achieve this generation and control by varying means.

I. HISTORICAL OVERVIEW

Upon discovering the controlled means of disordering heterostructures using impurity induced disordering (IID) at the beginning of the 80s,¹ the principle application for such technology has always been optoelectronics. The excessive free carrier absorption associated with techniques based on IID, lead to the development of QWI using impurity-free techniques. Implantation induced defect disordering, although first discovered in an attempt to use Si implants as a way to induce IID,² has been an effective method to induce QWI when neutral, or native lattice impurities are used as the implant species. Moreover, the advances and control of the implantation processes, was readily available to utilise in optoelectronics. Point defects, and hence QWI, can also be introduced by other means such as plasma and laser irradiation damage.^{3,4} The development of dielectric cap annealing processes, known as impurity-free vacancy disordering, IFVD, followed after implantation induced disordering. IFVD was discovered when the GaAs VLSI process technologies, at the time, were utilised to generate point defects in the vicinity of the QWs. This was achieved through dielectric cap annealing induced defects. The factors leading to the realisation of IFVD are:

- The understanding of disordering mechanisms, which suggested that Al/Ga interdiffusion is carried out through group III interdiffusion in GaAs heterostructures.
- VLSI technology, which provided information about the performance of GaAs/AlGaAs heterostructures at elevated temperatures, namely the interdiffusion of Al and Ga at the interfaces,⁵ and the diffusion behaviour of species like As and Ga into dielectric caps such as SiO₂, and Si₃N₄.

The technique has been a prominent means for realising regrowth-free photonic integrated circuits, PICs, and optoelectronic integrated circuits, OEICs, respectively. It is attractive due to the simplicity of the processes involved, and the optical losses produced, which are more than two orders of magnitude less than for the IID process. In this chapter a brief overview of the basics, advances and most noticeable applications of the major intermixing techniques reported to date will be presented. An emphasis is made on IFVD, being the process underpinned in this work.

II. INTERMIXING TECHNIQUES

Disordering mechanisms were first studied in the GaAs /AlGaAs material system. The principal role of group III vacancies, V_{III} , and interstitials, I_{III} in the process was soon identified. These studies were carried out to explain the process of impurity induced disordering. Driven by the initial understanding of the IID mechanisms, other schemes by

which one can generate group III point defects were developed. Naturally every new method developed was an attempt to overcome certain limitations, or drawbacks in the preceding scheme. For any technique to be useful, disordering has to be realised on a selective basis, therefore thermal stability of the lattice becomes of key element in the success of the selectivity of any process.⁵

Thermal Al/Ga interdiffusion in the heterostructures takes place with a certain activation energy E_A , with a Boltzman-like temperature dependence such that;

$$D_{Al \leftrightarrow Ga} = D_o \exp\left[-E_A/kT\right] \quad (1.1)$$

where D_o is the diffusion coefficient at infinite temperature, k is the Boltzmann constant, T is the temperature and E_A is the activation energy by which diffusion takes place. The goal of any intermixing technique is to selectively decrease the activation energy of the group III interdiffusion coefficient in given areas. Various important intermixing techniques will be presented below, they will be categorised by the means of generation of group III defect. For further reading, a collection of the most important papers published in the field was recently published by *SPIE*,⁶ and a special issue on inter-diffused quantum wells was also published in *IEEE Journal of Quantum Electronics*.⁷

II.A. Impurity Induced Disordering

Impurity induced disordering, being the first intermixing technique discovered by Laidig *et al.* in 1981, has the been the most investigated.¹ Despite the technological advances achieved after its discovery, little was known about the actual mechanisms by which intermixing takes place.^{2,8} In 1987 Tan and Gösele suggested the dependence of the equilibrium concentration of defects on the Fermi level.⁹ They also suggested in 1988 that the triply charged group III vacancies play a pivotal role in the interdiffusion on the group III sublattice.¹⁰ In the same year, Deppe and Holonyak Jr provided a more complete picture of the mechanisms involved by highlighting the effect of As overpressure on the intermixing behaviour.³ One decade later, the individual factors such as the Fermi level effect, the As overpressure, as well as the other experimental parameters have been correlated together using basic physical relationships such as the Gibbs phase rule by R. M. Cohn (more elaborate discussion on the subject will be presented in chapter 3).¹¹

Factors in excess of 10^5 increase in the Ga/Al interdiffusion coefficient were reported due to Zn diffusion at 600°C.¹² Various other impurities were studied; donors such as Si, Ge, S, Se, as well as acceptors such as Zn, Be, Mg have shown the same effect of disordering heterostructures upon annealing.³ Different schemes of introducing defects have also been explored; defect diffusion was the initial means of exploring the phenomenon, then came implantation of electrically active impurities, which induces intermixing due to

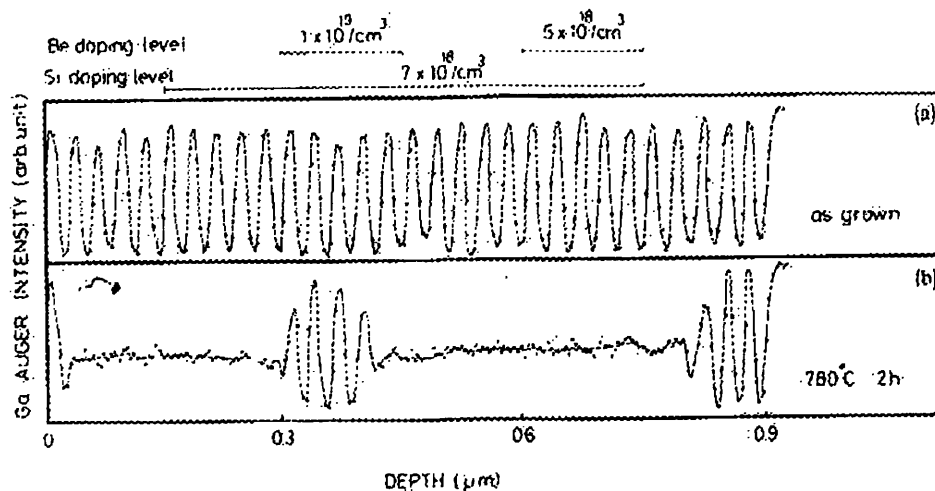


Fig. 2.1 Auger depth profiles of Ga in a superlattice doped with Be and Si, with profile as shown on the top of the graph. As grown profile is shown in (a), while (b) shows the profile after a 2 hr. furnace anneal at 780 °C. After Kobayashi *et al.*³⁶

the damage caused as well as the dopant diffusion that takes place during the subsequent annealing phase. Another means of diffusing dopants such as Si was laser annealing.¹³ Intermixing due to laser annealing, as will be explained in section II.B.3, is usually observed after irradiating samples for a suitable length of time using a laser with an appropriate wavelength. Moreover, IID can take place after subsequent annealing if a dopant such as Si is introduced and hence mobilised into the semiconductor during irradiation to become in the vicinity of the QWs.¹⁴ The incorporation of impurities during growth was also investigated as a means of IID,^{3,15} where a clear demonstration of this IID technique shown in Fig. 2.1. Samples were prepared which had a grown-in Si concentration, they were then implanted with Be to compensate for the effect of Si on the Fermi level at two given depths. The role of the Be implantation, having inhibited the intermixing where it takes place, clearly demonstrates the IID effect of Si, and how it can be quenched if the Fermi level can be altered.¹⁵

The process of IID, although very effective, will always have an inherent limitation regarding the associated optical losses, due to free carrier absorption. The different schemes by which defects are introduced in the lattice including implantation, diffusion from the surface, and incorporation during growth, in addition to the control over the diffusion of species such as Si in III-V semiconductors make the technique a powerful way to induce localised QW. IID will therefore always attract a suite of applications, which involve electrical pumping of the intermixed regions.¹⁶ It proved very beneficial to simplify the fabrication of otherwise complicated devices such as antiguided laser arrays. In these devices, neighbouring undoped SL laser stripes were intermixed using Zn diffusion, and then electrically pumped.¹⁷ The effect of the intermixing reduces the refractive index and

generates an antiguided laser diode array. It has also been used to improved the performance of VCSELS with no added complexity in the processing.^{18,19}

II.B. Irradiation Induced Disordering

Irradiation damage in semiconductors is caused by exposing the samples to a flux of particles such as electrons, ions, or photons. A considerable amount of the associated damage is comprised of native point defects. The lattice absorbs energy from the irradiated flux, which enables the release of a number of lattice atoms out of their sites, leaving them in interstitial positions, and consequently generating lattice vacancies or antisites where the atoms were knocked-off. In this section we shall review the techniques which utilise the irradiation-induced defects to enhance intermixing.

II.B.1. Implantation & Focused Ion Beam Induced Disordering

The notion of disordering using implantation induced defects dates from 1971, when ion beams were observed to cause atomic mixing to sharp semiconductor interfaces during sputtering of samples in secondary ion mass spectroscopy (SIMS) measurements.²⁰ Assuming that the effect was based on the collision cascades generated by the primary ion beam, calculations of atomic mixing were first derived using a diffusion model in 1977.²¹ Although ion implantation was systematically used to introduce extrinsic dopants into semiconductors, for impurity induced disordering, the implantation defect induced intermixing was recognised a few years latter in 1985.²² Frenckel defect pairs are the principle type of defects produced due to implanted ions. Such defects are generated by the atomic collisions between the implanted species and the lattice atoms.²³ The effect of ion implantation on compositional intermixing was not clearly identified at the beginning of the work on IID because the effect of implantation induced defects is usually convoluted with the effect of impurities on the Fermi level, as discussed in section II.A.³

For intermixing using implantation induced defects to have an edge over its predecessor, IID, it had to overcome the excessive optical losses associated with the electrically active species used in IID. Consequently, the work in the field developed in two main routes:

- The first was to use electrically inactive implantation species to induce intermixing.
- The second was use the native lattice matrix constituents as implantation species.

Although implantation induced intermixing was explored in other material systems,^{24,25,26} most of the work on implantation induced disordering has been in GaAs/AlGaAs. Despite the two distinct trends undertaken in the field to reduce the optical absorption coefficient, there has been some investigations of electrically active species such as Zn,^{22,27} S,²² Be,²⁸

Mg, & Se,²⁸ Ge,²⁹ Bi,³⁰ Xe & In,³¹ Si.^{22,27,28,32,33,34,35} Achievements can be summarised in the following points:

- A considerable part of the work in the field was carried out using Si, which was the key element used in IID at the time. Intermixing caused by Si implantation has two effects; the first is implantation defect induced disordering, which induced point defects within the implantation range and caused interdiffusion upon annealing. However, above certain implantation energy, the number of introduced defects coalesce and form extended defects, which annihilate point defects in their vicinity and hence, reduce intermixing.^{32,28,35,33} The second effect is impurity induced disordering, which uses the increased equilibrium concentration of point defects. The effect can extend for depths much greater than the implantation range due to Si diffusion.^{29,32} However, the effect of the position of the Fermi level on IID can be suppressed by co-doping any given region with an impurity to compensate for the doping causing the IID, as can be seen in Fig. 2.1 for a Si doped lattice after codoping with Be.³⁶ Investigations of other dopants showed results similar to those with Si, in particular Zn.^{22,27} Oxygen implantation has also been viewed as a potential technology for intermixing,^{37,38,39} since it can serve both as an implant species for intermixing as well as simultaneously decreasing the local free carrier concentration. In addition to low energy, low dose implantation, Oxygen has been investigated for MeV implantation, where it was found to cause initial collision intermixing prior to annealing.^{38,39} It was also found to cause collisional intermixing near the surface of the implanted samples as a result of the electronic energy loss mechanism.³⁷
- Electronically inactive implanted species were first investigated in 1985, when Kr ions were investigated by Gavrilovic *et al.*²² However many other species such as Ar,^{40,41} F, B,⁴⁰ Ne, He,²⁷ as well as isoelectric ³¹P⁺,⁴² were investigated. The ion mass and the implantation energy for such species affect the number of introduced defects, and their depth. The implantation dose, also, affects the number of defects, with an upper limit determined by the threshold dose for the formation of extended defects.
 - In recent years Boron and Fluorine have attracted much attention,^{43,44,45,46} after the initial work carried out by Hirayama *et al.* in 1985.⁴⁰ Boron was proposed to form both deep acceptor B_{As} and isoelectric B_{Ga} in p-type material. In n-type material, the majority of B was thought to have formed B_{Ga}. Significant diffusion was observed in GaAs p-type material due to the diffusion of B_{As}, while negligible diffusion was observed in n-type material, since B_{Ga} is relatively immobile at high temperatures. For AlGaAs p-type material, the formation of B_{As} reduces the equilibrium number of charged Ga interstitials and hence, the interdiffusion rate of Al and Ga. For n-type material, partial intermixing was observed and it was ascribed to charged Ga

vacancy.⁴⁷ Boron implantation was not found useful to QWI especially because of the extended defects observed in GaAs after boron implantation.⁴⁵ On the other hand Fluorine, which exhibits a very fast diffusion rate in n and p-type materials, has its diffusion mechanism related to the interstitials. This suggests that Fluorine does not occupy lattice sites, but rather reside on interstitial sites. Waveguides fabricated in F implanted regions exhibited optical absorption losses of 20 dB/cm, with a blue shifts in the order of 35 meV. Most importantly Fluorine did not contribute to the losses, the observed loss was due to bandedge absorption, which depends on the degree of intermixing not on the Fluorine concentration.⁴⁸

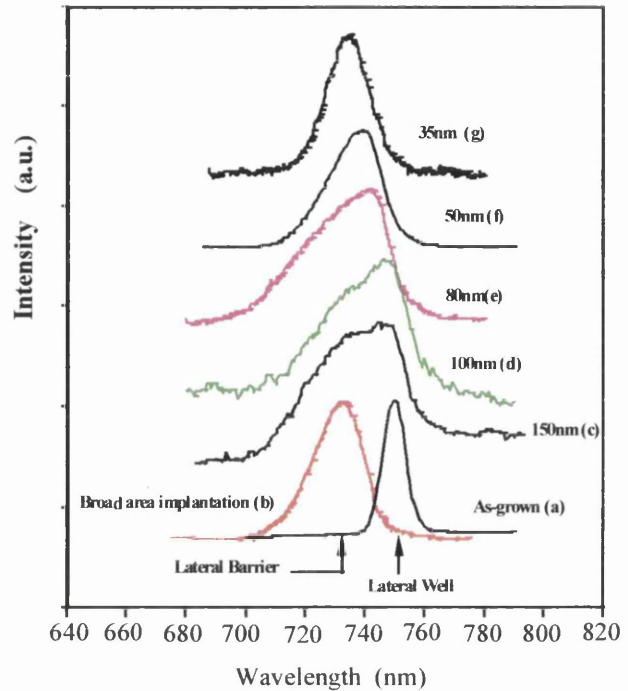


Fig 2.2 5 K photoluminescence spectra from (a) as-grown, (b) homogeneous implanted, and the wire samples of widths from 150 nm (c) to 35 nm (g). The samples were implanted with arsenic dose of $1 \times 10^{13} \text{ cm}^{-2}$, at 45 keV and annealed at 875°C for 30 s. After Ooi *et al.*⁶⁰

- Implantation induced intermixing using native matrix elements such as Al was investigated by Gavrilovic *et al.* in 1985.²² These initial experiments demonstrated that implantation damage alone, can induce considerable amounts of intermixing. However complete disordering of heterostructures can be achieved when electrically active implant species are used. Both the impurity, and implantation defects would then induce intermixing. Investigations of defect induced intermixing using Al as an implant species are limited in comparison with those carried out for Ga and As. That is due to the deep level lattice defects associated with the existence of excessive amounts of Al in the lattice.⁴⁹ QWI due to Al implantation shows similar results to those obtained for Ga and As in many aspects including the diffusion lengths for a given thermal treatment, the saturation behaviour of the intermixing, and the behaviour of the PL signal strength with the annealing conditions.⁵⁰
 - Gallium was studied next, and was the native implant species that has received most interest. Optimum annealing conditions and doses for broad area implantation

samples were deduced from experiments.^{51,52} Defects and damage introduced by Ga implantation were also investigated.^{41,27,53} Defects due to Ga implantation were found in GaAs and AlGaAs layers,⁵³ with induced intermixing occurring at lower temperatures than those for As, Ar, and Mg.²⁷ In addition, such damage was found to be annealed out more effectively than damage introduced by other

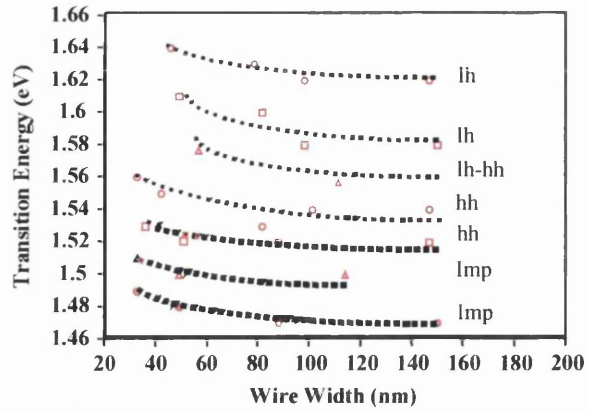


Fig 2.3 Transition energies from PR spectra. The equal energy separation of transitions from the heavy hole related transitions indicate harmonic potential confinements in the wires. In wires smaller than about 100 nm, the relatively flat trend of light hole transitions suggest that the light hole wavefunction is spread everywhere across the gratings with no effective hole confinement taking place. This can be ascribed to the significant effect of both the strong inter-wire coupling and the light hole effective mass. After Ooi *et al.*⁶⁰

species such as As, Si, and Ar.⁴¹ Studying the kinetics,⁵⁴ and the mechanisms of intermixing using Ga implantation induced defects,⁵⁵ along with the channelling effects during implantation,⁵² lead to the realisation of lateral features on the nanometer scale.⁵⁴ Various structures, such as wires and dots with varying sub-micron dimensions were reported using Ga implantation.^{31,51,56}

- Less progress has been achieved with arsenic implants, even though arsenic has a larger mass than Ga, giving a potentially higher resolution. This might be ascribed to the properties of Ga as an implantation source and especially its stability as a liquid metal ion source in focused ion beam technology.⁴⁰ However, As was investigated concurrently with Ga at the initial stages of the implantation damage induced intermixing work.^{34,40} Optimum annealing conditions as well as doses for broad area implantation were deduced for As implants.^{57,58} Studies of implantation damage,⁴¹ photogenerated carrier decay times,⁵⁹ in addition to comparative studies of the intermixing behaviour with that of other species including Ga, F, B and Si among,⁴⁰ were conducted for As implanted samples.
- Low dimensional structures have recently been reported, when As was studied for fabricating quantum well wires, QWW.⁶⁰ As has a relatively large atomic mass compared to other neutral species such as boron, fluorine and gallium, which leads to a corresponding low straggling length during ion implantation. The diffusion coefficient of As is also known to be relatively low.⁴⁰ The implantation energy of As and its corresponding lateral straggling length were then simulated and optimised using TRIM, a Monte-Carlo simulation software package.⁶¹ In order to introduce a high concentration

of point defects into the QW, the peak concentration of the ion was placed in the middle of the QW. Simulation showed that 45 keV drove the ions to an average range of 27 nm, with a lateral straggle of 5 nm. Using this implantation energy, the arsenic ions will not penetrate through 50 nm of $\text{SrF}_2/\text{AlF}_3$, which acts as an effective implant mask. Broad area (homogeneous) implantation into the shallow SQW structures was performed together with fields of 1:1 gratings with periods varying from 35 to 1000 nm. Low temperature PL and room temperature photoreflectance measurements were then carried out to study the optical properties of the QWW fields with optimum As doses for intermixing. From PL, the energies of the lateral wells were found to remain constant for wire widths between 1000 nm and 150 nm, and started to shift significantly towards high energy for 80 nm wires, showing 1-D confinement effects. The signal of the lateral well eventually merges with that of the lateral barrier for 35 nm wires, as can be seen in Fig. 2.2, hence an intermixing radius of about 17 nm was estimated for the process. Photoreflectance measurements were also carried out on these wire samples, showing that the wires appear to have a parabolic lateral potential from samples with barriers narrower than 50 nm, as can be seen in Fig. 2.3, which suggests coupling between QWWs' wavefunctions.⁶⁰

The knowledge acquired from the IC technology about the implantation induced defects enables high precision and control in introducing them. Therefore the process implantation induced defect disordering has great potential to offer to QWI, when compared with other, less understood, processes such as IFVD. Current challenges of the process include the dependence of the QWI resolution on the heterostructures' depth. Although QWWs were demonstrated using various implant species, the resolution of the patterns produced will always be a function of their depth. Another point of strength for implantation is that the surface layers of the lattice should not have a significant amount of defects when compared with other techniques based on surface defect diffusion.

As can be inferred from the research trends in implantation induced intermixing, native matrix elements seem to be the most promising implant species to study. However, it would seem that some implants could be used to perform more than one function; Examples can be oxygen being used to induce intermixing as well as passivate the carriers. Also As can be used for both intermixing and reducing the photogenerated carrier life time due to its presence in an interstitial form. It should also be noted that deep (a few micrometers) intermixing has been realised due to cascade damage of heavy implant species. This technique will always offer unique features, having exceptional characteristics of resolution versus depth.

Due to the thermal instability of the InP based quaternary III-V semiconductors, the implantation induced defect disordering have produced more promising results than IFVD techniques because they can be achieved at lower temperatures. However the pivotal factor in the success of implantation induced defect disordering, especially for fine features, is the availability of appropriate dielectric caps for annealing the defects. Therefore, implantation induced intermixing, although promising, needs to be used in conjunction with the dielectric cap annealing technology to produce a process with less drawbacks than those associated with each technique when used separately.

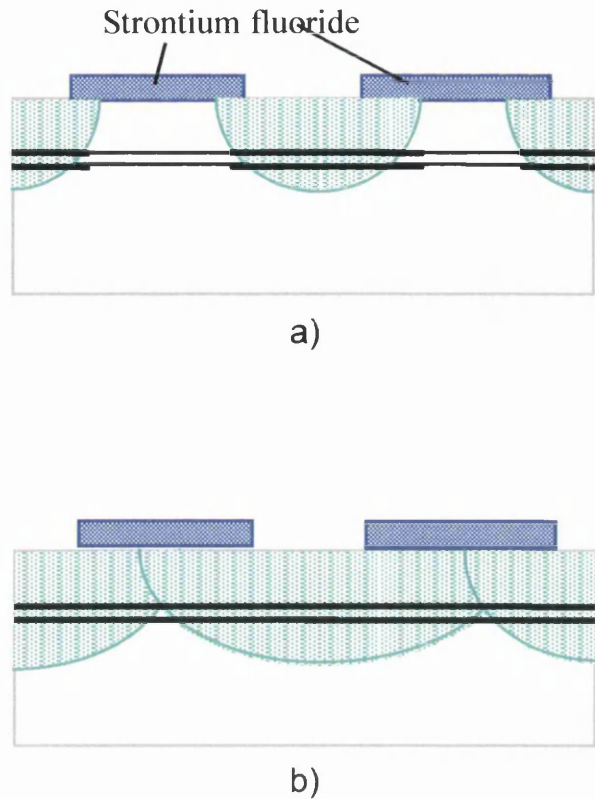


Fig 2.4 A schematic diagram for the gratings used to measure the resolution limit of the PIDLI process. Their effect on the quantum well energy gap is expressed in the width of the line representing them, a) shows partially intermixed region and b) shows fully intermixed region.

II.B.2. Plasma Induced Defect Layer Disordering

Reactive Ion etching, RIE, damage is particularly pronounced in MESFETS, where it was discovered to cause a reduction of the transconductance of the devices.⁶² The effect of RIE etching exposure can be considered as the exposure to a certain flux of ions. Damage mechanisms similar to those taking place during ion implantation are associated with plasma exposure. The generated defects, mainly point defects, can be directly related to the energy transfer.⁶³

The process of plasma induced layer intermixing (PIDLI) is based on Frenkel defect pairs introduced into the semiconductor material, using the hydrogen plasma generated in a RIE machine. The process of QWI using hydrogen plasma induced layer intermixing can be summed up in a few main steps:

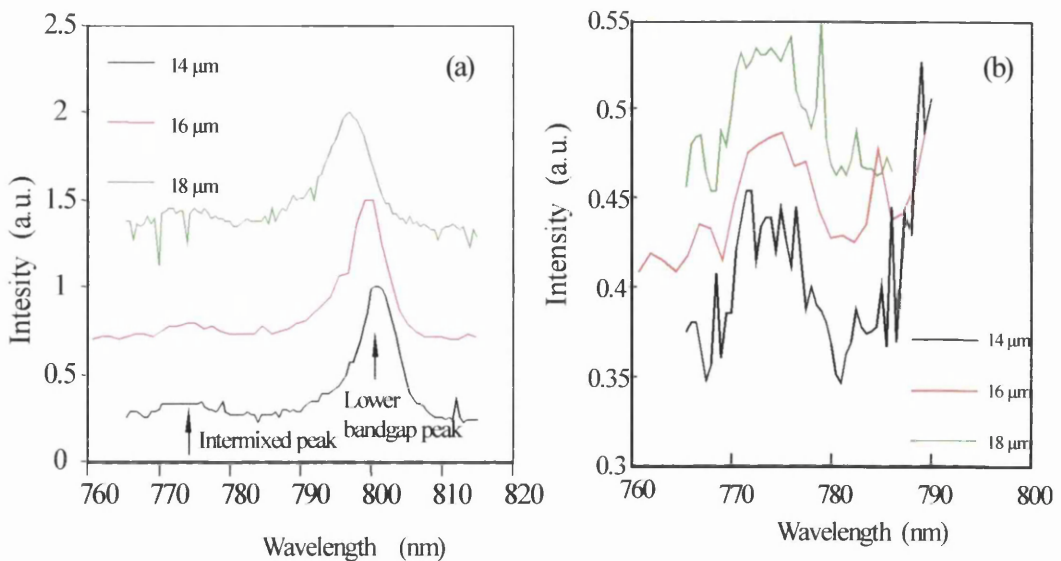


Fig 2.5 Photoluminescence spectra of different grating periods. In (a) the two peaks resembling the two bandgaps in the grating are marked by arrows, while (b) focuses on the smaller peak.

- The RIE machine used was the Electrotech SRS Plasmfab 340 (ET340), the hydrogen used was 99.999 % pure.
- The processes are carried out at a RF power of 150 W with a DC bias of about -1 kV, a gas flow rate of 20 sccm, a table temperature of 30 °C, and at an operating pressure in the range of 5-8 mTorr for 1 minute.
- The etch rate is dependent on the chamber contaminants, the preceding etching gases used, and compounds produced during etching. Etch rate was found to vary from a few $\text{nm}\cdot\text{min}^{-1}$, to $200 \text{ nm}\cdot\text{min}^{-1}$
- The PIDLI process has been found to etch SiO_2 at a relatively high etch rate of about $200 \text{ nm}\cdot\text{min}^{-1}$. On the other hand it was found to etch SrF_2 at a relatively slow rate of $5 \text{ nm}\cdot\text{min}^{-1}$. The range of the H_2 in the SrF_2 layer was computed to be approximately 25 nm using a TRIM simulation program.⁴⁷
- SrF_2 also suppresses intermixing at the temperatures used in the subsequent annealing phase. Layers of approximately 300 nm of SrF_2 were used as a cap for exposure and thermal processing.
- The samples are then thermally processed using RTA at a temperature of 875 °C for 40 seconds. Rise and fall times were set to 12 seconds.
- The amount of defects resulting from one cycle was not found to cause sufficient Al/Ga interdiffusion to achieve the desired intermixing. This is due to the small atomic mass of hydrogen, which governs the atomic interactions with the lattice atoms. Consequently defects are introduced for a short range of energies towards the extremity of the implanted range.

- To achieve the desired amount of defects it was found necessary to use several cycles while monitoring the degree of intermixing by measuring the PL shift of the samples. Typically 6 cycles were used, giving rise to a 27 nm shift in the QWs PL spectrum.⁶⁴

After the successful demonstration of laser diode operation in samples which have undergone the PIDLI process,⁶⁴ an attempt to measure the resolution limit of the PIDLI process was carried out. SrF₂ gratings, with periods ranging from 4 μm to 22 μm, were fabricated on the surface of the sample with a 1:1 ratio.⁶⁵ The material used was a standard laser double quantum well (DQW) material, see Appendix A for details. The samples were exposed to 6 cycles of plasma and subsequent annealing. Shifts of about 25 nm between the capped and uncapped layers were observed. Due to the etching effect of the plasma, gratings with features below 14 μm were etched away. Data for gratings of only larger features are presented. The grating samples should result in QWI with a repetitive profile—one region intermixed and the other is non-intermixed as shown in Fig. 2.4. We therefore expect a dual peaked PL spectrum resulting from recombination in the two regions. As can be observed in Fig. 2.5, the grating sample PL spectrum is indeed dual peaked. The longer wavelength peak has the higher intensity, since it corresponds to the narrowest bandgap region in the sample into which carriers diffuse prior to recombination. The grating spacing at which the two peaks overlap should represent the resolution limit. The PL peaks are well separated, even for the 14 μm pitch grating—the resolution limit is therefore less than 7 μm. The resolution limit of impurity free vacancy disordering, in comparison, process was reported to be about 3 μm for a 1.5 μm thick multiple quantum well waveguide.⁶⁶

Although the process of quantum well intermixing using damage introduced by a hydrogen plasma leads to successful device fabrication, the reliability and reproducibility of the process have not been found adequate for device production.^{47,67} One principal reason responsible for the failure in fabricating further PICs using this technique is thought to be the problems associated with SrF₂. Such problems are more profound in the PIDLI process as compared to the IFVD process, due to the multiple annealing cycles involved (see section II.E. for more details). Failure to remove, and hence electrically pump, PICs fabricated using this technique have consistently been encountered.⁶⁷ However, PIDLI served as a useful process to study the kinetics of intermixing,⁶⁸ due to the availability of models for the defects introduced during the plasma process used as will be discussed in chapter 3.⁶⁹

II.B.3. Laser Induced Disordering

Laser induced disordering uses laser irradiation to induce intermixing in III-V heterostructures. This is carried out primarily by two means: If the photon energy is larger than the absorption edge of the irradiated material, then the semiconductor will absorb the

photon leading to a rise in the lattice temperature. If the photon energy is smaller than that of the irradiated material, no absorption of the light is possible at low intensities. However, as the intensity increases multiphoton absorption takes place leading to the generation of point defects in the lattice. Upon annealing such samples, QWI can take place. Lasers can also be used indirectly to cause intermixing by assisting dopant diffusion from surface layers.

Laser irradiation was first used in disordering processes in 1986 when Epler *et al.* developed a process of disordering by focusing an Ar^+ laser beam on GaAs/AlGaAs SL samples.⁷⁰ Intermixing is primarily induced in the samples due to the rapid

melting and regrowth of the SL. In these experiments a layer of Si and a Si_3N_4 cap was used to cause Si diffusion through the AlGaAs during exposure.⁷⁰ Further annealing of such samples causes further intermixing due to the IID effect. Spatial resolution better than 70 nm was observed for 1 μm deep and 3 μm wide regions. Laser power densities of up to $4 \times 10^7 \text{ W.cm}^{-2}$ were used. In 1987 Ralston *et al.* used pulsed excimer laser irradiation for the same purpose, with pulse energy densities of up to $1 \times 10^7 \text{ W.cm}^{-2}$.⁷¹ An abrupt disordering profile, coinciding with the SL heterostructures interfaces, was observed. Such techniques use large photon energies to illuminate the samples, the temperature rises above the melting temperature of the semiconductor at depths beyond the reciprocal absorption length, α . In such a molten state the Al atoms from the QW, or the SL, barriers diffuse rapidly throughout the melted region. This phase is followed by epitaxial re-crystallisation on the underlying solid material forming a nearly perfect single crystal with a homogeneous distribution of the Al atoms. Upon cooling, the semiconductor becomes crystalline again with an average Al

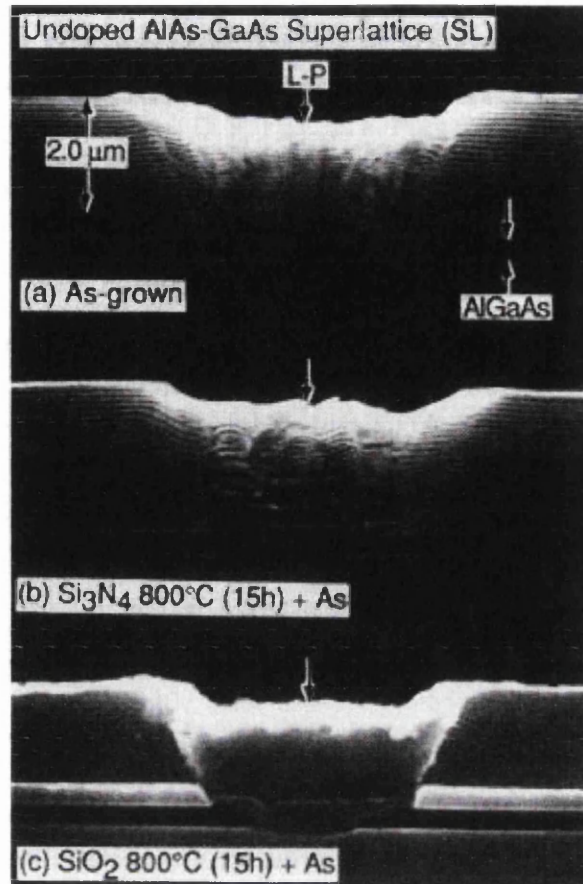


Fig. 2.6 SEMs from different GaAs/AlAs superlattice samples after laser processing. In (a) the as-grown sample is shown, (b) shows the sample after annealing with Si_3N_4 cap, and (c) shows a sample after annealing with SiO_2 cap. The damage of the lattice is apparent in the SEMs.

composition to that of the QW and the barriers.⁷² Despite the visible damage associated with such processes, as can be seen in Fig. 2.6, low threshold laser diodes were demonstrated using Ar^+ and excimer laser assisted disordering.^{73,74}

McLean *et al.* reported another QWI technique termed Photoabsorption Induced Disordering (PAID) for the InP material system in 1992.⁷⁵ In contrast with the technique discussed earlier, this process depends on the absorption of the laser radiation within the QW, i.e. the laser irradiation is not absorbed in the cladding.⁷⁶ This decreases the overall damage caused to the lattice while intermixing buried. Bandgap tuned MQW electroabsorption modulators were demonstrated using this technique, where the spatial selectivity was around 100 μm .⁷⁷ A variation on this process termed pulsed PAID (P-PAID), which uses pulsed laser irradiation instead of CW, was developed to overcome the poor spatial resolution due to thermal diffusion.⁷⁶ P-PAID depends on introducing native point defects in the lattice. The pulsed laser does not supply enough energy for thermally induced interdiffusion.⁷⁸ Spatially and temporally resolved PL measurements showed that the spatial resolution of the process is approximately 20 μm , and the carrier life time can be decreased by one order of magnitude after exposure to the laser pulses.⁷⁹ The technique was devised to fabricate basic PICs.^{80,81} It was the enabling vehicle for novel QWI applications such as in-situ laser wavelength trimming.⁸² This technique was not only successful in the InP system, but also in the GaAs system. Radiation from a Nd:YAG laser ($\lambda=1064$ nm) was used to produce bandgap shifts in GaAs/AlGaAs heterostructures through defects introduced by multiphoton absorption. This process has also been used to fabricate bandgap tuned lasers,⁴ which had threshold currents only a few percent higher than those of the unprocessed samples. CW and pulsed PAID demonstrate immense potential for fabricating OEICs and PICs, though they still lack optimisation and reproducibility to be commercially viable.

II.C. Impurity Free Vacancy Induced Disordering

IFVD uses native group three vacancies, generated at the surface of the semiconductor, to enhance the interdiffusion of the lattice elements responsible for intermixing. The vacancies are generated due to the diffusion of group three lattice atoms, namely Ga in the case of GaAs, out of the surface of the semiconductor and into a dielectric cap. Where the out-diffusion takes place, a resultant concentration of V_{III} is introduced into the lattice, in addition to the V_{III} concentration already introduced during growth. Interdiffusion of Al and Ga, which depends on the nature of the dielectric cap and the amount of V_{III} introduced, then takes place in the lattice. IFVD technology was conceived as a result of advances in two fields, the controlled Al/Ga interdiffusion phenomenon, and the

technology of using dielectric caps in various thermal processing phases of semiconductor manufacturing.

IFVD was first demonstrated in GaAs/AlGaAs in 1986 by Deppe *et al.*, where they fabricated channel waveguides due to the refractive index change induced by the interdiffusion of MQW structures.⁸³ Two main factors contributed to SiO₂ being the first, and most widely studied, cap for IFVD. The first was the importance of SiO₂ in various Si IC technologies such as masks for diffusion, both to prevent and introduce extrinsic dopants such as As and Ga.⁸⁴ The second was the emerging interest in GaAs ICs and the technologies associated, in which SiO₂ and Si₃N₄ caps were studied to keep the GaAs lattice intact during post-implantation annealing.⁸⁵ These initial studies showed that Ga diffuses through the SiO₂ caps at high temperatures, while As does not.^{86,87}

It is useful at this point to make a distinction between the IFVD using dielectric cap annealing, and other techniques of introducing defects, which include introducing defects during cap deposition or from a semiconductor layer grown with excess amount of point defects.

II.C.1. Dielectric Cap Annealing Induced Intermixing

Studies of SiO₂ caps started as early as 1957, when it was considered to protect the surface of Si samples at elevated temperatures, and also used as a diffusion mask for impurities such as As.⁸⁴ While such studies were still of great interest to the Si fabrication technology,⁸⁸ the use of such caps have proved also valuable for processing III-V semiconductors, which are much less thermally stable than Si. Initial studies were carried out on SiO₂ and Si₃N₄ caps using Rutherford Back Scattering (RBS).⁸⁵ Characterisation of the effect of SiO₂ and Si₃N₄ caps along with others such as AlN on the annealing of GaAs was reported.⁸⁷ Also the diffusion coefficients of various species such as Ga into the SiO₂ caps during furnace anneals were reported.⁸⁸ After the discovery of the QWI using dielectric cap annealing, IFVD induced by SiO₂ caps has been studied by numerous groups.^{89,90,91,92} The interdiffusion coefficient of Ga and Al in QWs annealed with SiO₂ caps on,⁹³ the saturation concentration of Ga in the caps,⁹² and the change of intermixing with depth were all studied.⁹¹ The SiO₂/GaAs interface has been investigated as well using X-ray photoelectron spectroscopy, XPS, showing evidence of an increase in the Ga diffusion coefficient in SiO₂ caps for rapid thermal processing by two orders of magnitude than that of conventional furnace annealing.⁹⁴ Further, the effects of the cap thickness, anneal temperature, and anneal duration, on the amount of intermixing were reported.⁹⁰ It was found out by using deep level transport spectroscopy, DLTS, that the nature of defects induced by annealing GaAs with caps such as Si₃N₄ and SiO₂ were similar to those of EL2 defects.⁹⁵ To the best of our knowledge, all the studies of SiO₂ have shown that such caps

are suitable caps for Ga diffusion, unlike Si_3N_4 , which was found to prevent Ga diffusion when deposited in certain ways.⁸⁷ Si_3N_4 was studied as a viable dielectric cap for inhibiting intermixing in IFVD at the same time as SiO_2 ,⁸³ leading however to results with less consistency than those of SiO_2 caps.^{92,96,97,98} Reasons behind the inconsistent observations for Si_3N_4 caps when compared to those of SiO_2 are thought to be due to existence of contamination in the films. Such contamination along with the intermittent deposition conditions lead to variation in film composition and matrix density. Difficulties have often been experienced in producing nitrides in a pure state. Since the deposition of Si_3N_4 is always associated with O_2 , it thus induces the formation of $\text{Si}_k\text{N}_y\text{O}$.⁹⁹ The density of the film matrix also affects the diffusion of elemental Ga and As into the film, hence affecting the amount of intermixing. This topic will be discussed in more details in chapter 4. Although in the early days of IFVD, laser devices were fabricated using the $\text{SiO}_2/\text{Si}_3\text{N}_4$ cap ensemble, little has been reported since then using Si_3N_4 . However, SiO_2 was often used in conjunction with areas with no caps, to produce differential shift in GaAs.^{100,101,102} Quantum well wires in the surface proximity were fabricated using this technique.¹⁰⁰ Intermixed waveguides with very interesting mode filtering characteristics were also reported.¹⁰¹ In addition, novel non-linear switches were demonstrated using this capping system to locally control the $\chi^{(3)}$ coefficient.¹⁰²

Selective disordering is necessary for device applications. Initially, layers that need not be disordered were thermally processed without dielectric caps. Although the heterostructures underneath such regions exhibited a limited but finite amount of intermixing, a differential shift could still be attained. However, the lattice quality underneath these regions have been observed to deteriorate upon thermal processing. Suitable caps are therefore necessary to keep the lattice intact.

SrF_2 was consequently explored as a potential cap to inhibit intermixing since it exhibited minimal PL shifts due to disordering.¹⁰³ The $\text{SiO}_2/\text{SrF}_2$ capping system has produced up to 240 meV differential shift.¹⁰⁴ The activation energy for the Ga/Al interdiffusion coefficient in regions underneath SrF_2 caps was found to be 6.4 eV,⁹³ which is larger than the activation energy observed for diffusion produced due to thermal-induced dissociation in GaAs/AlGaAs structures.¹⁰⁵ Successful optoelectronic devices have been realised using such capping system.^{106,107} The SrF_2 cap exhibited several unfavourable properties though. Excess damage and inefficient electrical pumping have been reported upon annealing GaAs with SrF_2 caps.¹⁰⁸ Further discussion of the damage will be presented in chapter 4. SrF_2 has been now replaced with another cap exhibiting less side effects, namely $\text{SiO}_2:\text{P}$.

In 1995 E.V.K. R o *et al.*¹⁰⁹ have announced $\text{SiO}_2:\text{P}$ as a universal QWI cap for III-V semiconductors, which was suggested to replace plain SiO_2 . Work has been carried out in

the Department of Electronics and Electrical Engineering at the University of Glasgow to verify this work. As will be discussed in the chapter 4, SiO₂:P caps have been shown to inhibit intermixing in almost all of the doped layer structures used. Different amount of phosphorous has however been used in these experiments.^{110,111} The negligible damage associated with this process allowed the demonstration of very efficient mode-locked laser diodes integrated with external cavities using this capping system.¹¹²

Further studies of the various characteristics of dielectric caps used in IFVD revealed that it is possible using a single type of dielectric caps to achieve selective intermixing. The technique depends on altering the dielectric cap properties to control the out-diffusion of Ga during annealing.¹¹³ The technique provides both, the promise of high resolution IFVD capping system, and improves the current understanding of the mechanisms of the dielectric cap annealing process.

II.C.2. Other IFVD Techniques

Dielectric cap annealing is not the only means by which we can induce IFVD. Some techniques introduce point defects by affecting the structures surface composition to enhance, or inhibit, Ga out-diffusion during annealing. Others introduce point defects by using hybrid techniques such as combining ion bombardment induced defects with dielectric cap annealing in one step.

The surface of the semiconductor plays a paramount role in controlling the Ga out-diffusion. Some recent techniques successfully made use of the surface structure as a means of controlling QWI. Native oxide growth using hydrogen plasma treatment was reported to inhibit QWI in the areas underneath. XPS studies on these surfaces showed the presence of a Ga₂O₃ rich native oxide, which lead to the conclusion that this oxide composition limits the Ga out-diffusion at elevated temperatures. Disordered MQW waveguides, produced by this technique were investigated showing up to 64% modulation in the non-linear self-phase modulation coefficient n_2 , as well as increased propagation losses at 1.55 μm from 0.94 dB.cm⁻¹ to 6 dB.cm⁻¹.¹¹⁴ Also a 17% modulation in the $\chi^{(2)}$ coefficient was achieved in asymmetric GaAs/AlGaAs quantum wells using this intermixing technique.¹¹⁵ Independently, a few months later, on the other side of the globe, anodic oxidation was reported to produce layers of native oxide on GaAs/AlGaAs structures, which enhance QWI.¹¹⁶ The anodic oxidation recipes were originally used as a means for current blocking in laser diodes. The technique was demonstrated to be viable when succeeded in enhancing the emission from QWVs grown on sawtooth-type non-planar GaAs pre-etched substrate.¹¹⁶ Anodic oxidation was then further studied and optimised.¹¹⁷ However, no conclusive evidence was presented to explain the enhanced QWI.¹¹⁸ No devices were demonstrated

using that technique and no spectroscopic investigation of the nature of the oxide was carried out either.

For enhancing Al/Ga interdiffusion through native point defects, another technique has been also reported. The technique utilises the fact that the mechanical treatment history of the semiconductor is crucial in determining the point defect concentration. Growth temperature of semiconductor is a detrimental factor in defining the amount and nature of defects incorporated in the semiconductor lattice. Interstitial As atoms, antisite defects, as well as Ga vacancies are usually associated with GaAs grown at temperatures within the vicinity of 200 °C.¹¹⁹ Several hundreds of nanometers of low temperature (LT) GaAs were therefore grown as the top layer of a SL structure to investigate the possibility of achieving differential QWI using the associated point defects. Upon thermally processing such structures using a RTA at temperatures varying between 700°C - 850 °C,¹²⁰ bandgap shift up to 200 meV, were observed in layers with only 100 nm of LT-GaAs on top of the SL. On the other hand uncapped regions experienced a shift of about 40 meV undergoing the same thermal treatment. Similar LT-GaAs layers grown beneath SL structures cause similar intermixing, but less than the one induced LT GaAs layers on top of the SL structures. The technique has been also used to induce disordering in InGaAs/GaAs QCHs, with activation energy of 1.63 eV for the In-Ga interdiffusion. Such energy is less than the thermally induced interdiffusion coefficient, 1.93 eV, which allows differential bandgap shift between capped and uncapped regions.¹²¹ This technique is seen as particularly attractive in replacing SiO₂ caps for samples incorporating SLs, since Si has been found to diffuse from the caps during RTA into the SL layers if they are within a few hundreds of nanometers from the semiconductor surface.¹²²

A technique was reported recently as an effective means to realise selective QWI, and was demonstrated for almost all III-V semiconductor material systems.¹²³ It uses sputtered SiO₂ caps to introduce point defects due to sputtering induced damage. The defects as well as the dielectric caps play a role in the QWI, which takes place where the cap is in direct contact with the semiconductor surface. Such conclusions were drawn upon investigating the damage induced by the film deposition using a special wafer with QWs at varying depths.¹²³ The intermixing due to deposition induced damage prior to thermal processing has been previously reported for Si₃N₄ deposition.^{96,97,98} However the recently reported techniques have been devised to fabricate functional PICs and OEICs such as external cavity lasers.^{124,125} Some investigations regarding the resolution of the process will be presented in chapter 5 of this thesis.

III. SUMMARY

In this chapter we have presented a brief overview of the main QWI intermixing techniques. The origin of each technology as well as the major advantages and disadvantages were also highlighted. An emphasis on the process of IFVD has been made due to the roll it plays in the research undertaken in this thesis. The latest advances in the IFVD technology were documented. Such an overview will be used to assist guiding the research undertaken. Concluding remarks can be summarised as:

Impurity induced disordering, although unsuitable for passive optoelectronic devices, can be a valuable technology for active devices. The potential IID has stems from the understanding of dopant diffusion, and the control of introducing such dopants. Implantation induced defect disordering is gaining much interest recently because of its unparalleled success in the InP material system. However the lack of appropriate capping system for annealing might be a limiting factor for the advances achieved by this technique. Interest in low dimensional patterning using implantation will be a major driving force behind the research. That is because the buried structures will have no shortcomings caused by interface states and hence the recombination associated with interface states will be eliminated.

Implantation induced defects using RIE machines is likely to be a strong candidate for replacing disordering using implantation induced defects. This is due to the economical overheads involved in using an implanting machine. However hydrogen is not a good implant species to use for intermixing purposes as demonstrated by investigating the PIDLI process. The hydrogen ion mass, and hence the multiple annealing cycles associated with the PIDLI process pose a detrimental obstacle in the success of this process and any similar processes. The PIDLI process, nevertheless, served as a useful pathway to develop quantitative methods to explain the kinetics of intermixing.

Intermixing techniques, which use laser annealing, lend themselves to mass production, in-situ intermixing during device operation, and in-situ monitoring of the degree of intermixing through optical spectroscopic techniques such as Raman spectroscopy. Industrial interest is likely to be shown if better control is demonstrated over such processes. This can be achieved by either using anti-reflection coatings, or using a laser beam with a reproducible intensity profile and a direct beam writing technology. The survival of this technology, and its transfer to industry, is perhaps primarily governed by the advances achieved in the fields of laser beam shaping, steering and optical multi-layer coating. One emerging science, which might greatly enhance this technology, is free space holography.

Impurity free vacancy disordering is the simplest technology to realise QWI. Process complexity and equipment overheads are the least when compared to irradiation

induced disordering. However, the defects are introduced from the surface, which imposes a limitation on the process resolution versus depth, as well as the status of the lattice above the intermixed heterostructure after annealing. An investigation of the reverse bias performance of structures processed by this technique has not yet been undertaken, and should prove useful in assessing the effect of the defects introduced on the lattice. Generally, principal challenges within IFVD lie in the reproducibility of the performance of the dielectric caps, and the ability of achieving a differential shift within the range of tens of meV to minimise bandedge absorption with a minimal associated shift under the unintermixed regions. This is not yet achieved due to the lack of comprehensive understanding of the mechanisms involved in processes such as intermixing using dielectric cap annealing. It is interesting to note that despite the whole host of applications which SiO₂ cap annealing, there has been no work explaining the reason of the elevated temperature diffusion of elemental Ga and As for the crystals.

IV. REFERENCES

- ¹ W.D. Laidig, N. Holonyak, Jr., M.D. Camras, K. Hess, J.J. Coleman, P.D. Dapkus, and J. Bardeen, *Appl. Phys. Lett.*, vol 38, P 776, 1981.
- ² J.A. Van Vechten, *J. Appl. Phys.*, vol. 53, P 7082, 1982.
- ³ D.G. Deppe and N. Holonyak Jr., *Appl. Phys. Lett.*, vol. 64, P R93, 1988.
- ⁴ B.S. Ooi, C.J. Hamilton K. McIlvaney, A. C. Bryce, R. M. De La Rue, J. H. Marsh, J. S. Roberts, *IEEE Photonic. Technolo. Lett.*, vol. 9, P 587, 1997.
- ⁵ L.L. Chang, A. Koma, *Appl. Phys. Lett.*, vol. 29, P 138, 1976.
- ⁶ E. H. Li, editor, "Quantum Well intermixing for Photonics," SPIE Optical Engineering Press, vol. 145, 1998.
- ⁷ Issue on Inter-diffused Quantum-Well Materials and Devices, *IEEE J. Sel. Topics Quantum Electron.*, vol. 4, 1998.
- ⁸ J. Kobayashi, M. Nakajima, Y. Bamba, T. Fukumaga, K. Matsui, K. Ishida, H. Nakashima, and K. Ishida, *Jpn. J. Appl. Phys.*, vol. 25, P L385, 1986.
- ⁹ T.Y. Tan, U. Gösele *J. Appl. Phys.*, vol. 61, P 1841, 1987.
- ¹⁰ T.Y. Tan, U. Gösele, *Appl. Phys Lett.*, vol. 52, P 1240, 1988.
- ¹¹ R. M. Cohen, *Mat. Sci. & Eng Reports*, vol R20, P 167, 1997.
- ¹² J.W.Lee, and W.D. Laidig, *J. Electron. Mater.*, vol. 13, P 147, 1984.
- ¹³ J. E. Epler, F. A. Ponce, F. J. Endicott, T. L. Paoli, *J. Appl. Phys.*, vol. 64, P 3439, 1988.
- ¹⁴ J. E. Epler R. D. Brunham, R. L. Thorton, T. L. Paoli, *Appl. Phys. Lett.*, vol. 51, P 731, 1987.
- ¹⁵ M. Kawabe, N. Shimizu, F. Hasegawa, and Y. Nannichi, *Appl. Phys. Lett.*, vol. 46, P 849, 1985.
- ¹⁶ E. Kappon, N. G. Stoffel, E. A. Dobisz, and R. Bhat, *Appl. Phys. Lett.*, vol. 52, P 351, 1988.
- ¹⁷ J. M. Gray, J. H. Marsh, and J. S. Roberts, *IEEE Photon. Technolo. Lett.*, vol. 10, P 328, 1998.
- ¹⁸ A. Khan, K. Woodbridge, M. Ghisoni, G. Parry, G. Beyer, J. Roberts, M. pate, and G. Hill, *J. Appl. Phys.*, vol. 77, P 4921, 1995.
- ¹⁹ P. D. Floyd, M. G. Peters, L. A. Coldern, and J. L. Merz, *IEEE Photon. Technolo. Lett.*, vol. 7, P 1388, 1995.
- ²⁰ J. A. Cairns, D. F. Holloway, and R. S. Nelson, *Radiaion. Effects*, vol. 7, P 167, 1971.
- ²¹ P.K. Haff, and Z.E. Switkowski, *J. Appl. Phys.*, vol 48, P 3383, 1977.

- ²² P. Gavrilovic D. G. Deppe, K. Meehan, N. Holonyak, Jr., J. J. Coleman, and R. D. Burnham, *Appl. Phys. Lett.*, vol. 47, P 130, 1985.
- ²³ Mayer, Eriksson, & Davies, "Ion Implantation," Academic press, 1970.
- ²⁴ W. Freiman, R. Beserman, Yu. L. Khait, M. Shanan, K. Dettermer, F. R. Kessler, *Phys. Rev. B*, vol. 48, P 2282, 1993.
- ²⁵ M. A. Bradely, F. H. Jullien, J. P. Gilles, Y. Gao, E. V. K. Rao, M. Razeghi, F. Omnes, *Electron. Lett.*, vol. 26, P 208 1990.
- ²⁶ P.G. Piva, R. D. Goldberg, I. V. Mitchell, H. Chen, R. M. Feenstra, G. C. Weatherly, D. W. McComb, G. C. Aers, P. J. Poole, S. Charbonneau, *Appl. Phys. Lett.*, vol. 72, P 1599, 1998.
- ²⁷ H. leier, A. Forchel, G. Hörcher, J. Hommel, S. Bayer, H. Rothfritz, G. Wienmann, and W. Schlapp, *J. Appl. Phys.*, vol. 67, P 1805, 1990.
- ²⁸ J. Ralston, G. W. Wicks, L.F. Eastman, D. C. De Cooman, and C. B. Carter, *J. Appl. Phys.*, vol. 59, P 120, 1986.
- ²⁹ P. Mei, T. Venkatesan, S. A. Shwarz, N. G. Stoffel, J. P. Harbison, D. L. Hart, and L. A. Florez, *Appl. Phys., Lett.*, vol. 52, P 1487, 1988.
- ³⁰ L. B. Allard, D. C. Aers, P. G. Piva, P. J. Poole, M. Buchanan, I. M. Tempelton, T. E. Jackson, S. Charbonneau, U. Akano, and I. V. Mitchell, *J. appl. Phys.*, vol. 64, P 2412, 1994.
- ³¹ F. E. Prins, G. Lehr, E. M. Fröhlich, H. Chweizer, G. W. Smith, *J. Appl. Phys.*, vol. 73, P 2376, 1993.
- ³² T. Venkatesan, S. A. Schwartz, D. M. Hawng, R. Bhat, M. Koza, H. W. Yoon, P. Mei, Y. Arakawa, and A. yariv, *Appl. Phys. Lett.*, vol. 49, P 701, 1986.
- ³³ S. A. Schwartz, T. Venkatesan, D. M. Hawng, H. W. Yoon, R. Bhat, Y. Arakawa, *Appl. Phys. Lett.*, vol. 50, P 281, 1987.
- ³⁴ P. Mei, T. Venkatesan, S. A. Schwartz, N. G. Stoffel, J. P. Harbison, D. L. Hart, and L. A. Florez, *Appl. Phys. Lett.*, vol. 52, P 1487, 1988.
- ³⁵ K. B. Kahn, G. Rajeswaren, *J. Appl. Phys.*, vol. 66, P 545, 1989.
- ³⁶ J. Kobayashi, M. Nakajima, T. Fukunaga, T. Takamori, K. Ishida, H. Nakashima, K. Ishida, *Jap J. Appl. Phys.*, vol. 25, P 1736, 1986.
- ³⁷ Fulin Xiong, T. A. Tombrello, C. L. Schwartz, and S. A. Schwartz, *J. Appl. Phys.*, vol. 57, P 896, 1990.
- ³⁸ B. L. Weiss, I. V. Bradely, and N. J. Whitehead, and J. S. Toberts, *J. Appl. Phys.*, vol. 71, P , 1992.

- ³⁹ P. J. Hughes, B. L. Weiss, Spirit Tlali, H. E. Jackson, *J. Vac. Sci. Technol. B*, vol. 15, P 845, 1997.
- ⁴⁰ Y Hirayama, Y Suzuki, H. Okamoto, *Jpn. J. Appl. Phys.*, vol.24, P 1498, 1985.
- ⁴¹ Y. Suzuki, Y. Hirayama, H. Okamoto, *Jpn. J. Appl. Phys.*, vol. 25, P L912, 1986.
- ⁴² J. Sapiel, E. V. K. Rao, R. Brillouet, J. Chavignon, P. Ossart, Y. Gao, P. Krauz, *Superlat. & Microstruc.*, vol. 4, P 115, 1988.
- ⁴³ J. H. Marsh, S. I. Hansen, A. C. Bryce, R. M. De La Rue, *Optical & Quantum Electron.*, vol. 23, P S941, 1991.
- ⁴⁴ C. Jagadish, B. G. Svensson, and N. Hausser, *Semicond. Sci. Technol.*, vol. 8, P 481, 1993.
- ⁴⁵ B.S.Ooi, A. C. Bryce, J. H. Marsh, J. Martin, *Appl. Phys. Lett.*, vol. 65, P 85, 1994.
- ⁴⁶ J. H. Marsh, *Semicond. Sci. Technol.*, vol. 8, P 1136, 1993.
- ⁴⁷ B. S. Ooi, A. C. Bryce, J. H. Marsh, and J. S. Roberts, *Semicond. Sci. Technol.*, vol. 12, P 121, 1997.
- ⁴⁸ S. R. Andrew, J. H. Marsh, M C. Holland, and A. N. Kean, *IEEE Photon. Technol. Lett.*, vol. 4, P 426, 1992.
- ⁴⁹ J.C. Bourgoin, H.J. von Bardeleben, D. Stievenard, *J. Appl. Phys.*, vol. 64, P R65, 1988.
- ⁵⁰ K. Kash, B. Tell, P. Grabbe, E. A. Dobisz, H. G. Craighead, and M. C. Tamargo, *J. Appl. Phys.*, vol. 63, P 1444, 1991.
- ⁵¹ C. Vieu, M. Schnieder, D. Mailly, R. Planel, H. Launios, J. Y. Marzin, and B. Descouts, *J. Appl. Phys.*, vol. 70, P 1444 1991.
- ⁵² F. Laruelle, A. Bagchi, M. Tsuchiya, J. Merz, P. M. Petroff, *Appl. Phys. Lett.*, vol. 56, P 1561, 1990.
- ⁵³ D. J. Werder, S. J. Pearton, *J. Appl. Phys.*, vol. 62, P 318, 1987.
- ⁵⁴ J. Cilbert, P. M. Petroff, D. J. Werder, S. J. Pearton, A. C. Gossard, and J. H. English, *Appl. Phys. Lett.*, vol. 49, 223 1986.
- ⁵⁵ Y. Hirayama, *Jap. J. Appl. Phys.*, vol. 28, P L162, 1989.
- ⁵⁶ F. E. Prins, G. Lehr, M. Burkard, S. Y. Nikitin, H. Schweizer, and Gilbert W. Smith, *Jap. J. Appl. Phys.*, vol. 32, P 6228, 1993.
- ⁵⁷ D. Kirillov, P. Ho, G. A. Davis, *Appl. Phys. Lett.*, vol. 48, P 53, 1986.
- ⁵⁸ I. V. Bradely, W. P. Gillin, K. P. Homewood, and R. P. Webb, *J. Appl. Phys.*, vol. 73, P 1686, 1993.
- ⁵⁹ P. G. Piva, S. Charbonneau, I. V. Mitchell, R. D. Goldberg, *Appl. Phys. Lett.*, vol. 68, P 2252, 1996.

- ⁶⁰ B.S. Ooi, Y.S. Tang, A. Saher Helmy, A.C. Bryce, J.H. Marsh, M. Paquette, J. Beauvais, *J. Appl. Phys.*, Vol. 83, P 4526, 1998.
- ⁶¹ F. Ziegler, J.P. Biersack, and U. Littmark, *The stopping and Range of Ions in Solids*, (Pergamon, New York, 1985).
- ⁶² S. Salimian C. Yuen, C. Shih, C.R. Cooper *J. Vac. Sci. Technol.*, vol 9 B, P 114, 1991.
- ⁶³ D. Lootens, P. Vandaele, P. Demeester, P. Clauws, *J. Appl. Phys.*, vol. 70, P 221, 1991.
- ⁶⁴ B.S. Ooi, A.C. Bryce, and J. H. Marsh, *Electronics Lett.*, vol. 31, P 449, 1995.
- ⁶⁵ A. Saher Helmy, B.S. Ooi, and J.H. Marsh, Integrated Photonics Research-Boston, paper IMH21, P 228, 1995.
- ⁶⁶ A. Saher Helmy, N. P. Johnson, M. L. Ke, A. C. Bryce, J. S. Aitchison, J.H. Marsh, I. Gontijo, G. S. Buller, J. Davidson, P. Dawson, *IEEE J. Selected Topics in Quantum Electronics*, vol. 4, P 661, 1998
- ⁶⁷ A. Saher Helmy, "Investigation of the process of hydrogen plasma induced defect layer intermixing," University of Glasgow, M.Sc. Thesis, 1995.
- ⁶⁸ A. Saher Helmy, J. S. Aitchison, and J. H. Marsh, *Appl. Phys. Lett.*, vol. 71, P 2998, 1997.
- ⁶⁹ M. Rahman M. A. Foad, S. Hicks, M. C. Holland, and C. D. W. Wilkinson, *Mat. Res. Soc. Symp. Proc.*, vol. 279, P 775, 1993.
- ⁷⁰ J.E. Epler, R.D. Burham, R.L. Thorton, T.L. Paoli, and M.C. Bashaw, *Appl. Phys. Lett.*, Vol 49, P1447, 1986.
- ⁷¹ J. Ralston, A.L. Moretti, R.K. Jain, F.A. Chambers, *Appl. Phys. Lett.*, vol 50, P1817, 1987.
- ⁷² J. E. Epler R. D. Brunham, R. L. Thorton, T. L. Paoli, *Appl. Phys. Lett.*, vol. 50, P 1637, 1987.
- ⁷³ J. E. Epler R. L. Thorton, T. L. Paoli, *Appl. Phys. Lett.*, vol. 52, P 1371, 1988.
- ⁷⁴ J. E. Epler R. L. Thorton, W. J. Mosby, T. L. Paoli, *Appl. Phys. Lett.*, vol. 53, P 1459, 1988.
- ⁷⁵ C. J. Maclean, J. H. Marsh, R. M. De La Rue, A. C. Bryce, B. Garrett, R. W. Glew, *Electronics Lett.*, vol. 28, P 1117, 1992.
- ⁷⁶ A. Mackee, C. J. Maclean, A. C. Bryce, J. H. Marsh, *IEEE J. Quantum Electronics*, vol. 33, P 45, 1997.
- ⁷⁷ C. J. Maclean, A. McKee, J. H. Marsh, R. M. De La Rue, *Electronics Lett.*, vol. 29, P 1657, 1993.
- ⁷⁸ C. J. McLean, A. McKee, G. Lullo, A. C. Bryce, R. M. De La Rue, J. H. Marsh, *Electronics Lett.*, Vol. 31, P1285, 1995.

- ⁷⁹ S. J. Fancy, G. S. Buller, J. S. Massa, A. C. Walker, C. J. McLean, A. McKee, A. C. Bryce, J. H. Marsh, R. M. De La Rue, *J. Appl. Phys.*, vol. 79, P 9390, 1996.
- ⁸⁰ A. McKee, C. J. McLean, A. C. Bryce, R. M. De La Rue, J. H. Marsh, C. Button, *Appl. Phys. Lett.*, vol. 65, P 2263, 1994.
- ⁸¹ G. Lullo, A. McKee, C. J. McLean, A. C. Bryce, C. Button, J. H. Marsh, *Electronics Lett.*, vol. 30, P 1623, 1994.
- ⁸² T. K. Sudoh, M. Kumano, Y. Nakano, K. Tada, *IEEE Photonic. Technolo. Lett.*, vol. 9, P 887, 1997.
- ⁸³ D. G. Deppe L. J. Guido, N. Holonyak, Jr., K. C. Hsieh, R. D. Burnham, R. L. Thorton, T. L. Paoli, *Appl. Phys. Lett.*, vol. 49, P 510, 1986.
- ⁸⁴ C. J. Frosch and L. Derick, "Surface protection and selective masking during diffusion in Silicon," *J. Electrochem. Soc.*, vol. 104, P 547, 1957.
- ⁸⁵ J. Gyulai, J. W. Mayer, I. V. Mitchell, and V. Rodriguez, "Outdiffusion through silicon dioxide and silicon nitride layers on GaAs," *Appl. Phys. Lett.*, vol. 17, P 332, 1970.
- ⁸⁶ B. Molnar, *J. Electrochem. Soc.*, vol. 123, P 767, 1976.
- ⁸⁷ K. V. Vaidyaathan, M. J. Helix, D. J. Wolford, B. G. Streetman, R. J. Battner, and C. A. Evans Jr., *J. Electrochem. Soc.*, vol. 124, P 1781, 1977.
- ⁸⁸ S. Wagner, and E. I. Povilonis, *J. Electrochem. Soc.*, vol. 121, P 1488, 1974.
- ⁸⁹ J. D. Ralston, S. O'Brien, G. W. Wicks, L. F. Eastman, *Appl. Phys. Lett.*, vol. 52, P 1511 1988.
- ⁹⁰ X. Wen, J. Y. Chi, E. S. Koteles, B. Elman, P. Melman, *J. Electron. Mat.*, vol. 19, P 539, 1990.
- ⁹¹ S. J. Lycett, A. J. Dewdney, M. Ghisoni, C. E. Norman, R. Murray, D. Sansom, J. S. Roberts, *J. Electron. Mat.*, vol. 24, P 197, 1995.
- ⁹² S. Bürkner, M. Maier, E. C. Larkns, W. Rothemund, E. P. O'Rielly, J. D. Ralston, *J. Electron. Mat.*, vol. 24, P 805, 1995.
- ⁹³ I. Gontijo, T. Krauss, J.H. Marsh, and R. M. De La Rue, *IEEE J. Quantum Electron.*, vol 30, P S779, 1994.
- ⁹⁴ M Katayama, Y. Tokuda, N. Ando, Y. Inoue, A. Usami, T. Wada, *Appl. Phys. Lett.*, vol. 54, P 2559, 1989.
- ⁹⁵ F. Hasegawa, N. Yamamoto, Y. Nannichi, *Appl. Phys. Lett.*, vol. 45, P 461, 1984.
- ⁹⁶ W.J. Choi, J.I. Lee, I.K. Han, K.N. Kan, Y. Kim, H.L. Park, and K. Cho, *J. Mat. Sci. Lett.*, vol 13, P 326, 1994.
- ⁹⁷ W.J. Choi, S.K. Lee, J. Zhang, Y. Kim, S.K. Kim, J. I. Lee, K.N. Kang, and K. Cho, *Jpn. J. Appl. Phys.*, vol 34, P L418, 1995.

- ⁹⁸ W.J. Choi, S.K. Lee, Y. Kim, S.K. Kim, J. I. Lee, K.N. Kang, N. Park, H.L. Park, and K. Cho, *J. Mat. Sci. Lett.*, vol 14, P 1433, 1995.
- ⁹⁹ M.Kuzuhara et al., *J. Appl. Phys.*, Vol. 66, P 5833, 1989.
- ¹⁰⁰ A. Pepin, C. Vieu, M. Schnieder, G. Ben Assayag, R. Planel, J. Bloch, H. Launois, J. Y. Marzin, Y. Nissim, *Superlattices & Microstructures*, vol. 18, P 229, 1995.
- ¹⁰¹ Y. Suzuki, H. Iwamura, O. Mikami, *Appl. Phys. Lett.*, vol. 56, P19, 1990.
- ¹⁰² A. Kan'an, P. LiKamWa, Mitra-Dutta, J. Pamulapati, *J. Appl. Phys.*, vol. 80, P 3179, 1996.
- ¹⁰³ J. Beauvais, J.H. Marsh, A. H. Kean, A. C. Bryce, C. Button, *Electronics, Lett.*, vol. 28, P 670, 1992.
- ¹⁰⁴ S.G. Ayling, J. Beauvais, and J.H. Marsh, *Electron. Lett.*, vol 28, P 2240, 1992.
- ¹⁰⁵ T.Y. Tan, and U. Gosele, *Appl. Phys. Lett.*, vol 52, P 1383, 1988.
- ¹⁰⁶ B.S. Ooi, N.W. Street, S.G. Ayling, A.C. Bryce, J.H. Marsh, and J.S. Roberts, *Int. J. of Optoelect.*, vol 10, P 257, 1995.
- ¹⁰⁷ I. Gontijo, T. Krauss, R.M. De La Rue, J.S. Roberts, and J.H. Marsh, *Electron. Lett.*, vol 30, P 145, 1994.
- ¹⁰⁸ Shinya Sudo, Hirofumi Onish, Yoshiaki Nakano, Yukihiro Shimogaki, Kunio Tada, Mark J. Mondry, and Larry A. Coldern, *Jpn., J. Appl. Phys.*, vol 35, P 1276, 1996.
- ¹⁰⁹ E.V.K. Rao, A. Hamoudi, Ph. Krauz, M. Juhel, and H. Thibierge, *Appl. Phys. Lett.*, vol 66, P 472, 1995.
- ¹¹⁰ P. Cusumano, A. Saher Helmy, B. S. Ooi, S. G. Ayling, A. C. Bryce, J. H. Marsh, B. Voegelé, and M. J. Rose, *Mat. Res. Soc. Symp. Proc.*, vol. 450 , P 419, 1996.
- ¹¹¹ P. Cusumano, B. S. Ooi, A. Saher Helmy, S. G. Ayling, A. C. Bryce, J. H. Marsh, B. Voegelé, and M. J. Rose, *J. Appl. Phys.*, vol. 81, P 2445, 1997.
- ¹¹² A.C. Bryce, F. Camacho, E.A. Avrutin, and J.H. Marsh, *IEEE J. Quantum Electron.*, vol. 33, P 1784, 1997.
- ¹¹³ A. Saher Helmy, S. K. Murad, A. C. Bryce, J. S. Aitchison, J. H. Marsh, S. K Hicks, C. D. W Wilkinson, *Appl. Phys. Lett.*, Accepted.
- ¹¹⁴ C. J. Hamilton, J. H. Marsh, D. C. Hutchings, J. S. Aitchison, G. T. Kennedy, W. Sibbett, *Appl. Phys. Lett.*, vol. 68, P 3078, 1996.
- ¹¹⁵ M. W. Street, N. D. Whitbread, D. C. Hutchings, J. M. Arnold, J. H. Marsh J. S. Aitchison, G.T. Kennedy, and W. Sibbett, *Opt. Lett.*, vol.22, P 1600, 1997.
- ¹¹⁶ Y. Kim, S. Yuan, R. Leon, C. Jagadish, M. Gal, M. B. Johnston, M. R. Phillips, M. A. Stevens Kalceff, J. Zou, D. J. H. Cockayne, *J. Appl. Phys.*, vol 34, P 5014, 1996.

- ¹¹⁷ S. Yuan, Y. Kim, C. Jagadish, P. T. Burke, M. Gal, J. Zou, D. Q. Cai, D. J. H. Cockayne, R. M. Cohen, *Appl. Phys. Lett.*, vol. 70, P 1269, 1997.
- ¹¹⁸ S. Yuan, Y. Kim, H. H. Tan, C. Jagadish, P. T. Burke, L. V. Dao, M. Gal, M. C. Y. Chan, E. H. Li, J. Zou, D. Q. Cai, D. J. H. Cockayne, R. M. Cohen *J. Appl. Phys.*, vol. 83, P 1305, 1998.
- ¹¹⁹ M. Kaminska, E.R. Weber, Z. Liliental-weber, and Leon, and Z.U. Rek, *J. Vac. Sci. Technol.*, vol B7, P 710, 1989.
- ¹²⁰ Jian-Shih Tsang, Chien-Ping Lee, Jenn-Chyuan Fan, Shing-Horng Lee, and Kaung-Lung Tsai, *Jpn. J. Appl. Phys.*, vol 34, P 1089, 1995.
- ¹²¹ J.S. Tsang, C.P. Lee, S.L. Lee, K.L. Tsai, C.M. Tsai, and J.C. Fan, *J. Appl. Phys.*, vol 79, P 664, 1996.
- ¹²² J. Gray, A. Saher Helmy, A. C. Bryce, and J. H. Marsh, Unpublished results.
- ¹²³ O. P. Kowalski, C. J. Hamilton, S. D. McDougall, J. H. Marsh, A. C. Bryce, C. C. Button, J. S. Roberts, *Appl. Phys. Lett.*, vol. 72, P 581, 1998.
- ¹²⁴ J. H. Marsh, O. P. Kowalski, S. D. McDougall, B. C. Qiu, A. McKee, C. J. Hamilton, R. M. De La Rue, A. C. Bryce, *J. Vac Sci. Tecnolo. B*, vol. 16, P 810, 1998.
- ¹²⁵ S. D. McDougall, O. P. Kowalski, B. C. Qiu, A. McKee, C. J. Hamilton, J. H. Marsh, R. M. De La Rue, A. C. Bryce, *IEEE J. Selected Topics in Quantum Electronics*, vol. 4, P 661, 1998.

QUANTIFYING INTERMIXING KINETICS

Although the exact mechanisms are not completely understood, it is agreed that compositional intermixing in III-V semiconductors takes place through the diffusion of the native point defects of the lattice. Therefore, modelling the intermixing behaviour will depend substantially on understanding the kinetics of the motion of point defects. At equilibrium the distribution of these defects will be governed by the means that generated them, and hence their characterisation is relatively simple. However, non-equilibrium situations are far from trivial to represent. This is partially because experiments are highly sensitive to every parameter in the surrounding ambient of the sample. Therefore proper experiments need excessive degrees of control on the experiments' environment.

I. MOTIVATION

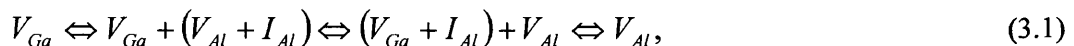
The deployment of quantum well intermixing (QWI) as a replacement for regrowth and overgrowth processes, which are used in realising optoelectronic and photonic integrated circuits (OEICs and PICs) has been steadily increasing ever since it was first reported in 1981.¹ However, most work to date towards characterising the phenomenon has been primarily technological. No comprehensive explanations of the mechanisms involved were presented until 1988,² when a quasi-equilibrium Fermi level model was developed to describe the intermixing of GaAs/AlGaAs heterostructures. Although limited modelling work has followed, it is mostly either incomplete or has only described trends rather than relating the underlying physics to experimental measurements.^{3,4,5,6,7} One decade later, the effects of factors such as the Fermi level effect, the As overpressure, as well as the other experimental parameters were unveiled using basic physical relationships such as the Gibbs phase rule.⁸

A comprehensive qualitative model would permit further process optimisation. Such a model would not only result in improved control of existing processes such as Impurity Free Vacancy Disordering (IFVD) in GaAs based semiconductors, but is also necessary for extending the technology to more complicated semiconductor systems, such as IFVD in InP based semiconductors.

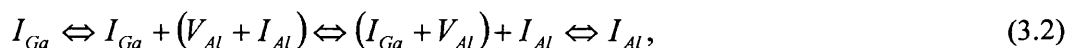
In this chapter we develop such a model, and start by highlighting the physical assumptions underlying the model. The process of hydrogen plasma induced defect layer intermixing (PIDLI) will then be briefly explained. The model is then used to calculate the amount of intermixing expected from the defect profile introduced by the PIDLI process, and compared with the amount of intermixing actually measured. Similar calculations and comparisons are also made for the process of IFVD. A discussion and evaluation of the developed model are then presented, followed by a summary.

II. INTERMIXING MECHANISMS

Compositional intermixing,⁹ and hence Al and Ga interdiffusion, in GaAs/AlGaAs heterostructures is either carried out directly through diffusion of group III vacancies, V_{III} , as described by the equation,



or is assisted by the formation of group III Frenkel defect pairs, through diffusion of group III interstitials, I_{III} ,²



Therefore, the interdiffusion coefficient of group III sublattice atoms through the heterostructure is dependent on the diffusion coefficient, as well as the concentration, of both group III point defects. Each defect is created with a certain activation energy, which primarily depends on the Fermi level of the semiconductor, the As surface concentration, the ambient temperature, and the scheme by which it was created.⁸

Group III point defects and Frenkel defect pairs can be introduced by various schemes. Impurity induced disordering, IID,¹ uses the dependence of the equilibrium defect concentration on the Fermi level in the semiconductor to increase the number of group III defects. IID, however, introduces excessive free carrier absorption.¹⁰ Implantation defect induced disordering,¹¹ PIDLI,¹² and pulsed photoabsorption induced disordering (P-PAID),¹³ utilise point defects and Frenkel defect pairs introduced due to the interaction between the semiconductor lattice atoms and implanted ions, plasma ions, and photons respectively, to enhance Ga/Al interdiffusion. Limitations then arise due to the other types of defects introduced by such processes. Line defects and dislocation loops are examples of defect types, which are not annealed out at elevated temperatures, and can even act as sinks for point defects.¹⁴ On the other hand, IFVD uses the group III vacancies introduced due to Ga out-diffusion into dielectric caps at elevated temperatures to assist Ga/Al interdiffusion.¹⁵ IFVD has been utilised extensively to fabricate OEICs and PICs, due to its simplicity and the resulting low optical losses.^{10,16} A given defect profile introduced by any of the aforementioned means will diffuse within the lattice when being thermally processed. Since we are interested in the kinetics of the interactions between point defects and lattice atoms, investigating the statistical behaviour of the point defect diffusion will reveal the underlying physical mechanisms more comprehensively.

III. ELEMENTS OF THE MODEL

Because QWI is carried out primarily at elevated temperatures through diffusion of native point defects in the semiconductor, the model starts by studying such diffusion in the lattice. The statistical nature of the behaviour of an arbitrary defect profile at elevated temperatures is modelled, and hence its contribution to the Al/Ga interdiffusion in GaAs/AlGaAs heterostructures is quantified. The approach shows promising agreement when compared with experimental results.^{17,18} In principle, similar calculations can be performed for any intermixing technique for the GaAs/AlGaAs system.

The diffusion coefficient on a given sublattice can be expressed as,¹⁹

$$D_{vac} = \frac{f \cdot w_v}{2} \left(\frac{a_o}{2} \right)^2, \quad (3.3)$$

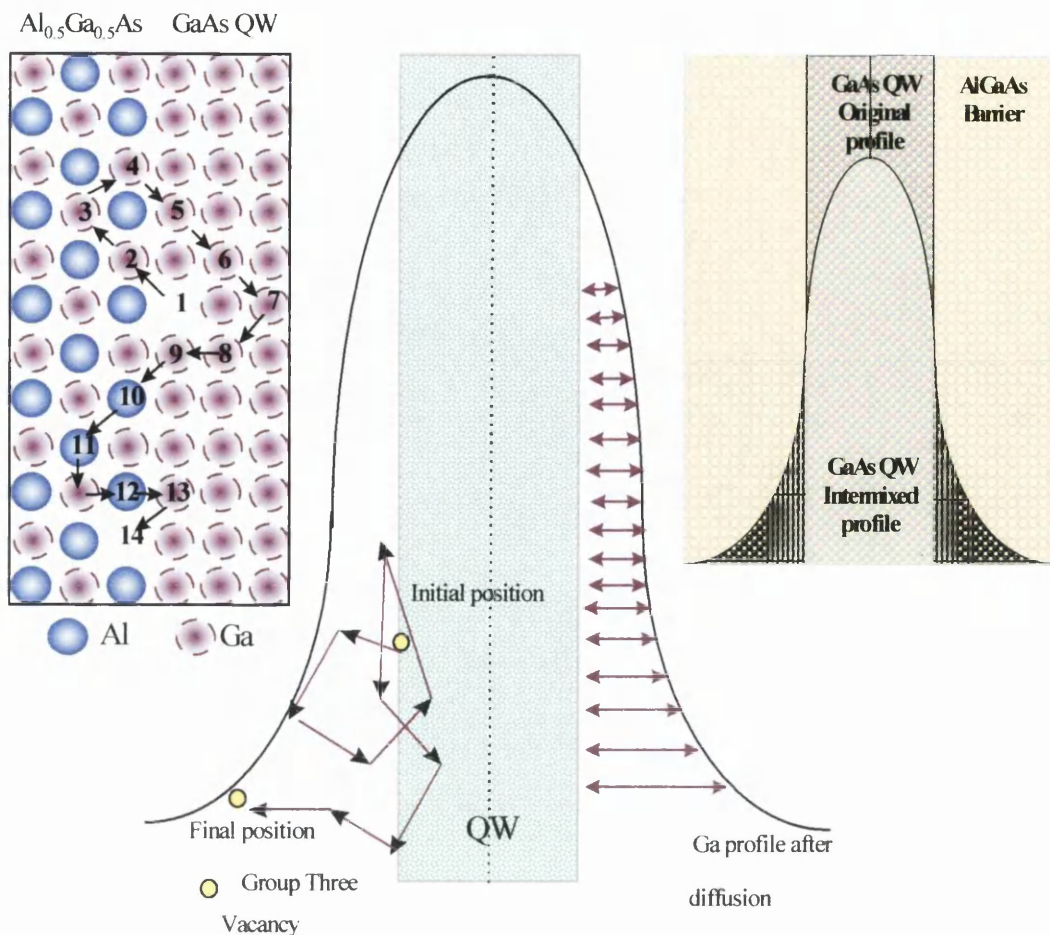


Fig. 3.1 Schematic diagram of the lattice hops comprised in Ga out-diffusion from the quantum wells, and the quantum well interface crossings carried out by group three vacancies during the random walks associated with their diffusion.

where w_v is the effective defect hop frequency, a_o is the lattice constant of GaAs, and $a_o/2$ is the hop length between group III lattice planes, given that the group III point defects will primarily diffuse on the group III sublattice. We consider here that hops between lattice planes are those responsible for interdiffusion across the QW/barrier interface. The factor f is the reciprocal of the number of directions of the nearest neighbouring sites to which the vacancy can hop. For three-dimensional diffusion in the crystal, f is equal to $1/3$. This picture suggests that, within the regions where $[V_{III}] \gg [I_{III}]$, diffusion is determined primarily by vacancies. It should also be noted that the background equilibrium concentration of V_{III} ought to be taken into consideration if it was found to have a significant effect on the amount of intermixing induced. However, the reported V_{III} background equilibrium concentration in undoped QWs is equal to $1.25 \times 10^{31} \exp[-3.28/k_B T] \text{ cm}^{-3}$,³ and will have no significant effect on the amount of induced intermixing at annealing temperatures below 1000 °C, as will be shown in this chapter.

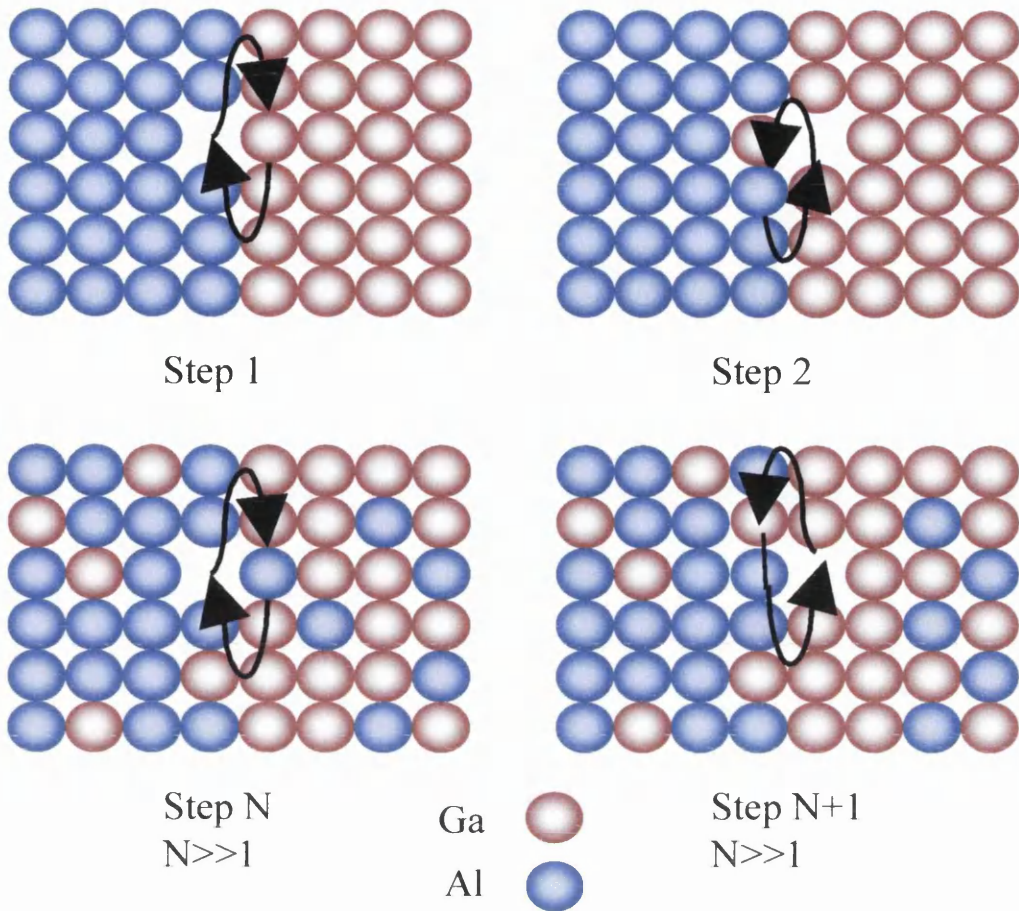


Fig. 3.2 Schematic of the group III GaAs/AlAs sublattice showing the different steps of vacancy diffusion across the QW/barrier interface. early stage of a AlAs/GaAs heterostructure, and after a long diffusion time, where there is a finite amount intermixing on the group III sublattice.

At the early stages of diffusion (step 1&2), all the vacancy interface crossings, N_{QW} , will result in Ga, Al interdiffusion from the QW, barrier respectively. However after some time (step N&N+1), the probability that a Ga atom diffuses out of the well, when a V_{III} moves in is finite, and is equal to C_{Ga}^{QW} / C_o . Similarly the probability that an Al atom diffuses into the well, when a V_{III} moves out is finite, and is equal to $C_{Al}^{barrier} / C_o$. That is why the total number of lattice hops result in interdiffusion should have a factor to account for the initial and time induced change in the Ga/Al concentration in the QW/barrier respectively. The coefficient should be the product of the probabilities that the transported across the interface is the one required (i.e. Ga out of the QW, and Al into the QW).

Prior to annealing, GaAs/AlGaAs heterostructures have an abrupt change in the Ga concentration at the QW interface. In the presence of a given concentration of group III defects, at elevated temperatures Ga/Al interdiffusion will take place across the interface, giving rise to an error function-like profile. Assuming a GaAs/AlAs heterostructure, the Ga profile at one interface can thus be expressed as,⁵

$$C_{QW} = \frac{C_o}{2} \operatorname{erfc} \left[\frac{z - L_z/2}{2\sqrt{D_{QW}t}} \right], \quad (3.4)$$

where C_{QW} and D_{QW} are the concentration and the diffusion coefficient of Ga atoms out-diffused from the quantum well respectively, C_o is their initial concentration in the wells, L_z is the quantum well thickness, and z is the spatial depth parameter. The movement of Ga atoms takes place through vacancy diffusion, therefore the profile of the diffused Ga arises from a certain number of discrete lattice hops. It should be noted that the diffusion profile of the QW is taken in this case as an *erfc* as opposed to a Gaussian, because the diffusion lengths studied in QWI do not exceed a few nanometers, which is much less than the well width, and hence presenting the Ga concentration of the QW as a delta function is not a valid approximation in our case. The number of lattice hops can be obtained by integrating the spatial parameter over all the Ga concentration outside of the well boundary, and normalising it with respect to the lattice hop length, as shown in Fig. 3.1. The number of lattice hops required to achieve a given diffusion profile is calculated from,

$$N_{QW} = \frac{k}{a_o/2} \int_0^{C_{QW}(L_z/2)} z(C_{QW}) d(C_{QW}), \quad (3.5)$$

$$z(C_{QW}) = 2\sqrt{D_{QW}t} \operatorname{erfc}^{-1} \left[\frac{2C_{QW}}{C_o} \right], \quad (3.6)$$

where $C_{QW}(L_z/2)$ is the concentration of Ga at the edge of the well and k is a constant. The purpose of the constant k will be discussed below. This means that if we are able to predict a number of lattice hops generated by the diffusion of a given V_{III} profile, then by substituting this value as N_{QW} and solving equation (3.5), one can obtain an associated value of D_{QW} for a given V_{III} concentration. Because we study a single heterostructure interface to calculate the number of lattice hops, the diffusion profile is an *erfc*, whereas for a QW (or a double QW) the diffusion profile is a superposition of the *erfc* profiles at every interface (see also chapter 1).^{20,21}

The expression for N_{QW} above was found, however, for a GaAs/AlAs interface, under the assumption that the Ga concentration in the barrier always remain sufficiently small that every Ga atom out-diffusing from the well is replaced by an Al atom from the barrier. When the barrier Al concentration is not ~100%, the fluxes of Ga and Al will change by a factor depending on their concentrations in the atomic layers on either side of the QW/barrier interface. Therefore, a factor k is introduced in equation (3.6) to account for the fact that the Al concentration in the barrier will not generally be 100%; (k is equal to unity in case of a GaAs/AlAs heterostructure). It must also be a time dependent coefficient to account for the

changes in Ga and Al concentrations at the interface as intermixing takes place. As explained in Fig. 3.2, the factor k is equal to $1/(x_{Al}^{barrier}(t)x_{Ga}^{well}(t))$, where $x_{Ga}^{well}(t)$ and $x_{Al}^{barrier}(t)$ are the time dependent Ga and Al concentrations in the atomic layers on either side of the QW/barrier interface normalised by C_o , the concentration of group III atoms in the lattice. When the factor k is added to equation (3.5) the expression then represents the actual number of lattice hops, by taking into account the finite probability of an Al atom diffusing from the barrier to the quantum well, and of it being replaced by a Ga atom out-diffusing from the QW to the barrier. Using the *erfc* approximation, for an AlAs/GaAs at $t=0$ we find that $k=1$, while when t tends to infinity, k is equal to 4, which is the reciprocal of the product of the normalised Al and Ga concentrations at infinite time, 0.5×0.5 . For an $Al_{0.2}Ga_{0.8}As/GaAs$ at $t=0$ we find that $k=5$, which is the reciprocal of the product of the initial normalised Al and Ga concentrations in the barrier and QW respectively, 0.2×1 . When t tends to infinity, k is equal to 11, which is the reciprocal of the product of the normalised Al and Ga concentrations in the barrier and QW respectively at infinite time, 0.1×0.9 .

After calculating the number of lattice hops we substitute for N_{QW} in equation (3.5) and solve to give the corresponding D_{QW} . The PL shift resulting from this diffusion coefficient calculated can then be obtained and compared with the experimental one. PL shifts corresponding to a given diffusion length are calculated by solving the Ga diffusion equation in a QW in conjunction with the Schrödinger wave equation to obtain the confined energy levels for a given diffusion length.²⁰ The Ga diffusion is assumed to follow Fick's law resulting in a diffusion profile represented by double *erfc*. To calculate the number of lattice hops induced by a given vacancy concentration, we therefore need to study the effect of V_{III} on a heterostructure interface during annealing.

At the interface of a heterostructure, each time a V_{III} crosses the plane into the quantum wells, a Ga atom moves one lattice site, in the opposite direction, out of the well into the barrier. A subsequent un-correlated interface crossing of a V_{III} in the opposite direction is needed to transport an Al atom one lattice site towards the well, as illustrated in equation (3.1). Therefore on average, for each two crossings of the barrier/QW interface carried out by V_{III} , one Al atom can move one lattice hop towards the interface eventually replacing the out-diffused Ga atom. In the calculations reported here, we assume $[V_{III}]$ is the same at both interfaces of a particular QW.

The total number of barrier/QW interface crossings undertaken by the atoms, N_{IC} , will therefore correspond to the total number of lattice site-hops available for the Al/Ga interdiffusion, which can be calculated for a time span t by,

$$N_{IC} = \int_0^t \frac{w_v}{2} \cdot N_v(d_{QW}, t) dt, \quad (3.7)$$

where $N_v(d_{QW}, t)$ is the time dependent V_{III} concentration at one of the QW interfaces. For a given vacancy concentration $N_v(d_{QW}, t)$ generated by any means, the model predicts N_{IC} lattice hops are available for group III interdiffusion across that interface. The value of N_{IC} calculated from the model above must therefore be the same as N_{QW} in equation (3.5), and hence the corresponding values of D_{QW} and $L_{D_{QW}}^2$ for a given vacancy profile, $N_v(d_{QW}, t)$, can be calculated, from which the predicted PL shift is obtained.²⁰

In the rest of the chapter the validity of the model is demonstrated through the agreement between the calculated and measured PL shifts calculated from the diffusion coefficient as discussed above.

IV. MODELLING THE KINETICS OF DIFFERENT INTERMIXING PROCESSES

The model presented above does not put any restrictions on the means by which the defects are introduced, which makes it suitable for modelling intermixing of the whole range of intermixing processes available. However, the model requires knowledge of the kinetics of introducing the defects in the lattice, which might not be readily available for every intermixing technology. Before comparing the model predictions with experiment, it should be noted that, although the model is process independent in the means by which it treats the defects, care should be taken in determining the defects that contribute to the interdiffusion for a given process. As an example, implantation defect induced disordering and PIDLI produce primarily Frenkel defect pairs, some of which may then recombine through interaction with neighbouring interstitial-vacancy pairs. However, in the steady state, the remaining defects would be distributed with a sufficient separation from one another to minimise recombination. For IFVD, on the other hand, the primary type of defect introduced is the Schottky defect, namely V_{III} or V_V , hence $I_{III}-V_{III}$ recombination plays a minor role. Such considerations are of paramount significance when attempting to quantify defect profiles resulting from experimental processes.

IV.A. Kinetics of Plasma Induced Defect Layer Intermixing

PIDLI is based on multiple cycles of exposing heterostructure samples to hydrogen plasma in an RIE machine, followed by thermal processing in a rapid thermal annealer (RTA). As discussed in Chapter 2, bandgap shifts in excess of 40 meV have been achieved with such a process in 8 cycles.¹² RIE damage has adverse effects on many devices, and in

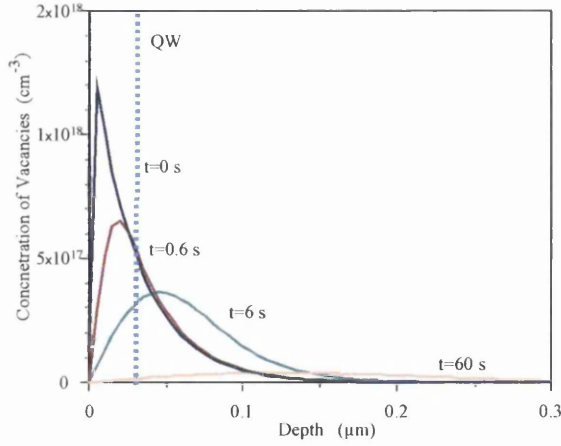


Fig. 3.3 Group three vacancy concentration in the GaAs/AlGaAs single quantum well structure for different annealing time spans for the PIDLI process. The surface recombination velocity of group three vacancies used in the calculations is 0.1 cm.s^{-1} .

particular MESFETS where it was discovered that it caused a reduction of the transconductance when gate recess etching had been carried out using RIE.²² Irradiation damage is caused by the hydrogen ions in the plasma impinging on the semiconductor surface during the plasma exposure. Energy is therefore transferred to the lattice, introducing point defects,²³ mainly interstitials resulting from the incident ions and neutrons, or lattice atoms knocked off due to the momentum transfer. There can also be vacancies resulting from the knocked off atoms, the vacancies being created where the knock off has occurred.

The defect profile produced by a RIE process similar to PIDLI, based on a H_2/CH_4 plasma, has previously been studied and characterised.²⁴ Phenomenological expressions for the defect profile have been obtained. The distribution function of the defects can be written as,

$$N(z, v(t - t_o)) = \frac{\lambda g_o}{v} \exp[-(z - v(t - t_o)) / \lambda] [1 - \exp[-v(t - t_o) / \lambda]], \quad (3.8)$$

where z is the distance from the surface of the semiconductor, v is the etch rate in nm.s^{-1} , t is the plasma exposure time, g_o with dimensions of $\text{cm}^{-3}.\text{s}^{-1}$ is a parameter related to the number of bombarding ions, and λ with dimensions of nm is dependent on the ion energy. The term vt_o is to account of any etching of the sample surface during the plasma exposure when describing the damage as a function of depth from the surface. In the referenced work, the defects studied were deep level traps, quantified through quantum wire conduction measurements. The concentration of group III defects is expected to have the same functional dependence as that of the deep level defects, since both are created by hydrogen ion bombardment.¹⁷ Therefore equation (3.8) was assumed to give the initial vacancy profile in our calculations. By integrating (3.8) and substituting the numerical values of the parameters

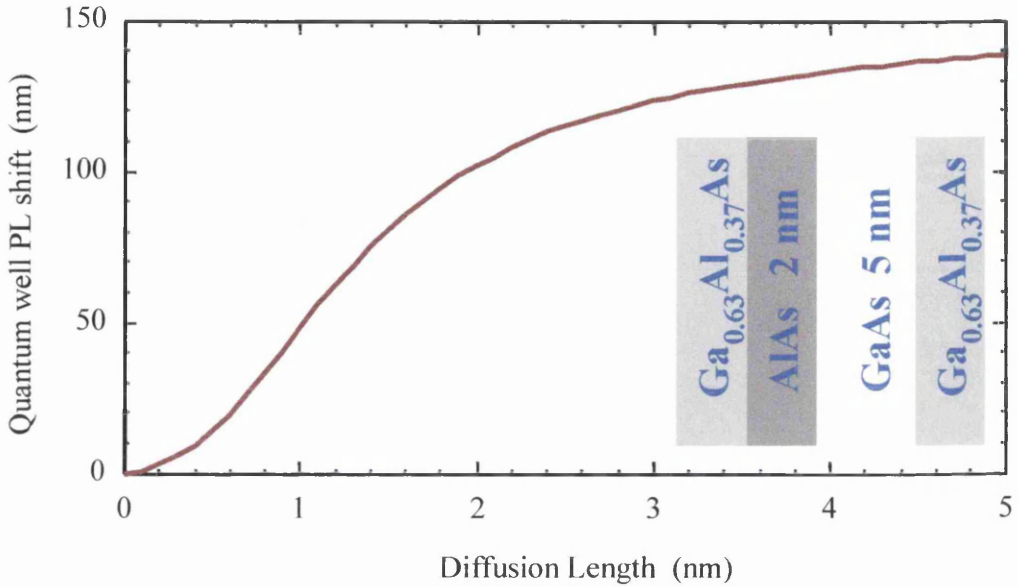


Fig. 3.4 Plot for the PL shift versus the corresponding diffusion length for an asymmetric quantum well. The inset shows the QW composition.

quoted for the H_2/CH_4 RIE process with the exposure time of the PIDLI process, which is 40 s, the sheet density of induced defects is,²⁵

$$C_{defects}(z,t) = \int_z^{\infty} N(z,v(t-t_o)) dz, \quad (3.9)$$

where the values of the phenomenological expression reported by Rahman *et al.*²⁵ were used, where g_o is $6 \times 10^{16} \text{ cm}^{-3} \cdot \text{s}^{-1}$, t is 40 s, λ is 30 nm, and v is $15 \text{ nm} \cdot \text{s}^{-1}$. After evaluating the above integral, and substituting with the constant's values, the sheet density of the defect profile introduced was found to be,¹⁷

$$C_{defects}(z,40) = 5.6 \times 10^{12} \exp\left[-z/3 \times 10^{-6}\right] \text{ cm}^{-2}. \quad (3.10)$$

Vacancies and interstitials will be created in almost equal numbers during plasma exposure. Although a fraction of these will recombine instantaneously, the diffusion coefficient of interstitials is sufficiently large, even at room temperature,⁴ to allow some of them to diffuse into the bulk of the sample, leaving behind a vacancy profile given by (3.9). It should be noted that diffusion of interstitials alone does not necessarily lead to significant intermixing, as can be seen in equation (3.2). At elevated temperatures, the vacancies' behaviour will be primarily governed by their diffusion into the bulk of the semiconductor and by their annihilation at the semiconductor surface. Because of the large concentration gradient immediately below the surface, the preferential direction of diffusion, dictated by the derivative of the concentration gradient, will be towards the surface rather than towards the substrate. The concept of recombination of carriers at the surface with a certain recombination velocity has been adopted, in the model, to describe the annihilation of

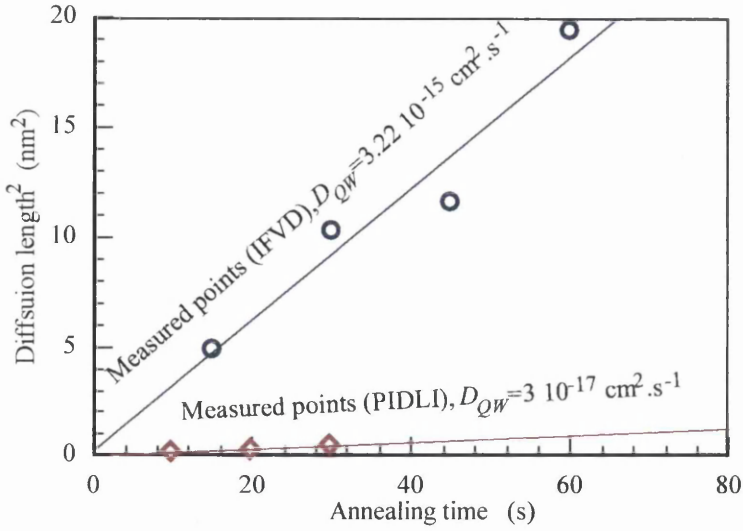


Fig .3.5 Plot for the square of the diffusion length and the anneal time for the both the PIDLI (red points) and IFVD (blue points) processes. The lines are linear fit of the experimental data represented by the points. The slope of the lines passing through the measured points is approximately constant giving a value of D_{QW} equal to $3 \times 10^{-17} \text{ cm}^2 \cdot \text{s}^{-1}$ for the PIDLI process, and equal to $3.22 \times 10^{-15} \text{ cm}^2 \cdot \text{s}^{-1}$ for the IFVD process.

vacancies at the surface of the semiconductor exposed to the hydrogen plasma in the PIDLI. Assuming the surface of the semiconductor is at an arbitrary position l , where vacancies have a surface release velocity v_{PIDLI} , the diffusion equation governing the behaviour of the vacancies and the appropriate boundary conditions, can be expressed as,

$$D_{vac} \frac{\partial^2 C_{vac}}{\partial z^2} = \frac{\partial C_{vac}}{\partial t}, \quad (3.11)$$

$$@ t = \infty \rightarrow C_{vac} = 0,$$

$$@ t = 0 \rightarrow C_{vac} = C_{defecis}(l - z, 40), \quad (3.12)$$

$$@ z = l \rightarrow v_{PIDLI} C_{vac} = D_{vac} \frac{\partial C_{vac}}{\partial z},$$

Solutions for such a boundary value problem are obtained according to Sturm-Liouville theory.²⁶ In this approach, the time varying concentration profiles are expanded as a series of orthogonal functions. We chose to define the initial problem in way that results in odd symmetry, which allows us to use one set of orthogonal functions, namely odd trigonometric functions, to describe the behaviour. This therefore simplifies the boundary-condition equations. The concentration can be written described by,

$$N_v(z, t) = \sum_{n=1}^{\infty} k_n \cdot \sin[\lambda_n z] \exp[-\lambda_n^2 D_{vac} t], \quad (3.13)$$

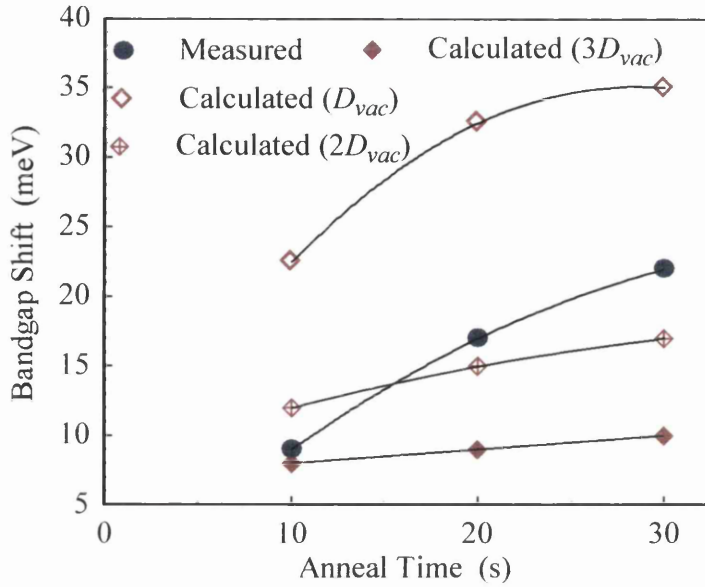


Fig. 3.6 Measured and calculated PL shifts resulting from the PIDLI process in a shallow single quantum well for different values of D_{vac} .

$$k_n = \frac{\langle C_{defects}(z, 40) \sin[\lambda_n z] \rangle}{\langle \sin[\lambda_n z] \sin[\lambda_n z] \rangle}, \quad (3.14)$$

$$\lambda_n \Rightarrow n^{\text{th}} \text{ root of: } \tan[l \cdot \lambda_n] = \frac{-\lambda_n \cdot D_{vac}}{v}, \quad (3.15)$$

The diffusion profile of $N_v(z, t)$ is shown in Fig. 3.3. The predicted number of lattice hops contributing to intermixing, N_{IC} , can then be calculated from equation (3.13) using the reported process parameters.²⁴

To obtain the actual number of lattice hops, N_{Ga} , an experiment has been carried out to measure the diffusion coefficient of Ga out-diffusing into the barriers. This diffusion coefficient can then be used to calculate N_{Ga} from equation (3.5). The wafer used was grown on a n-type GaAs substrate with a shallow quantum well placed at a depth of 30 nm. Starting from the substrate, an un-doped GaAs buffer layer of 100 nm was grown followed by 500 nm of n-type $\text{Ga}_{0.63}\text{Al}_{0.37}\text{As}$ doped to $7 \times 10^{16} \text{ cm}^{-3}$. The QW, 5 nm of un-doped GaAs was then grown followed by 2 nm of AlAs, and 20 nm of p-type $\text{Ga}_{0.63}\text{Al}_{0.37}\text{As}$ doped to $7 \times 10^{16} \text{ cm}^{-3}$, and a 10 nm GaAs p^+ cap. Samples with 3 mm \times 3 mm area were then exposed to a single cycle of the plasma and annealed for different time spans, namely 10, 20 and 30 s. The PL spectra of the samples were then measured, from which the diffusion length was obtained by solving Al/Ga diffusion equations in conjunction with the Schrödinger wave equation for the QW.²⁰ In Fig. 3.4 the PL shift vs. the diffusion length obtained from the calculations is plotted. Upon plotting the square of the diffusion length against time, as shown in Fig. 3.5,

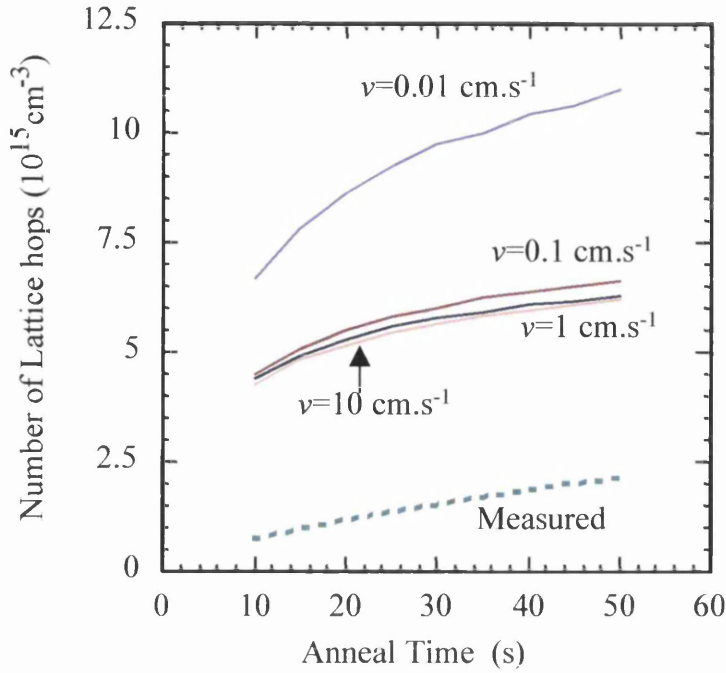


Fig. 3.7 Measured and calculated PL shifts resulting from the PIDLI process in a shallow single quantum well for different values of D_{vac} .

the relation was found to be linear. This produces a time invariant Ga diffusion coefficient, for the range of anneal time spans and parameters of the process used. The slope of the line is directly proportional to the diffusion coefficient, $L_{D_{Ga}}^2 = D_{Ga}t$, hence the Ga diffusion coefficient was found to be $3 \times 10^{-17} \text{ cm}^2\text{s}^{-1}$. Using the reported value for D_{vac} , which is $0.96 \exp[-2.72/k_B T] \text{ cm}^2\text{s}^{-1}$, the value of w_v can be obtained from (3.3). It was found to be $2.8 \times 10^3 \text{ hop.s}^{-1}$.³ Because $N_v(d_{QW}, t)$ is now known, N_{IC} and the associated PL shifts calculated from the model can be compared to those measured. The plot of the measured and predicted PL shifts is shown in Fig 3.6.

During diffusion, vacancies are expected to be annihilated at the free surface of the semiconductor, *i.e.* the probability of a vacancy being reflected is almost negligible. The expected vacancy surface release velocity v is, therefore, effectively infinity. The saturation effect of the surface recombination velocity on N_{IC} is seen in the model for values of v larger than $1 \times 10^{-4} \text{ cm.s}^{-1}$.¹⁷ It was found that the PL shifts predicted by the model for the PIDLI process have an order of magnitude agreement with experiment carried out at 875 °C, for surface recombination velocities larger than $1 \times 10^{-4} \text{ cm.s}^{-1}$ as can be seen in Fig. 3.7. In other words, the PL shifts predicted by the model agree best when v tends to infinity, which was expected for the condition of the semiconductor surface after plasma exposure in the PIDLI process. However, if the value of D_{vac} is increased, better agreement between the calculated and measured values is achieved, as can also be seen in Fig. 3.6. When D_{vac} increases, the resulting intermixing decreases because $[V_{III}]$ exists in the vicinity of the QW for shorter time

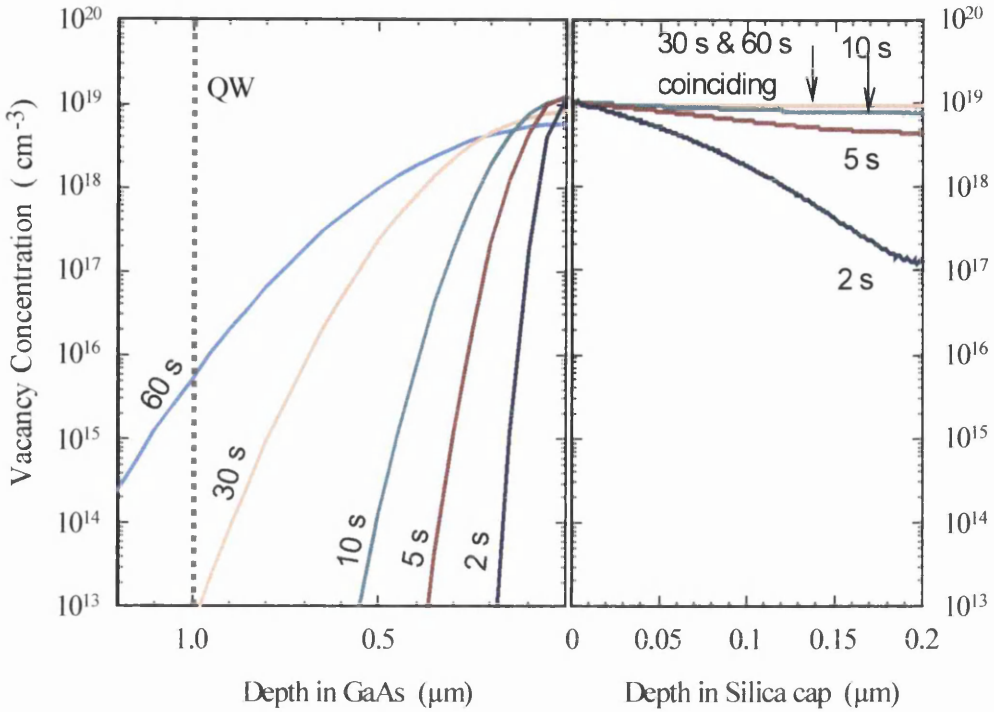


Fig. 3.8 Plot for the Ga profile in a 200 nm SiO₂ film, and the resulting group III vacancy profile in the semiconductor for different annealing times at 950 °C.

spans due to its rapid diffusion out of the sample. For v equal 1×10^{-4} cm.s⁻¹ and a value for D_{vac} , twice the reported value, 1.13×10^{11} cm² s⁻¹ at 875 °C, the measured PL shifts are in close agreement with those predicted from the model. Inaccuracy in the reported values for D_{vac} are likely to take place, and can be ascribed to the indirect means by which these measurements were carried out. The values reported for D_{vac} in the reference quoted were extracted from the rate of interdiffusion in a GaAs/AlGaAs QWs. This rate, as discussed in this chapter, is not fully understood and is not likely to be accurately quantified. Therefore finding the best fit for a value of D_{vac} twice this reported value is not surprising, and should be a source of considerable concern at this stage.

IV.B. Kinetics of Impurity Free Vacancy Disordering

IFVD utilises Ga out-diffusion into dielectric caps at elevated temperatures to introduce group III point defects.²⁷ Since its discovery,²⁸ it has been widely used to fabricate OEICs and PICs.^{12,10} It can be readily understood from the mechanism that the defect type introduced is the Schottky defect, specifically V_{III} . The concentration of Ga atoms out-diffused in dielectric caps has previously been measured using various techniques, and was reported to have a saturation concentration of the order of $1-7 \times 10^{19}$ cm⁻³.^{29,30,31,32} The out-diffusion of a single Ga atom into the cap will result in the formation of one V_{III} . An identical flux of vacancies will consequently be generated with the same rate at the semiconductor

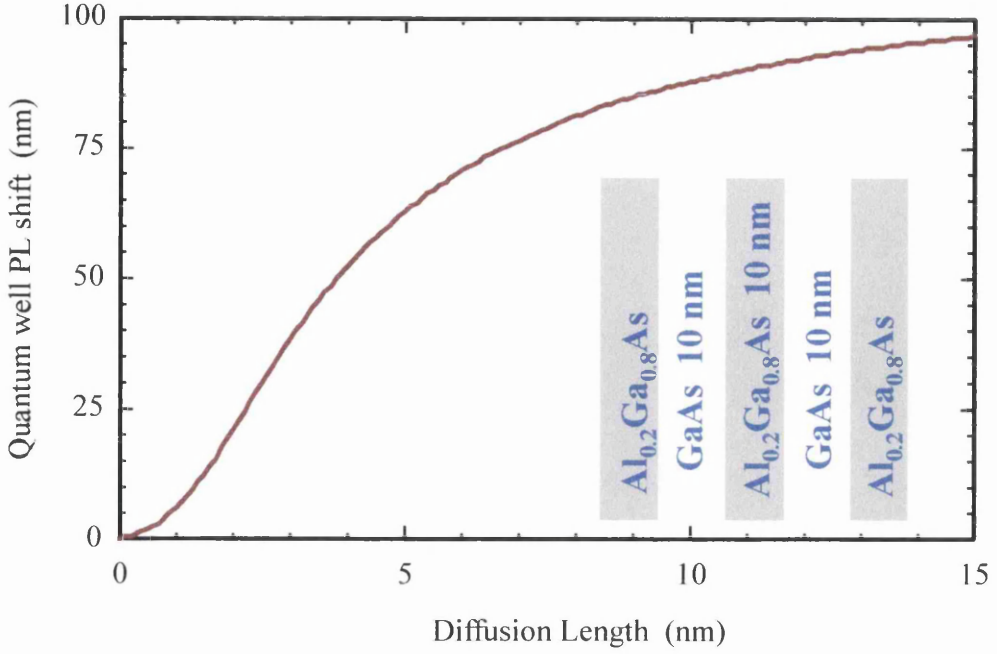


Fig. 3.9 Plot for the PL shift versus the corresponding diffusion length for a double quantum well. The inset shows the QW composition.

surface due to this flux of Ga out-diffusion. Therefore, to quantify the vacancies in the semiconductor one has to determine the flux of the Ga diffusing into the dielectric cap. The boundary conditions associated with the Ga out-diffusion assume that diffusion is governed by equation (3.12) and that Ga diffuses into the cap approaching its solubility limit as time goes to infinity,³³ with an initial Ga concentration equal to zero in the cap. The boundary conditions can be expressed as:

$$\begin{aligned}
 @t = 0 &\rightarrow C_{Ga} = 0 \\
 @t \Rightarrow \infty &\rightarrow C_{Ga} = C_{sol} \\
 @z = d &\rightarrow \frac{d}{dx}C_{Ga} = 0
 \end{aligned} \tag{3.16}$$

The solubility limit of the caps is termed C_{sol} , while d is the thickness of the cap, and is typically of the order of 200 nm. Different, and more complicated, boundary conditions would be necessary to describe the diffusion of Ga in the silica cap while taking into account some of the possibilities such as Ga pile up at the surface of the cap and at the GaAs/cap interface beyond saturation. However, the above boundary conditions can be solved giving a profile expressed as,

$$C_{Ga}(z, t) = \sum_{n=1}^{\infty} k_n \sin[\lambda_n z] \{1 - \exp[-\lambda_n^2 D_{Ga} t]\} \tag{3.17}$$

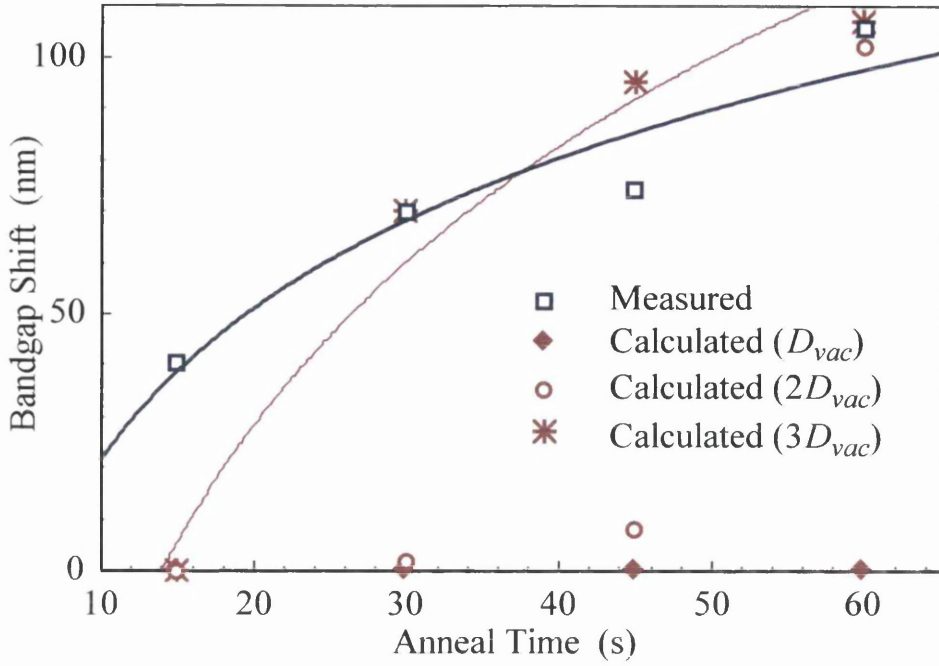


Fig. 3.10 Plot for measured and calculated PL shifts resulting from the IFVD process in a double quantum well for different values of D_{vac} .

$$k_n = \frac{\langle C_{sol} \cdot \sin[\lambda z] \rangle}{\langle \sin[\lambda z] \cdot \sin[\lambda z] \rangle}, \quad (3.18)$$

$$\lambda_n = \frac{n\pi}{d} \quad (3.19)$$

where D_{Ga} is the Ga diffusion coefficient in SiO_2 , reported to be $5.2 \times 10^{-1} \exp[-1.77/k_B T]$ cm^2s^{-1} , and equal to $2.7 \times 10^{-11} \text{cm}^2\text{s}^{-1}$ at 950°C . The resulting Ga profiles for various anneal times are plotted in Fig. 3.8. As can be seen in the Figure, saturation of Ga in the cap takes places after about 10 s of annealing, which matches very well the reported measurements.³³

Due to this Ga flux, there exists a similar flux of vacancy in-diffusion into the semiconductor. Therefore at the GaAs/ SiO_2 interface the following boundary condition should be satisfied,

$$D_{vac} \frac{d}{dz} N_v(z,t) \Big|_{z=0} = D_{Ga} \frac{d}{dz} C_{Ga}(z,t) \Big|_{z=0} \quad (3.20)$$

where, D_{vac} and $N_v(x,t)$ are the vacancy diffusion coefficient and concentration in the semiconductor respectively. Using the Laplace transform to solve the diffusion equation (3.11), with the boundary conditions in (3.20) and initial vacancy concentration equal to zero, the vacancy concentration can be expressed as a convolution of two functions,²⁶ such that,

$$\begin{aligned}
N_v(z, t) &= \int_0^t f(t - \tau)g(\tau)d\tau, \\
f(t) &= \frac{\partial}{\partial z} N_v(z, t)|_{z=0} = \frac{D_{Ga}}{D_{vac}^{1/2}} \frac{\partial}{\partial z} C_{Ga}(z, t)|_{z=0} \\
g(t) &= \frac{1}{\sqrt{\pi t}} \exp\left[\frac{-z^2}{4D_{vac}t}\right]
\end{aligned} \tag{3.21}$$

The vacancy profile was obtained using the reported D_{vac} , which, at 950 °C, is $6.1 \times 10^{12} \text{ cm}^2 \text{ s}^{-1}$. The value of w_v can be then be obtained from equation 3.3, and was equal to $15 \times 10^3 \text{ hop.s}^{-1}$.³ Also a value of $1 \times 10^{19} \text{ cm}^{-3}$ was used as the Ga solubility limit in the silica caps.³¹ As can be seen in Fig. 3.8, the vacancy concentration at the surface decreases as the Ga concentration in the cap saturates, which also explains the commonly observed saturation in the dielectric caps used in IFVD,³⁰ and the effect of the cap thickness on the amount of QWI obtained. Upon evaluating $N_v(d_{QW}, t)$, N_{IC} and the associated PL shifts can be calculated in a similar manner to the PIDLI process. In Fig. 3.9 the PL shift vs. the diffusion length obtained from the calculation is plotted. For the parameters stated above, the predicted amount of intermixing is negligible for annealing times less than 60 s, as can be seen in Fig. 3.10. However, if D_{vac} is increased, the predicted intermixing is in better agreement with the measured values. For a value of D_{vac} three times the reported value, $1.13 \times 10^{11} \text{ cm}^2 \text{ s}^{-1}$ at 875 °C, the measured PL shifts are in close agreement with those predicted from the model. The vacancy diffusion coefficient, D_{vac} , used in these calculations is the one used for the PIDLI calculations. Therefore a factor of 2-3 discrepancy between the expected from the model here and the reported should raise concerns at these early stages of modelling the process kinetics.

V. SUMMARY

We have developed an atomic-scale model for the kinetics of intermixing of GaAs/AlGaAs quantum confined heterostructures starting from first principles. The model hypothesis has been validated by successfully predicting the amounts of quantum well intermixing induced by the processes of hydrogen plasma induced defect layer intermixing and impurity free vacancy disordering, two different techniques for quantum well intermixing. The predictions are in good agreement with the measurements for both processes of the vacancy diffusion coefficient is increased by a factor of 2 to from its reported value. The results show a good degree of accuracy considering the uncertainty in the parameters used. It is obvious that a more rigorous model would take into account effects such as defect recombination, as well as correlation effects in diffusion, and hence predict more accurately the effect of Al/Ga mixing at the interface of the well and barrier. The error function profiles

assumed for the diffusion profiles could also be substituted with exact diffusion profiles calculated by solving the diffusion equation in its statistical form using parameters, which were accurately measured. Moreover, the concept of the defect surface recombination velocity should prove useful in characterising various technological factors such as the state of the surface of the semiconductor.

Although not comprehensive, the model is currently limited by the parameters used within it. Further sophistication in the model meant the need for knowing the values for more parameters, or instead, fitting the results obtained to more unknown variables. Instead, it was found more appropriate to carry out the necessary characterisation needed to identify the mechanisms and parameters necessary for more accurate representation of the process.

VI. REFERENCES

- ¹ W.D. Laidig, N. Holonyak, Jr., M.D. Camras, K. Hess, J.J. Coleman, P.D. Dapkus, and J. Bardeen, *Appl. Phys. Lett.*, vol. 38, P 776, 1981.
- ² D.G. Deppe and N. Holonyak Jr. *Appl. Phys. Lett.*, vol. 64, P R93, 1988.
- ³ K. B. Kahen D. L. Peterson, G. Rajeswaran, and D. J. Lawrence, *Appl. Phys. Lett.*, vol. 55, P 651, 1989.
- ⁴ S.Y. Chiang and G.L. Pearson, *J. Appl. Phys.*, vol. 46, P 2986, 1975.
- ⁵ I. Gontijo, T. Krauss, J.H. Marsh, and R. M. De La Rue, *IEEE J. Quantum Electron.*, vol. 30, P 1189, 1994.
- ⁶ Y.T. Oh, T.W. Kang, C. Y. Hong, K.T. Kim, T.W. Kim, *Solid State Comm.*, vol. 96, P 241, 1995.
- ⁷ W. P. Gillin, A. C. Kimber, D. J. Dunstan, R. P. Webb, *J. Appl. Phys.*, vol. 76, P 3367-, 1994.
- ⁸ R. M. Cohen, *Mat. Sci. & Eng Reports*, vol. R20, P 167, 1997.
- ⁹ T.Y. Tan, U. Gösele *J. Appl. Phys.*, vol. 61, P 1841, 1987.
- ¹⁰ J. H. Marsh, P. Cusumano, A. C. Bryce, B. S. Ooi, and S. G. Ayling, *Proc. SPIE*, vol. 74, P 2401, 1995.
- ¹¹ P.K. Haff, and Z.E. Switkowski, *J. Appl. Phys.*, vol. 48, P 3383, 1977.
- ¹² B.S. Ooi, A.C. Bryce, and J. H. Marsh, *Electronics Letters*, vol. 31, P 449, 1995.
- ¹³ C.J. McLean, A. Mckee, G. Lullo, A.C. Bryce, R.M. De La Rue, and J.H. Marsh, *Electronics Letters*, vol. 31, P 1285, 1995.
- ¹⁴ W. Hayes, and A. M. Stoneham, “ Defects and defect processes in non-metallic solids,” John Wiley & Sons, 1985.
- ¹⁵ D. G. Deppe, L. J. Guido, N. Holonyak, Jr., K. C. Hsieh, R. D. Burnham, R. L. Thorton, and T. L. Paoli, *Appl. Phys. Lett.*, vol. 49, P 510, 1986.
- ¹⁶ B.S. Ooi, K. McIlvaney, M.W. Street, A. Saher Helmy, S.G. Ayling, A.C. Bryce, J.H. Marsh, and J.S. Roberts, *IEEE J. Quantum Electron.*, vol. 33, P 1784, 1997.
- ¹⁷ A. Saher Helmy, J. S. Aitchison, and J. H. Marsh, *Appl. Phys. Lett.*, vol. 71, P 2998, 1997.
- ¹⁸ A. Saher Helmy, J. S. Aitchison, and J. H. Marsh, *IEEE J. Selected Topics in Quantum Electronics*, vol. 4, P 653, 1998.
- ¹⁹ R. J. Borg, and G. J. Dienes, “An Introduction to solid state diffusion,” Academic Press, 1988.
- ²⁰ B.S. Ooi, M.W. Street, S.G. Ayling, A.C. Bryce, J.H. Marsh, and J.S. Roberts, *Int. J. of optoelectronics*, vol. 10, P 257, 1995.

- ²¹ T.E. Schlesinger and T. Kuech, *Appl. Phys. Lett.*, vol. 49, P 519, 1986.
- ²² S. Salimian C. Yuen, C. Shih, C.R. Cooper, *J. Vac. Sci. Technol.*, vol 9 B, P 114, 1991.
- ²³ D.Lootens, P. Vandaele, P. Demeester, P. Clauws, *J. Appl. Phys.*, vol. 70, P 221, 1991.
- ²⁴ M. Rahman M. A. Foad, S. Hicks, M. C. Holland, and C. D. Wilkinson, *Mat. Res. Soc. Symp. Proc.*, vol. 279, P 775, 1993.
- ²⁵ M. Rahman, N. P. Johnson, M. A Foad, A. R. Long, M. C. Holland, and C. D. Wilkinson, *Appl. Phys. Lett.*, vol. 61, P 2335, 1992.
- ²⁶ M. D. Greenberg, "Advanced Engineering Mathematics," Prentice Hall, 1968.
- ²⁷ K.V. Vaidyanathan, M. J. Helix, D. J. Wolfrod, and B. G. Streetman, R. J. Blattner, and C. A. Evans Jr., *J. Electrochem. Soc.*, vol. 124, P 1781, 1977.
- ²⁸ D. G. Deppe, L. J. Guido, N. Holonyak, Jr., K. C. hsieh, R. D. Burnham, R. L. Thorton, and T. L. Paoli, *Appl. Phys. Lett.*, vol. 49, P 510, 1986.
- ²⁹ Sigurd Wagner, and Edward I. Povilonis, *J. Electrochem. Soc.*, vol. 121, P 1487, 1974.
- ³⁰ Xin Wen, Jim Y. Chi, Emil S. Koteles, Bori Elman and Paul Melman, *J. Electronic Materials*, vol. 19, P 539, 1990.
- ³¹ T. Haga, N. Tachino, Y. Abe, J. Kasahara, A. Okubora, and H. Hasegawa, *J. Appl. Phys.*, vol. 66, P 5809, 1989.
- ³² S. Bürkner, M. Maier, E. C. Larkins, W. Rothemund, E. P. O'Rielly, and J. D. Ralston, *J. Electron. Mat.*, vol. 24, P 805, 1995.
- ³³ Masayaku Katayama, Yutada Tokuda, Nobuo Ando, Yajiro Inoue, Akira Usami, and Takao Wada *Appl. Phys. Lett.*, vol. 54, P 2559, 1989.

TECHNOLOGY OF DIELECTRIC-CAP- ANNEALING INDUCED INTERMIXING

In GaAs/AlGaAs structures, IFVD utilises Ga out-diffusion into dielectric caps at elevated temperatures to introduce group III point defects.¹ Since its discovery,² it has been widely used to fabricate OEICs and PICs.^{3,4,5} The principal IFVD techniques utilise dielectric caps such as Si₃N₄ and SiO₂ to control the activation energies of As and Ga out-diffusion in GaAs/AlGaAs epitaxial layers at elevated temperatures. Because of the varying diffusivity of particular matrix atoms in different dielectric caps, selective intermixing can also be achieved. For a given semiconductor structure, this can be done by choosing dielectric cap ensemble which enhances/impedes the out-diffusion of the species necessary for intermixing. However there are other IFVD techniques that do not use dielectric cap annealing induced intermixing. Although quantum well intermixing is an alternative to low yield expensive processes such as overgrowth, it is still chiefly used within the research laboratories with very limited industrial interest. This is principally due to the lack of reliable and reproducible processes for it, a goal that needs non-trivial characterisation and control over the properties of the dielectric caps used.

I. IFVD BACKGROUND

When dielectric caps were first investigated in GaAs based IC technologies, they were ranked according to how well they prevented impurities from diffusing through them. At the time, dielectric caps were used as masks for impurity diffusion, and annealing caps for maintaining the lattice integrity. A few decades later, quantum well intermixing became a promising technique for realising optoelectronic and photonic integrated circuits, PICs and OEICs respectively. Matrix element diffusion into dielectric caps as a means for introducing lattice defects then became a method for achieving quantum well intermixing due to its simplicity, and the resultant low optical losses. The development of IFVD processes can be ascribed to a correlation between the partial understanding of disordering mechanisms at the time, and GaAs LSI process technologies.

- The contribution from LSI technology covered the behaviour of GaAs/AlGaAs heterostructures at elevated temperatures, namely the interdiffusion of Al and Ga across the interfaces.⁶
- Understanding of disordering mechanisms contributed the knowledge about group III interdiffusion in GaAs/AlGaAs heterostructures and the fact that inter-diffusion takes place through diffusion of native point defects in the semiconductor lattice.

Characterisation and control of the properties of dielectric films involved in IFVD are vital to achieve a reliable and reproducible process. The properties of the films as well as the condition of the dielectric/semiconductor interface are thought to be the main factors that control the amount of Ga out-diffusion, as will be seen later in the chapter.

In this chapter the usefulness of various dielectric caps for IFVD will be investigated. The caps will be ranked according to their properties and the bandgap shifts they produce after annealing at elevated temperatures. A discussion will then be presented, about the optimum cap ensemble to be used for IFVD. Finally an optimised process is then developed and its performance characterised.

II. INVESTIGATION OF DIELECTRIC CAPS FOR IFVD

To draw a conclusion about the important factors for achieving a reproducible and selective IFVD process, it is vital to deposit a set of dielectric caps with known properties, so we can correlate such properties with the caps' performance in QWI.⁷ This section will investigate the performance of various dielectric films as annealing caps for IFVD. From the results obtained and other work reported on the subject, some conclusions are drawn about the optimum means for IFVD technology.

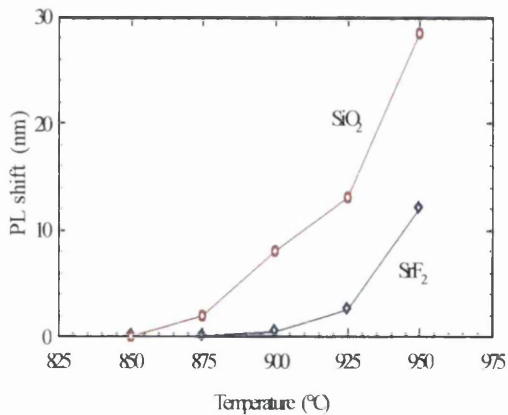


Fig. 4.1 Plot for the bandgap shifts as a function of anneal temperature for samples capped with SrF₂ and SiO₂ and annealed for 30 s with 15 s rise time.

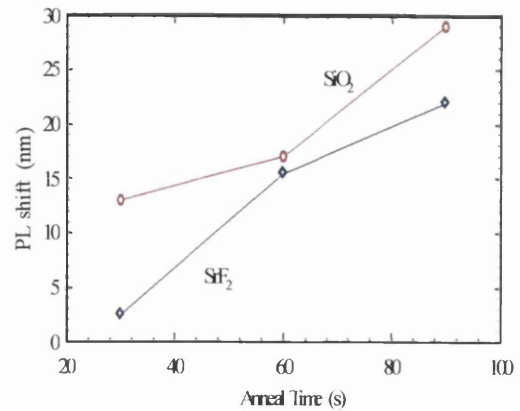


Fig. 4.2 Plot for the bandgap shifts as a function of anneal time for samples capped with SrF₂ and SiO₂ and annealed at 925 °C with 15 s rise time.

II.A. Silica; SiO₂

Because of the early importance of SiO₂ caps in semiconductor technologies,⁸ this was the first to be investigated for IFVD.² Shortly after, the technique was widely used in this technology,^{9,10,11,12} and parameters such as the interdiffusion coefficient of Ga and Al in QWs annealed with SiO₂ caps,¹³ the saturation concentration of Ga in the caps,¹² and the change of the amount of intermixing with depth were all studied.¹¹ Other studies included X-ray photoelectron spectroscopy, XPS, of the SiO₂/GaAs interface,¹⁴ deep level transport spectroscopy, DLTS, and Rutherford Back Scattering, RBS, of GaAs annealed with SiO₂ caps.^{15,16} The effects of the cap thickness, anneal temperature, and anneal duration, on the amount of intermixing were also reported.¹⁰ Attempts to summarise the performance parameters resulting from using SiO₂ in IFVD show great variance. Values like interdiffusion activation energies and bandgap shifts usually depend on the type, mechanical treatment history, doping, and thermal stability of the structures and SiO₂ caps used. Therefore it will be necessary to explain the circumstances of every result along with the numbers produced from it. The results reported using SiO₂ caps, however, are much more consistent than those achieved by any other cap. Because of the consistency of its performance SiO₂ is an ideal candidate to be part of an optimised selective IFVD process.

II.B. Silicon Nitride; Si₃N₄

Si₃N₄, as discussed in chapter 2, was one of the popular dielectric caps developed for semiconductor integrated circuit technologies, to prevent Ga diffusion when deposited in certain ways.¹⁷ Even now it still plays a pivotal role in semiconductor devices, and not in IFVD.¹⁸ Although Si₃N₄ has been studied as a viable dielectric cap for inhibiting intermixing

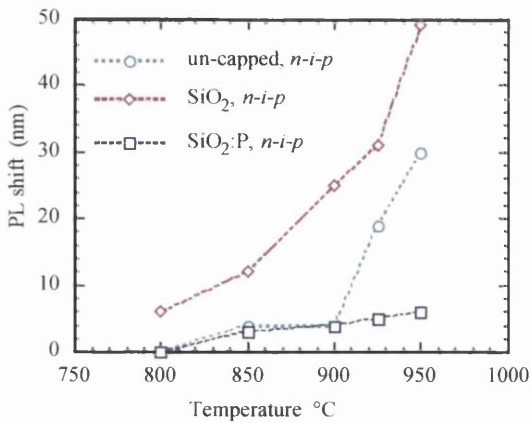


Fig. 4.3 Plot for the bandgap shifts as a function of anneal temperature for *n-i-p* DQW samples capped with SiO₂:P and SiO₂. Samples were then annealed for 30 s with 15 s rise time.

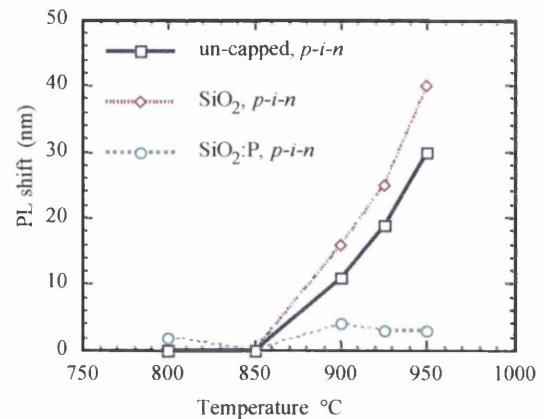


Fig. 4.4 Plot for the bandgap shifts as a function of anneal temperature for *p-i-n* DQW samples capped with SiO₂:P and SiO₂. Samples were then annealed for 30 s with 15 s rise time.

in IFVD,¹⁹ the lack of consistency in its performance has limited its usefulness.^{20,21,22,23} However laser devices have been fabricated using the SiO₂/Si₃N₄ cap ensemble.¹⁹ Difficulties have often been experienced in producing nitrides in a pure state, despite studies devoted to depositing the films with a reproducible composition.^{24,25} The unintentional presence of O₂ during the deposition of Si₃N₄ assists the formation of silicon oxynitrides Si_xN_yO instead.²⁶ Si₃N₄ films were therefore not chosen as a potential dielectric film for IFVD process, despite the degrees of freedom (such as internal stress) they potentially offer in controlling the film properties, because of the difficulties encountered in depositing optimised films reproducibly.

II.C. Strontium Fluoride; SrF₂

Thin films of SrF₂ have been used in a number of applications within the III-V semiconductor technology.^{27,28,29,30} It has been used to form metal-insulator-semiconductor structures on InP^{27,28} and GaAs,²⁹ where it was found to form good quality interfaces with a low density of interface states.³⁰ SrF₂ was also used as a mask during dry etching because of the low etch rate it exhibits at high plasma biases.³¹ SrF₂ was consequently explored as a mask for IFVD due to such properties, where it exhibited minimal intermixing and hence minimal bandgap shifts.³² An example of the cap performance is shown in Figs 4.1 and 4.2. The SiO₂/SrF₂ capping system has produced up to a 240 meV differential shift.³³ The activation energy for the Ga/Al interdiffusion coefficient in regions underneath SrF₂ caps was found to be 6.4 eV,³⁴ which is larger than the activation energy observed for diffusion due to thermal-induced interdiffusion in GaAs/AlGaAs structures.³⁵ Optoelectronic devices were realised successfully using such a capping system. External cavity lasers with low optical losses,³⁶ broad area lasers with improved far field performance,³⁷ lasers with band-gap widened saturable absorbers,³⁸ and lasers with integrated waveguide modulators have all been

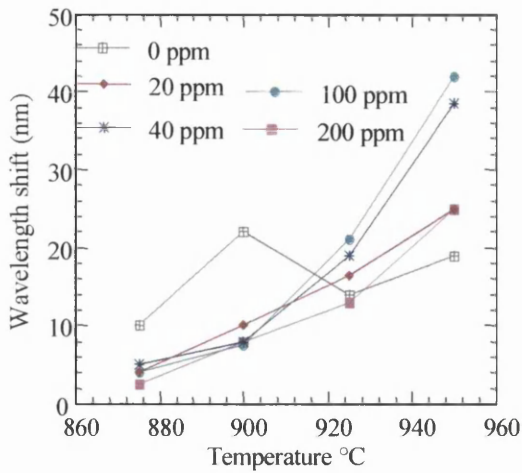


Fig. 4.5 Plot for the bandgap shifts as a function of fluorine content for different anneal temperature for DQW samples capped with SiO₂:F. Samples were annealed for 60 s with 15 s rise time.

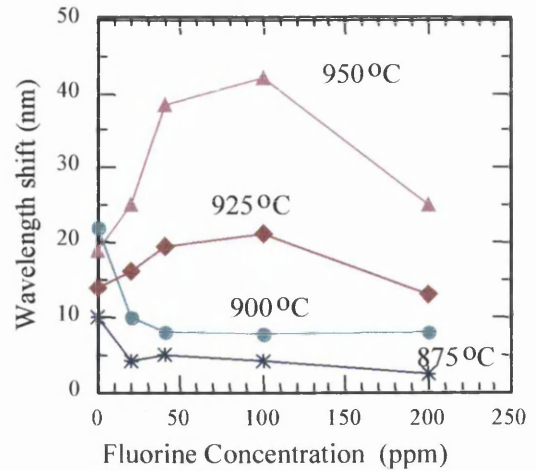


Fig. 4.6 Plot for the bandgap shifts as a function of fluorine content for different anneal temperature for DQW samples capped with SiO₂:F. Samples were annealed for 60 seconds with 15 s rise time.

demonstrated using this technique.³⁹ Also SrF₂ was used to develop a technology by which the extent of intermixing can be spatially controlled in a continuous fashion. This is achieved by changing the area covered with SrF₂ as compared to that covered with SiO₂ in a given region of the semiconductor.^{33,40,41} Successful multi-wavelength integrated laser diodes and detectors were fabricated using this technique.^{40,41}

Within the course of using SrF₂ as an inhibiting cap, it was found to exhibit several unfavourable properties despite its superior performance in inhibiting QWI. Excess damage in the GaAs, in the form of cracks, at the SiO₂/SrF₂ interfaces was reported upon annealing in GaAs.^{42,43} Defects, in the form of pits, were also observed underneath the SrF₂ caps. Such shortcomings were ascribed to the mismatch in the linear thermal expansion coefficient between GaAs, SiO₂ and SrF₂.^{44,43} In addition to the damage introduced in the GaAs, difficulties in etching the SrF₂ cap were encountered for annealing temperatures over 900 °C. The difficulties in removing the SrF₂ are also accompanied by non-uniformity in the degree of intermixing under the SiO₂ and SrF₂.⁴² The useful annealing temperatures for IFVD are between 915 °C and 950 °C, which makes SrF₂ unsuitable for successful device fabrication. Recently Rutherford Back Scattering (RBS) studies were carried out on GaAs/AlGaAs structures annealed with SiO₂ and SrF₂ caps. The measurements showed an interface broadening of ~16 nm at the GaAs/SrF₂ interface for annealing temperatures above 900 °C.⁴⁵ This broadening can certainly explain the damage observed on the surfaces, the difficulty in removing the SrF₂, and it can also account for the inefficient electrical pumping of devices annealed with SrF₂.

Table 4.1 Parameters of the set of experiments carried out to investigate the effects of oxide growth on the QWI using IFVD.

Sample Type	Treatment	PL Shift (nm)
DQW	200 nm SiO ₂	33
DQW	200 nm SiO ₂ +30 s HCL	39
DQW	200 nm SiO ₂ +60 min. CH ₄ O	43
DQW	200 nm SiO ₂ +30 s HCL+60 min. CH ₄ O	47
DQW	200 nm SiO ₂ +60 min. H ₂ O	41
DQW	200 nm SiO ₂ +30 s HCL+60 min. H ₂ O	41
DQW	200 nm SiO ₂ +60 min. (H ₂ O+ CH ₄ O)	47
DQW	200 nm SiO ₂ +30 s HCL+60 min. (H ₂ O+ CH ₄ O)	36
MQW	200 nm SiO ₂	57
MQW	200 nm SiO ₂ +30 s HCL	60
MQW	200 nm SiO ₂ +60 min. CH ₄ O	58
MQW	200 nm SiO ₂ +30 s HCL+60 min. CH ₄ O	60
MQW	200 nm SiO ₂ +60 min. H ₂ O	55
MQW	200 nm SiO ₂ +30 s HCL+60 min. H ₂ O	50
MQW	200 nm SiO ₂ +60 min. (H ₂ O+ CH ₄ O)	66.5
MQW	200 nm SiO ₂ +30 s HCL+60 min. (H ₂ O+ CH ₄ O)	45

II.D. Phosphorous doped Silica; SiO₂:P

In 1995 E.V.K. Rao *et al.*⁴⁶ announced SiO₂:P was a universal QWI cap for III-V semiconductors, and suggested that it would replace plain SiO₂. Phosphorous doped SiO₂ films play a critical role in the reliability of VLSI technologies.⁴⁷ The phosphorous helps neutralise the effect of mobile ion species and improve the glass flow, resulting in better gap filling and improved planarisation.^{48,49} In this section, work carried out in the department is described, which demonstrates that SiO₂:P caps inhibit intermixing in almost all of the structures used, irrespective of the doping order of the structure (undoped, p-i-n, or n-i-p).

Two GaAs/AlGaAs DQW laser wafers having similar configurations, but with opposite doping orders, *p-i-n* and *n-i-p*, as shown in Appendix A, were used in this experiment. Dielectric films of SiO₂ and SiO₂:P, both having thicknesses of 200 nm, were deposited on the surface at a temperature of 330 °C using a conventional PECVD apparatus equipped with a separate PH₃ flow line for P doping. The P content was measured by energy dispersive x-ray (EDX) spectroscopy on a 200 nm thick layer of SiO₂: P deposited, using the same PECVD system and in the same experimental conditions, on a Si wafer. EDX measurements showed a P content of 5% by weight in the caps, with a 1:2 atomic ratio between Si and O₂. Samples were annealed for 60 s in flowing N₂ at temperatures between 800 °C and 950 °C. Uncapped samples were annealed at the same time to study the thermal stability of the wafer under the conditions described above. Figs 4.3 and 4.4 show the shift in the PL from that of as-grown material as a function of the annealing temperature. After

annealing, differential band gap shifts > 40 nm can be easily obtained in samples partially masked with $\text{SiO}_2\text{:P}$ and capped with SiO_2 , with excellent surface morphology, including the edge interface between $\text{SiO}_2\text{:P}$ and SiO_2 . The wavelength shifts in the PL peak of the $p\text{-i-n}$ are smaller than those of the $n\text{-i-p}$ structures because intermixing n type material is carried out chiefly through V_{III} , which is the main defect generated during IFVD, and in p type material through I_{III} .⁵⁰ Even so, it can be seen that $\text{SiO}_2\text{:P}$ acts as a very effective mask for preventing Ga out-diffusion, limiting the band gap shift to no more than 5 nm, for both $n\text{-i-p}$ and $p\text{-i-n}$ structures at temperatures up to 950 °C. Moreover, no surface damage was produced by this dielectric cap under the annealing conditions studied here. In contrast, the blue shifts for both $p\text{-i-n}$ and $n\text{-i-p}$ samples capped with SiO_2 increase with temperature and are always greater than those for uncapped samples, demonstrating the enhanced out-diffusion of Ga into pure SiO_2 caps as compared with uncapped samples. The negligible damage associated with this process allowed very efficient mode-locked laser diodes to be realised using this capping system.⁵¹

Possible explanations for the masking properties of $\text{SiO}_2\text{:P}$ films, are related to the densification of the glass matrix caused by the P. Films of $\text{SiO}_2\text{:P}$ with a weight ratio $\text{P}_2\text{O}_5 / \text{SiO}_2$ of 4% have been used as caps for open-tube thermal activation of Si implants in GaAs, and it has been found that the diffusion coefficient of implanted Si in semi-insulating GaAs is about one order of magnitude smaller for $\text{SiO}_2\text{:P}$ than for SiO_2 .⁵² Another possibility might be due to the reduction in internal film stress caused by P. Strain is thought to play a role in promoting Ga out-diffusion at elevated temperatures. The thermal expansion coefficient of GaAs is about ten times larger than that of SiO_2 and, as a consequence, the SiO_2 film is under tensile strain and the GaAs surface layer is under compressive strain. Under this condition, because of the high diffusion coefficient of Ga in SiO_2 , the out-diffusion of Ga atoms into the SiO_2 film is an energetically favourable process because it minimises strain in the system. The addition of P into the SiO_2 film leads to an increase in the thermal expansion coefficient⁴⁷ and a decrease in the glass softening temperature.⁵³ Therefore, less compressive strain will be induced in the GaAs surface layer during the annealing step and, as a result, the number of Ga vacancies will be reduced due to less Ga out-diffusion. In chapter 6 SIMS measurements will confirm directly that P does not diffuse into the semiconductor and also shows that P inhibits the Ga out-diffusion. Also in chapter 5, spatially resolved PL and Raman measurements will discuss the studies carried out to investigate the resolution of the IFVD using the $\text{SiO}_2/\text{SiO}_2\text{:P}$ capping system.

It should also be noted that the addition of small amounts of P (1 wt%) does not drastically change the properties of $\text{SiO}_2\text{:P}$ as compared with SiO_2 and hence both caps are

expected to have similar effect on intermixing.⁴⁷ This shows that the results presented here^{54,55} do not conflict with those reported by Rao *et al.*⁴⁶

II.E. Fluorine doped Silica; SiO₂:F

SiO₂:F films have been studied extensively for use in ultra high scale integrated circuit technology as low dielectric constant insulating layers to reduce the capacitance between adjacent interconnections.^{56,57,58} In addition to the reduced interface stress, SiO₂:F films offer reduced thermal stresses because they can be deposited at lower temperatures. Improved mechanical properties of layers with sub micron lateral dimensions can therefore be achieved. In addition, fluorine was found to dramatically reduce the trapped charge density at the Si/SiO₂ interface, the dielectric break-down voltage, and reduce the water absorption of the films.^{59,60} Such features make the film a strong candidate for improved operational characteristics of sub-micron M.O.S. field effect transistors with a SiO₂:F gate oxide.^{61,62} Also the incorporation of fluorine induces a change in the index of refraction of the doped silica films which can be used for guided wave optoelectronic applications.⁶³ The features mentioned above drove a great deal of research characterising fluorine incorporation in SiO₂ films.^{64,65} Therefore we studied the performance of SiO₂:F in QWI of GaAs/AlGaAs heterostructures. If the films have the same effects of reducing the interface stress, and trap charge density for GaAs as they do for Si, it would be of great interest to investigate the role these parameters have on QWI.

Samples of a DQW p-i-n doped heterostructure, as shown in Appendix A, were used in this experiment. PECVD silica films with fluorine contents of 0, 20, 40, 100, and 200 ppm of were deposited. Samples were then annealed 1 month after deposition at temperatures between 875 °C and 950 °C for 60 s with 15 s rise time. The shifts in the bandgap as a function of temperature are plotted in Fig. 4.5. Samples capped with SiO₂ containing various amounts of fluorine doping exhibit intermixing which increases with the increase of the annealing temperature, and their behaviour is very similar to that of the control sample with no Fluorine. When plotting the amount of bandgap shift as a function of the fluorine content for different annealing temperatures, as can be seen in Fig. 4.6, the behaviour of the samples can be divided in two groups. Samples annealed at temperatures < 900 °C exhibit bandgap shifts that increase with the fluorine content. Samples annealed above 900 °C show the opposite trend. From this simple experiment, it was found that the behaviour of samples does not differ significantly as the fluorine concentration is varied from 0 to 200 ppm. SIMS studies showed no evidence of fluorine diffusion into the semiconductor, as will be presented in chapter 6. Although no conclusions of the effect that fluorine may have on the GaAs surface can be drawn from these experiments, the performance of such caps, when annealed

at high temperatures, was not promising for selective QWI applications. Therefore no further studies were conducted.

II.F. Surface effects

The surface of the semiconductor plays a paramount role in controlling Ga out-diffusion. Some recent techniques have therefore successfully made use of the surface condition as a means of controlling QWI. Native oxide growth using hydrogen plasma treatment has been reported to inhibit QWI.⁶⁶ A modulation of 17% in the $\chi^{(2)}$ coefficient was achieved in asymmetric GaAs/AlGaAs quantum wells using this intermixing technique.⁶⁷ Also, anodic oxidation was reported to produce layers of native oxide on GaAs/AlGaAs structures, which enhance QWI.⁶⁸ More recently, considerable differential shifts were achieved, with almost no intermixing underneath the control caps, by growing a thermal oxide on the GaAs surface before annealing, which promotes intermixing, and using Al to reduce this oxide, which suppresses intermixing.⁶⁹ These approaches, although successful, might affect the quality of the surface after processing, jeopardising the electrical contact quality of the surfaces. Moreover no conclusive evidence was presented to explain the enhanced QWI.⁷⁰ No devices have been demonstrated using such techniques and no thorough spectroscopic investigation of the nature of the oxide has been carried out either.

Surface treatment is not a suitable technique for fabricating PICs and OEICs because of its effect on the surfaces. Nevertheless it will still affect any other IFVD technique used. Therefore, an experiment was designed to reveal some of effects of the standard surface treatments used in semiconductor processing on IFVD. The material used in this experiment was the standard DQW laser structure shown in Appendix A. Pieces with sizes of $2 \times 2 \text{ mm}^2$ were soaked in either H_2O , CH_4O , or a 1:1 mixture of both for 60 min. with and without a pre-clean using HCl. Immediately after the surface treatments, the samples were covered with 200 nm of E-gun deposited SiO_2 , and annealed at $925 \text{ }^\circ\text{C}$ for 60 s, with rise and fall times of 15 s.

- The effects of soaking in H_2O and CH_4O have been previously reported to enhance the growth of As rich, and Ga-rich oxides, respectively.⁷¹
- As can be seen in Table 4.1, the amount of intermixing using the SiO_2 caps before and after these treatments is quite different. In addition the amount of intermixing in all the cases studied is affected by the HCl treatment.
- The soaking durations used in these experiments are longer than what is typically used for cleaning the samples. However it is the principle of how sensitive the surface of the

semiconductor is to prior treatments that should be noted and hence studied and controlled.

- Substantial differences were observed in these experiments; 42% change in the PL shift was measured for the sample exposed to 60 min. of CH_4O and H_2O without previous HCl clean. Conversely, instead of enhancing intermixing like the effect it has on the rest of the samples, the HCl treatment caused intermixing to decrease in this sample.

The status of the GaAs surface was proven to be a prime source of inconsistency for the performance of any IFVD process, and should be controlled for reproducible consistent results. Systematic studies should therefore be conducted on the matter.

III. DISCUSSION

Before IFVD can have a real future in realising PICs, and OEICs outside of the research lab, in an industrial environment, its shortcomings must be minimised. The damage associated with annealing dielectric caps such as SrF_2 is not acceptable. Also the irreproducible film properties, and hence variation in QWI behaviour, encountered with Si_3N_4 caps is not at all suitable for industrial processes. Time dependent effects reported for $\text{SiO}_2\text{:P}$, is a serious drawback, but can be avoided by optimising the film parameters during deposition. However, the $\text{SiO}_2\text{-SiO}_2\text{:P}$ capping system is the most promising process reported to date.

Although quite successful, not enough is yet known about dielectric cap annealing with prior surface oxidation and treatment. For example its effect on the electrical quality of the GaAs surface and possibly the device degradation have not yet been assessed. The solubility limit of Ga in the films as well as the films' density, porosity and ability to absorb humidity are all parameters that can play significant role in Ga out-diffusion. Thorough experimental studies are needed to unfold the mechanisms taking place in IFVD, and hence allow a better-informed choice about the dielectric caps to be made. However, because of the nature of the problem, rigorous experiments are very time, and resource consuming.⁷²

From the performance perspective for integrated devices, the IFVD process should have minimal effects on the properties of the as-grown structure apart from changing the band-gap, and hence the optical properties depending on it. It is clear from the above discussion that the use of dielectric caps is preferred to surface treatment provided a similar performance can be achieved. It is essential that such caps can be etched reproducibly and efficiently. Silica caps, are by far the most reproducible and damage free performance, are ideal candidates for exploiting in IFVD. In the next section we shall present work carried out using silica for a single-cap, selective IFVD process. It should be noted that although attempts were previously

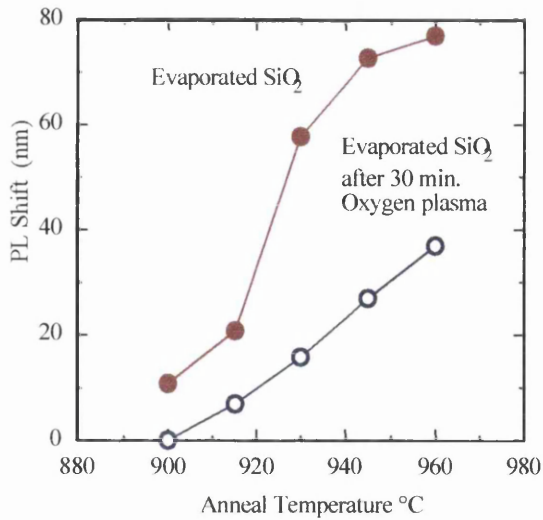


Fig. 4.7 Plot for the bandgap shifts as a function of anneal temperature for DQW samples capped with E-gun deposited SiO₂ and exposed to oxygen plasma for 30 mins. Samples were annealed for 60 seconds at 925 °C with 15 s rise time.

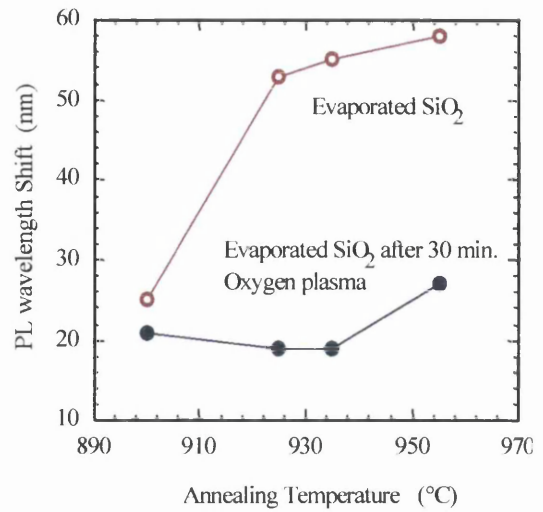


Fig. 4.8 Plot for the bandgap shifts as a function of anneal temperature for MQW samples capped with E-gun deposited SiO₂ exposed to oxygen plasma for 30 mins. Samples were annealed for 60 seconds at 925 °C with 15 s rise time.

made to obtain such a selective single cap process, no success has been reported in having sufficient control over the dielectric film properties to produce a differential shift adequate for device applications.⁷³

IV. PLASMA TREATMENT OF SiO₂ FILMS: A MEANS OF INHIBITING QWI

Increasing the resistance of dielectric caps to erosion during reactive ion etching (RIE) is a topic of current interest, especially for SiO₂ and Si₃N₄ films.^{74,75} One approach is film densification, and was demonstrated for SiO₂ films.⁷⁴ It is based on annealing silica at temperatures above 875 °C, however such high annealing temperatures make the processes only suitable for Si wafers and not for the III-V semiconductors because of their low thermal stability. Another technique of film densification is based on ion bombardment and was demonstrated for Si₃N₄ films.⁷⁵ In this technique, Si₃N₄ films are exposed to oxygen plasma, which was found to increase their resistance to erosion during etching. This technique of exposing the dielectric films to oxygen plasma was also reported to cause an increase in the refractive index of the films, reaching a maximum of 3.7% after 30 min of treatment for a 140 nm Si₃N₄ film. The operating conditions for the oxygen plasma used in the treatment were: an RF power of 50 W, an O₂ flow rate of 25 sccm, and a gas pressure of 100 mTorr, resulting in a DC self-bias of 110 V. Since the process is thought to have an effect on SiO₂

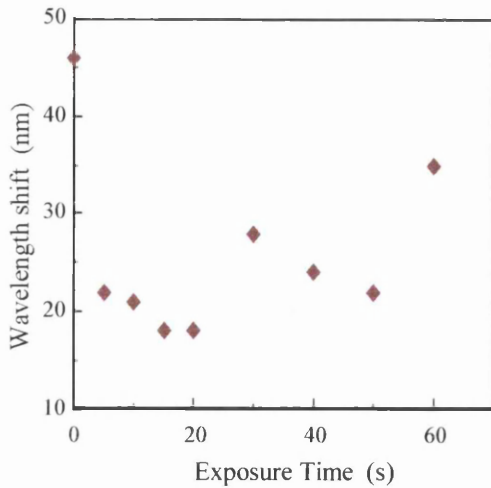


Fig. 4.10 Plot for the bandgap shifts as a function of exposure time for DQW samples capped with E-gun deposited SiO_2 exposed to oxygen plasma for different times. Samples were annealed for 60 s at 925°C with 15 s rise time.

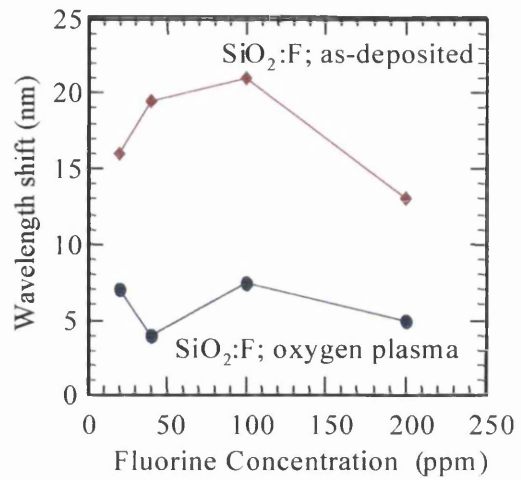


Fig. 4.11 Plot for the bandgap shifts as a function of Fluorine content for DQW samples capped with $\text{SiO}_2\text{:F}$. Two sets of samples are shown, exposed and unexposed to oxygen plasma for 30 mins. Samples were annealed for 60 s at 925°C with 15 s rise time.

caps, a set of experiments were conducted to investigate the effect of exposing the SiO_2 caps used in IFVD to the same treatment that increases the resistance of the masks to erosion.

The experiments presented in this section were to investigate whether plasma exposure has any effect on the silica caps used for IFVD. This stems from the belief that if the diffusivity and/or solubility limit of the Ga in a film can be controlled, then the amount of intermixing under such caps can also be controlled (see discussion in section III). Two MOVPE grown wafers were used in this experiment, see *MQW waveguide structure*, and *DQW laser structures* in Appendix A. Samples from both wafers were capped with 200 nm of electron beam evaporated SiO_2 and exposed to the oxygen plasma for 30 minutes, using the parameters reported by Hicks *et al.*⁷⁵ They were then annealed along with control unexposed samples at different temperatures. The amount of the PL shift versus the annealing temperature is plotted in Figs 4.7 and 4.8. The unexposed samples show amounts of intermixing 3 times larger than for the exposed samples. Differential bandgap shifts in excess of 110 meV were achieved between the exposed and un-exposed samples when annealed at 925°C for both doped DQW and un-doped MQW sample. It was also important to investigate whether the effect works for different types of silica or not. Another experiment is thus necessary to investigate the effect on the plasma exposure on different caps.

Samples from the DQW structure were therefore capped with 200 nm of electron beam evaporated SiO_2 and sputtered SiO_2 . They were then exposed to the oxygen plasma for different time spans, with the same set of parameters used in the first experiment.⁷⁵ Samples were then annealed using parameters identical to those used in the first experiments. The

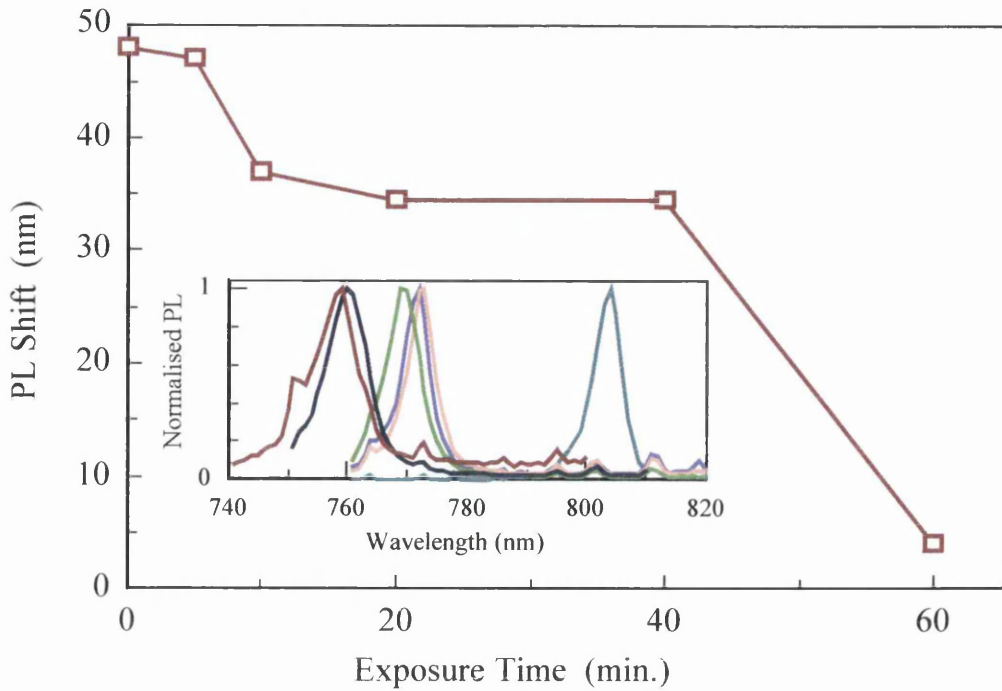


Fig. 4.12 Plot for the bandgap shifts as a function of exposure time for DQW samples capped with sputter deposited SiO_2 exposed to oxygen plasma for different times. Samples were annealed for 60 seconds at 925°C with 15 s rise time.

amount of the PL shift versus the exposure time is plotted in Fig 4.9 and 4.10. It is clear that, as the exposure time increases, the amount of intermixing also decreases, reaching almost zero for sputtered silica, after 60 min. exposure time. It is interesting to note that, in the case of the electron beam evaporated SiO_2 , the intermixing starts to rise again after a certain amount of exposure time. This effect is interesting and cannot be explained readily if one considers that the oxygen plasma causes film densification.

Results from samples covered with 200 nm PECVD $\text{SiO}_2:\text{F}$ are shown in Fig. 4.11. The figure shows the PL shifts as a function of the fluorine concentration for samples exposed and unexposed to oxygen plasma. As before, the samples exposed to the oxygen plasma show amounts of intermixing less than the unexposed ones, irrespective of the fluorine concentration in the cap. In addition, samples with 200 nm of sputtered silica were deposited, and the amount of intermixing was monitored as a function of time of exposure to the plasma. Samples were annealed for 60 s at 925°C and, again, the amount of intermixing decreases as a function of intermixing as can be seen in Fig. 4.13.

Although the samples exposed to oxygen plasma intermix considerably less than the un-exposed ones, they do show PL shifts as high as 20 nm. This is an unfavourable feature when looking for a cap which inhibits intermixing completely. Also there are interesting effects that cannot be readily explained such as the U shaped behaviour of the PL shifts observed for electron beam evaporated SiO_2 when exposed for different time spans, as shown

in Fig. 4.10. The effects observed so far in reducing QWI encouraged further optimisation of the plasma parameters for suppressing intermixing, as will be shown below. Also in section IV.C, we shall suggest possible explanations for such behaviour

IV.A. Single cap IFVD

The optimum performance was obtained after exposing the samples for 70 minutes to oxygen plasma with the following parameters: film thickness of

350 nm, with a 5 sccm O_2 flow rate, a pressure of 10 mTorr and a power of 275 W. This set of conditions results in a self DC bias of 800 V. As shown in Appendix 2, a longer exposure time is expected to result in even less intermixing. However, due to the high RF power needed for the process, the RIE machine could not be operated for longer, and so the process performance was limited by the practical operating conditions of the RIE machine.

A set of samples capped with 350 nm of electron beam evaporated SiO_2 was then processed using the same parameters. Another set of samples without SiO_2 caps were exposed to the plasma, and had an identical 350 nm of electron beam evaporated SiO_2 deposited after plasma exposure. A third set of samples was used as a reference, also coated with 350 nm of electron beam evaporated SiO_2 . The PL shift versus the annealing temperature for the three sets of samples is plotted in Fig 4.13. The samples with un-exposed SiO_2 films exhibit intermixing within the expected range for the thickness of the cap, and the annealing temperatures used.⁷⁶ However, the samples exposed to the plasma exhibit minimal intermixing, 10 meV, for temperatures below 945 °C, above which intermixing extends to a few tens of meVs. The samples exposed to the oxygen plasma prior to the deposition of silica caps show intermixing behaviour very similar to that of the unexposed silica caps. This suggests that the plasma exposure does not affect the GaAs surface, and the observed effects are due to changes in the cap properties. As can be seen in Table 1, the refractive index of the silica films, at 633 nm, changed from 1.532 before to 1.474 after the exposure to plasma. The thickness of the film decreased by 10% after the exposure. This can be explained by the high bias, ≈ 800 V of the plasma, which results in sputtering of the film by ion bombardment. Also, the etch rate of the exposed films is 5% less than that of the unexposed film.

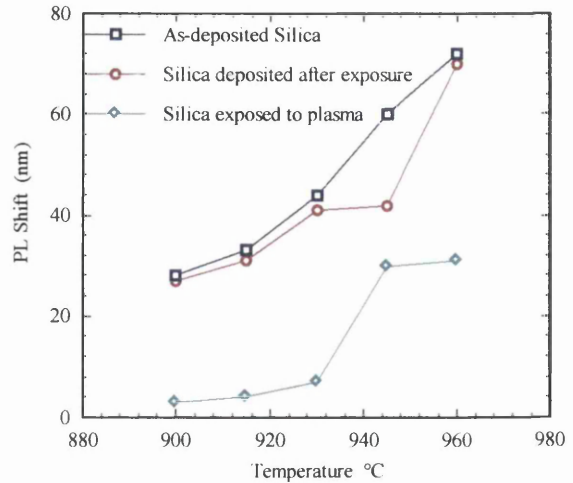


Fig. 4.13 Change in bandgap emission wavelength as a function of temperature for p-i-n doped DQW samples annealed for 60 s with 350 nm of evaporated SiO_2 cap

Table 4.2 Properties of the Silica caps before and after exposure to 70 minutes of oxygen plasma with a flow rate of 5 sccm, at a pressure of 10 mTorr, and a power of 275 W.

Film Property	Before Exposure	After exposure	Relative change
Thickness (nm)	355	320	-9.8%
Refractive index	1.532	1.474	-3.9%
Etch Rate (nm.min ⁻¹)	30	27	-10%

The refractive index of the as-deposited films, being greater than that of the thermal oxide, indicates a Si rich film agreeing with previous reports for the same type of deposition of SiO₂.⁷⁷ The observed reduction in the refractive index after plasma exposure can be explained in one of two ways. The first proposes that oxygen is incorporated in the films during plasma exposure, so reducing the refractive index of the layer but this could only happen within the ion penetration range. This would mean that the refractive index we measured after exposure is an average of two layers, one identical to that of the original film, and the other oxygen rich. However, the ion energy is sufficient to allow penetration no further than >5 nm in such an amorphous material, and so the observed reduction in refractive index is larger than would be expected from such a hypothesis. Recent experiments showed that E-gun deposited SiO₂ can have a pore fill factor of 0.23. Also a 4.1% increase in the refractive index of the as-grown at 633 nm films after their exposure to air was observed. According to the effective medium approximation, this increase in the refractive index was ascribed to the incorporation of H₂O in the film pores.⁷⁸ Another explanation proposes that, during the oxygen treatment, the H₂O in the film pores will be desorbed and the pores, now free from H₂O, may be sealed by the ion exposure. This makes the effective refractive index of the pores 1 (the refractive index of air), instead of 1.33 (the refractive index of H₂O). The measured reduction in the refractive index for our process, 3.9 %, therefore agrees well with what has been previously reported due to the incorporation of H₂O.⁷⁸ Clearly this hypothesis of sealed pores needs verification by electron microscopy and this will be attempted. However, this assumption would indicate that H₂O and air in the film pores respectively play a key role in assisting and preventing Ga out-diffusion, and hence QWI.⁷⁹

V. SUMMARY

Work characterising the performance of various dielectric caps used for IFVD has been presented in this chapter:

- SrF_2 caps have a good performance, but induce excessive damage in the semiconductor and are not etched away easily.
- Si_3N_2 caps were not investigated because of the difficulty in obtaining reproducible film quality.
- $\text{SiO}_2\text{:F}$ caps showed no interesting performance for selective intermixing. We have shown that, by adding 5 % in wt. P to SiO_2 caps, these caps inhibit quantum well intermixing.
- Problems with $\text{SiO}_2\text{:P}$ caps include the hygroscopic nature of the films, and hence their time dependent performance in inhibiting intermixing.
- The effect of exposing the surface of the GaAs to a HCl clean, H_2O , and CH_4O treatments has been investigated. It was found that changes in the observed PL shift of up to 42 % in the amount of intermixing could be obtained by exposing the GaAs to a 1:1 mixture of H_2O and methanol for 60 min.
- In section I it was concluded that the best caps are those with the least amount of damage associated, and with the most reproducible performance. Optimum performance, from the perspective of reproducibility and low damage, would be therefore obtained by using single SiO_2 caps for selective IFVD without altering the GaAs surface.

We have demonstrated control of the extent of QWI in various GaAs/AlGaAs heterostructures by exposing the SiO_2 films used in the process of impurity free vacancy disordering to an oxygen plasma in a reactive ion etching machine. Control was observed for doped and undoped GaAs/AlGaAs samples. Control was also obtained for different types of SiO_2 . According to our understanding of the process, inhibition of intermixing can be ascribed to the plasma exposure reducing the diffusivity of Ga in the cap. It seems that the reduced diffusivity of Ga in plasma exposed films is due to change in the properties of and the amount of pores in the SiO_2 film. Further investigations of the effect of plasma on the films are in progress. Such studies should unfold some of the mechanisms involved in IFVD. Selective exposure to oxygen plasma has been used to realise a selective IFVD process using a single silica capping layer, with bandgap shifts in excess of 100 meV achieved with <10 meV shift in the un-intermixed regions. The process has the potential to offer a single step, low damage, spatially controllable IFVD process.

Within the course of optimising the process parameters, we have utilised experimental design tools to gain insight about the process response. This helped us to predict the effects of the changes in parameters outside the ranges used for the parameter without resorting to more experiments. The RIE machine operating limitations, however, dictated the final parameters used. The experimental design tools were proven to be valuable for use in developing multivariable technological processes.

VI. REFERENCES

- ¹ K.V. Vaidyanathan, M. J. Helix, D. J. Wolfrod, and B. G. Streetman, R. J. Blattner, and C. A. Evans Jr., *J. Electrochem. Soc.*, vol. 124, P 1781, 1977.
- ² D. G. Deppe, L. J. Guido, N. Holonyak, Jr., K. C. Hsieh, R. D. Burnham, R. L. Thorton, and T. L. Paoli, *Appl. Phys. Lett.*, vol. 49, P 510, 1986.
- ³ J. H. Marsh, P. Cusumano, A. C. Bryce, B. S. Ooi, and S. G. Ayling, *Proc. SPIE*, vol. 74, P 2401, 1995.
- ⁴ M. W. Street, N. D. Whitbread, D. C. Hutchings, J. M. Arnold, J. H. Marsh, J. S. Aitchison, G.T. Kennedy, and W. Sibbett, *Opt. Lett.*, vol. 22, P 1600, 1997.
- ⁵ E. H. Li, "Selected papers on Quantum Well Intermixing," SPIE Optical Engineering Press, vol. 154, 1998.
- ⁶ L.L. Chang, A. Koma, *Appl. Phys. Lett.*, vol 29, P 138, 1976.
- ⁷ Shinya Sudo, Hirofumi Onish, Yoshiaki Nakano, Yukihiro Shimogaki, Kunio Tada, Mark J. Mondry, and Larry A. Coldern, *Jpn., J. Appl. Phys.*, vol 35, P 1276, 1996.
- ⁸ C. J. Frosch and L. Derick, *J. Electrochem. Soc.*, vol. 104, P 547 1957.
- ⁹ J. D. Ralston, S. O'Brien, G. W. Wicks, L. F. Eastman, *Appl. Phys. Lett.*, vol. 52, P 1511 1988.
- ¹⁰ X. Wen, J. Y. Chi, E. S. Koteles, B. Elman, P. Melman, *J. Electron. Mat.*, vol. 19, P 539, 1990.
- ¹¹ S. J. Lycett, A. J. Dewdney, M. Ghisoni, C. E. Norman, R. Murray, D. Sansom, J. S. Roberts, *J. Electron. Mat.*, vol. 24, P 197, 1995.
- ¹² S. Bürkner, M. Maier, E. C. Larkns, W. Rothemund, E. P. O'Rielly, J. D. Ralston, *J. Electron. Mat.*, vol. 24, P 805, 1995.
- ¹³ I. Gontijo, T. Krauss, J.H. Marsh, and R. M. De La Rue, *IEEE J. Quantum Electron.*, vol 30, P S779, 1994.
- ¹⁴ M Katayama, Y. Tokuda, N. Ando, Y. Inoue, A. Usami, T. Wada, *Appl. Phys. Lett.*, vol. 54, P 2559, 1989.
- ¹⁵ F. Hasegawa, N. Yamamoto, Y. Nannichi, *Appl. Phys. Lett.*, vol. 45, P 461, 1984.
- ¹⁶ J. Gyulai, J. W. Mayer, I. V. Mitchell, and V. Rodriguez, *Appl. Phys. Lett.*, vol. 17, P 332 1970.
- ¹⁷ K. V. Vaidyaathan, M. J. Helix, D. J. Wolfrod, B. G. Streetman, R. J. Battner, and C. A. Evans Jr., *J. Electrochem. Soc.*, vol. 124, P 1781 1977.
- ¹⁸ T. P. Ma, *IEEE Trans. Eletron. Dev.*, vol. 45, P 680, 1998.

- ¹⁹ D. G. Deppe L. J. Guido, N. Holonyak, Jr., K. C. Hsieh, R. D. Burnham, R. L. Thorton, T. L. Paoli, *Appl. Phys. Lett.*, vol. 49, P 510, 1986.
- ²⁰ S. Bürkner, M. Maier, E. C. Larkns, W. Rothmund, E. P. O'Rielly, J. D. Ralston, *J. Electron. Mat.*, vol. 24, P 805, 1995.
- ²¹ W.J. Choi, J.I. Lee, I.K. Han, K.N. Kan, Y. Kim, H.L. Park, and K. Cho, *J. Mat. Sci. Lett.*, vol 13, P 326, 1994.
- ²² W.J. Choi, S.K. Lee, J. Zhang, Y. Kim, S.K. Kim, J. I. Lee, K.N. Kang, and K. Cho, *Jpn. J. Appl. Phys.*, vol 34, P L418, 1995.
- ²³ W.J. Choi, S.K. Lee, Y. Kim, S.K. Kim, J. I. Lee, K.N. Kang, N. Park, H.L. Park, and K. Cho, *Mat. Sci. Lett.*, vol 14, P 1433, 1995.
- ²⁴ D. L. Smith, *J. Vac. Sci. Technol.*, vol. 11, P 1843, 1993.
- ²⁵ T. Blaz, R. Brendel, R. Hezel, *J. Appl. Phys.*, vol. 76, P 4811, 1994.
- ²⁶ M.Kuzuhara, *J. Appl. Phys.*, vol. 66, P 5833, 1989.
- ²⁷ A.Hidaka, H. Ikoma, *Jap. J. Appl. Phys.*, vol.34, PART-1, P 4641, 1995.
- ²⁸ B. Mombelli, A. Elfajiri, C. Couturier, A. S. Barriere, *Thin Solid Films*, vol. 256, P 80, 1995.
- ²⁹ M. Yamamoto, T. Negishi, J. Igarashi, H. Ikoma, *Jap. J. Appl. Phys.*, vol.33, PART-1, P 4820, 1994.
- ³⁰ G. N. Chaudhari, V. J. Rao, *Semicond. Sci. technolo.*, vol. 8, P 412, 1993.
- ³¹ B.S. Ooi, A.C. Bryce, and J. H. Marsh, *Electron. Lett.*, vol. 31, P 449, 1995.
- ³² J. Beauvais, J.H. Marsh, A. H. Kean, A. C. Bryce, C. Button, *Electron. Lett.*, vol. 28, P 670, 1992.
- ³³ S.G. Ayling, J. Beauvais, and J.H. Marsh, *Electron. Lett.*, vol 28, P 2240, 1992.
- ³⁴ I. Gontijo, T. Krauss, J.H. Marsh, R.M. De La Rue, *IEEE J. Quant. Electron.*, vol. 30, P 1189, 1994.
- ³⁵ T.Y. Tan, and U. Gosele, *Appl. Phys. Lett.*, vol 52, P 1383, 1988.
- ³⁶ I. Gontijo, T. Krauss, R.M. De La Rue, J.S. Roberts, J.H. Marsh, *Electron. Lett.*, vol. 30, P145, 1994.
- ³⁷ K. McIlvaney, J. Carson, A. C. Bryce, J. H. Marsh, R. Nicklin, *Electron. Lett.*, vol. 31, P553, 1995.
- ³⁸ X. Haung, A. J. Seeds, J. S. Roberts, *Appl. Phys. Lett.*, vol. 71, P 765, 1997.
- ³⁹ J. H. Marsh, P. Cusumano, A. C. Bryce, B. S. Ooi, S. G. Ayling, *Proc. SPIE*, vol. 74, P 2401, 1995.
- ⁴⁰ B.S. Ooi, N.W. Street, S.G. Ayling, A.C. Bryce, J.H. Marsh, and J.S. Roberts, *Int. J. Optoelectron.*, vol. 10, P 257, 1995.

- ⁴¹ B. S. Ooi, K. Mcilvaney, M. W. Street, A. S. Helmy, S. G. Ayling, A. C. Bryce, J. H. Marsh, J. S. Roberts, *IEEE J. Quant. Electron.*, vol. 33, P 1784, 1997.
- ⁴² F. Camacho Paez, "Comparative study of passive configuration in semiconductor lasers," Ph.D. Thesis, Glasgow University, P 113, 1997.
- ⁴³ C. J. Hamilton, "Novel Structures and fabrication techniques for the observation of solitons in AlGaAs," Ph.D. Thesis, Glasgow University, P 115, 1995.
- ⁴⁴ "Thermophysical properties of matter," TPRC Data series, vol. 13.
- ⁴⁵ C. Jeynes, "Internal reports on RBS studies of GaAs/AlGaAs, and GaAs/InGaAs structures capped with SiO₂ and SrF₂," (1993, 1995, and 1998).
- ⁴⁶ E.V.K. Rao, A. Hamoudi, Ph. Krauz, M. Juhel, and H. Thibierge, *Appl. Phys. Lett.*, vol 66, P 472, 1995.
- ⁴⁷ S. K. Ghandhi, *VLSI Fabrication Principles*, Wiley, New York, P530, 1994.(and references therein)
- ⁴⁸ F. C. Schilling, K. G. Steiner, Y. S. Obeng, *J. Appl. Phys.*, vol. 78, P 4174, 1995.
- ⁴⁹ W. L. Warren, M. R. Shaneyfelt, D. M. Fleetwood, P. S. Winokur, *Appl. Phys.Lett.*, vol. 67, P 995, 1995.
- ⁵⁰ D. G. Deppe and N. Holonyak, Jr., *J. Appl. Phys.*, vol. 64, P R93, 1988.
- ⁵¹ A.C. Bryce, F. Camacho, E.A. Avrutin, and J.H. Marsh, *IEEE J. Quantum Electron.*, vol. 33, P 1784, 1997.
- ⁵² S. Singh, F. Baiocchi, A. D. Butherus, W. H. Grodkiewicz, B. Schwartz, L. G. Van Uitert, L. Yesis, and G. J. Zydzik, *J. Appl. Phys.*, vol. 64, P 4194, 1988.
- ⁵³ T. Y. Tien and F. A. Hummel, *J. Am. Ceram. Soc.*, vol. 45, P 422, 1962.
- ⁵⁴ P. Cusumano, A. Saher Helmy, B. S. Ooi, S. G. Ayling, A. C. Bryce, J. H. Marsh, B. Voegelé, and M. J. Rose, *Mat. Res. Soc. Symp. Proc.*, vol.450 , P 419, 1996.
- ⁵⁵ P. Cusumano, B. S. Ooi, A. Saher Helmy, S. G. Ayling, A. C. Bryce, J. H. Marsh, B. Voegelé, and M. J. Rose, *J. Appl. Phys.*, vol. 81, P 2445, 1997.
- ⁵⁶ S. M. Lee, M. Park, K. C. Park, J. T. Bark, J. Jang, *Jpn. J. Appl. Phys.*, vol. 35, P 1579, 1996.
- ⁵⁷ M. Yoshimaru, S. Koizumi, K. Shimokawa, *J. Vac. Sci. Technol. A*, vol. 15, P 2908, 1997.
- ⁵⁸ S. W. Lim, Y. Shimogaki, Y. Nakano, K. Tada, H. komiyama, *Appl. Phys. Lett.*, vol. 68, P 832, 1996.
- ⁵⁹ H. Kudo, R. Shinohara, S. Takeishi, N. Awaji, M. Yamada, *Jpn. J. Appl. Phys.*, vol. 35, P 1583, 1996.
- ⁶⁰ M. Yoshimaru, S. Kizumi, K. Shimokawa, *J. Vac. Sci. Technol. A*, vol. 15, P 2915, 1997.

- ⁶¹ E. F. da Silva, Jr., Y. Nishioka, T. P. Ma, *IEEE Trans. Nuc. Sci.*, vol. 34, P 1190, 1987.
- ⁶² Y. Nishioka, E. F. da Silva, Jr., Y. Wang T. P. Ma, *IEEE Electron Dev. Lett.*, vol. 9, P 38, 1988.
- ⁶³ M. V. Bazylenko, M. Gross, A. Simonian, P. L. Chu, *J. Vac. Sci. Technol. A*, vol. 14, P 336, 1996.
- ⁶⁴ S. M. Han, E. S. Aydil, , *J. Vac. Sci. Technol. A*, vol. 15, P 2893, 1997.
- ⁶⁵ K. Kim, J. Song, D. Kwon, G. S. Lee, *Appl. Phys. Lett.*, vol. 72, P 1247, 1998.
- ⁶⁶ C. J. Hamilton, J. H. Marsh, D. C. Hutchings, J. S. Aitchison, G. T. Kennedy, W. Sibbett, *Appl. Phys. Lett.*, vol. 68, P 3078, 1996.
- ⁶⁷ M. W. Street, N. D. Whitbread, D. C. Hutchings, J. M. Arnold, J. H. Marsh J. S. Aitchison, G.T. Kennedy, and W. Sibbett, *Opt. Lett.*, vol. 22, P1600, 1997.
- ⁶⁸ Y. Kim, S. Yuan, R. Leon, C. Jagadish, M. Gal, M. B. Johnston, M. R. Phillips, M. A. Stevens Kalceff, J. Zou, D. J. H. Cockayne, *J. Appl. Phys.*, vol 34, P 5014, 1996.
- ⁶⁹ R. M. Cohen, G. Li, C. Jagadish, P. T. Burke, and M. Gal, *Appl. Phys. Lett.*, vol. 73, P 803, 1998.
- ⁷⁰ S. Yuan, Y. Kim, H. H. Tan, C. jagadish, P. T. Burke, L. V. Dao, M. Gal, M. C. Y. Chan, E. H. Li, J. Zou, D. Q. Cai, D. J. H. Cockayne, R. M. Cohen, *J. Appl. Phys.*, vol. 83, P 1305, 1998.
- ⁷¹ H. Barbe, R. L. Van Meirhaeghe, F Cardon, *Semicond. Sci. Technol.*, vol. 3, P 853, 1988.
- ⁷² R. M. Cohen, *Mat. Sci. & Eng Reports*, vol. R20, P 167, 1997.
- ⁷³ S. Brunkner, M. Maier, E. C. Larkins, W. Rothmund, E. P. O'Reilly, and J. D. Ralston, *J. Electron. Mat.*, vol. 24, 805, 1995.
- ⁷⁴ W. K. Choi, C. K. Choo, K. K. Han, J. H. Chen, F. C. Loh, and K. L. Tan, *J. Appl. Phys.* , vol. 83, P 2308, 1998.
- ⁷⁵ S. Hicks, S. K. Murad, I. Sturrock, C. D. W. Wilkinson, *Microelectronics Engineering*, vol 35, P 41, 1997.
- ⁷⁶ W. J. Choi, S. Lee, S. K. Kim, J. I. Lee, K. N. Kang, N. Park, H. L. Park, and K. Cho, *J. Mat. Sci. Let.*, vol. 14, P 1433, 1995.
- ⁷⁷ G. Emiliani, S. Scaglione, *J. Vac. Sci. Technolo., A*, vol. 5, P 1824, 1987.
- ⁷⁸ A. Brunet-Bruneau, J. Rivory, B. Rafin, J. Y. Robic, P. Chaton, *Appl. Phys. Lett.*, vol. 82, P 330, 1998.
- ⁷⁹ A. Saher Helmy, J. S. Aitchison, and J. H. Marsh, *IEEE Journal of Selected Topics in Quantum Electronics*, vol. 4, P 653, 1998.

CHARACTERISATION USING OPTICAL TECHNIQUES

Along with the interest in exploiting the various processes of intermixing came the need to characterise the amount of compositional intermixing associated with each process. When a QWI process is considered for realising PICs and OEICs, there is a set of parameters, which must be characterised. These parameters include features, figures of merit, limitations and drawbacks of any given process. Optical, electrical, and other diagnostic means have been utilised in these studies. Characterisation tools, however, are lagging in comparison to technology, this might be due, partially, to the lack of comprehensive mathematical models of the processes involved, and partially to the complexity of the parameters that need to be characterised. There is therefore a need for a powerful, comprehensive, yet simple and versatile, set of measurement techniques to characterise QWI processes.

I. OPTICAL SPECTROSCOPY

To investigate QWI, the bandgap energies and the change of composition in the structures need to be probed. Optical characterisation of semiconductors means monitoring the interaction between semiconductors and optical fields. Optical fields are defined here to include a region of the electromagnetic spectrum from the ultraviolet all the way through to the deep infrared, this regime being sufficiently wide to probe almost every property of bulk, and structured semiconductors. There are many motivations for using optical measurements to characterise semiconductors.¹ They stand out because they are non-destructive, and need little sample preparation, as opposed to TEM for example. Optical measurements are thought to be more versatile than electrical measurements because they do not need electrical contacts to be made to the samples. They have the ability of producing two and three-dimensional maps of semiconductor parameters, by simply scanning a laser beam across the sample, with an appropriate data acquisition and control system. Aspects such as depth of focus, spot size and absorption length play an significant role in setting the limits of optical measurements. Depth of focus is the distance along the direction of propagation of the optical field where the beams are sufficiently focused to give a output signal with a detectable signal to noise ratio. It is related to the numerical aperture, NA , and the wavelength, λ , by the relation,²

$$\Delta z = \pm \frac{\lambda}{2(NA)^2} \quad (5.1)$$

The spot size of an optical beam is important since it sets the lower boundary of the spatial resolution of measurement set-up. It relates the wavelength, λ , the focal length of the lens, F , and the its diameter, D , through the relation,¹

$$d = 1.22 \frac{F\lambda}{D} \quad (5.2)$$

Also equally important, is the absorption length of the light field. For a field intensity in the form of,

$$I = I_0 \exp[-\alpha z] \quad (5.3)$$

where α is the absorption coefficient of the field. The distance $1/\alpha$ is where the field intensity is reduced to $1/e$ of its peak value.

Although the first report of IFVD demonstrated intermixing by observing the lasing wavelength of lasers fabricated out of the intermixed material,³ measurements of the position of the PL peak are the most widely used means of measuring intermixing for all compound semiconductors.⁴ These can provide information about the amount of QWI with

depth by placing QWs at different depths in the structure.^{5,6,7} In addition, appropriate PL techniques can convey information about the spatial distribution of compositional intermixing,^{8,9,10} and the photogenerated carrier lifetime.^{10,11} The bandgap shifts can be measured using absorption and photocurrent, but PL is simpler to implement and interpret.^{12,13} Raman backscattering has also been used to investigate structural properties of the disordered lattice of various material systems.^{14,15} In principle such measurements can be quite informative, however practical probing of the QWs within the lattice and the interpretation of the results is an involved task.¹ The bound energy levels in a QW have been measured using photoluminescence excitation, PLE, and Photoreflectance, PR. Profiles of inter-diffused and as-grown QWs can be obtained when using the bound energy levels measured using PLE or PR in conjunction with a Schrödinger equation solver. The Schrödinger solver can fit the energies measured for the bound states to an appropriate potential profile.^{16,17}

In this chapter we shall present a number of optical measurements carried out to characterise various aspects of the process of QWI using IFVD. Time resolved PL is used to investigate the effect of intermixing on the photogenerated carrier life times in intermixed lattice. A PL micro-probe is used to carry out spatially resolved measurements, by which the variation in the PL energy along gratings with alternating intermixed and inhibited regions can be investigated. Also Raman micro-probe analysis is used to carry out spatially resolved investigations of the change in Raman signals as a function of intermixing. PLE was finally used to investigate QW shapes prior to, and after annealing.

II. PHOTOLUMINESCENCE SPECTROSCOPY

Photoluminescence is the light emitted by a material when optically excited. In semiconductors luminescence occurs mainly due to radiative recombination following the absorption of an electron hole pair across the bandgap. Other radiative transitions depend on the energy levels available in the crystal lattice. In addition to the conduction and valence levels, neutral donors and neutral acceptor, for example, can contribute to radiative transitions. The energy of excitation for any radiative transition has to be the same or larger than the energy levels associated with this transition. When discussing photoluminescence, absorption will also have to be involved since both processes are closely coupled. Because of the importance of excitons in GaAs/AlGaAs QWs, emphasis will be made on the PL resulting from exciton transitions.

An exciton is a bound electron hole pair, which then has a single particle nature. This binding energy stems from the Coulomb interactions when electrons and holes are in proximity. In bulk semiconductors exciton-dominated-recombination is not observed

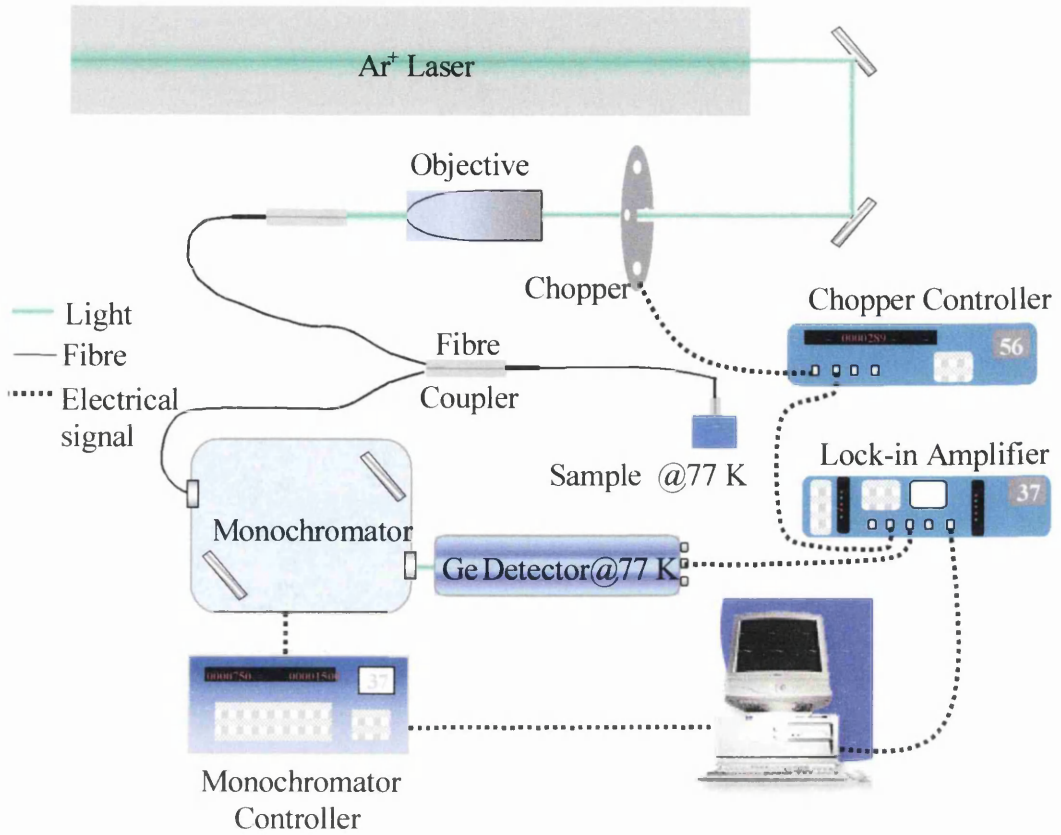


Fig. 5.1 A schematic for the PL set-up used at Glasgow University.

readily. However, due to the proximity posed in a quantum-confined heterostructure, their 2D binding energy is larger than that in 3D. Therefore it is possible to observe PL signals resulting from exciton recombination even at room temperature in quantum confined heterostructures with energies expressed as,

$$\hbar\nu = E_{gap} - E_{ex}^1 \tag{5.4}$$

where $\hbar\nu$ is the energy of the emitted photon, E_{gap} is the bandgap energy of the semiconductor, and E_{ex}^1 is the binding energy of the exciton of the ground level, e1-hh1. If the dimensions of the heterostructure, where the excitons reside, are much less than the effective Bohr radius, $a_b \approx 10$ nm, then the energy of the bound excitons can be expressed by the Rydberg value, $R_{n,2D}$, such that,

$$R_{n,2D} = R_{3D} \frac{1}{\left(n - \frac{1}{2}\right)^2} \tag{5.5}$$

Where R_{3D} is the 3D exciton binding energy, and is equal to 4.2 meV for GaAs,¹⁸ so the e1-hh1 transition $R_{n,2D} = 4R_{3D}$.¹⁹ These excitonic transitions are observed upon exciting a piece of quantum confined heterostructure with a photon energy larger than that of the bandgap

energy. Upon monitoring the energy of the PL signal obtained from the semiconductor, information can be obtained about the band gap of the probed material. Moreover, the quality and uniformity of the quantum confined heterostructures investigated will affect both, the full width at half maximum (FWHM) and the intensity of the PL signal.

The set-up used within this work to carry out the PL measurements is shown in Fig. 5.1. Where an Ar^+ modulated laser is shone on the sample, using a fibre 3dB coupler. The resulting luminescence is collected in the same fibre and partially directed by the coupler to a spectrometer, and a Ge detector operating at 77 K. The signal from the detector is then routed to a lock-in amplifier where it is collected using a computer running *LabView*, a data acquisition software. The same software package controls the spectrometer drivers.

As a consequence of the short, $< 1 \mu\text{m}$, wavelengths used to excite the PL signal, the spatial resolution of the measurements can be less than $1 \mu\text{m}$ when using far-field optics.¹ Spatially resolved measurements were realised by scanning the surface of the sample across the beam using

precision X-Y stage. As the laser excitation, and hence the PL collection, is scanned across the sample, images of the PL can be obtained. A drawback inherent in the PL technique lies in the fact that carriers generated during excitation can diffuse before band-to-band recombination takes place. Such photogenerated carriers will diffuse beyond the excitation region. Where the carriers take place, the resulting PL signal will be generated from the region with the fastest recombination rate. A PL signal with photon energy equal to that of the smallest bandgap in the vicinity of the excitation beam is the outcome of such a sequence of events. The carrier recombination in lower bandgap

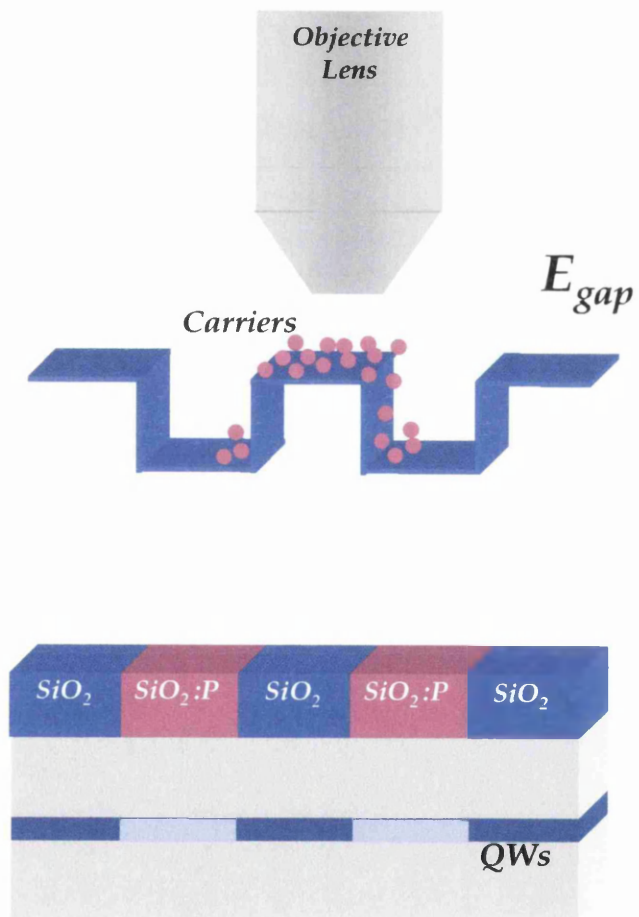


Fig. 5.2 A schematic for the photogenerated carriers in a bandgap grating induced by IFVD using $\text{SiO}_2:\text{P}/\text{SiO}_2$ caps. The significance of the carrier diffusion depends on both, the spot size of the excitation laser beam, and the period of the bandgap grating.

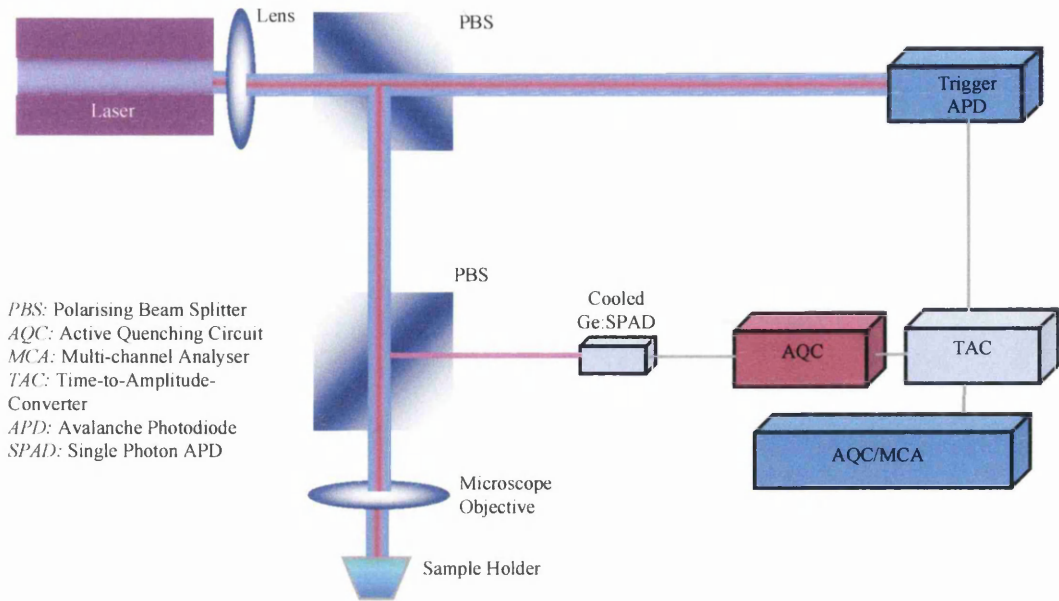


Fig. 5.3 A schematic of the setup used for spatially and temporally resolved PL measurements.

regions is shown schematically in Fig. 5.2. It should be noted that vicinity in this context is of the order of the diffusion length of carriers, which is $\sim 0.68 \mu\text{m}$ for a 10 nm GaAs QW with $\text{Al}_{0.3}\text{Ga}_{0.7}\text{As}$ barriers.²⁰ This poses a limitation on the PL technique when measuring different bandgaps in close proximity and ultimately sets a lower limit on the spatial resolution of the measurement.

Another way of using PL signals to probe further the semiconductor parameters is to temporally resolve the PL emission process. Using time histogram of the PL, the average lifetime of the carriers, inducing the radiation, can be calculated. Several factors, mainly the concentration of the non-radiative recombination centres in the excited material, govern the time decay of the radiative recombination process.

When both temporally and spatially resolved PL measurements are carried out on samples with different bandgap features on them, valuable information can be obtained about the change of, not only the bandgap, but also the carrier life time in the samples, as will be presented below.

II.A. Studying the Extent of Quantum Well Intermixing using a Photoluminescence Micro-Probe

Temporally and spatially resolved PL measurements were carried out, using a set-up shown in Fig. 5.3, to investigate the spatial resolution of the intermixing process as well as the effect of intermixing on the photogenerated carrier lifetime. The samples used were from a nominally un-doped MQW structure, as shown in Appendix A (*waveguide MQW structures*). Samples were prepared with grating fields consisting of alternating intermixed

and non-intermixed stripes with different dimensions. Gratings with a 1:1 mark to space ratio with periods varying from 4 μm to 22 μm were fabricated. The intermixed and non-intermixed regions were capped with SiO_2 and $\text{SiO}_2\text{:P}$ respectively.²¹ Two $2 \times 2 \text{ mm}^2$ rectangular fields adjacent to the grating were also formed, one of which was capped with SiO_2 and the other with $\text{SiO}_2\text{:P}$ to produce control areas for PL studies. The samples were annealed at 925 $^\circ\text{C}$ for 60 s. In Fig. 5.4 (c) the 77 K PL spectra measured from the intermixed and non-intermixed areas adjacent to the gratings are shown. A differential shift of $\sim 30 \text{ nm}$ can be seen for the sample. Temporally and spatially resolved PL measurements were then performed.

A passively Q-switched semiconductor laser producing picojoule pulses of $\sim 20 \text{ ps}$ duration at a repetition rate of 1 MHz,²² was used as the excitation source, and a Si single-photon avalanche diode (Si-SPAD) was used for detection of the luminescence.²³ Besides the general advantages found in using solid-state devices when compared with photomultipliers, Si-SPADs have a superior photon detection efficiency as well as a faster and undistorted time response.^{24,25} The whole instrument is mounted on a

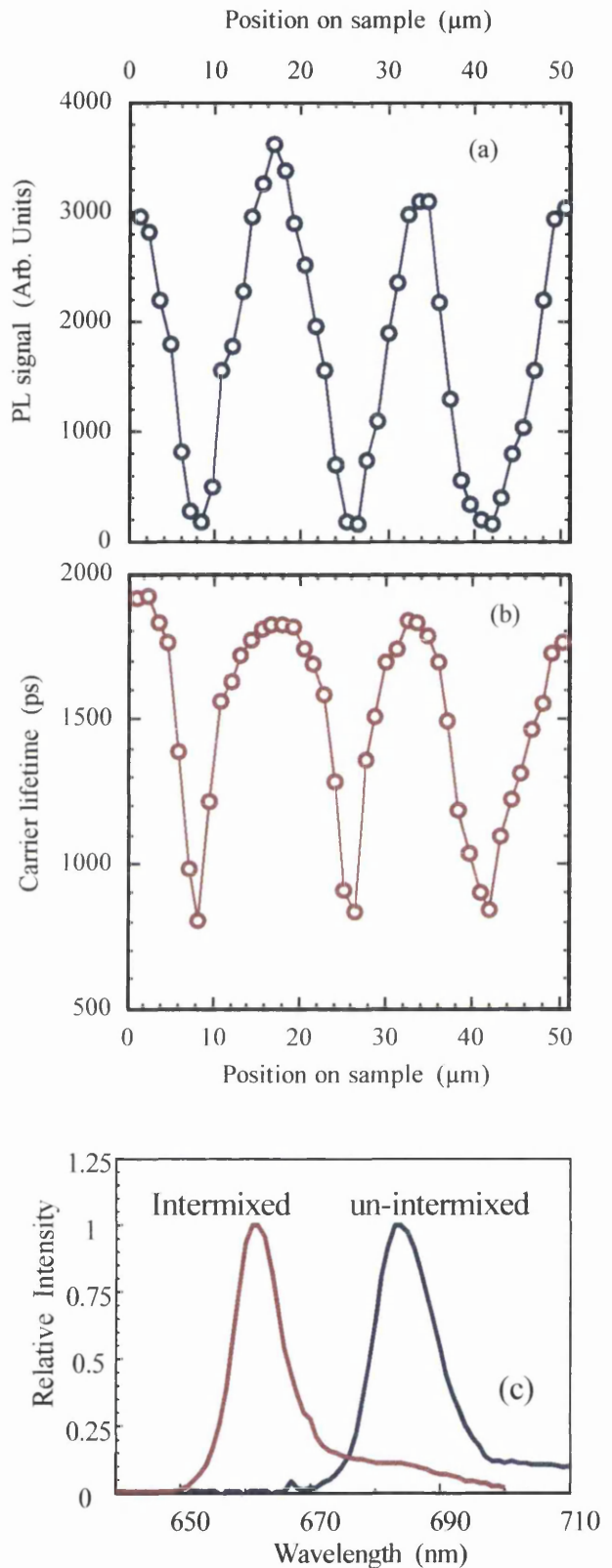


Fig. 5.4. Scan across a grating sample with a period of 16 μm for (a) the PL signal at the un-intermixed wavelength peak, (b) the photogenerated carrier lifetime and (c) the PL signals from the intermixed and un-intermixed parts of the sample.

microscope which launches and collects the light as can be seen in Fig. 5.3. In addition to producing a PL signal, the laser pulses trigger the avalanche photodetector, which starts the time-to-amplitude converter. This converter is terminated by the PL signal detected from the sample. From the amplitude of the time-to-amplitude converter signal, the luminescence decay time can then be obtained after taking the instrument time response into account.²⁶ The time domain instrumental response in the system is around 80 ps (FWHM).

The small active area used ($\sim 7 \mu\text{m}$ diameter), is a considerable advantage in spatially resolved applications, giving a high spatial

resolution with low sensitivity to spurious backscatter. However the detector size will be a limiting factor for grating periods of a comparable size.

The wavelength of excitation was 677 nm and the laser was focused onto the sample to a spot size of $\sim 2 \mu\text{m}$. PL was detected in the wavelength band $690 \pm 5 \text{ nm}$, which corresponds to the peak of emission of the non-intermixed material. Data were acquired for a fixed amount of time for each point of measurement, which were equally spaced by about $1.5 \mu\text{m}$. Once the PL decay times had been measured, their FWHM, peak of emission, and area (the integrated PL intensity) could be calculated. The experimental PL decays were further analysed by deconvolution of the instrumental response with an exponential function, to obtain the sample (1/e) decay times.²⁷ In general, the decays fitted well by single exponential functions, with time constants varying between 3 ns, for the non-intermixed regions, to approximately 1 ns, for the intermixed regions.

In Fig. 5.4 (a) and (b), the integrated PL intensity and the decay time FWHM as functions of position are shown respectively. The grating is clearly evident in both curves, having a period of approximately $16 \mu\text{m}$. The spatial resolution of the intermixing process

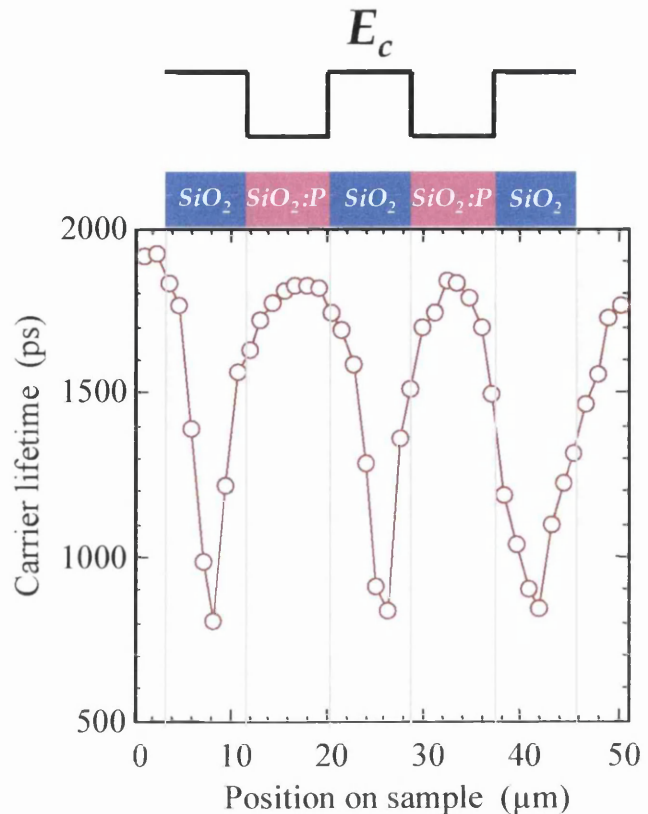


Fig. 5.5. Scan across a grating sample with a period of $16 \mu\text{m}$ for the photogenerated carrier lifetime. The dielectric cap grating used for intermixing and the resulting bandgap grating are also shown.

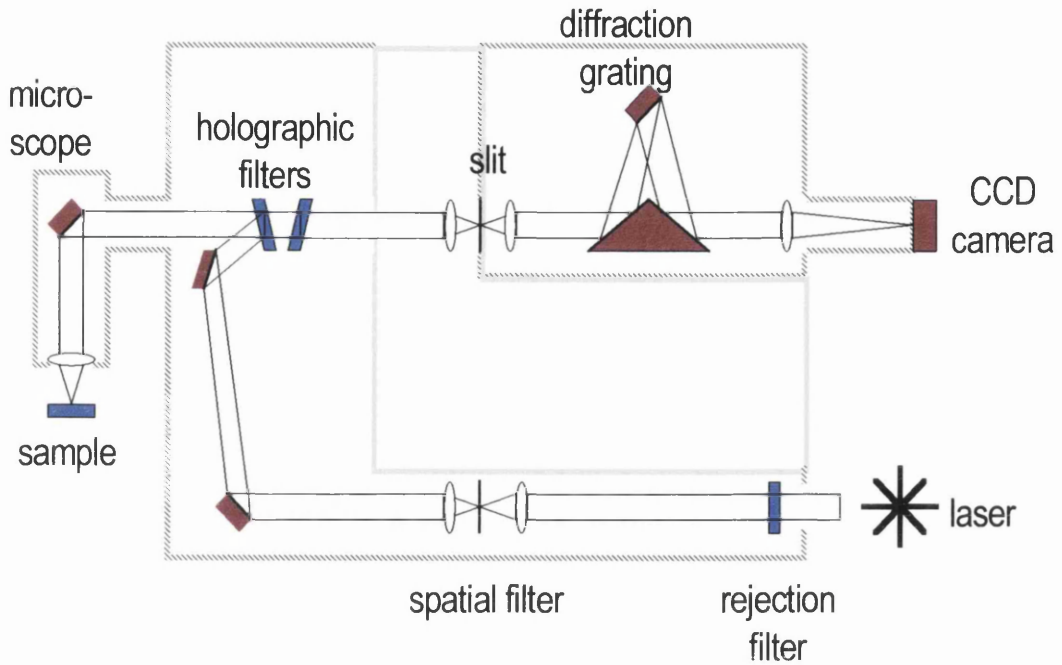


Fig. 5.6 A schematic diagram for the Raman microprobe instrument, from Renishaw, used to acquire the measurements presented in this work.

can be estimated by taking it to be half of the distance between the 10%-90% points in the oscillations in Fig. 5.4. Using data from the FWHM results and from exponential fitting, the spatial resolution and standard deviation obtained are $2.2 \mu\text{m}$ and $0.6 \mu\text{m}$ respectively. If, instead, data from the spatially resolved integrated PL peak are used, the values obtained are $3 \mu\text{m}$ and $0.4 \mu\text{m}$ respectively. The photogenerated carrier lifetime is strongly dependent on the concentration of the non-radiative recombination centres in the lattice. In the samples investigated, some non-radiative recombination centres are produced during growth phase, and are uniformly distributed within the lattice. The IFVD process also generates point defects. These defects will have a concentration related to the position with respect to the dielectric caps used, and hence the amount of intermixing achieved. In the case of the grating, the defect concentration will also have a spatial variation following that of the dielectric caps, and the bandgap. The effects of the laser spot size and the finite detection area on the spatial resolution presented above have not been taken into account. By knowing the laser spatial profile, it should be possible to de-convolute the finite sizes of the laser spot and detected area from the measured results, to obtain the true spatial resolution. The scan profiles obtained, however, imply that the spatial resolution is equal to or better than that observed in this experiment.

By analysing the information obtained here, the following points can be made:

- The detection area of the microscope is in the order of $7 \mu\text{m}$ and the laser spot size was $2 \mu\text{m}$.

- The minority carrier diffusion length in 10 nm QWs with $\text{Al}_{0.3}\text{Ga}_{0.7}\text{As}$ barriers was reported to be $0.68 \mu\text{m}$ at room temperature.²⁰
- It is interesting to note that the FWHM line scan has maxima, which are wider than its minima. This agrees very well with the assumptions presented above. As illustrated in Fig. 5.2, one would expect a larger and more flat region where the smaller bandgap takes place since this is where the smallest recombination lifetime will take place. It is thought that the 10 nm tolerance of the spectral filter at the detector allows this effect to be more apparent since the carriers recombining in the lower bandgap region will have a different energy from those recombining in the illuminated, higher bandgap, region (see Fig. 5.2). Therefore a narrow-band notch filter will allow us to monitor only the monitor the recombination from the higher bandgap region while illuminated by the excitation laser.
- The integrated PL intensity curve is more symmetrical. This may be due to the size of the detection area, being $\sim 7 \mu\text{m}$, and hence collecting PL signal beyond the $2 \mu\text{m}$ excitation area. Another factor is the spectral bandwidth of the detection filter, being 10 nm, which leads to measuring a PL signal integrated over the spectral width. These two factors allow the PL photons generated by the diffused carriers to contribute to the total number of detected photons, even though being of different energy, and hence result in an apparently symmetric scan profile.
- For carrier diffusion not to affect the resolution of the measurement in a bandgap grating (see Fig. 5.2), two conditions must be satisfied:
 - The spot size of the excitation laser beam plus twice the carrier diffusion length should be much smaller than, the minimum feature in the bandgap grating. This is to minimise the number of generated carriers that can diffuse and recombine in the lower bandgap region.
 - The detection area in the PL set up, determined by the numerical aperture of the detector optics, should be much smaller than the minimum feature in the bandgap grating. A detection area equal to or less than the excitation area can eliminate the contribution from the carriers that diffuse beyond the excitation area. The limit of this criterion is to use near field optics such as SNOM and STM, for excitation and detection sizes $\geq \lambda/40$.²⁰

Nevertheless, the measurements above indicate that the spatial resolution of the intermixing process is better than $3 \mu\text{m}$, with the measurements being limited by photogenerated carrier diffusion and the size of the detection aperture. To the best of our knowledge, this is the highest spatial resolution measured of QW intermixing using the TRPL technique. Previous measurements of QWs intermixed using, similar IFVD process

as well as a pulsed laser technique had established an upper limit of about 5 and 20 μm respectively for the spatial resolution of these processes.^{10,28} Although the resolution observed is that of the bandgap patterning, the measurements do not confirm that the bandgap difference between the intermixed and un-intermixed region within the grating is the same as that of the large areas tested (30 nm). This is because the measurements are not spectrally resolved, and instead is based on detecting the PL signal magnitude in a constant spectral region. This can be overcome if the following points are taken into account:

- A map of the photogenerated carrier lifetime across the grating should be generated, but after comparing the obtained lifetimes with those of large areas of uniform, intermixed and un-intermixed regions. This will ensure the detection of the deviation of the degree of intermixing in different parts of the grating from those obtained in large area.
- Being able to resolve each PL measurement spectrally along the grating so the actual PL peak at each point is obtained.

II.B. Spectrally Resolved Photoluminescence Micro-Probe Measurements

Probing the absolute amount of intermixing in gratings with dimensions of $\sim 10 \mu\text{m}$ was not possible by the set-up used in the previous section. However such bandgap-shifted gratings have many attractive applications in the field of integrated optics. They can be used for light reflection or to periodically modulate optical coefficients, such as $\chi^{(2)}$, to achieve phase matching.²⁹ Although the task of measuring such bandgap gratings can be carried out using scanning near field optical and tunnelling microscopy, SNOM and STM,³⁰ more simple experiments devised to measure the bandgap of such features should prove valuable.

Measurements were carried out on gratings fabricated in a similar way to that of the samples investigated using the spatially and temporally resolved PL system discussed in the previous section. The wafer structure used for this experiment consisted of four QW *p-i-n* doped heterostructure, as described in Appendix A (*wide optical waveguide 4QW laser structure*). A Renishaw 'Ramascop' equipped with a sample positioning stage with a precision XYZ mechanical system was used, and is shown in Fig. 5.6. At every position, the spectrometer of the Ramascop was scanned across a pre-set spectral regime to cover the spectral region of the PL emission. Hence, at every point in the sampled area, a whole spectrum was obtained, after which the PL peak position could be determined using curve fitting.

The peak wavelength as a function of position along a 4 and a 12 μm grating are shown in Fig. 5.7 (a) and (b). The PL wavelength varies between 850.5 nm and 851.5 nm in case of the 4 μm grating, resulting in a differential shift of 1 nm. For the 12 μm grating, the

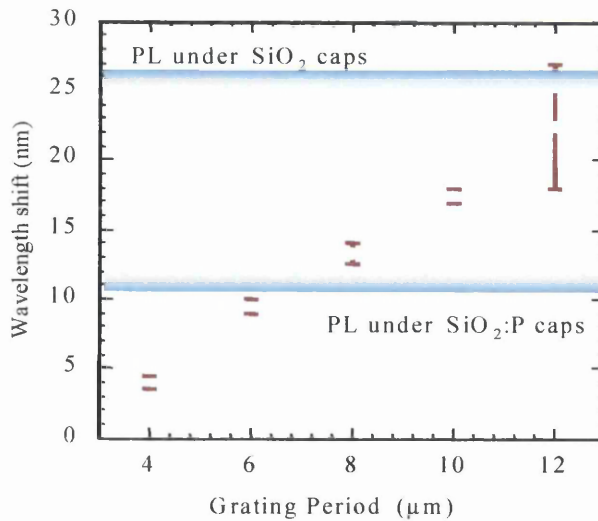


Fig. 5.8 PL wavelength shift as a function of the grating period obtained from (error bars) the spectrally and spatially resolved PL. The blue horizontal lines indicate the lower and upper limits in annealing with large area caps

measurements to obtain the resolution limit of the dielectric cap annealing induced intermixed were conducted using a constant duty cycle grating with a varying filling factor of the intermixing cap. While this technique can give some information about the ultimate resolution of the process, it can be very difficult to resolve the effect we have seen in our measurements because:

- i. The observations reported here take place for grating periods $\leq 12 \mu\text{m}$, where the effect of excitation spot size, PL collection area, and photogenerated carrier life time have detrimental impact on the results and can surely impact the interpretation of the results.
- ii. A single micrometer-scale stripe of dielectric cap that inhibits intermixing within a larger area of a cap that promotes intermixing, or vice versa can be used to eliminate the carrier diffusion from affecting the resolution studies. However such measurements will not give accurate information about what takes place in 1:1 grating sample with the same stripe dimensions. This is because the effects of the size dependent intermixing will give different results in both samples.

In this section we have investigated the spatial resolution of the dielectric cap annealing induced intermixing process. From spatially and temporally resolved PL measurements, resolution better than $3 \mu\text{m}$ was observed. However, indications of carrier diffusion into the neighbouring, low bandgap regions, were evident from the TRPL measurements. We have also seen sufficient evidence to believe that dielectric cap annealing induced intermixed is dependent on the area of the caps used for enhancing and inhibiting intermixing. This can be seen in the amounts of intermixing induced in 1:1 grating periods below $8 \mu\text{m}$. Intermixing observed in these gratings is less than that obtained

underneath large area covered with caps such as SiO₂:P, which is known to inhibit intermixing. This result will have a profound impact on applications such as gratings for quasi phase matching applications, where a periodic grating with an approximate period of 1.7 μm is needed at a wavelength of 1.55 μm. Systematic studies to further investigate the phenomenon are in progress.

III. RAMAN SPECTROSCOPY

The light scattered from a laser beam incident onto a sample, when of sufficient intensity, is shifted in energy from that of the original incident laser beam. The shift in energy is due to the interaction of the incident photons with the mechanical modes of the lattice, namely phonons. A resultant net exchange in energy takes place between the laser photons and the lattice phonons. The Raman-scattered photons gain energy upon absorbing a phonon, anti-stoke shifting, or lose energy upon emitting one, stoke shifting. The energy and momentum conservation laws for the scattered photons imply that,

$$\begin{aligned}\hbar v_s &= \hbar v_i \pm \hbar \Omega, \\ \hbar k_s &= \hbar k_i \pm \hbar K,\end{aligned}\tag{5.6}$$

Where v_s and v_i are the scattered and incident photon frequencies, k_s , and k_i are the scattered and incident photon wavevectors. The phonon frequency and wavevector are denoted by Ω and K respectively.

Raman spectroscopy is based on studying the change in energy shift between the incident and scattered optical field. The full theory of Raman scattering is complex, which explains why detailed line shape analysis is seldom used to analyse the results.¹ Different phonon modes correspond to the different configurations by which the lattice can vibrate. There are both transverse and longitudinal phonon modes. Raman modes are also either optical, where atoms of opposite charge vibrate out of phase to give an oscillating dipole moment which couples to light, or acoustic, which are not necessarily between opposite charged atoms and have a constant speed of propagation as $k \rightarrow 0$.¹ In case of compound semiconductors, there will be different vibration modes, and hence Raman peaks, for different sublattices in the crystal. For example, there are AlAs-like and GaAs-like modes in an AlGaAs lattice, which corresponds to the two sublattices available. Much information about a lattice can be obtained by monitoring its different phonon modes, through their interactions with the incident photons.

Raman scattering has been used extensively to characterise a wide variety of lattice parameters of almost all the semiconductor compounds of current interest.¹ The electronic properties, lattice quality, and alloy composition of GaAs/AlGaAs heterostructure layers have been thoroughly investigated using Raman measurements, e.g. by Abstreiter *et al.* in

1978.³¹ For GaAs/AlGaAs heterostructures, the laser penetration depth can vary from 15 nm to 1 μm for excitation wavelengths of 400 nm and 800 nm respectively. These are typical values, since laser penetration depth depends on the compound bandgap and therefore on its composition. For first order Raman back scattering from GaAs alloys (e.g. AlGaAs, InGaAs), only the LO mode appears when the Raman shifts are excited by an optical field along a $\langle 100 \rangle$ surface, only the TO appears when the Raman shifts are excited by an optical field along a $\langle 110 \rangle$ surface and both LO and TO appear when the Raman shifts are excited by an optical field along a $\langle 111 \rangle$ surface. Any mode appearing where it should not (these are called forbidden modes) for a given measurement set up indicates imperfections in the crystal lattice ordering. That is because the crystal order is what determines the lattice vibration configurations and hence the Raman modes. Raman scattering is therefore a suitable tool for investigating lattice disruption due to implantation and annealing induced disordering. Many efforts to utilise Raman scattering were therefore put together to investigate implantation and annealing induced disordering.^{32,33} Because Si still plays a pivotal role in the present semiconductor technology, Raman characterisation has been developed to characterise a vast variety of its properties. Raman scattering was also identified as a valuable tool in studying Si/SiGe lattices as early as 1973 by Brya *et al.*³⁴ Doping and impurity probing, stress and interface characterisation,^{33,35} crystal lattice quality³⁶ and implantation induced damage are some of the properties that can be characterised by Raman scattering. Raman spectroscopy is not only a research tool: it is now systematically used for in-situ monitoring of fabrication processes in industry, because of the high throughput of new system designs.³⁷

Although the spatial resolution of IFVD was studied using spatially resolved PL, the resolution was limited by the excitation spot size, collection area, and diffusion length of the photogenerated carriers. Raman scattering measurements, in contrast, are only limited by the laser spot size, since the scattered light is produced from only the part of lattice illuminated by the laser. Raman measurements have served before as a sensitive technique for detecting and studying disordering in GaAs/AlGaAs heterostructures.³¹ The aim of this study is to examine the use of Raman microprobe techniques in characterising QWI, since they have the potential of better resolution than that of spatially resolved PL. Raman measurements can also give depth information by changing the laser wavelength and/or point of focus.

In this section we show:

- i. It is possible to detect compositional intermixing in GaAs/AlGaAs MQW structures, 1 μm below the surface, using Raman spectroscopy.
- ii. Provisional results on using Raman spectroscopy to quantify the amount of compositional intermixing taking place in GaAs- AlGaAs heterostructures.

- iii. Raman spectroscopy can clearly detect periodic bandgap grating structures, fabricated by intermixing.

Compositional intermixing is expected to take place where the defects exist. Defects are introduced by several fashions depending on the intermixing technology used. For example, in the case of IFVD, defects diffuse

Table 5.1 Observed and reported Raman peaks for the 4QW GaAs/AlGaAs p-i-n structure. The reported peaks are after Abstriter *et al.*³¹

Sample	<i>D</i>		<i>Q</i>	<i>W</i>
	Observed	Closest Reported	GaAs/AlAs	Designation
1	384	382	AlAs like	LO Al _{0.4} Ga _{0.6} As
2	375	374	AlAs like	LO Al _{0.2} Ga _{0.8} As
3	277	274	GaAs like	LO Al _{0.4} Ga _{0.6} As
4	268	269	GaAs like	TO Al _{0.2} Ga _{0.8} As

from the surface towards the QWs, inducing excessive intermixing near the surface, where their concentration is maximum. Therefore the amount of intermixing induced close to the surface will be much more than that induced in the vicinity of the QWs. Hence the aim of this work is to detect the compositional intermixing from the heterostructures associated with the QW layers to acquire accurate information about the compositional intermixing that leads to the bandgap energy shift in the QWs. This will be realised by trying different laser wavelengths, which have different probing depths.

III.A. Studying the Extent of Quantum Well Intermixing using Raman Backscattering Measurements

In this study, two structures are used to investigate whether Raman spectroscopy can detect and quantify the amount of intermixing. A four QW p-i-n doped heterostructure, as shown in Appendix A (*wide optical waveguide 4QW laser structures*), and a nominally un-doped MQW structure, as shown in Appendix A (*waveguide MQW structures*). One set of the 4QW and two sets of the MQW structure were covered with 200 nm of E-gun evaporated SiO₂ and annealed for 60 s at different temperatures between 875 °C and 975 °C.

The Ramascope used, as shown in Fig. 5.6, has a photon energy resolution of 1 cm⁻¹ and uses a CCD electrically cooled to -70 °C. The maximum wavelength is limited by the sensitivity of the CCD camera used for detection and is ~ 1 μm. The room temperature PL spectra of the samples were first measured. After, Raman measurements were carried out and the change in the energy shift of the Raman peaks together with their FWHM were observed as a function of the PL shift measured. Initial experiments to measure the Raman spectra were carried out using a SDL 785 nm laser diode. This was the laser with the lowest energy available, and was used since it will suffer minimal absorption and hence have the

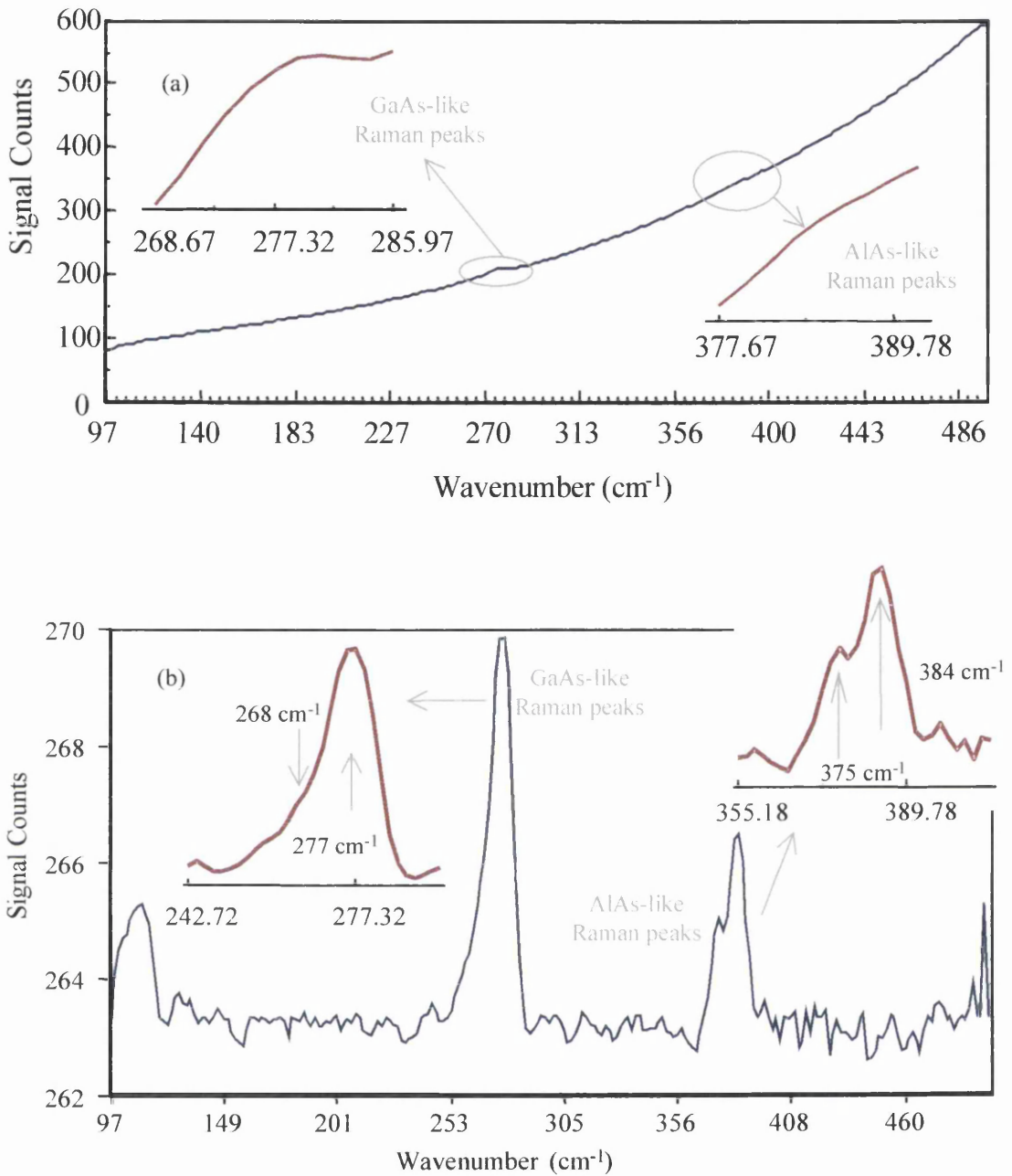


Fig. 5.9 Raman spectra from the as-grown 4QW sample. The Raman spectrum is shown (a) before and (b) after removing the photoluminescence background line. The GaAs-like and AlAs-like Raman spectra are indicated.

longest interaction depth. A strong Raman signal can hence be expected from the QWs. However, no Raman signal was detected using this laser because of the strong PL signal it generates from the QWs. The intense PL signal, with a wavelength of ~ 750 nm for the MQW sample and ~ 850 nm for the 4QW sample, is superimposed on the, relatively weaker, backscattered light from the sample, which is with a wavelength of ~ 800 nm. The Raman signal could not, therefore, be resolved from the background luminescence. A HeNe laser was therefore used instead in the measurements that follow to study the Raman peaks. The incident beam was linearly polarised, in the (111) plane of the samples, the Raman

signal detection was un-polarised, to ensure the detection of all the Raman modes.³⁸ The light was focused with a $\times 50$ objective in a spot size of $0.34 \mu\text{m}$, giving a power density of $38 \text{ mW}\cdot\text{cm}^{-2}$.

III.A.1 p-i-n Laser Structure

The 4QW structure contains GaAs in the QWs and in the 100 nm capping layer, $\text{Al}_{0.2}\text{Ga}_{0.8}\text{As}$ in the lower and upper barrier with a thickness of 300 nm and $\text{Al}_{0.4}\text{Ga}_{0.6}\text{As}$ in the lower and upper cladding, as shown in Appendix A. The photons from the HeNe laser have an energy of 1.96 eV, and will have an absorption length of $\sim 0.4 \mu\text{m}$ GaAs. To avoid absorption within the 100 nm GaAs cap, it was removed after annealing using a $\text{NH}_3:\text{H}_2\text{O}_2$ solution with the ratio of 5:95 for 60 s. The photon will have an absorption length of $1 \mu\text{m}$ in the $\text{Al}_{0.4}\text{Ga}_{0.6}\text{As}$ upper cladding layer and $0.66 \mu\text{m}$ in the $\text{Al}_{0.2}\text{Ga}_{0.8}\text{As}$ barrier region.³⁹ Light will therefore predominately interact with the $\text{Al}_{0.4}\text{Ga}_{0.6}\text{As}$ upper cladding layer producing a Raman spectra, with chances of acquiring Raman spectra also from the $\text{Al}_{0.4}\text{Ga}_{0.6}\text{As}-\text{Al}_{0.2}\text{Ga}_{0.8}\text{As}$ interface.

Raman measurements were carried out on the samples, and the luminescence line from the QWs was subtracted from the spectra after. Curve fitting was carried out subsequently, to identify the energy shift and the FWHM of each Raman peak in every sample. From the spectra, 4 peaks were clearly detected and curve fitted. The information about the Raman peaks is shown in Table 5.1. The table also gives the closest peaks reported for GaAs/AlGaAs lattice.^{31,40}

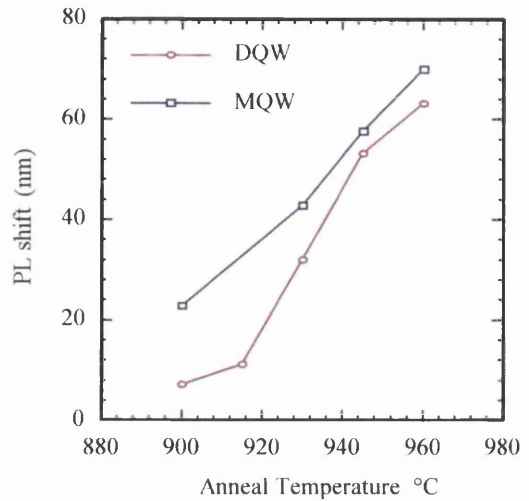


Fig. 5.10 PL wavelength shift for the 2 sets of samples used in the Raman measurements. One set of DQW samples and two other of MQW samples.

Table 5.2 Observed and reported Raman peaks for the MQW GaAs/AlGaAs undoped structure. The reported peaks are after Abstriter *et al.*³¹

Sample	<i>M</i>		<i>Q</i>	<i>W</i>
	Observed	Closest Reported	GaAs/AlAs	Designation
1	382	382	AlAs like	LO $\text{Al}_{0.4}\text{Ga}_{0.6}\text{As}$
2	374	373	AlAs like	TO $\text{Al}_{0.4}\text{Ga}_{0.6}\text{As}$
3	367.8	-	-	-
4	275.1	275	GaAs like	LO $\text{Al}_{0.4}\text{Ga}_{0.6}\text{As}$
5	269	269	GaAs like	TO $\text{Al}_{0.4}\text{Ga}_{0.6}\text{As}$

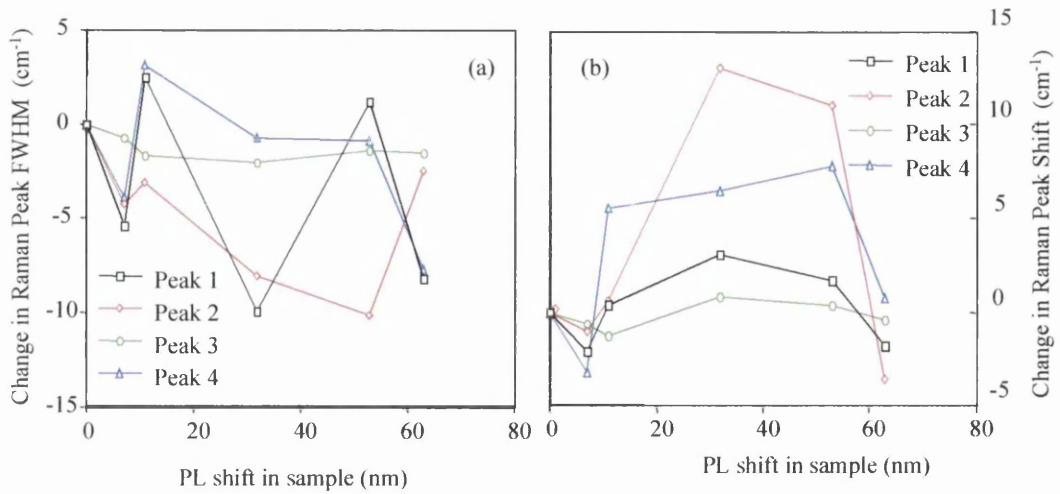


Fig. 5.11 The change in the FWHM and energy shift the peaks detected in the 4QW samples as a function of the PL wavelength shift are shown in (a) and (b) respectively. No consistent trend can be seen in the change of both parameters as a function of the amount of intermixing.

Raman spectra of the as-grown sample, before and after removing the background luminescence tail are shown in Fig. 5.9, with the Raman peaks identified.

Samples annealed at different temperatures exhibit different degrees of intermixing, as can be seen in Fig. 5.10. The energy shift and the FWHM of the Raman peaks are plotted as a function of the PL wavelength shift due to intermixing in Fig 5.11. Although changes of up to 13 cm⁻¹ and 10 cm⁻¹ in the energy shift and the FWHM of the Raman peaks respectively between the as-grown and intermixed samples are observed, changes do not show a consistent trend with intermixing. Obtaining no meaningful results from this set of samples can be ascribed to the absorption of the light in the cladding and barrier regions. As a consequence, the light intensity will be too low to generate a detectable Raman signal from the QWs. This implies that the only expected Raman signal with a detectable magnitude will be from the cladding/barrier interface. In addition, compositional intermixing will occur within 1-2 nm at each heterostructure interface, which is much smaller when compared to signals generated from the rest of the epitaxial layer. If one compares the volume of the intermixed region in cladding/barrier interface to the volume of the 1 μm Al_{0.4}Ga_{0.6}As upper cladding layer on top, it will be clear how small is the interaction between the intermixed part of the lattice and the photons.

Ways to overcome such obstacles of detecting the lattice disorder near the QWs include:

- i. Detecting the Raman signal in a waveguide structure, where the signal propagates for a few millimeters before detection. However this technique is not spatially resolved, and more importantly, it is a destructive test. Non-destructive means of measurement are essential for wafer diagnostic purposes at different PIC device fabrication stages.

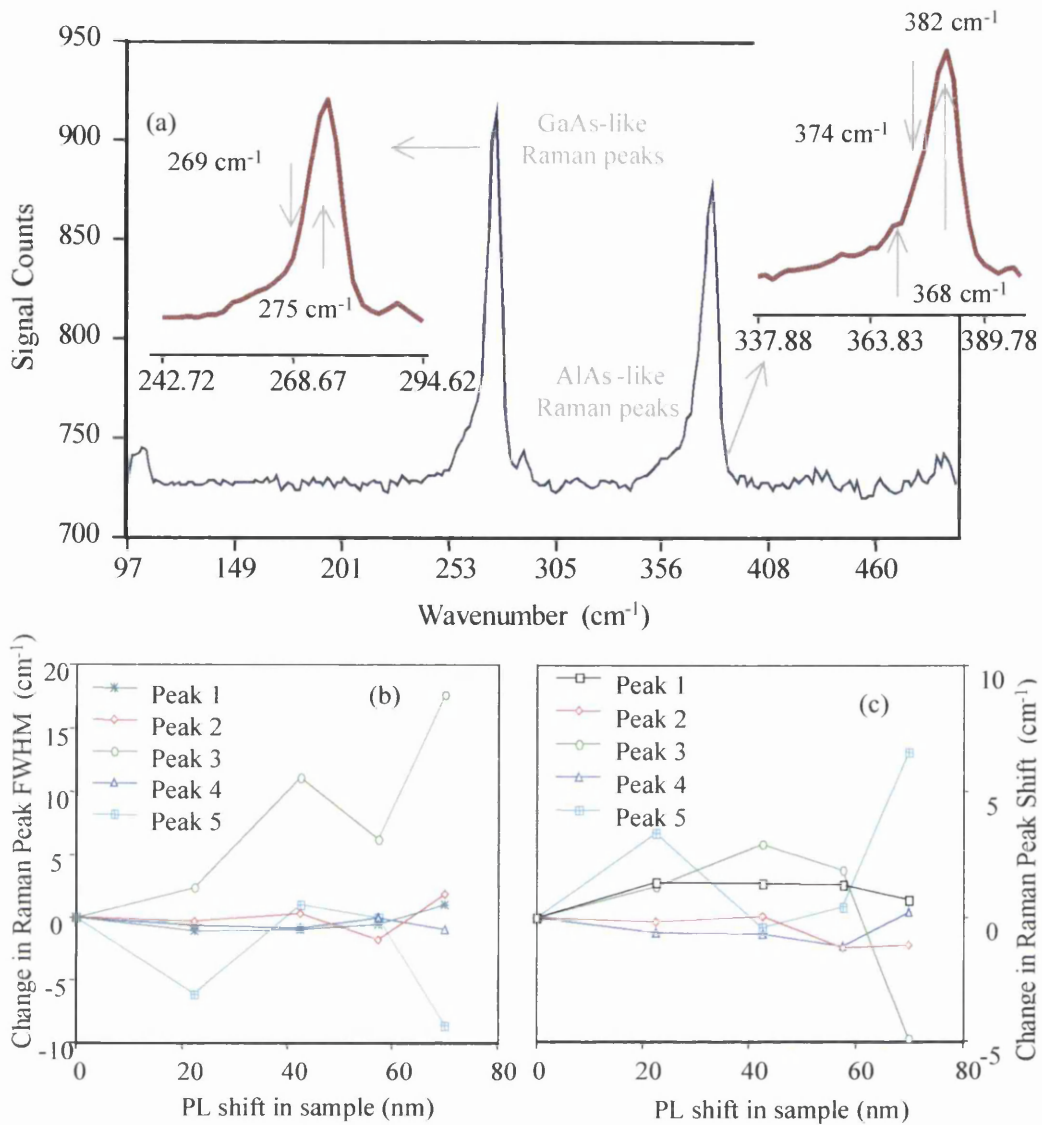


Fig. 5.12 Raman spectra from the as-grown MQW sample with a top GaAs layer. The Raman spectrum were induced using a HeNe laser and are shown after removing the photoluminescence background line. Also shown are the two groups of the Raman spectra belonging to the GaAs-like and the AlAs-like modes. The change in the FWHM and the energy shift all the peaks as a function of the PL wavelength shift is shown in (b) and (c) respectively.

- ii. Etching the cladding and most of the barrier layers can also alleviate the associated absorption. However this is also a destructive means, and is not trivial to implement, due to the challenges of the precision of wet etching of GaAs/AlGaAs heterostructures.

III.A.2 Undoped Waveguide Structure

The MQW structure contains GaAs in its 76 QWs and in the 100 nm capping layer, and $Al_{0.4}Ga_{0.6}As$ in the barriers as well as the lower and upper cladding layers, as shown in Appendix A. The potential photon interaction with the QW/barrier interface lattices will be generally greater in MQW structures, due to the increased number of wells in comparison to that of the 4QW sample. The same 632 nm HeNe laser set up, used in the previous

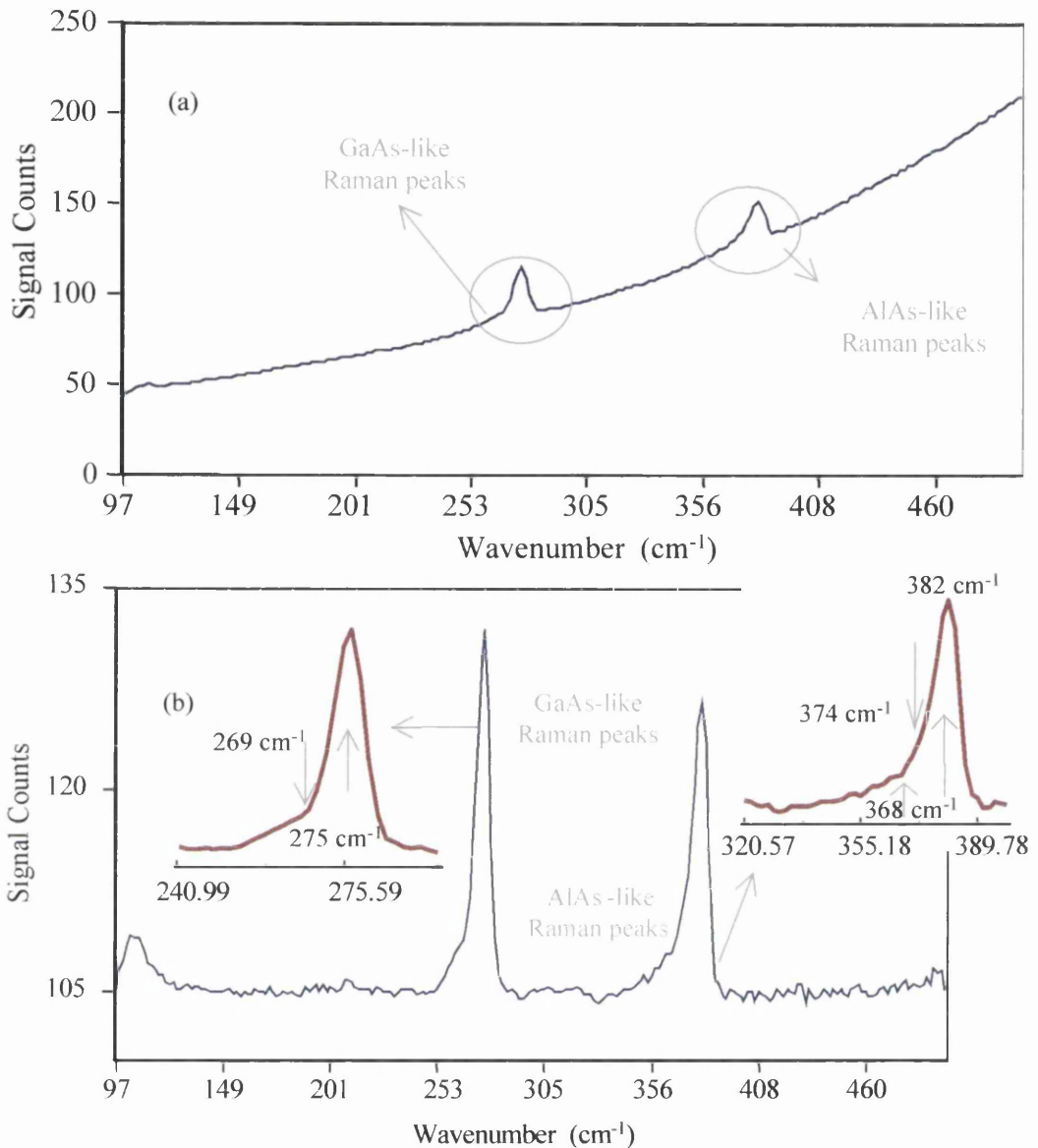


Fig. 5.13 Raman spectra from the MQW as-grown with the top GaAs contact layer removed. The Raman spectrum is shown (a) before and (b) after removing the photoluminescence background line. The GaAs-like and AlAs-like Raman spectra are indicated.

section, was also used to induce the Raman signal. In this set of samples, with the GaAs cap on, photons will suffer considerable absorption in the 100 nm GaAs cap, where the absorption length is 400 nm. The Raman modes will therefore be expected to originate from the interface of the contact GaAs layer and the $Al_{0.4}Ga_{0.6}As$ upper cladding, but less likely to be from the QW/barrier interfaces. Samples were coated with E-Gun SiO_2 and annealed along with the 4QW batch, as presented in the previous section. The PL shifts as a function of the annealing temperature are shown in Fig. 5.10. After removing the background PL signal, and curve fitting the Raman spectra, 5 peaks were clearly detected. The information about the peaks and their designation are listed in Table 5.2 along with the closest peaks

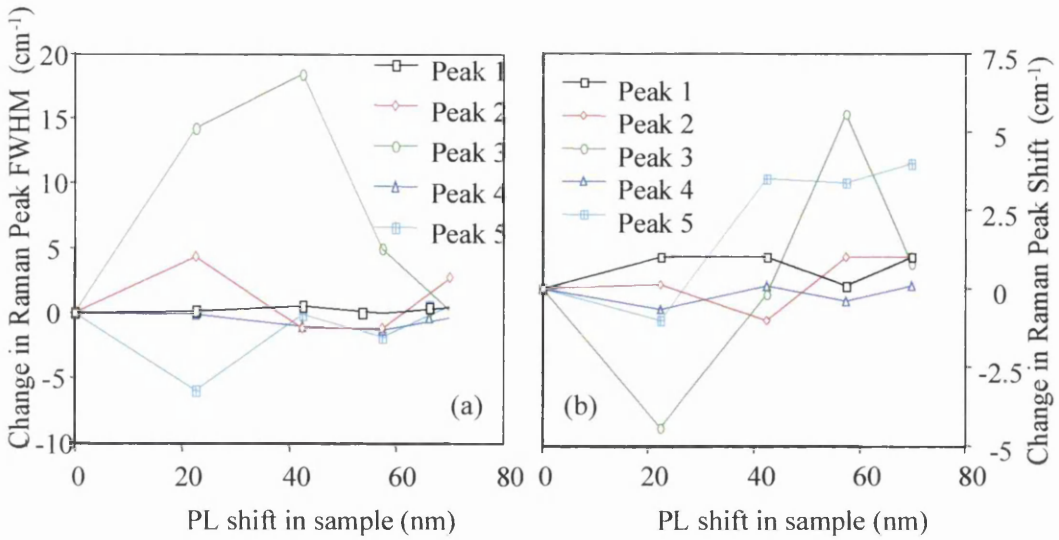


Fig. 5.14 The change in (a) the FWHM and (b) the energy shift for all the Raman peaks detected as a function of the PL wavelength shift.

reported in Abstrieter *et al.*^{31,40} The Raman spectrum of the as-grown sample, after removing the background luminescence tail, is also shown in Fig. 5.12 (a).

As was done for the 4QW sample, the energy shift and the FWHM of the Raman peaks of the MQW samples with GaAs cap on are plotted as a function of the PL shift due to intermixing in Fig. 5.12 (b) and (c) respectively after curve fitting. The FWHM of the Raman peaks of the $Al_{0.4}Ga_{0.6}As$ cladding layer do not show any appreciable change as a function of PL shift. However the FWHM of the unidentified peak at 376.8 cm^{-1} exhibits a monotonic increase as a function of the wavelength shift in the PL peak. This energy shift was not found to correspond to any of the Raman modes of the compositions available in the epitaxial layer, namely GaAs $Al_{0.2}Ga_{0.8}As$ and $Al_{0.4}Ga_{0.6}As$. Although more samples should be fabricated and examined, this peak might be associated with the p-like doping of the structure.¹ Similar to the FWHM, the energy shift of the Raman peaks of the $Al_{0.4}Ga_{0.6}As$ cladding layer do not show any appreciable change as a function of PL shift. The maximum energy shift of the TO mode of the AlAs-like / GaAs-like Raman peaks increase / decrease by $\sim 2\text{ cm}^{-1}$, respectively, as seen in Fig. 5.12 (c). However the sign of the change in their energy shift indicates an increase in the Al content of the effective composition of the layer inducing this Raman signal. This effective increase in the Al content clearly does not match what is expected from compositional intermixing of GaAs/ $Al_{0.4}Ga_{0.6}As$ interface. The AlAs-like TO mode shows, in contrast, a reduction in the energy shift, although no more than $\sim 2\text{ cm}^{-1}$, yet the change indicates an increase in the effective Al content of the layer inducing the Raman signal. The energy shift of the rest of the peaks shows no consistent trend of change as a function of the amount of intermixing. Further analysis of the Raman peaks' behavior was not carried out since the photons used will be mostly absorbed in the GaAs

layer, and hence the signal observed is most likely generated from the single interface of the top GaAs contact layer and the $\text{Al}_{0.4}\text{Ga}_{0.6}\text{As}$ cladding. Therefore, even if we detect a meaningful signal from this interface, it will convey little, if any, useful information about the compositional intermixing taking place at the QW/barrier interface. We hence move on to test the MQW samples with the GaAs caps removed, since they have the potential to provide useful information about the compositional intermixing at the interfaces QWs and the corresponding barriers.

III.A.3 Undoped Waveguide Structure after Etching the Contact Layer

The second set of MQW samples was prepared along with the samples investigated in the last two sections. This set of samples had its GaAs contact layer etched using a $\text{NH}_3:\text{H}_2\text{O}_2$ solution with the ratio of 5:95 for 60 s. Similar to the previous set of MQW samples, after removing the PL background signal and curve fitted the Raman peaks 5 peaks were clearly detected in this set of samples as listed in Table 5.2. The Raman spectra of the as-grown sample, before and after removing the background luminescence tail, is shown in Fig. 5.13. The PL shift as a function of the anneal temperature are shown in Fig. 5.10. The FWHM and energy shifts of the Raman peaks are plotted as a function of the PL shift in Fig. 5.14 (a) and (b) respectively. The FWHM of the AlAs-like and GaAs-like LO Raman modes of the $\text{Al}_{0.4}\text{Ga}_{0.6}\text{As}$ cladding layer do not show any appreciable change as a function of PL shift. On the other hand, the FWHM of the AlAs-like and GaAs-like LO Raman modes exhibit changes as large as 5 cm^{-1} with no consistent trend of change observed as a function of the shift in PL peak wavelength. An increase approaching 20 cm^{-1} was observed in the unidentified peak, similarly with no trend of change. The energy shift of the AlAs-like and GaAs-like LO Raman modes of the $\text{Al}_{0.4}\text{Ga}_{0.6}\text{As}$ cladding layer do not show any appreciable change as a function of PL shift. Moreover, the sign of their change indicate an increase in the effective Al content of the lattice inducing the Raman signal. The energy shift of the GaAs like TO peak of $\text{Al}_{0.4}\text{Ga}_{0.6}\text{As}$ layer however, exhibits a monotonic increase with the increase of PL shift. This suggests that a lattice with an effective Al content less than 40% induces the Raman signal. This reduction in the Al composition of the intermixed MQWs matches expectations from compositional intermixing of GaAs QWs and $\text{Al}_{0.4}\text{Ga}_{0.6}\text{As}$ barriers. The Raman spectrum of the sample annealed at $960\text{ }^\circ\text{C}$ for 60 s, before and after removing the background luminescence tail, is shown in Fig 5.15. This sample exhibited a PL shift of 70 nm, with a change in the GaAs TO Raman peak of 4 cm^{-1} from that of the original sample,⁴¹ which matches the energy shift of the TO GaAs-like Raman mode of $\text{Al}_{0.3}\text{Ga}_{0.7}\text{As}$, still explaining well the expected intermixing of 2.8 nm GaAs QW and 10 nm $\text{Al}_{0.4}\text{Ga}_{0.6}\text{As}$ barrier.⁴² The reason of observing the compositional intermixing only in one of the Raman peaks and not all of them is not known at this point in time, and requires further

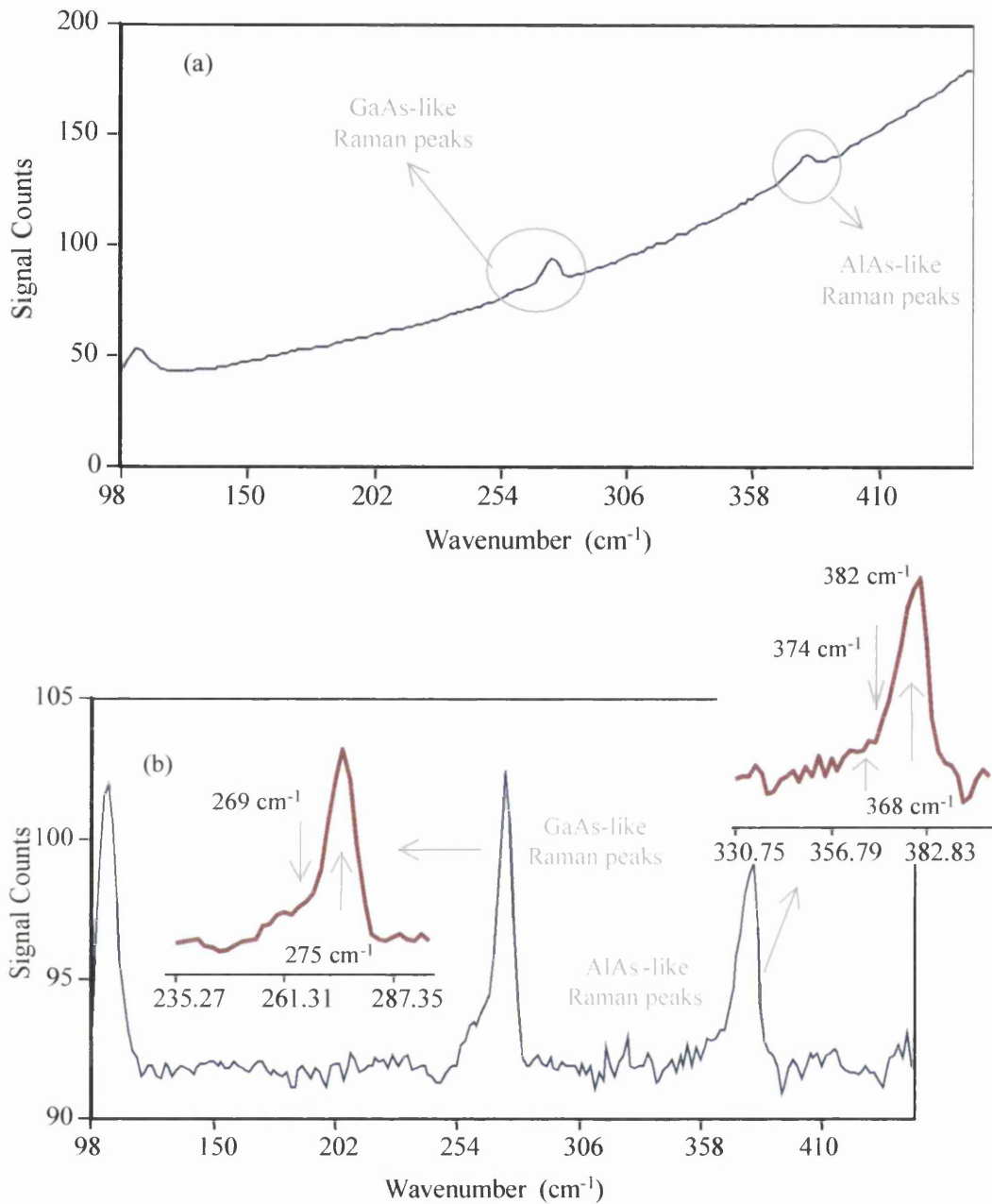


Fig. 5.15 Raman spectra from the MQW sample annealed with E-gun deposited SiO₂ caps at 960 °C for 60 s. The Raman spectrum is shown (a) before and (b) after removing the photoluminescence background line. The GaAs-like and AlAs-like Raman spectra are indicated.

investigation. Although this will be investigated in more detail, two factors might be contributing to these results.

- The photons used (632 nm) have absorption lengths of approximately 1 μm in the Al_{0.4}Ga_{0.6}As upper cladding layer. Although relatively long, the absorption length is still finite and probably affects the strength of the detected signal. It should also be noted that the absorption of the backscattered Raman signal is smallest for the energies of the GaAs-like modes.

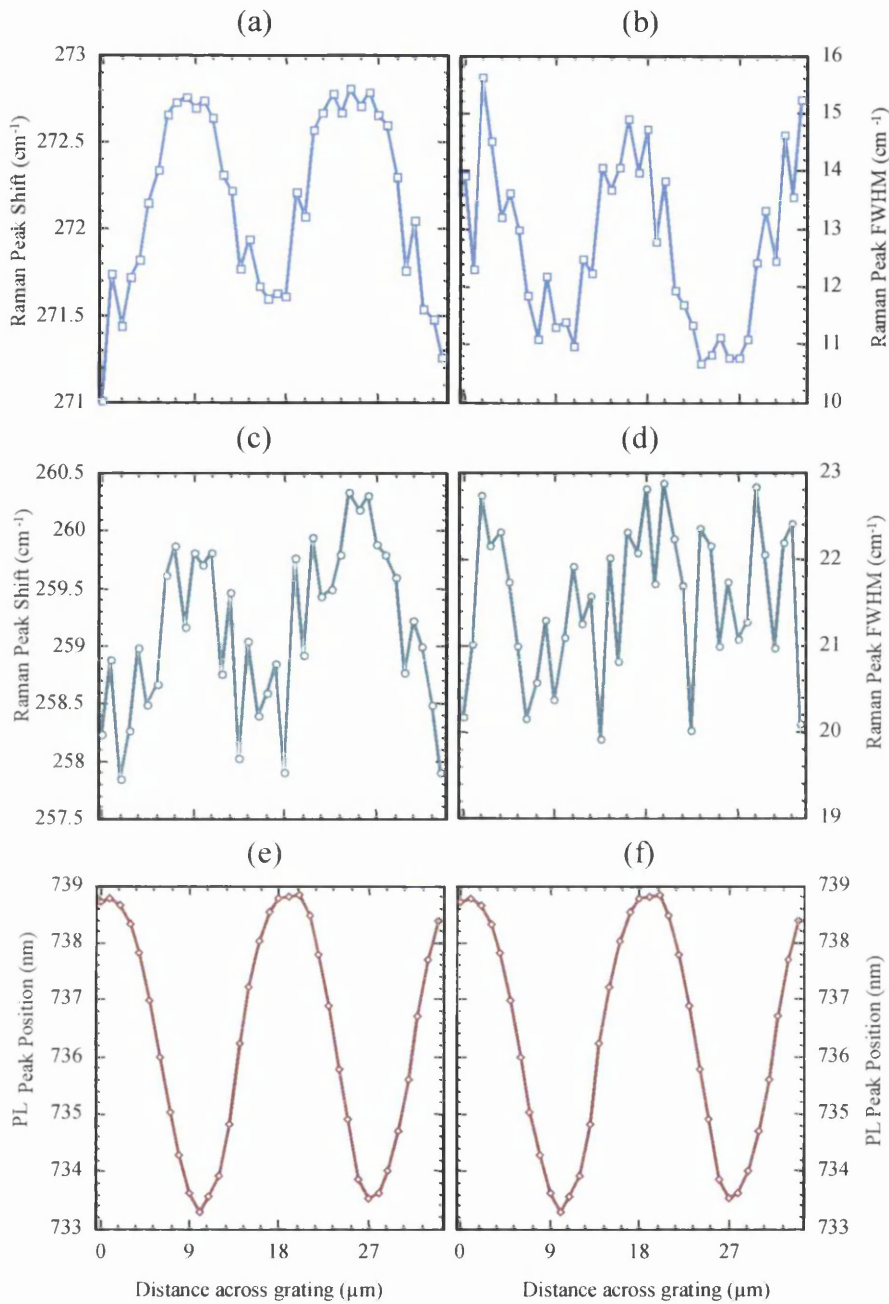


Fig. 5.16 Line scans for the PL shift across two periods of an intermixed grating of a MQW sample without the GaAs layer annealed for 60 s at 950 °C with SiO₂/SiO₂:P caps are shown in (e) and (f). The scan of the (a) FWHM and the (b) position of the LO GaAs like Raman peak of the Al_{0.4}Ga_{0.6}As cladding layer, and another scan of the (c) FWHM and the (d) TO GaAs like Raman peak of the Al_{0.4}Ga_{0.6}As cladding layer are also shown.

- The strong PL generated by the HeNe laser will result in poor Raman signal to background ratio. The PL signal, being smallest at the energies of the GaAs-like modes as seen in Fig. 5.15 (a), will have the least effect on such modes. The GaAs-like modes are, therefore, expected to be the most sensitive to small change.

III.B. Summary of Raman Measurements

From studying the energy shift and the FWHM of various Raman peaks in 4QWs and MQW structures qualitative evidence of QWI in was observed in MQW samples without the top GaAs. QWI could not be detected in samples with the top GaAs cap layer on because of photon absorption in this layer. It was also not possible to detect intermixing in samples with 4QW photon absorption in the QW barrier regions and due to the reduced number of interfaces where compositional intermixing will take place.

III.C. Studying the spatial localisation of Quantum Well Intermixing using Raman Micro-Probe

To investigate laterally-localised intermixing, a sample from the MQW structure was used for spatially resolved Raman backscattering. An experiment is designed to investigate the change of properties of the different Raman peaks associated with the different layers in the structure with a periodically varying intermixing grating. This work is particularly interesting for applications involving the use of QWI with μm scale patterning for quasi phase matching in compound semiconductors.⁴³

Samples were coated with 200 nm of PECVD $\text{SiO}_2\text{:P}$, then a grating pattern with different 1:1 periods was etched away from this cap. Another 200 nm of E-gun SiO_2 was evaporated after, to cover etched parts of the grating, where it enhances intermixing.⁴⁴ Samples were then annealed at 950 °C for 60 s. The dielectric cap and the top GaAs contact layer were wet etched after, using a HF solution for 30 s and a $\text{NH}_3\text{:H}_2\text{O}_2$ solution with the ratio of 5:95 for 60 s, respectively. The Raman and PL spectra were induced using an Ar^+ 514.5 nm laser, with a $\times 50$ objective giving a spot size of 0.276 μm and power density of 83 $\text{mW}\cdot\text{cm}^{-2}$. The absorption length at this wavelength is ~ 400 nm in the $\text{Al}_{0.4}\text{Ga}_{0.6}\text{As}$ cladding layer. A scan of the PL peak across 2 periods of 1:1 grating was carried out with a step of 1 μm . A plot of the Raman peak shift as a function of position in the grating is shown in Fig. 5.16 (e) and (f). As can be seen, the grating structure is clearly evident in the wavelength of the PL peak with a 6 nm shift between the intermixed and un-intermixed regions. The Raman modes studied here were the GaAs like LO and TO modes for the $\text{Al}_{0.4}\text{Ga}_{0.6}\text{As}$ cladding layer. The LO mode varies between 271.5 cm^{-1} and 272.5 cm^{-1} , which indicates a change in the AlGaAs composition between 45 % and 35 %.⁴⁵ Also the FWHM of this peak decreases from 15 cm^{-1} in the region where there is minimal intermixing, to 11 cm^{-1} , where there is enhancement in intermixing. Less contrast was seen in the modulation of the Raman energy shift of the TO mode when compared to that of the LO signal. The TO mode varies between 258 cm^{-1} and 260 cm^{-1} , which implies a decrease in the effective Al fraction of the AlGaAs alloy inducing the Raman signal, indicating composition mixing between the GaAs

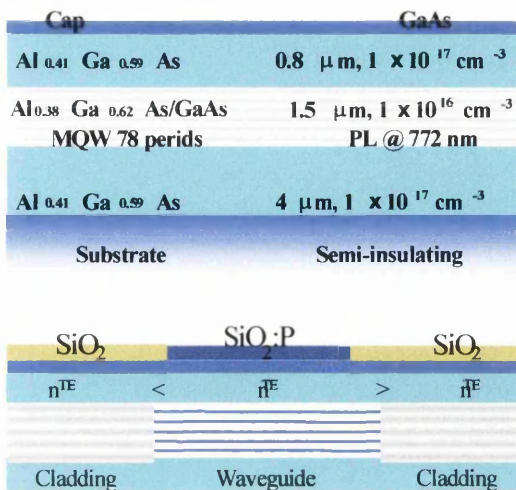


Fig.5. 17 As-grown wafer and waveguide schematics.

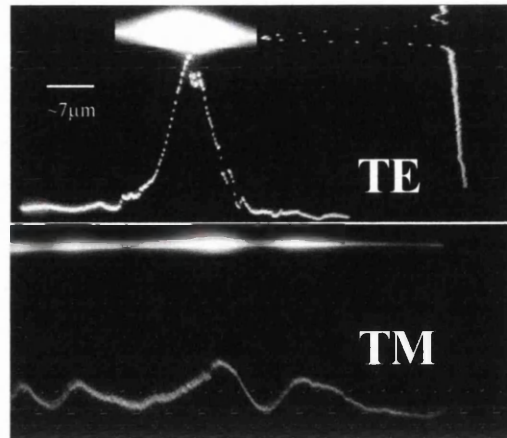


Fig.5. 18 Mode profiles for a 7 μm wide waveguide. The outputs in the TE guided mode and the TM slab mode cases are shown.

QWs and the Al_{0.4}Ga_{0.6}As barriers.⁴⁵ Also the FWHM of this peak decreases from 23 cm⁻¹ in the region where there is minimal intermixing, to 20 cm⁻¹, where there is enhancement in intermixing. The change in the FWHM of both Raman peaks is opposite to what was reported for a superlattice (SL) layer with the same effective AlGaAs composition.⁴⁶ These studies reported an increase of FWHM from 11 cm⁻¹ for the SL to 13 cm⁻¹ for the bulk.⁴⁶ As can be seen in Fig 5.16 the changes in the Raman shift and FWHM of these peaks coincide with the grating pattern, as identified by the variation in the PL peak. This confirms that Raman scattering can detect spatially localised QWI, at least qualitatively, through the position of the energy shift and the FWHM of the Raman peaks.⁴¹ It should be emphasised that in these measurements the signal is generated from the QW/barrier interface.

III.C.1 Raman micro-probe of intermixed waveguide structures

Since Raman measurements are attractive for probing QWI with sub μm dimensions, studies must be carried out on samples with the GaAs cap layer on, to ensure that indication about intermixing can still be detected from such structures. Intermixed waveguide with different widths were fabricated and tested using MQW samples as will be explained below:

- Low loss waveguides defined by impurity-free vacancy disordering (IFVD) have shown promise as viable low losses interconnect waveguide in optoelectronics.⁴⁷ They add new functionality due to their polarisation guiding characteristics.⁴⁸ Such waveguides also have potential applications as novel non-linear switching elements based on soliton emission using the half bandgap non-linearity at 1.55 μm.⁴⁹

- Waveguides are defined using the refractive index change induced by quantum well intermixing. Previous results were based on a surface superlattice (SL) structure and resolution was limited by lateral defect diffusion.
- The $\text{SiO}_2/\text{SiO}_2:\text{P}$ IFVD capping system, was used to fabricate the waveguides. Waveguides were fabricated by intermixing the whole wafer except where the guides were located. This results in a buried waveguide region below the SiO_2 cap, where n^{TE} is lower than that of the original MQW, below the $\text{SiO}_2:\text{P}$ cap, as can be seen in Fig. 5.17.
- Single mode guiding was observed for waveguides up to $7\ \mu\text{m}$ wide, at a wavelength of $1.55\ \mu\text{m}$, which implies that Δn_{IFVD} even at sub-half the bandgap of the MQW is large enough to sustain waveguiding. The mode profile of a $7\ \mu\text{m}$ guide is plotted in Fig. 5.18.

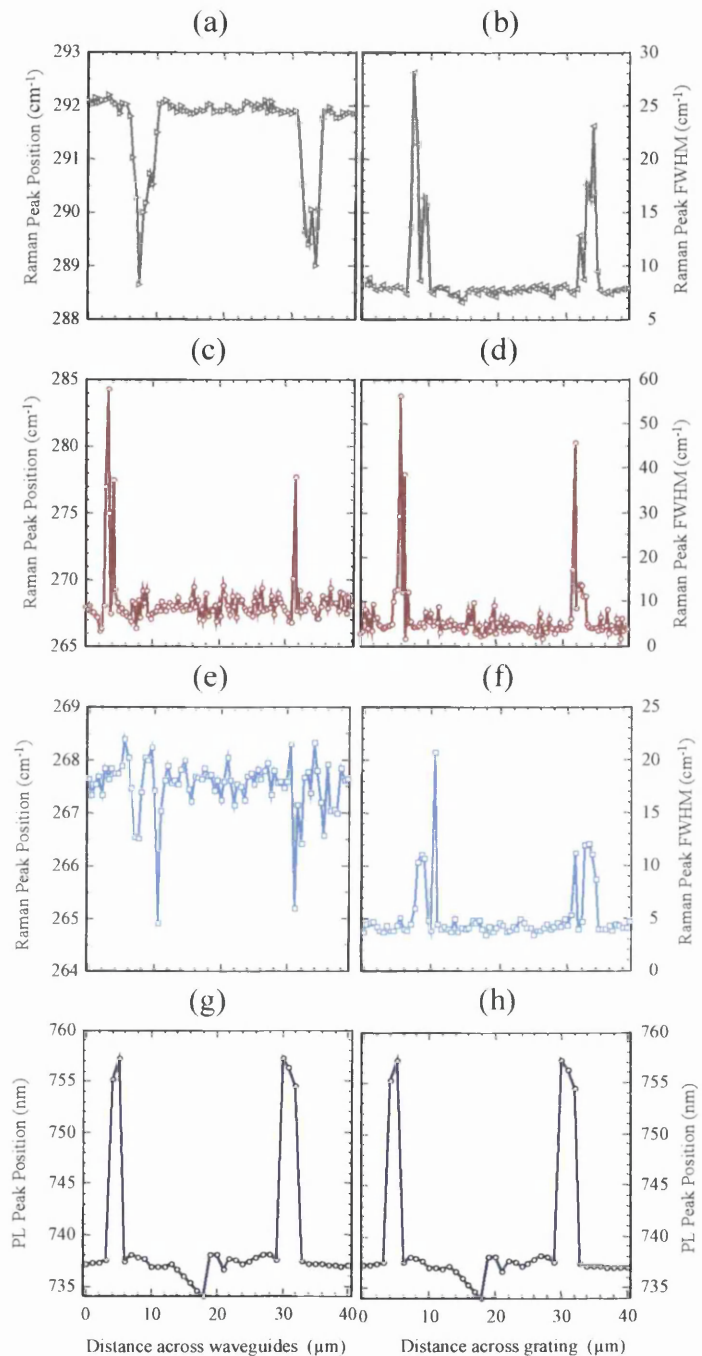


Fig. 5.19 Line scans for the PL shift across two waveguides of an intermixed MQW waveguide sample, with the GaAs layer and intermixed using sputtered silica technique, are shown in (g) and (h). The scan of the (a) position of the LO GaAs like Raman peak, and (b) the FWHM of the GaAs layer, of the (c) TO GaAs like Raman peak, and (d) the FWHM of the GaAs layer, and of the (e) TO GaAs like Raman peak, and (f) the FWHM of the $\text{Al}_{0.4}\text{Ga}_{0.6}\text{As}$ cladding layer, are also shown.

- Propagation losses were found to lie in the range 4-5 dB.cm⁻¹, although the background doping is in the mid 10¹⁶ cm⁻³ for this structure. This value is the same as that reported for low background doping MBE grown SL structures.⁴⁷
- The waveguides also act as TE filters, as seen in Fig. 5.18. This confirms that the TE/TM refractive indices change in the same way to that previously reported in SL.⁴⁷

The Raman and PL spectra were collected using the same Ar⁺ laser set up as in the previous experiment, with the same spot size and an average power of 207 mW.cm⁻². A scan of the PL peak position across 2 waveguides of width of 2 and 3 μm is shown in Fig. 5.19 (g). As can be seen, the evidence of the waveguides can be clearly see in the position of the PL peak with a 20 nm shift between the cladding and waveguiding regions. Raman peaks studied here were the GaAs like LO and TO modes for the top GaAs layer as well as the LO mode from the Al_{0.4}Ga_{0.6}As cladding layer. The LO mode of the GaAs layer varies between 271.5 cm⁻¹ and 272.5 cm⁻¹, again indicates a change in the AlGaAs composition between 45 % and 35 %, which matches well what is expected from the barrier/QW intermixing.⁴⁵ Further, the FWHM of this peak decreases from 25 cm⁻¹ in the region where there is minimal intermixing, to 7 cm⁻¹, where there is enhancement in intermixing. The TO mode varies between 258 cm⁻¹ and 260 cm⁻¹, which indicates a decrease in the Al fraction in the AlGaAs lattice and matches well what is expected from the barrier/QW intermixing.⁴⁵ Also the FWHM of this peak decreases from 45 cm⁻¹ in the region where there is minimal intermixing, to 3 cm⁻¹, where there is enhancement in intermixing. The change in the FWHM for both Raman modes is also in contrast with that reported for a superlattice layer with the same effective AlGaAs composition as previously discussed.⁵⁰ As can be seen in Fig 5.19 the change in the position as well as the FWHM of these peaks coincides with the waveguide pattern determined from the PL peak wavelength. This confirms that Raman scattering can detect QWI, at least qualitatively through the position of the Raman peaks, which convey information about the lattice composition, and through the FWHM of the peaks, which convey information about the lattice order.

IV. PHOTOLUMINESCENCE EXCITATION SPECTROSCOPY

When only the lowest interband transition energy is used to characterise the intermixing process errors are likely to occur, as pointed out by E. H. Li *et al.*⁵¹ This is due to the factors affecting QWI, which are all convoluted to contribute to the observed bandgap energy shifts. Factors such as the heterostructure shape, the amount of barrier / well compositional mixing, the modification of the QW dimensions, and the strain related effects

all have a roll in the final out come of the QWI process. Therefore studying the higher energy transitions should help provide more accurate information about what actually takes place within the heterostructure.

Photoluminescence excitation (PLE) is a technique by which all the bound energy transitions taking place in a quantum well can be measured. PLE uses a similar set-up to that of the PL as shown in Fig. 5.1. In contrast to the conventional sequence of events for PL measurements, the monochromator is set at a wavelength, which is a few meVs less than the ground state energy. The latter is determined from PL measurements. A tuneable laser source

is then used to scan the range of energies, which correspond to the available bound energy levels (usually the energy span is limited by the tuning capabilities of the laser used).¹ As the laser irradiation energy is increased from that of the bandgap to higher energies, the photons are absorbed between the higher bound states, with consequent emission at similar energies. The various peaks in the collected spectrum correspond, therefore, to the various available transitions in the heterostructure that are within the scanning range of the laser. The bound energy determined from PLE convey information about the heterostructures' dimensions, interface profile, and hence the composition distribution of the heterostructure. The dependence of the QW optical transitions on the density of states and the optical matrix elements pose a set of rules, which govern the transitions between bound states from such structures. They stem primarily from the assumptions associated with the heterostructures, of which the orthogonality of the wavefunctions is a dominant factor. These rules are termed the selection rules, and they dictate a set of the permitted transitions to take place between the bound states. If the designed structure deviates from the ideal QW by a significant extent, then the restrictions on the transitions set by the selection rules are relaxed and hence forbidden transitions are detected in the PLE spectra. These forbidden transitions are, therefore, an indicator of the deviation of quantum wells from the infinite barrier approximation. Fundamentally the selection rules for interband transitions can be summed in 3 points, which are,

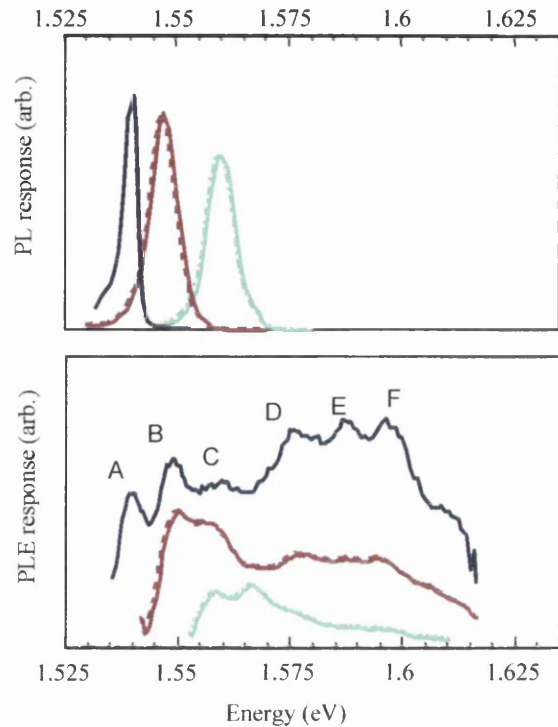


Fig. 5.20. Plot of PL spectra of the samples used in the PLE experiment, and typical PLE spectra obtained from the samples.

- 1- The allowed transitions must conserve the moment vector k , i.e. vertical transitions take place unless interactions with phonons take place.
- 2- Transitions are only allowed from bands with similar parity, i.e. bands with similar symmetry such as $e1 \rightarrow h3$, $e2 \rightarrow h4$, etc.
- 3- Due to the orthogonality of the wavefunctions in infinite QWs, transitions only of the same energy level number are allowed, i.e. $e1 \rightarrow h1$, $e2 \rightarrow h2$, etc., however this rule is not strictly true in real QWs where the confining potential is finite. Transitions between same energy level number bands are usually the strongest.

Upon obtaining the energies of the ground and higher states of a QW, and by solving the Schrödinger wave equation for a QW with an arbitrary potential profile, a fit for the QW shape can be deduced. Similarly, the shapes of the inter-diffused QWs can also be obtained by fitting the measured energies of the ground state and higher confined states to an appropriate Al/Ga diffusion profile.

Table 5.3. Experimentally observed transition energies for a non-intermixed reference sample (column 2). The calculated results from both a square well (column 3) and an exponential well profile (column 4) are also included.

Transitions	E_{measured} (eV)	$E_{\text{calculated}}$ (eV) Square well	$E_{\text{calculated}}$ (eV) Exponential well
E1-HH1 (A)	1.539	1.541	1.537
E1-LH1 (B)	1.549	1.551	1.547
E1-HH2 (C)	1.560	1.563	1.558
E1-HH3 (D)	1.576	1.586	1.579
E2-HH1 (D)	1.576	1.587	1.578
E1-LH2 (E)	1.588	1.604	1.590
E2-LH1 (E)	1.588	1.602	1.589
E2-HH2 (F)	1.597	1.616	1.598

VI.A. Studying Quantum Well profiles using Photoluminescence Induced Excitation

PLE was used to determine the energies of the confined states in double quantum well (DQW) separate confinement heterostructure (SCH) *pin* laser material, as shown in Appendix A. The samples were cleaved up into square pieces of $3 \times 3 \text{ mm}^2$, and were coated with 200 nm of SiO_2 deposited by electronic gun evaporation. The samples were then annealed, with the SiO_2 caps present, at temperatures in the range 875-950 °C for 60 s.

PLE measurements were performed on the annealed samples along with one control un-annealed sample as a reference. A He-Ne laser was used for the PL measurement and a Ti:Sapphire laser for PLE. PL and PLE data obtained from three representative samples are shown in Fig. 5.20. The model and parameters used in the energy calculations are carried out reported by M. L. Ke *et al.*^{52,53} A conduction band offset of $0.65 \Delta E_g$ was used and band

non-parabolicity was included as suggested by Ekenberg.⁵⁴ The electron band edge effective mass was taken to be $0.0665m_0$, while the Luttinger parameters, as devised by Lawaetz, were used to derive the heavy and light hole masses.⁵⁵ From the PL data (Fig. 5.20(a)), it is obvious that the lowest band edge transition energy increases with increasing annealing temperature. This is also confirmed by the PLE data (Fig. 5.20(b)), where the lowest energy peak represents the excitonic transition between the lowest energy electron states and heavy hole states ($e1-hh1$). Many

other transitions are also visible in the PLE spectra, which provide information about the behaviour of the higher subbands with intermixing. Also clear from the spectra, is the decrease of the higher states' energies with the increase of the annealing temperature, which opposes the trend for the lowest two bound states.

Another interesting result from the PLE data is that many of the observed transitions are in fact forbidden. As discussed earlier, it is well known from the selection rules, that for an ideal infinitely deep square well, only transitions with the same energy level are allowed because the wavefunctions of all other transitions are

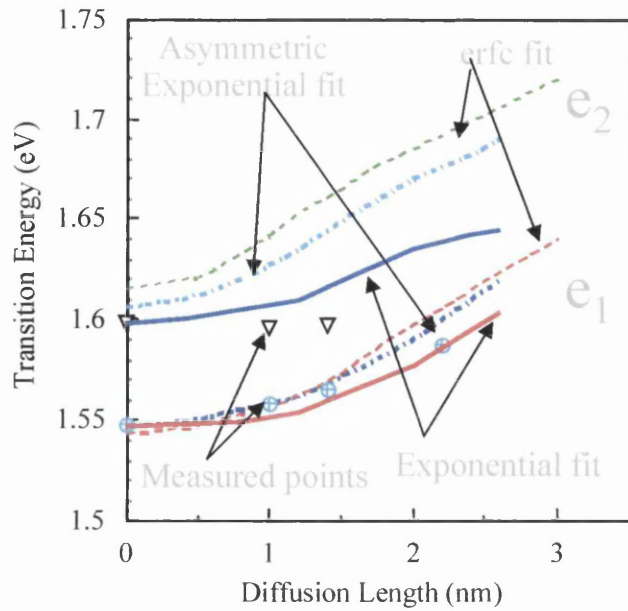


Fig. 5.21. Plot of the measured $e1 \rightarrow hh1$, and $e2 \rightarrow hh2$ transitions obtained from PLE measurements. Transitions fitted for an initial square, exponential, and single sided exponential QW profiles are also plotted and represented by the dashed, solid, and dashed- dotted lines respectively.

Table 5.4. Experimentally observed transition energies for an intermixed sample (column 2), which was annealed at 925 °C for 60 s. The calculated results for the diffusion of both an initial abrupt well (column 3) and an exponential well profile (column 4) are also included.

Transitions	$E_{measured}$ (eV)	$E_{calculated}$ $L_D=8 \text{ \AA}$ Square well (eV)	$E_{calculated}$ $L_D=10 \text{ \AA}$ Exponential (eV)
E1-HH1	1.549	1.549	1.546
E1-LH1	1.559	1.560	1.557
E1-HH2	1.567	1.574	1.566
E1-HH3	1.578	1.602	1.584
E2-HH1	1.578	1.603	1.585
E1-LH2	1.587	1.616	1.595
E2-LH1	1.587	1.615	1.596
E2-HH2	1.595	1.635	1.604

orthogonal. This means that $\Delta l \Rightarrow m-n=0$, where m and n are the subband indices for the conduction and valance band respectively. However, for a real QW, which has a finite depth and may contain graded interfaces, the orthogonality of the wavefunctions is relaxed, resulting in a modified selection rule, where $\Delta l \Rightarrow \text{even}$ transitions are allowed. This is why all possible transitions can be observed in the emission spectra.⁵⁶

The electronic band profile of the reference sample was initially calculated using a finite difference method, assuming a square well shape as shown in Fig. 5.21. Also Table 5.3 shows the various transition energies from both simulated and PLE data. While the two sets of data agree well for the lower transitions, there is, however, a noticeable discrepancy for the higher ones. Apparently, the calculated energies for the higher subbands are always larger than those observed experimentally, suggesting a wider well is needed for the higher subbands. In order to take the behaviour of the higher energy subbands into account, an exponential interface profile was used instead of the square well approximation. A well profile of the form,

$$\begin{aligned} \zeta &= \zeta_o \exp[-\beta/(z^2 - (L_w/2)^2)] \dots |x| \geq L_w/2 \\ \zeta &= 0 \dots |x| \leq L_w/2 \end{aligned} \quad (5.7)$$

was used, where ζ is the energy profile of the well, β is the curvature parameter, L_w the initial well width (i.e. the width of the bottom of the well). Using this profile a much better fit for all the transition energies was obtained as shown in Table 5.4. Similar work has been reported recently indicating that an initial exponential profile for the QWs fits the measured data better than a square profile.⁵⁷ Error function profiles were also used to fit the data from the reference sample, but the calculated energies did not match the measured experimental data. The subband energies of the samples annealed at higher temperatures were fitted both to error function profiles and to Ga diffusion profiles resulting from an initial exponential QW profile, assuming a Fick's law diffusion. The latter fit leads to diffused quantum well profiles described by the following equation,

$$C(z) = \frac{C_o}{2\sqrt{\pi Dt}} \int_{\frac{L_w}{2}-z}^{\infty} \zeta(\eta) \cdot e^{-\frac{\eta^2}{4Dt}} d\eta + \frac{C_o}{2\sqrt{\pi Dt}} \int_{\frac{L_w}{2}+z}^{\infty} \zeta(\eta) \cdot e^{-\frac{\eta^2}{4Dt}} d\eta \quad (5.8)$$

where $\zeta(\eta)$ is the initial exponential QW profile as given by equation (5.7). The equation was solved numerically, and the energies of the diffused wells were obtained.¹⁷ The resulting diffusion profiles of the square and exponential as-grown profiles are shown in Fig 5.22. Also as can be seen in Table 5.3 and Fig 5.21, for an initial exponential profile with $\beta=500$ and subsequent diffusion, there is good agreement between experimental and calculated energy values of all of the transitions, not merely the ground level transition.

As well as the exponential profile discussed, others were also studied including an initial *erfc* profile, which produced energy levels further away from the measured energies than those produced by the initial square well profile. Initial square wells with a thickness different than that specified during growth were also investigated giving rise to good fit for the lower energy level, e1-lh1, but inaccurate fit for the higher levels. In addition, asymmetric profiles were studied: results for single sided exponential profiles produced energy levels which fitted experimental results better than those produced by the square wells but not as good as those produced by the symmetric exponential profile, as can be seen in Fig 5.21. A QW profile with one side being an *erfc* profile and the other being an exponential profile was investigated giving rise to higher energy levels in good agreement with the measured ones, but the ground level, e1-lh1, was in poor agreement with the measured value.

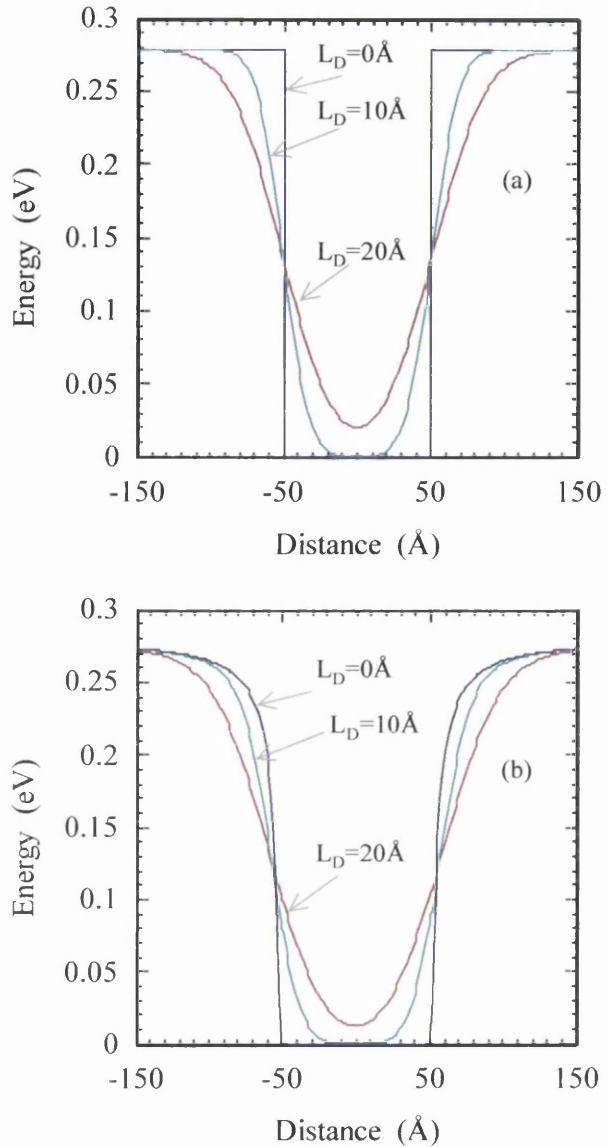


Fig. 5.22. Plot of the as-grown and interdiffused QW profiles of (a) a square QW approximation and (b) an exponential QW approximation.

Although the as grown QW interface gradient is evident in the fitted calculations presented in the experiments above, the exact interface shape is thought to be asymmetrical. Considering the growth dynamics at the QW interface closer to the substrate, the only intermixing expected at this heterostructure for the system to be causal can be induced due to growth related effects. Such effects are reported to be negligible for GaAs/AlGaAs heterostructures. Therefore, any gradient on that interface is expected to be much smaller to that expected at the upper interface of the QW, where a longer response time is expected for epitaxial layers with the desired Al content to be formed, even with Al cell set to the right

temperature.⁵⁸ More formal multi-band k,p model should be used for accurate calculations of the higher bound energy levels.¹⁹ An asymmetric profile should then describe the behaviour of the bound energy levels more accurately, since it relates better to the physical conditions of growth. An element of error will also be introduced from the failure of the effective mass approximation used in these calculations to accurately predict the behaviour of higher energy levels in a graded QW.

V. SUMMARY

The PL experiments have shown a decrease in the photogenerated carrier lifetime from 3 ns to 1 ns between the un-intermixed and intermixed regions respectively. However the asymmetry in the reproduction of the grating pattern in the lifetime results is a strong indication of carrier diffusion and subsequent recombination across the grating periods. From these measurements a resolution better than 3 μm was predicted for the dielectric cap annealing induced intermixing process. Spectrally resolved micro-PL measurements were also carried out across the same grating. From these measurements it was found that gratings less than 8 μm have an induced intermixing much less than that induced under the inhibiting cap, namely $\text{SiO}_2\text{:P}$. Also the differential shift induced underneath gratings of these sizes is much less than the differential shifts obtained between large area SiO_2 and $\text{SiO}_2\text{:P}$ caps. This is the first experimental observation of the direct role of the dielectric cap area on the intermixing it induces.

We have demonstrated that studies using micro Raman probes are a useful tool to investigate QWI. Evidence of the intermixing was observed in the wavelength of the PL peak, from the cladding layer, as well as from the barrier/QW interface. However this correlation between Raman signals and the amount of intermixing could only be detected for MQW structures, where there is a sufficient number of QWs/barrier interfaces to produce a detectable signal, and where there are barriers non-absorbing to the excitation wavelength. Similar results could not be obtained for the samples with 4 QWs even after etching away the top GaAs layer. Raman peaks indicating intermixing were detected from the barrier/QW in a periodically intermixed 1:1 gratings, which were identified using spatially resolved PL. In addition, the energy shift and the FWHM of the Raman peaks were observed as a function of distance for waveguides defined by QWI, and were also detected using spatially resolved PL. Because the GaAs cap was not etched away from these samples, the Raman peaks generated were from the cladding/top GaAs contact layer interface, which is expected to undergo an amount of intermixing dissimilar to that of the QW/barrier interface. Therefore a laser of 900 nm is needed to induce a detectable Raman signal from the QW/barrier interface.

From PLE experiments, the potential profile of as grown QWs was found not to be square shaped in GaAs/AlGaAs heterostructures. By fitting the QW bound energies to various potential profiles, it was found that symmetric exponential profiles give the best fit for the energy levels of both the initial and the interdiffused QW profiles. The observed non-abruptness of the heterostructure interface can be confirmed by difference techniques including high resolution TEM. On the other hand, the exact interface profile can not be known accurately without carrying out more PLE measurements on a group of samples and obtain statistically the profile that fits best the energy transitions, since growth runs will not be identical. The calculations shown here are carried out for the ground as well as the higher energy levels. For these higher levels, the effective mass approximation is quite inaccurate, and hence a more formal k,p approach should be used to calculate such bound states. The consequences of such findings have a direct impact on the QW diffusion behaviour. The profiles calculated for a square initial QW profile would obviously lead to errors in the obtained diffusion coefficients, which can be a considerable source of inaccuracy in the model developed to quantify the intermixing, as described in Chapter 3.

VI. REFERENCES

- ¹ S. Perkowitz, "Optical Characterisation of Semiconductors," Academic Press, Second edition, 1994.
- ² Mells Griot Catalogue, 1995-1996.
- ³ D. G. Deppe, L. J. Guido, N. Holonyak Jr., M. D. Camras, K. Hess, J. J. Coleman, P. D. Dapkus, J. Bardeen, *Appl. Phys. Lett.*, vol. 49, P 510, 1986.
- ⁴ E. H. Li, editor, "Selected Papers on Quantum Well Intermixing for Photonics," SPIE optical Engineering Press, vol. MS 145, 1998.
- ⁵ T. E. Schlesinger, T. Keuch, *Appl. Phys. Lett.*, vol. 49, P 519, 1986
- ⁶ W. J. Taylor, N. Kuwata, I. Yoshida, T. Katsuyama, H. Hayashi, *Appl. Phys. Lett.*, vol. 73, P 8653, 1993.
- ⁷ K. Mukai, M. Sugawara, S. Yamazaki, *Phys. Rev. B*, vol. 50, P 2273, 1994.
- ⁸ S. Sudo, H. Onishi, Y. Nakano, Y. Shimogaki, K. Tada, M. J. Mondry, L. A. Coldern, *J. Appl. Phys.*, vol. 35, P 1276, 1996.
- ⁹ C. J. McLean, A. McKee, G. Lullo, A. C. Bryce, R. M. De La Rue, J. H. Marsh, *Electron. Lett.*, vol. 31, P 1285, 1995.
- ¹⁰ S. J. Fancy, G. S. Buller, J. S. Massa, A. C. Walker, C. J. McLean, A. McKee, A. C. Bryce, J. H. Marsh, R. M. De La Rue, *J. Appl. Phys.*, vol. 79, P 9390, 1996.
- ¹¹ W. J. Choi, S. Lee, Y. Kim, D. Woo, S. K. Kim, S. H. Kim, J. I. Lee, K. N. Kang, J. H. Chu, S. K. Yu, J. C. Seo, D. Kim, K. Cho, *Appl. Phys Lett.*, vol. 67, P 3438, 1995.
- ¹² J. D. Ralston, W. J. Schaff, D. P. Bour, L. F. Eastman, *Appl. Phys Lett.*, vol. 54, P 534, 1989
- ¹³ M. Ghisoni, P. J. Stevens, G. Parry, J. S. Roberts, *Opt. Quant. Electron.*, vol. 23, P S915, 1991.
- ¹⁴ K. Mizoguchi, S. Nakashima, A. Fujii, A. Mitsuishi, H. Morimoto, H. Onoda, T. Kato, *Jpn. J. Appl. Phys.*, vol. 26, P 903, 1987.
- ¹⁵ R. Schorer, E. Friess, K. Ebrel, G. Abstreiter, *Phys. Rev. B*, vol 4, P 1772, 1991.
- ¹⁶ Y. T. Oh, T. W. Kang, T. W. Kim, *J. Appl. Phys.*, vol. 78, P 3376, 1995.
- ¹⁷ M. Ke, A. Saher Helmy, A. C. Bryce, J. S. Aitchison, J.H. Marsh, J. Davidson, P. Dawson, *J Appl. Phys.*, vol. 84 P 2855, 1998.
- ¹⁸ C. Kittel, "Introduction to Solid State Physics," Academic Press, Sixth edition, 1986.
- ¹⁹ C. D. Weisbuch, B. Vinter, "Quantum Semiconductor structures, Fundamentals and Applications," Academic Press, 1991.

- ²⁰ A. Gustafsson, M. E. Pistol, L. Montelius, L. Samuelson, *J. Appl. Phys.*, vol. 84, P 1715, 1998.
- ²¹ P. Cusumano, B.S. Ooi, A. Saher Helmy, S.G. Ayling, A.C. Bryce, J.H. Marsh, B. Voegelé, and M. J. Rose, *J. Appl. Phys.*, vol. 81, P 2445, 1997.
- ²² E.L. Portnoi, N.M. Stelmakh, A.V. Chelnokov, *Sov. Tech. Phys.Lett.* (USA), vol. 15, P 432, 1989. Translation of: *Pis'ma v Zh. Tekh. Fiz.* (USSR).
- ²³ S. Cova, M. Ghioni, A. Lacaita, C. Samori and F. Zappa, *Appl. Opt.*, vol. 35, P 1956, 1996.
- ²⁴ A. Lacaita, M. Ghioni, S. Cova, *Electron. Lett.*, vol. 25, P 841, 1989.
- ²⁵ S. Cova, A. Lacaita, M. Ghioni, G. Ripamonti and T. A. Louis, *Rev. Sci. Instrum.*, vol. 60, P 1104, 1989.
- ²⁶ G. S. Buller, J. S. Massa and A. C. Walker, *Rev. Sci. Instrum.*, vol. 63, P 2994, 1992.
- ²⁷ D. V. O'Connor and D. Phillips, "Time-correlated single photon counting," Academic Press, New York, 1983.
- ²⁸ S.G. Ayling, J. Beauvais, and J.H. Marsh, *Electron. Lett.*, vol 28, P 2240, 1992.
- ²⁹ M. W. Street, N. D. Whitbread, D. C. Hutchings, J. M. Arnold, J. H. Marsh J. S. Aitchison, G.T. Kennedy, and W. Sibbett, *Opt. Lett.*, vol. 22, P 1600, 1997.
- ³⁰ A. Gustafsson, M. E. Pistol, L. Montelius, L. Samuelson, *J. Appl. Phys.*, vol. 84, P 1715, 1998.
- ³¹ G. Abstreiter, E. Bauser, A. Fischer, and K. Ploog, *Appl. Phys.*, vol. 16, P 345, 1978.
- ³² S. Nakashima, M. Hangyo, *IEEE J. Quantum Electron.*, vol. 25, P 265, 1989.
- ³³ J. B. Hopkins, L. A. Farrow, G. J. Fisanick, *Appl. Phys. Lett.*, vol. 44, P 535, 1984.
- ³⁴ W. J. Brya, *Solid State Commun.*, vol. 12, P 253, 1973.
- ³⁵ K. Yamazaki, R. K. Uotani, R. K. Nambu, M. Yamada, K. Yamamoto, K. Abe, *Jpn. J. Appl. Phys.*, vol. 23, P L403, 1984.
- ³⁶ R. J. Nemanich, *Mat. Res Soc. Symp. Proc.*, vol. 69, P 23, 1986.
- ³⁷ Renishaw Transducer Catalogue, Raman Group, *Renishaw Transducer Systems Division*, Gloucestershire, GL12 7DH, UK.
- ³⁸ Ian Wilcock, and Ian Hayward, Renishaw Transducers, Private communication.
- ³⁹ S. Adachi, *J. Appl. Phys.*, 58, P R1, 1985.
- ⁴⁰ Z. C. Feng, S. Perkowitz, D. K. Kinell, R. L. Whitney, D. N. Tawlar, *Phys. Rev. B*, vol. 47, P 13466, 1993.
- ⁴¹ B. Jusserand, J. Sapiel, *Phys. Rev. B*, vol. 24, P 7194, 1981.
- ⁴² C. Melteni, L. Colombo, L. Miglio, G. Benedek, M. Bernasconi, *Phil. Mag. B.*, vol. 65, P 325, 1992.

- ⁴³ J. S. Aitchison, M. W. Street, N. D. Whitbread, D. C. Hutchings, J. H. Marsh, G. T. Kennedy, W. Sibbett, *IEEE J. Selected Topics Quant. Electron.*, vol. 4, P 695, 1998.
- ⁴⁴ P. Cusumano, B. S. Ooi, A. Saher Helmy, S. G. Ayling, A. C. Bryce, J. H. Marsh, B. Voegelé, and M. J. Rose, *J. Appl. Phys.*, vol. 81, P 2445, 1997.
- ⁴⁵ O. K. Kim W. G. Spitzer, *J. Appl. Phys.*, vol. 50, P 4362, 1979.
- ⁴⁶ D. Kirillov, P. Ho, G. A. Davies, *Appl. Phys. Lett.*, vol. 48, P 53, 1986.
- ⁴⁷ Y. Suzuki, H. Iwamura, O. Mikami, *Appl. Phys. Lett.*, vol. 56, P 19, 1990.
- ⁴⁸ Y. Suzuki, H. Iwamura, O. Mikami, *IEEE Photon. Technol. Lett.*, vol. 2, P 818, 1990.
- ⁴⁹ P. Dumais, A. Villeneuve, A. Saher Helmy, J. S. Aitchison, *Optics Express*, vol. 2, P 455, 1998.
- ⁵⁰ D. Kirillov, P. Ho, G. A. Davies, *Appl. Phys. Lett.*, vol. 48, P 53, 1986.
- ⁵¹ E. H. Li, B. L. Weiss, and K. S. Chan, *Phys. Rev. B.*, vol. 46, P 15181, 1992.
- ⁵² M. L. Ke, and B. Hamilton, *Phys. Rev. B.*, vol. 47, P 4790, 1993.
- ⁵³ M. L. Ke, J. S. Rimmer, B. Hamilton, et al, *Phys. Rev. B.*, vol. 45, P 14114, 1992.
- ⁵⁴ U. Ekenberg, *Phys. Rev. B.*, vol. 36, P 6152, 1987.
- ⁵⁵ P. Lawaetz, *Phys. Rev. B.*, vol. 4, P 3460, 1971.
- ⁵⁶ W. T. Masselink, P. J. Pearah, J. Klem, C. K. Peng, H. Morkoc, G. D. Sanders, and Y. C. Chang, *Phys. Rev. B.*, vol. 32, P 8027, 1985.
- ⁵⁷ W. C. H. Choy, P. J. Hughes, and B. L. Weiss, *Mat. Res. Soc. Symp. Proc.*, vol. 450, P 425, 1997.
- ⁵⁸ W. C. H. Choy, P. J. Hughes, and B. L. Weiss, E. H. Li, K. Hong, D. Pavlidis, *Appl. Phys. Lett.*, vol. 72, P 338, 1998.

CHARACTERISATION OF LATTICE CONSTITUENTS AND DEFECT DIFFUSION

Native point defects and lattice atoms play a major role in inter-diffusion. Studying the effect of such particles' concentration, profile, and thermodynamic properties on intermixing is of prime importance for understanding the mechanisms and modelling the kinetics of the process. Direct measurement of point defects is still an open question, while the resolution by which we can depth-profile native matrix elements is not usually great, when compared to the abruptness of heterostructure interfaces. Therefore there is a pressing need for a comprehensive, yet simple and versatile means to characterise the different mechanisms involved in the process of quantum well intermixing. While optical techniques proved valuable in characterising the distribution of intermixing in the semiconductor structures, as discussed in the previous chapter, they are harder to use to probe the particles associated with inter-diffusion. Non-optical techniques will, therefore, have to be used for this task.

I. NON-OPTICAL CHARACTERISATION TECHNIQUES

Although optical spectroscopy techniques are widely used to investigate intermixing,^{1,2} the accuracy of the values provided by many of these techniques is still a topic of current research.^{3,4} Other, destructive, measurement techniques such as cathodoluminescence, deep level transient spectroscopy and Rutherford backscattering, can be however used to provide more accurate answers. Tedious sample preparation is needed, though, in some of these techniques. Another drawback of destructive techniques is that they cannot be used for monitoring the performance of intermixing processes at different stages of PIC fabrication. In addition, direct measurements of some important parameters, such as vacancy/Ga flux at a GaAs/SiO₂ interface, are not possible to carry out, while others have to be measured indirectly. The diffusion coefficients of point defects, for example, are often inferred indirectly from other parameters such as sample conductivity, or the amount of induced intermixing in QWs.^{5,6} Indirect measurements of any given parameter leaves room for much uncertainty and inaccuracy.

One important reason for the difficulties found in measuring parameters describing lattice constituents from optical techniques, is the probing range of an optical beam in a given material. The probing range of an optical beam is dependent on its wavelength and the absorption the photon suffers. The lower limit on the accuracy of probing the surface layers of any structure using visible and infrared photon energies is approximately 15 nm.⁷ While this is a fairly low value, averaging parameters over such layer thicknesses is not accurate enough for many measurements and is also the upper limit for ion-beam techniques. Such techniques use ions and electrons as a means of probing the lattice. Typical probing depths of these particles can be ~ 1 nm for ions, ~ 2 nm for electrons, and from 15 to 1000 nm for photons, depending on their absorption in the material.⁸ Due to their atomic-scale penetration depths, the ions and electrons, when used under ultra-high-vacuum, UHV, can investigate the top most few monolayers of a material.^{8,9,10} When used with sputtering mechanisms, they can also be a powerful tool for quantitative depth profiling of defects and lattice constituents, with an atomic-layer accuracy.

Physical properties, such as particle mass, chemical activity, and particle binding energy are used to characterise the lattice atoms and point defects.^{9,10,13} Various techniques such as X-ray photoelectron spectroscopy (XPS), secondary mass ion spectroscopy (SIMS), Auger electron spectroscopy (AES), and Rutherford backscattering (RBS), are available for semiconductor lattice analysis:

XPS is based on illuminating samples in a vacuum with X-rays. The X-rays will induce photo-generated carriers in the material as a result. The binding energy of the chemical configuration of the surface elements governs the energy of the photo-emitted carriers. Different atoms in different chemical configurations can hence be identified using the energy of the photo-emitted carriers. Depending on the incidence angle of the X-rays, the probed depth can be varied from fractions of nanometer, to a few nanometers. In conjunction with a sputtering system, XPS can depth profile the constituents of any material, which can be sputtered using an ion beam.^{9,10,13} It has been used lately to investigate the surface treatments used in certain IFVD process. In one example, XPS was used to identify the nature of the oxide on the surface and its relation to the induced intermixing for a particular IFVD process.¹¹ It is a particularly attractive technique because of the low damage induced by the X-rays, and hence the minimal redistribution it causes to the topmost monolayers of the sample surface.

AES is based on detecting the electrons excited when an electron beam is incident on the sample. The excited electrons are called Auger electrons, and are emitted with characteristic energies depending on the elemental composition of the sample.^{9,10,13} AES was one of the first techniques used to investigate inter-diffusion in heterostructures due to QWI,¹² it was also used to profile thermally induced Ga/Al inter-diffusion.¹³

SIMS uses a beam of low energy ions to knock-off the constituents of a sample's surface. The sputtered particles are then detected directly using a mass spectrometer. A sputtering source with sufficient energy can be used to enable depth profiling of the sample, which makes the technique very attractive for semiconductor studies. This mode of measurement is often called dynamic SIMS, and has been used extensively to investigate various aspects of intermixing processes. It has been used to profile the inter-diffusion of QW/barrier constituents, out-diffusion of lattice atoms in IFVD, and impurity diffusion in impurity induced intermixing.²

While the techniques discussed above probe the particles' physical and chemical properties, other methods exist to characterise the electronic properties of the particle,⁵ of which deep level transient spectroscopy, DLTS, is powerful example.¹⁴ By making temperature scanned transient capacitance measurements of *p-n* junctions or Schottky barriers, one can identify emission and/or capture centres located within the energy bandgap of semiconductors. Identification can take place at various depths within the depletion region of the sample.¹⁵ Different traps existing at different energies within the bandgap, can have their energy, concentration profile, and spatial variation, resolved, each corresponding to a different type of lattice defect or impurity.^{16,17} DLTS has proven very useful in identifying

and studying impurities, it has also been used to investigate defects introduced during annealing of compound semiconductor structures.¹⁸

In this chapter we shall investigate two issues:

- i. Identification of the native point defects associated with IFVD and their change with the annealing temperature and hence the amount of intermixing. This will be carried out using DLTS measurements.
- ii. The out-diffusion of the semiconductor matrix elements into the dielectric caps used within this work, and how the diffusion of lattice atoms affect intermixing. This will be conducted using SIMS measurements to trace the GaAs lattice atoms within the dielectric cap.

II. CHARACTERISATION OF POINT DEFECT

Most processes of QWI take place through diffusion of point defects and therefore require a means of introducing the defect concentrations. Accordingly, QWI will benefit a great deal if native point defects are better understood and characterised. The properties of native point defects in compound semiconductors are not well documented. Various means of studying defects have been exploited over the past few decades, of which DLTS, positron annihilation (PA), and electron paramagnetic resonance (EPR), are the most effective.¹⁹ Despite being powerful in detecting point defects, these techniques do not provide much information about the thermodynamic properties of defects. Defect thermodynamics is important because of its direct relevance to the process of intermixing. From the thermodynamic properties of a defect, one can obtain information about its energy of formation, its diffusion and recombination, all of which have a direct impact on intermixing kinetics.²⁰ In addition, differential thermal analysis has been proven to be a powerful technique for identifying thermodynamic properties of point defects.¹⁹ In this study, we shall use DLTS to measure the deep level traps generated during IFVD of GaAs/AlGaAs samples and then match the traps to the point defects most likely to be generated by this QWI process.^{1,2,20, 21}

DLTS is an electrical method to characterise deep level traps. It relies on high frequency (MHz regime), thermal scanning of capacitance transients caused by the charging and discharging of traps available within the depletion region of a p - n junction or a Schottky barrier. After the traps are charged, monitoring their subsequent discharge behaviour to reach equilibrium-state again, as a function of temperature conveys information about the concentration, electrical charge, and the position of these traps in bandgap.¹⁴ Several conditions must be fulfilled for DLTS measurements to convey valid results:¹⁹

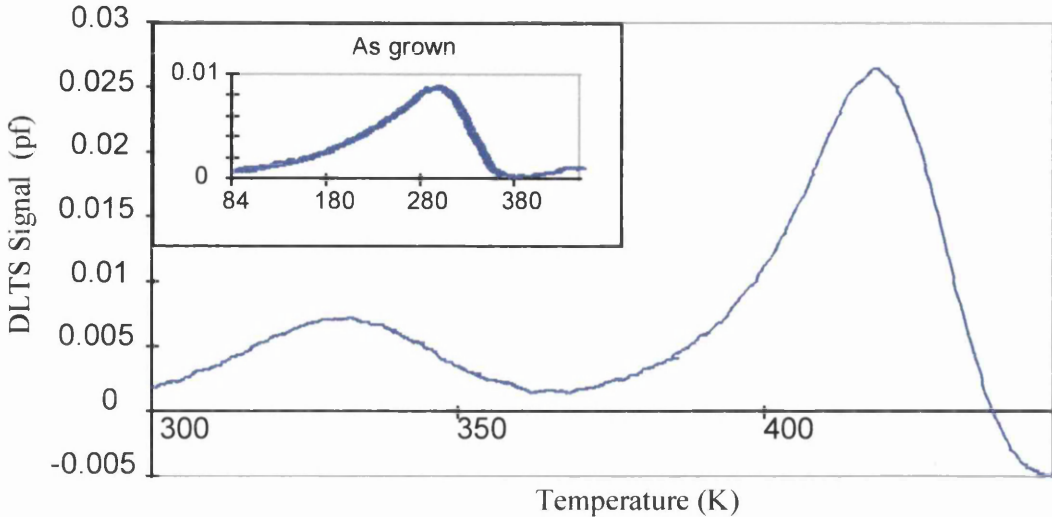


Fig. 6.1 Plot of the DLTS signal of a sampled annealed at 925 °C for 120 s.

- The width of the space charge region, which is determined by the free carrier concentration, must remain unchanged throughout the whole emission stage. This requires a trap concentration at least one order of magnitude lower than the background carrier concentration in the lattice. Failure to meet this condition results in a non-exponential emission and hence an apparent shift in the temperature at which the defect induces maximum capacitance (defect signature). This leads to an apparent reduction in the defects' concentration, and has been previously reported for the EL2 defect in GaAs.^{22,19}
- Leakage current and recombination centres, when are of a magnitude comparable to the defect emission rate, can reduce the apparent concentration of the detected traps.¹⁹ Therefore they should be minimised. One way of insuring such a condition can be done by testing devices with the lowest leakage currents. In addition, the leakage current can be plotted as a function of the device area for a range of device sizes. For an insignificant contribution from side-wall, leakage the leakage current measured should be linear with the change in area.
- Trap signatures should be compared at similar rates,^{23,19} because the change of emission rate with the electric field can change the apparent trap signature. It should be noted that this change of emission rate with the electric field also increases with the doping concentration for a given applied bias.

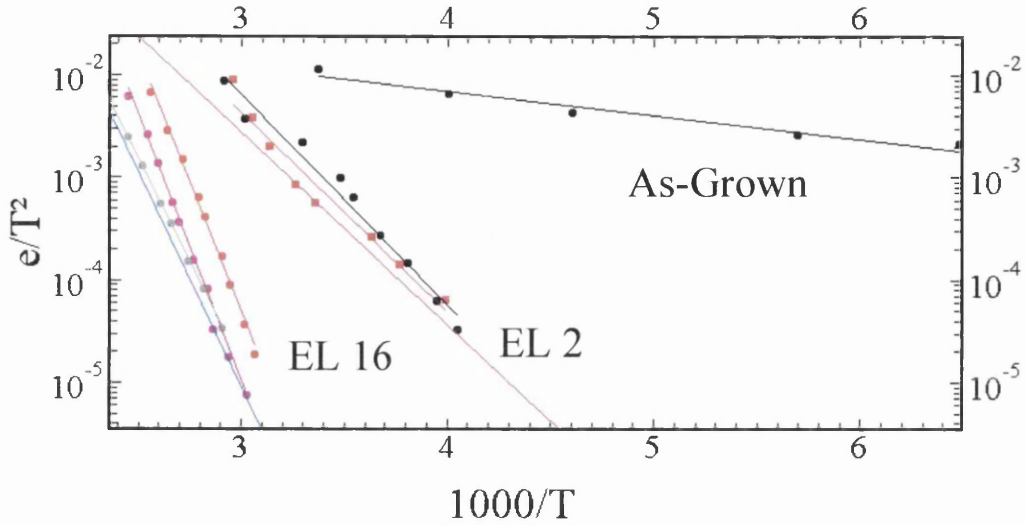


Fig. 6.2 Arrhenius plot of the signature of deep level traps identified in the various samples tested using DLTS.

II.A. Studying Vacancy Diffusion using DLTS

The defects introduced during IFVD are known to be primarily V_{III} .^{1,2,20} Most of the evidence for this assertion has been obtained indirectly by measuring the Ga concentration in the dielectric caps,^{24,25} and the Al/Ga interdiffusion coefficient during annealing,⁶ etc. It would be an advantage to monitor the movement of such defects directly, but in general, the concentration and type of vacancy can be difficult to establish. A powerful method for characterising defects both in semiconductor material and in devices is DLTS.¹⁴ Laser structures are not suitable for DLTS measurements, as it is not possible to move the depletion region through the gain section, which is the region of interest. In order to estimate the concentration of vacancies and other defects induced by the IFVD process, GaAs samples containing a p^+n junction were fabricated for DLTS measurements.

The structure, shown in Appendix A (*DLTS structure*), consisted of an n^+ substrate with a 1.5 μm thick unintentionally doped ($2 \times 10^{16} \text{ cm}^{-3}$) layer, which is the minimum n-type background doping achievable with the machine used. It is then capped by 0.05 μm of p^+ GaAs ($6 \times 10^{18} \text{ cm}^{-3}$) grown by MOCVD. The reverse bias was varied between 0 V and -5V so allowing the depth 0.8 to 1.3 μm to be probed, leaving some margin for variation in doping concentration. This depth range is located at the same depths as the QWs in the SCH *pin* laser structures (see *Laser structures* in Appendix A). Samples were cleaved to dimensions of $\sim 6 \times 6 \text{ mm}^2$ and were processed in exactly the same fashion as for the PLE samples (see chapter 5).²⁶ The samples were then patterned with four different diameter diodes. After removing the SiO_2 cap by wet etching using buffered HF for 30 s. P-type contacts were

formed using Ti/Pd/Au with thicknesses of 33 nm/33 nm/150 nm respectively by evaporation and lift-off. N-type contacts were formed using Au/Ge/Au/Ni/Au with thicknesses of 11 nm/11 nm/11 nm/14 nm/240 nm respectively. Both contacts were annealed at 360 °C for 60 s. The devices were then mesa isolated by wet etching in a H₂O₂:NH₄ solution with a composition of 95:5 for 60 s using the p-contact as a mask, leading to a 1 μm etch depth for isolation.

The reverse bias leakage current of the diodes was measured after fabrication. Some diodes from both processed and control samples showed large variations in leakage current. These were discounted, and only diodes falling on a straight line of leakage current versus diode area (confirming the absence of leakage from the edges) were wire-bonded for measurement.

For the as-grown sample, capacitance-voltage measurements indicated a doping concentration of around 10¹⁶ cm⁻³ at 0 V, which was confirmed using an electrochemical profiler, rising to 10¹⁷ cm⁻³ at -3.5 V. This, higher than expected, doping gives a relatively small probe range of ~ 0.01 μm at a depth of ~ 1 μm, depending on the particular doping concentration each sample. A comparison of results for the as-grown samples and for the same structure subjected to the IFVD process at 925 °C for 120 s is shown in Fig. 6.1. The as-grown sample has a relatively shallow level at 46 meV, which is native to the material. This may be the Si shallow donor at 58 meV, but with the emission energy influenced by field emission.¹⁹ The level is not detectable in the processed material and may be masked by the two induced deep levels shown in Fig. 6.1. The spectra were taken at a rate window of 1000/s with reverse bias of ~3.5 V with a fill pulse duration of 3.8 ms. Arrhenius plots for several samples are shown in Fig. 6.2 which were obtained by varying the rate window over the range 1000/s to 0.8/s (the fill pulse width was also varied to match the measurement time). The variation in signature (activation energy and apparent cross-section) has been confirmed as being due to the field dependence rather than sample variation. The closely identified levels EL2 and EL16 are shown in Fig. 6.2 for comparison.²⁷

- The origin of EL2 has long been a source of controversy, though many authors agree that it is a complex involving an As antisite i.e. arsenic on a gallium site As_{Ga}, coupled to an arsenic interstitial I_{As}. Phenomenologically,¹⁹ EL2 is found in bulk, VPE, and MOCVD material, and increases in concentration with As rich conditions. This is consistent with out-diffusion of Ga into the SiO₂ cap leaving As rich complexes behind associated with the excess Ga vacancy concentration. An increase in the EL2 concentration has also been observed before for similar processing procedures.²⁸

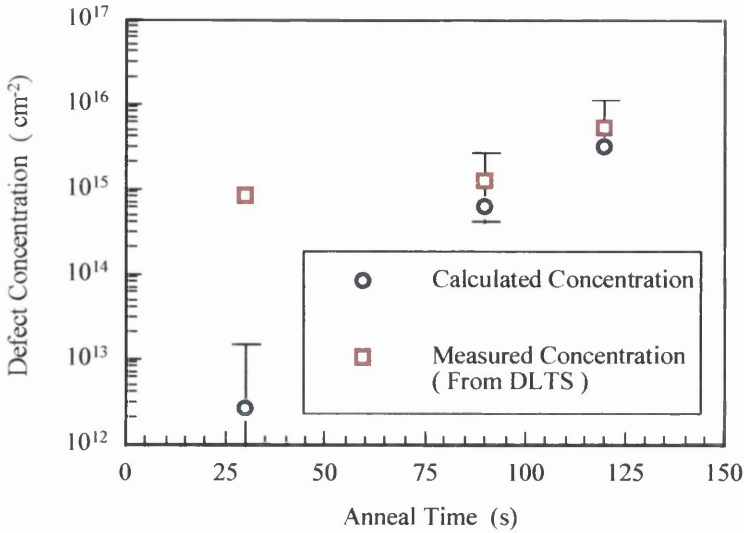


Fig. 6.3 Comparison of the number of point defects obtained from the DLTS measurements and those calculated from the model for the same annealing parameters.

➤ EL16 is a trap also associated with VPE material, although it has not been studied in much detail.

Measurements made at low reverse bias ~ 0.5 V produce an added complication of sign reversal for the trap assigned EL2, which can lead to the trap being misinterpreted as a hole trap. This well-known artifact occurs when the series resistance is large compared with the capacitive reactance at the measurement frequency.¹⁹ The series resistance was independently measured on a HP LCR meter and found to be comparable to the capacitive reactance of the samples for samples showing sign reversal at low reverse bias, again confirmed by observation of the sign reversal from the 20/s rate window (normal electron trap) to 50/s rate window (reversed, apparent hole trap) at 1 V reverse bias. The conclusion is that any hole like traps are merely artifacts of the high series resistance of the samples.²⁹

To obtain the trap concentration, the approximate formula,¹⁴ $N_T = 2N_D \Delta C/C$ can be used. For N_D of $3 \times 10^{17} \text{ cm}^{-3}$, the formula gives a trap concentration value of $N_T = 4 \times 10^{15} \text{ cm}^{-3}$ for EL2 and $1.4 \times 10^{15} \text{ cm}^{-3}$ for EL16 for the sample annealed at 925 °C for 120 s. Broadly, it was found that the EL2 trap concentration increases with annealing temperature, though detailed analysis of the behaviour with annealing temperature and time requires further investigation. The peak concentrations of the EL2 trap have been calculated³⁰ and are plotted in Fig. 6.3. On the same graph, the defect concentrations calculated from the model described in chapter 3 are also plotted for the same anneal temperatures and at the same probing depth of 1 μm . As can be seen, an order of magnitude agreement between the measured EL2 trap concentration and the defect concentration predicted by the model is

obtained, except for the shortest anneal time of 30 s.³⁰ This is attributed to the limitations in the model. The inaccuracy in the model for defect diffusion, and the parameters used for the diffusion calculations are thought to be the main source of error in the model (see chapter 3).³⁰

II.B. The EL2 Defect and More DLTS Experiments

The results obtained in the previous sections have to be analysed in order to help plan further experiments. The EL2 is of particular interest, since it is known to be a composite defect associated with As antisites.¹⁹ Its observation was not surprising, however, in the experiment presented above. The EL2 has been often observed when annealing GaAs-based compounds at elevated temperatures. The agreement between the measured EL2 concentration with that of the defects expected to induce the observed intermixing is a promising and important result which. It spawned further investigations about the nature and characteristics of EL2, of which the next few points are thought to be worth noting:

- i. Contrary to beliefs when EL2 was first discovered, EL2 is not related to the presence of oxygen in GaAs.^{16,19}
- ii. The EL2 trap is not related to an impurity within the GaAs, it is related to lattice point defects and/or lattice defect complexes.^{16,19}
- iii. The EL2 trap can only be observed in singly or doubly charged donor states.^{16,19}
- iv. Although EL2 is usually observed in a normal fundamental state, it can also be observed in a metastable state, which is a different configuration from that of the fundamental one. The EL2 switches between the two states depending on the thermal and optic excitations applied on the lattice.^{16,19}
- v. The As antisite, As_{Ga} , defect is one of the constituents of EL2 and matches well its metastable behaviour.^{16,19}
- vi. Thermodynamic studies of EL2 suggest that lattice vacancies, V_{III} and V_V , are part of its composition. On the other hand, EPR studies suggest that the Arsenic interstitial, I_{As} , is one of the constituents of EL2.

The nature of EL2, being known to represent an As_{Ga} based defect, matches the understanding of the IFVD process well; at non-equilibrium, as a result of Ga out-diffusion into the dielectric caps, group III vacancies, V_{III} , and interstitial As atoms, I_{As} , will be generated. At equilibrium V_{III} will tend to combine with I_{As} , and form As_{Ga} based defects.

Further experiments were carried out on MOVPE and MBE samples. Two batches of samples, one from each growth technique, were processed in a similar manner to that described above, and diodes were fabricated. The traps detected included EL2, but this time the deep level trap E5A was also detected. This process was different in one respect from that

in section the previous section, the deposition of the e-gun silica was carried out at 90 °C, instead of room temperature, to enhance silica adhesion. Further characterisation is under way. The most noticeable observation is that the EL2 trap is not readily observable in all the parameter space of the DLTS measurement system, and it disappears for some parameter settings. This phenomenon is being characterised, and may be linked to the metastable state of the defect. However before going further, a separate experiment to determine the origin of the E5A should be carried out. DLTS measurements conducted on samples coated with e-gun silica deposited at different temperatures are underway.

III. OUT-DIFFUSION OF LATTICE CONSTITUENTS

Quantum well intermixing takes place because of the in-diffusion of native point defects from the semiconductor surface due to out-diffusion of lattice constituents into the caps. The out-diffusion of different lattice constituents into the dielectric caps, when annealed at elevated temperatures, is therefore fundamental to the IFVD process. Studying out-diffusion into dielectric caps can convey information and show indications about the process mechanisms. In addition, it provides quantitative information for modelling the QWI processes.^{31,30} The concentration of Ga in dielectric films after annealing has been observed in several previous studies using various techniques such as XPS, AES, and SIMS.^{32,33,34} Although essentially a destructive technique, SIMS is well suited to study this phenomenon because it can quantify the concentration of the elements diffusing into the cap, and into the semiconductor. For certain elements its sensitivity can be as good as 10^{13} cm^{-3} , with lateral and depth resolution better than 1 μm and 2 nm respectively. SIMS can also be used for conducting and non-conducting materials by choosing the appropriate primary ion source, and hence can be used to profile both the dielectric cap and the semiconductor.⁹

SIMS is based on analysing sputtered secondary ions, by using a primary ion source impinging on the sample surface. When the primary ions strike the sample surface, energy is transferred elastically, in a collision cascade process, to atoms within the sample matrix. Some of the energy is transferred to the surface atoms and causes their dissociation from the sample matrix. The desorbed particles may be atoms or molecules, in a neutral, ionised or excited states. In such measurements, the ions are accelerated, mass resolved using a mass spectrometer, and then detected. The sputtered particles are usually generated within 10 nm of the sample surface, however this is dependent on the primary ion beam. In static SIMS, where the measurement is only conducted on the surface of the sample, a low primary ion beam energy secures minimal disruption of the original status of the matrix. On the other

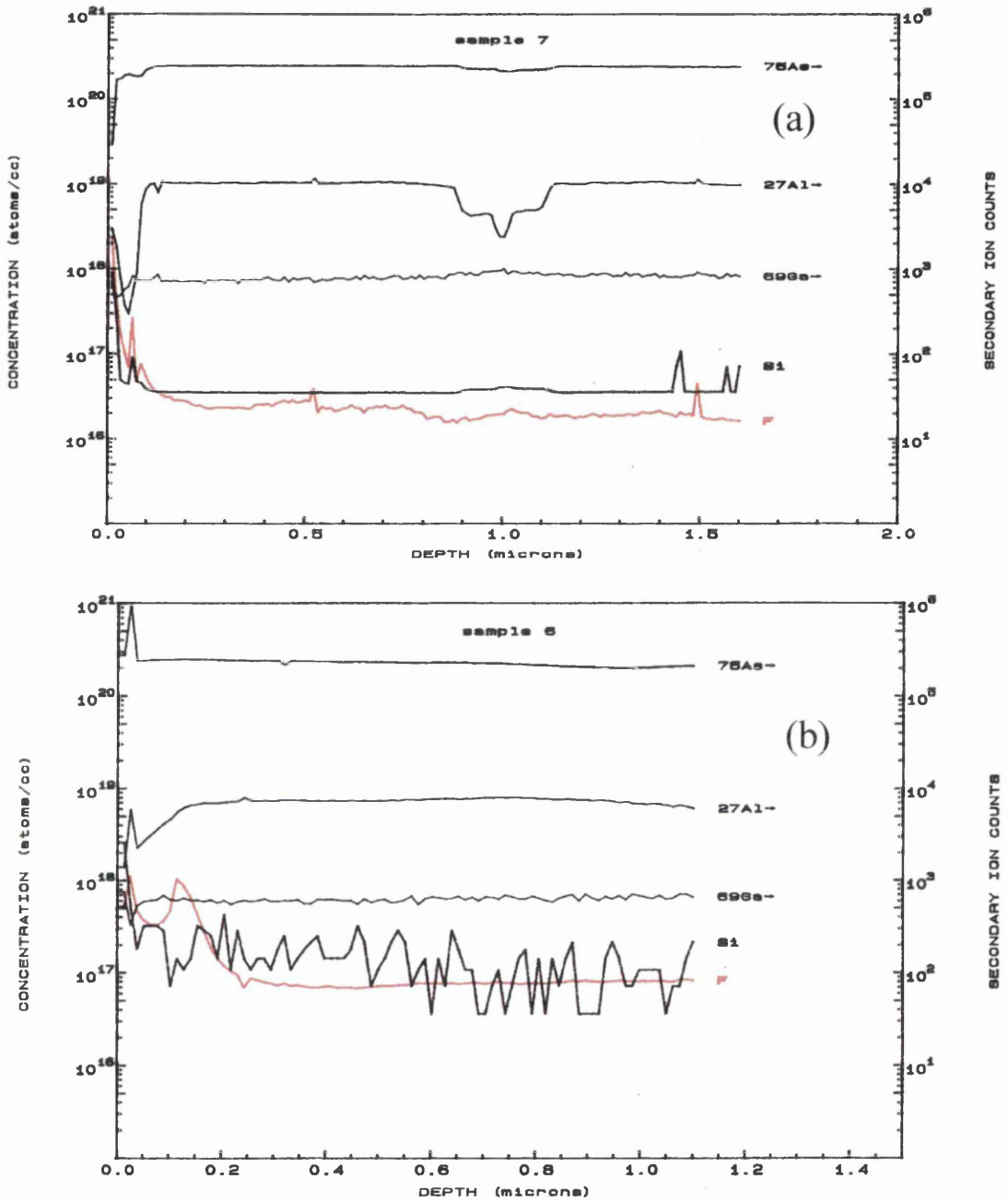


Fig. 6.4 SIMS profile of various GaAs and SiO₂:F constituents in the semiconductor with different depth resolutions.

hand, for dynamic SIMS, where there is sufficient energy in the primary ion source to scan the sample constituents with depth, the sputtering process can modify the matrix.

The varying yield of the same element within different matrixes has a notable effect on the quantitative accuracy of the concentrations provided when using SIMS in a multiple layer sample. Because this is exactly the case for in the samples tested in this work, where there is a semiconductor crystal lattice covered by several hundreds of nanometers of an

amorphous cap, the calibration of the measurements was conducted for the semiconductor lattice only. Therefore the concentrations obtained from the dielectric cap should not be taken quantitatively.⁹

An O_2^- ion source is usually used as a means of enhancing the yield of positive secondary ions and, hence, the system sensitivity.⁹ Also Cs^+ can be used for detecting negatively charged sputtered ions. However when sputtering the dielectric region using this ion source, charging effects are possible and can mask the signal detection from the surface.

In the following section we shall describe measurements of dielectric caps' matrix and the semiconductors' lattice elements on samples annealed with various dielectric caps. The results will be correlated with the amount of intermixing observed in these samples.

III.A. Studying Out-Diffusion in Dielectric Caps using SIMS

SIMS has been extensively used for investigating intermixing of III-V structures.² Measurements of superlattice (SL) disordering due to IID have been carried out, both in early and recent work of intermixing, giving clear representation of the disordering.^{35,36} It was also used to investigate implantation induced intermixing in SL structures,³⁷ and to trace the out-diffusion of semiconductor species into dielectric caps after annealing.³⁸ Although SIMS is a useful means for investigating disordering in heterostructures, it does suffer from some drawbacks. Depth profiling using SIMS depends on sputter etching, which might affect the distribution of the species studied. Furthermore, monolayer depth resolution is not readily available using such a technique. Such depth resolution is necessary to be comparable with heterostructure interfaces. Therefore SIMS, although powerful, has serious limitations concerning the accuracy of the measurements it can provide. In static SIMS however, the sputtering beam has less impact on the surface elements because the typical ion source energy, which varies between 1 and 15 keV is too low to cause 'knock-on' artifacts.⁸ In this section, we shall investigate

the out-diffusion of the lattice constituents into various dielectric caps, some of which enhance intermixing and others that suppress it. The caps investigated here are $SiO_2:P$, $SiO_2:F$ and SiO_2 . The $SiO_2:F$ cap did not show any sign of inhibiting intermixing, as discussed in Chapter 4,

Table 6.1 Experimental conditions for both ion species used in the SIMS experiments.³⁹

Primary Ion Source	Cs^+	O_2^-
Primary Ion Energy	10 keV	12.5 keV
Primary Ion Current	0.1 μA	0.1 μA
Raster Size	250 μm	250 μm
Secondary ions	+&-	+
Transfer Lens	150 μm	150 μm
Analysed Area	60 μm	10 μm
Mass Resolution	250	250

however it was thought to be interesting to observe whether fluorine diffuses into the semiconductor (see discussion about the effect of fluorine on intermixing in Chapter 2). The SiO₂:P cap has been demonstrated to be a nearly ideal cap for inhibiting intermixing because of the minimal damage associated with annealing such caps, and the degree by which it suppresses intermixing. It is hence of great importance to investigate whether there is any P diffusion into the semiconductor and what are the diffusion rates of Ga and As into the cap. As for SiO₂, being the dielectric cap with the most consistent performance in enhancing intermixing (see chapters 2 and 4 for details), the final aim of this work is to be able to measure the diffusion kinetics of Ga in the cap and hence find out the boundary conditions for its diffusion. This information can then be used to model the associated vacancy diffusion.

Samples were covered with 200 nm of PECVD SiO₂:P, SiO₂:F and SiO₂, then were annealed for 60 s at 925 °C with a rise time of 15 s. SIMS measurements were carried out using O₂⁻ and Cs⁺ ion sources with the experimental conditions presented in Table 6.1. For profiling in the semiconductors, Cs⁺ ions were used with satisfactory accuracy, however when charging effects were observed and caused by the dielectric caps, an O₂⁻ ion source had to be used.³⁹

The samples covered with SiO₂:F were investigated first using the Cs⁺ ion source and the results are shown in Fig 6.4. The position of the heterostructure is obvious from the Al signal in Fig. 6.4 (a), where the profiled depth was large enough to include QWs. It can be clearly seen that, within the semiconductor, there is no F signal, indicating that F did not diffuse during annealing. In Fig. 6.4 (b), a lower sputter rate was used to provide better depth resolution, and it indeed shows the F signal peak within the first 200 nm of the sample, which is the cap thickness, and then drop to the noise level within the semiconductor. From both Figs 6.4 (a) and (b), the tendency of F to accumulate at the SiO₂:F cap surface and the SiO₂:F/GaAs interface is quite apparent. It is also clear that there is no Si diffusion from the cap into the semiconductor that might contribute to intermixing. Although the Ga signal was seen to extend to the cap region, it should be noted that the concentration measured is not to scale since the calibration of the signal is not valid within the dielectric region.³⁹ While the signal decreases rapidly in the dielectric cap confirming the lack of any significant Al in the dielectric caps, the As signal peaks within the SiO₂:F film, confirming also the property of SiO₂ caps to permit As out-diffusion at temperatures over 875 °C.¹ The enhancement of intermixing induced by the SiO₂:F caps reported in Chapter 4, can therefore be ascribed to Ga out-diffusion, and not to a F induced enhancement in the interdiffusion on the group III sublattice.⁴⁰

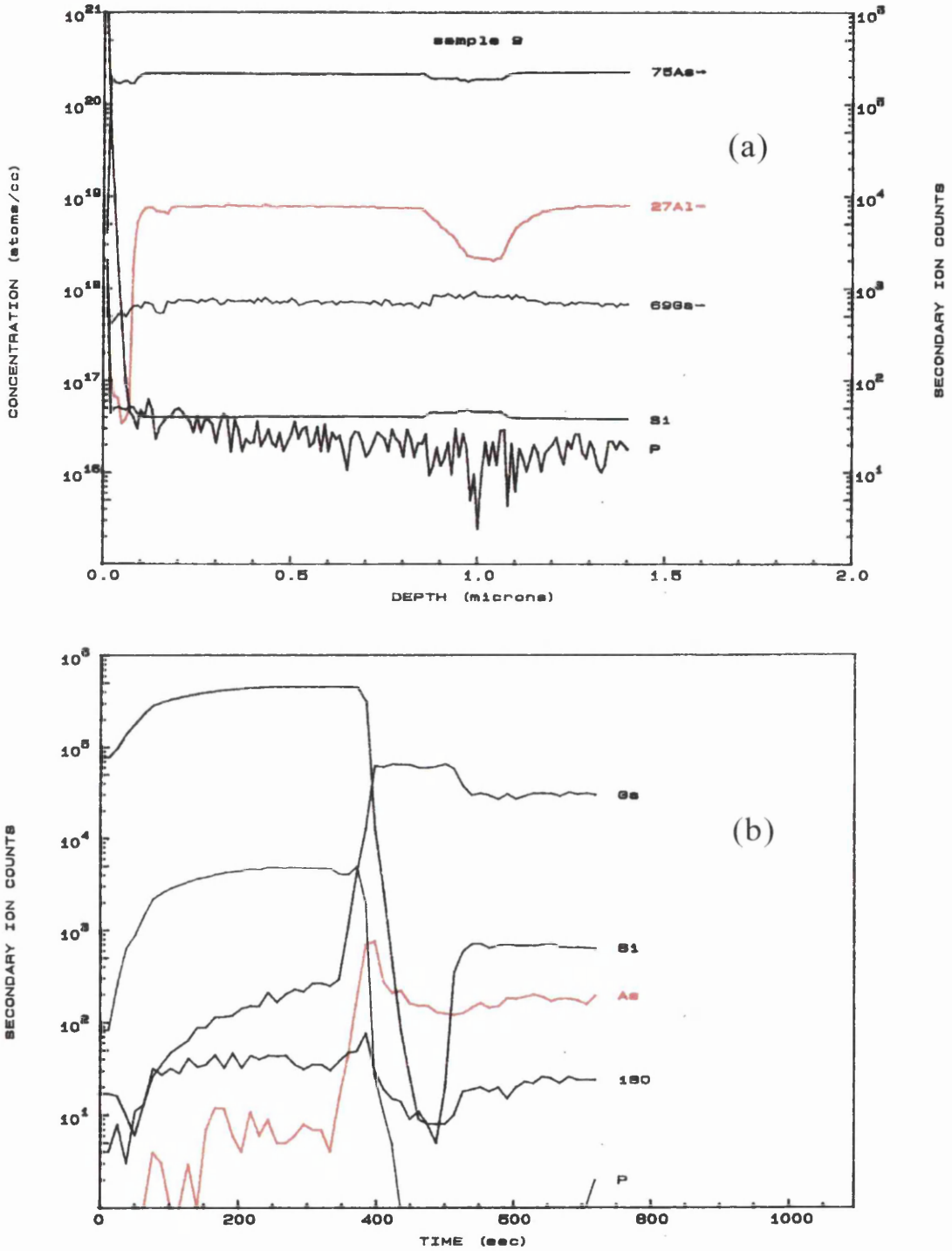


Fig. 6.5 SIMS profile of various GaAs and SiO₂:P constituents (a) in the semiconductor, and (b) in the SiO₂:Pcap

The samples covered with SiO₂:P were investigated next using the Cs⁺ ion source and the results are shown in Fig. 6.5. Similar to the previous samples, the heterostructure position can be seen by monitoring the Al profile, which has a dip at the QWs position, as seen in Fig.

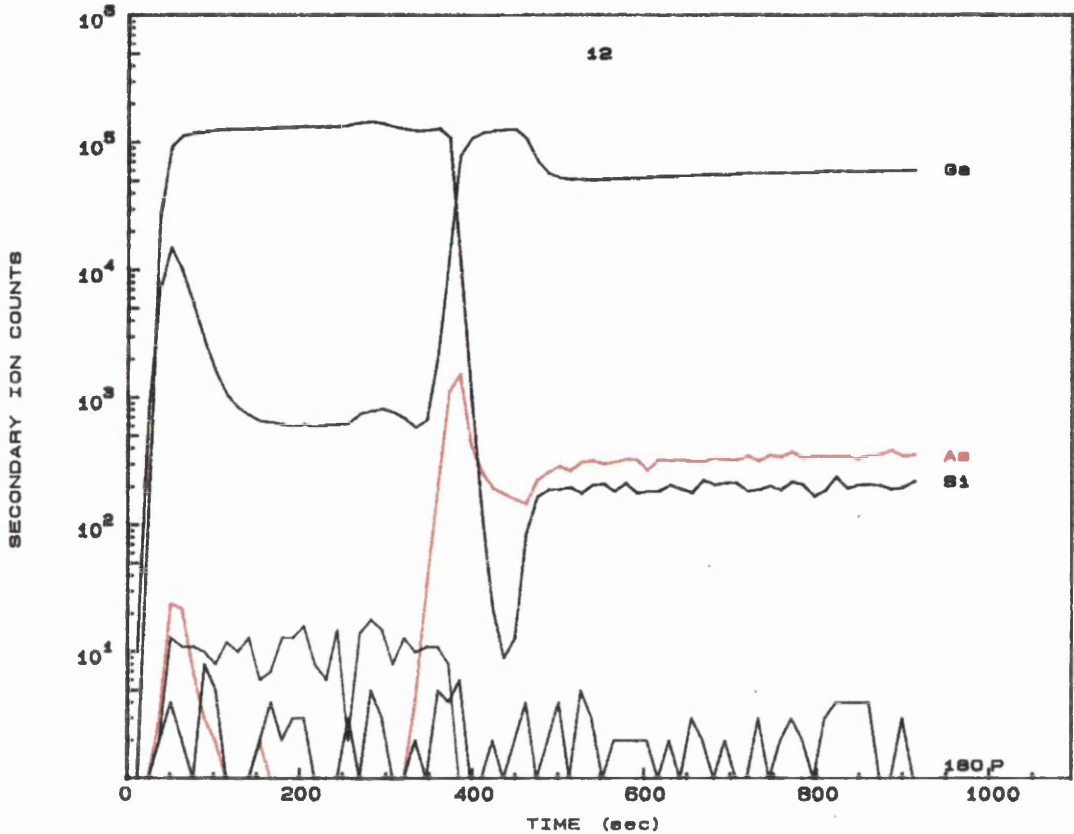


Fig. 6.6 SIMS profile of various GaAs and SiO₂ constituents in the SiO₂ cap.

6.5 (a). However there is no evidence of P diffusion within the semiconductor. It is very interesting to observe that the Ga and As profiles show no signs of diffusion within the dielectric film, agreeing with the observations of minimal intermixing exhibited by such caps at these temperatures. Indeed it is clear that P doping reduces Ga and As diffusion into the SiO₂ caps, and hence minimises QWI.⁴¹ The Cs⁺ ion source was then replaced by the O₂⁻ source to enable high resolution SIMS within the SiO₂:P cap. As can be seen in Fig. 6.5 (b), the profiles of the Si, O₂ and P are clear in the film. Again it can be seen that the concentration of Ga and As can barely be distinguished from the noise level of the signal, confirming that there is no significant Ga or As out-diffusion into SiO₂:P caps during annealing. It should also be noted that, despite the negligible Ga out-diffusion into the cap, slight Ga pile up at the dielectric film surface is evident. This pile-up might explain, in part, the small, but significant, amount of intermixing observed in samples annealed with SiO₂:P caps.⁴² A PL shift of ~ 6 nm is obtained upon annealing GaAs/AlGaAs at 925 °C with SiO₂:P caps, as seen in Fig. 4.4. Although the reasons behind the inhibition of out-diffusion exhibited by SiO₂:P caps is not known, it should be noted that its hygroscopic nature, and the fact that

its performance in inhibiting intermixing degrades by time, are probably related. Further investigations of this as an indication for the mechanisms involved (see section in chapter IV for comments on the effect of water vapour on Ga out-diffusion).

The samples covered by PECVD SiO_2 were measured using the O^- ion source, focusing primarily on the profiles within the dielectric cap to compare them with those of the $\text{SiO}_2\text{:P}$ and $\text{SiO}_2\text{:F}$ caps. As can be seen in Fig. 6.6, the concentration of Ga in the dielectric film is significant, being two orders of magnitude larger than the noise level. It is also evident that there is an accumulation of the Ga atoms at the film surface and at the SiO_2/GaAs interface. In contrast, there was no measurable concentration of As in the cap, but there was some accumulation at the SiO_2/GaAs interface. In addition the P concentration was measured to investigate whether there is any the migration of P from the $\text{SiO}_2\text{:P}$ caps into the SiO_2 cap after annealing samples with SiO_2 and $\text{SiO}_2\text{:P}$ side by side in the same chamber. Another point of interest that was not addressed in this work is to study Ga diffusion profiles in before saturation. Information obtained from such study can help determine the diffusion mechanism of Ga in dielectric caps, and hence quantify the subsequent vacancy in-diffusion from the semiconductor/dielectric interface.

In Summary the measurements show clearly that, in the case of annealing GaAs with $\text{SiO}_2\text{:F}$ caps, the observed intermixing can be ascribed to the out diffusion of Ga in the film. Fluorine atoms, when diffusing interstitially in GaAs, can enhance the inter-diffusion on the group III sublattice, however no F diffusion was evident in the measurements, implying that the intermixing observed in these samples is due to IFVD solely. As for the $\text{SiO}_2\text{:P}$ caps, the absence of Ga in the caps correlate with the inhibition of intermixing. SIMS can be used, with another technique that is sensitive to the chemical configuration of species investigated, to investigate the hygroscopic nature of $\text{SiO}_2\text{:P}$, and its role in the time dependent inhibition of intermixing exhibited by this cap. When profiling the SiO_2 caps, the Ga profile in the caps correlates with the enhancement of intermixing. The apparent accumulation of the Ga on the surface of the cap and at the semiconductor/cap interface requires further study since it affects both the theoretical and technological fronts of the process. It affects the theoretical front, since it proposes unconventional boundary conditions for the diffusion equation at the interface where he accumulation takes place. It will also affect the process where no intermixing is required since this accumulation will produce a small, yet finite, number of vacancies, which can in turn induce some QWI.

IV. SUMMARY

DLTS measurements showed that the EL2, E5A and EL16 deep level traps are introduced upon annealing the samples with SiO₂ dielectric caps. In the first batch of samples, the EL2 concentration at the depth of the QWs was found to match that calculated at the same depth from the model developed for intermixing in chapter 3. The concentrations, however, were only closely matched for anneal times longer than 30 seconds, which might be attributed to limitations of the model to describe the vacancy diffusion for short anneal times. Although there is still some confusion, DLTS measurements have shown promise in identifying the nature of the defects introduced due to the IFVD process.

From the SIMS measurements, it was confirmed that the enhancement of intermixing induced by the SiO₂:F caps, reported in Chapter 4, is due to Ga out-diffusion into the dielectric cap, and not due to F diffusion into the semiconductor. As for the annealed SiO₂:P caps, no evidence of Ga and/or As out-diffusion in the cap was observed. Also no measurable amount of P was found to diffuse into the semiconductor. These observations correlate with the measured amounts of intermixing obtained when annealing GaAs/AlGaAs structures with a SiO₂:P cap. The samples annealed with SiO₂ films showed a considerable Ga concentration within the cap, again correlating with the measured intermixing. The Ga pile-up phenomenon is thought to have significant implications from both the technological and theoretical viewpoints of IFVD and should be further studied.

V. REFERENCES

- ¹ D.G. Deppe and N. Holonyak Jr., *Appl. Phys. Lett.*, vol 64, P R93, 1988.
- ² E. H. Li, editor, "Quantum Well intermixing for Photonics," SPIE Optical Engineering Press, vol. 145, 1998.
- ³ S. Perkowitz, "Optical Characterisation of Semiconductors," Academic Press, Second edition, 1994.
- ⁴ A. Gustafsson, M. E. Pistol, L. Montelius, L. Samuelson, *J. Appl. Phys.*, vol. 84, P 1715, 1998.
- ⁵ S.Y. Chiang, G. L. Pearson, *J. Appl. Phys.*, vol. 46, P 2986, 1975.
- ⁶ K. B. Kahen D. L. Peterson, G. Rajeswaran, and D. J. Lawrence, *Appl. Phys. Lett.*, vol. 55, P 651, 1989.
- ⁷ G. Abstreiter, E. Bauser, A. Fischer, and K. Ploog, *Appl. Phys.*, vol. 16, P 345, 1978.
- ⁸ J. C. Vickerman, editor, "Surface analysis; the principal techniques," John Wiley & Sons, 1997.
- ⁹ J. M. Wallis, editor, "Methods of surface analysis; techniques and applications," Cambridge University Press, 1990.
- ¹⁰ D. P. Woodruff, T. A. Delchar, "Modern techniques of surface science," Cambridge University Press, 1986.
- ¹¹ C. J. Hamilton, J. H. Marsh, D. C. Hutchings, J. S. Aitchison, G. T. Kennedy, W. Sibbett, *Appl. Phys. Lett.*, vol. 68, P 3078, 1996.
- ¹² K. V. Vaidyaathan, M. J. Helix, D. J. Wolford, B. G. Streetman, R. J. Battner, and C. A. Evans Jr., *J. Electrochem. Soc.*, vol. 124, P 1781, 1977.
- ¹³ L.L. Chang, A. Koma, *Appl. Phys. Lett.*, Vol 29, P 138, 1976.
- ¹⁴ D.V. Lang, *J. Appl. Phys.*, vol. 45, P 3023, 1974.
- ¹⁵ A. G. Milles, "Deep impurities in semiconductors," John Wiley & Sons, 1973.
- ¹⁶ S. T. Pantelides, editor "Deep centers in semiconductors," second edition, Gordon & Breach Science Publishers, 1992
- ¹⁷ M. O. Manasreh, H. J. Bardeleben, G. S. Pomrenke, M. Lannoo, D. N. Talwar, editors, "Physics and applications of defects in semiconductors," *Mat. Res. Sci. Sympos.*, vol. 325, 1994.
- ¹⁸ F. Hasegawa, N. Yamamoto, and Y. Nannichi, *Appl. Phys. Lett.*, vol. 45, P 461, 1984.
- ¹⁹ J.C. Bourgoin, H.J. von Bardeleben, D. Stievenard, *J. Appl. Phys.*, vol. 64, P R65, 1988.
- ²⁰ R. M. Cohen, *Mat. Sci. & Eng Reports*, vol. R20, P 167, 1997.

- ²¹ A. G. Milnes, "Deep impurities in semiconductors," John Wiley & Sons, 1973.
- ²² M. O. Watanabe, A. Tanaka, T. Udagawa, T. Nakaniski, Y. Zohta, *Jpn. J. appl. Phys.*, vol. 22, P 923, 1983.
- ²³ S. Makram-ebeid, *Appl. Phys. Lett.*, vol. 37, P 464, 1980.
- ²⁴ Xin Wen, Jim Y. Chi, Emil S. Koteles, Bori Elman and Paul Melman, *J. Electronic Materials*, vol. 19, P 539, 1990.
- ²⁵ T. Haga, N. Tachino, Y. Abe, J. Kasahara, A. Okubora, and H. Hasegawa, *J. Appl. Phys.*, vol. 66, P 5809, 1989.
- ²⁶ A. Saher Helmy, N. P. Johnson, M. L. Ke, A. C. Bryce, J. S. Aitchison, J.H. Marsh, I. Gontijo, G. S. Buller, J. Davidson, P. Dawson, *IEEE J. Selected Topics in Quantum Electronics*, vol. 4, P 661, 1998
- ²⁷ G.M. Martin, A. Mitonneau, A. Mircea, *Electron. Lett.*, vol. 13, P 191, 1977.
- ²⁸ F. Hasegawa, N. Yamamoto, and Y. Nannichi, *Appl. Phys. Lett.*, vol. 45, P 461, 1984.
- ²⁹ D. K Schroder, "Semiconductor Material and Devices Characterisation," Wiley, New York, 1990.
- ³⁰ A. Saher Helmy, J. S. Aitchison, and J. H. Marsh, *IEEE J. Selected Topics in Quantum Electronics*, vol. 4, P 653, 1998.
- ³¹ Y.T. Oh, T.W. Kang, C. Y. Hong, K.T. Kim, T.W. Kim, *Solid State Comm.*, vol. 96, P 241, 1995.
- ³² Sigurd Wagner, and Edward I. Povilonis, *J. Electrochem. Soc.*, vol. 121, P 1487, 1974.
- ³³ Xin Wen, Jim Y. Chi, Emil S. Koteles, Bori Elman and Paul Melman, *J. Electronic Materials*, vol. 19, P 539, 1990.
- ³⁴ T. Haga, N. Tachino, Y. Abe, J. Kasahara, A. Okubora, and H. Hasegawa, *J. Appl. Phys.*, vol. 66, P 5809, 1989.
- ³⁵ J. Kobayashi, M. Nakajima, T. Fukunaga, T. Takamori, K. Ishida, H. Nakashima, K. Ishida, *Jap J. Appl. Phys.*, vol. 25, P 1736, 1986.
- ³⁶ W. Xia, S. A. Pappert, B. Zhu, A. R. Clawson, P. K. L. Yu, S. S. Lau, D. B. Poker, C. W. White, S. A. Schwarz, *J. Appl. Phys.*, vol. 77, P 5616, 1995.
- ³⁷ P. Chen, A. J. Steckl, *J. Appl. Phys.*, vol. 71, P 2602, 1992.
- ³⁸ S. Bürkner, M. Maier, E. C. Larkins, W. Rothmund, E. P. O'Rielly, and J. D. Ralston, *J. Electron. Mat.*, vol. 24, P 805, (1995).
- ³⁹ A. Chew, *Test Report*, Institute of Surface Science and Technology Loughborough University, 1997.

⁴⁰ B. S. Ooi, A. C. Bryce, J. H. Marsh, and J. S. Roberts, *Semicond. Sci. Technol.*, vol. 12, P 121, 1997.

⁴¹ P. Cusumano, A. Saher Helmy, B. S. Ooi, S. G. Ayling, A. C. Bryce, J. H. Marsh, B. Voegelé, and M. J. Rose, *Mat. Res. Soc. Symp. Proc.*, vol.450 , P 419, 1996.

⁴² K. McIlvaney, A. Saher Helmy, A. C. Bryce, S. G. Ayling, J. H. Marsh, C. Jeaynes, unpublished work.

CONCLUSIONS AND FUTURE WORK

The work presented in this thesis studied the kinetics, technology, and some characterisation methods associated with the process of impurity-free vacancy disordering using dielectric cap annealing techniques. The research has generated some results that answered several questions and helped to increase our understanding of the technology. However, this work has also raised many questions about the new mechanisms and phenomena observed. These serve as pointers to some of the limitations of the IFVD technology. The investigations focused on the technology without extending the effort to other aspects such as fabricating device demonstrators. This allowed a variety of measurements and experiments to be carried out with a more concise scope. This chapter will present review the major findings of this work. Some pointers and indications, which also suggest some future work, are presented in the final section of this chapter.

I. CONCLUSIONS

The investigations of modelling the quantum well intermixing kinetics resulted in few findings that are summarised in the following points, together with their implications. Also discussed, are the limitations of the model, the measurements carried out to quantify the parameters necessary for an improved model, and the results obtained from those measurements.

- Statistical models for defect diffusion successfully described the kinetics of compositional intermixing in GaAs. Predictions were obtained for different processes since the model does not depend on the means by which defects are introduced. It could therefore be used to describe implantation damage induced intermixing, as well as dielectric cap annealing induced intermixing.
- Order of magnitude agreement between the predicted and experimentally measured PL shifts was achieved.
- The calculated PL shifts for the process of plasma induced defect layer disordering and the process of impurity free vacancy disordering, were in good agreement with the PL shifts measured, for vacancy diffusion coefficients $2-3 \times \exp[-2.72/k_B T] \text{ cm}^2 \text{ s}^{-1}$. This is a factor of 2-3 more than what has been reported in the literature. However, due to the spread of values reported for the V_{III} diffusion coefficient in GaAs, this agreement is thought to be satisfactory at this stage of the study.
- The important implication in the model is that; if we have a small defect concentration at the QW depth and allow it to stay in the QW vicinity for an extended length of time, this will enable such a relatively small defect concentration to induce a considerable amount of intermixing. We can therefore apply this principle to use minimal defect concentration to induce the bandgap shifts needed for various applications.
- Further improvements of the model will have to be preceded by an accurate characterisation of the various parameters used in the intermixing process modelled.
- For the dielectric cap annealing induced intermixing there are a few points that had to be characterised:
 - The QW diffusion profile, and how it compares with the initial, as grown, QW shape. This will convey information about the diffusion mechanisms of the QW constituents, and whether they follow Ficks' law.
 - The Ga diffusion coefficient in the dielectric caps used in the IFVD process at the annealing temperatures studied.
 - The diffusion coefficient of the V_{III} in the GaAs/AlGaAs heterostructures.

The following experiments were carried out to underpin the parameters mentioned above:

- PLE measurements on as grown samples indicated that as grown QW profiles are not abrupt, as considered in the calculations. PLE measurements on samples intermixed to different extents indicated that the initial and interdiffused QW profiles are best fitted with a symmetric exponential profile. Such a finding means that there are errors when using initial square QW profiles in equations (3.5) and (3.6) to calculate the lattice hops needed for inter-diffusion.
 - Other techniques such as SIMS could not be used since the regions of interest do not exceed 1-2 nm at every heterostructure interface, a thickness which can be easily smeared by the Ar ion beam used for etching away the surface in the depth profiling of SIMS.
- DLTS detected the deep level traps, EL2, EL16 and E5A after annealing MOVPE and MBE grown structures. The EL2 level was further investigated since it is related to the As antisite. This matches well the picture drawn for intermixing being carried out through Ga out-diffusion, which leaves As interstitials and V_{III} behind. At thermal equilibrium, these defects are likely to be found in the form of an As antisite. The concentration of the EL2 trap, when measured at the depths where QWI are situated, matched the concentration predicted from the model describing intermixing. The encouraging results found from the DLTS measurements will have to be re-investigated further and cross-examined using other techniques such as positron annihilation. Even though, DLTS has proven to be a promising technique to investigate defects resulting from the QWI processes.
- SIMS measurements of Ga and As diffusion during annealing showed excessive Ga out-diffusion into the dielectric caps where enhancement in intermixing was observed, and less Ga in the cap, where minimal intermixing was observed. This direct relation between the Ga out-diffusion and the amount of intermixing observed confirms the role of Ga in the process of dielectric cap annealing induced intermixing. It also paves the way for using SIMS to characterise the Ga diffusion profiles, and hence diffusion coefficient into silica caps after rapid thermal processing.
 - Some of the problems include the large diffusion coefficient of Ga in silica, which causes the Ga to saturate within the silica for practical annealing conditions. Therefore, much thicker caps and much shorter anneal times should be used in these investigations to ensure that we can accurately measure the diffusion coefficient.

The investigations of technology of dielectric cap annealing induced intermixing resulted in a new process as well as new pointers to the mechanisms involved in IFVD generally. The performance of the most promising dielectric caps investigated and the new single cap selective intermixing process are summarised below.

- Various dielectric caps were investigated, of which SrF_2 , SiO_2 , $\text{SiO}_2\text{:P}$ are most the important.
- SrF_2 has the best performance in inhibiting intermixing, but surface damage and other technological drawbacks are associated with annealing SrF_2 at high temperatures.
- $\text{SiO}_2\text{:P}$ has a good performance in inhibiting intermixing but has a time dependent performance and is not available in the department where this work is carried out.
- SiO_2 caps are by far the most reliable one, since they always show a similar amount of intermixing each time SiO_2 caps are tested, given that the surface condition is the same.
- Also investigated was PECVD $\text{SiO}_2\text{:F}$, which showed performance very similar to that exhibited by normal PECVD SiO_2 .
- The condition of the surface prior to dielectric cap deposition was also investigated using oxide grown by H_2O , CH_4O and HCl surface treatment was proven to play a substantial role in the intermixing performance observed.
- A selective intermixing process using only SiO_2 was developed, by processing the caps in oxygen plasma to suppress intermixing. Differential shifts in excess of 100 meV at an anneal temperature of 925 °C were achieved with 10 meV shifts underneath the un-intermixed regions.
- The plasma exposure has reduced the amount of attained intermixing in PECVD, sputtered, and E-gun deposited SiO_2 caps. It reduced the amount of intermixing in $\text{SiO}_2\text{:F}$ caps too.
- The plasma was effective in reducing the bandgap for undoped MQW structures as well as DQW p-i-n QW laser structures.

In the final part of the thesis the feasibility of fabricating a bandgap grating, using laterally controlled intermixing was investigated using some optical characterisation techniques. Spatially and temporally resolved PL measurements and Spatially resolved Raman measurements were carried out on intermixed gratings.

- Spatially and temporally resolved PL showed that the resolution of intermixing process is better than 3 μm for 1.5 μm MQW stack 1 μm below the surface. Due to the defects associated with intermixing, carrier lifetime was reduced by a factor 3, where enhanced Ga out-diffusion, and hence intermixing takes place.
- The asymmetry in the grating profiles seen in the line scans of the carrier lifetime as a function of position in the grating samples is a clear evidence of the diffusion of the carriers beyond the excitation point and their subsequent recombination in neighbouring regions with the smaller bandgap.

- Spatially and spectrally resolved PL showed that 1:1 gratings fabricated using IFVD, with periods $< 8 \mu\text{m}$, are a very efficient means of inhibiting intermixing. Such gratings show bandgap shifts less than that exhibited by the inhibiting cap. Also the contrast between the intermixed and un-intermixed regions tend to reach that achieved in large area intermixing for grating periods $> 12 \mu\text{m}$. These results show a direct evidence of the important role of stress in the IFVD process.
- Intermixed gratings and waveguides were also detected, with bandgap shifts as low as 6 nm, using spatially resolved Raman spectroscopy by studying the energy shift and line width of different Raman peaks.
- Possibilities of using Raman spectroscopy as a non-destructive technique to quantify, and detect, spatially, quantum well intermixing are very promising.

II. FUTURE WORK

It seems that the thesis raised questions as often as it has provided answers about several aspects of the dielectric cap annealing induced intermixing process. The suggested work to follow on the findings and implications of this work are:

- Defect recombination on the surface of the semiconductor should be considered and can be readily introduced in equation (3.20).
- The defect recombination during diffusion should also be accounted for.
- The diffusion of the QW/barrier constituents should be modified to fit the profiles experimentally observed.
- To further use the model for InP quaternaries:
 - A model for the change in bandgap of the QW as the interdiffusion takes place on both sublattices should be developed.
 - The model parameters such as the defect diffusion coefficients and QW diffusion profiles should be investigated as was carried out for the GaAs/AlGaAs material system.

Before the process of dielectric cap annealing induced intermixing is acclaimed to be incapable of producing intermixed gratings with sub $12 \mu\text{m}$, the area dependence of this process should be thoroughly investigated. The following points are thought to be a suitable start for this aim:

- The inhibiting performance of the single dielectric cap selective intermixing process should be further optimised and then fully characterised.
- A surface treatment process that preserves the condition of the GaAs surface before dielectric cap deposition should be developed and characterised.

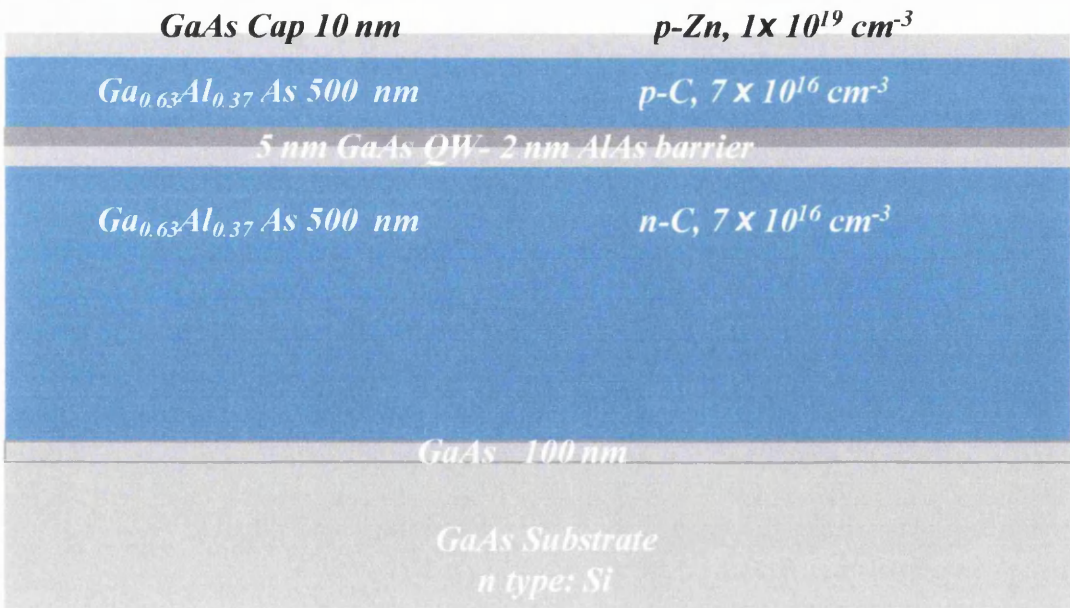
- The effect of varying the area of the intermixed and/or inhibited regions on the intermixing performance should be studied, from which the role of stress as a possible mechanism of the process can be identified.
- Hybrid intermixing processes, such as the sputtered silica process, should be investigated as an alternative for high resolution intermixed gratings. This can be implemented using an initial implantation stage followed by a dielectric cap deposition stage and a subsequent annealing. The enhanced Ga out-diffusion and the implantation induced defect intermixing can be simultaneously used to achieve a low temperature, high resolution intermixing process.

Raman spectroscopy as a suitable means of characterising intermixed gratings should be further investigated and developed. This can be carried out by using photon energies less than that of the bandgap and hence avoid the Photoluminescence which can screen the Raman signal. Also superlattice structures should be used as the upper cladding of the QWs. Such structures will produce strong Raman peaks due to the large number of heterostructure interfaces, and hence provide clearer information about the compositional intermixing, where it takes place. Having the superlattice structure in the barriers just next to the QWs can also provide accurate information about the extent of intermixing since the defect concentration at both the QWs and the barriers will be similar.

APPENDIX 1

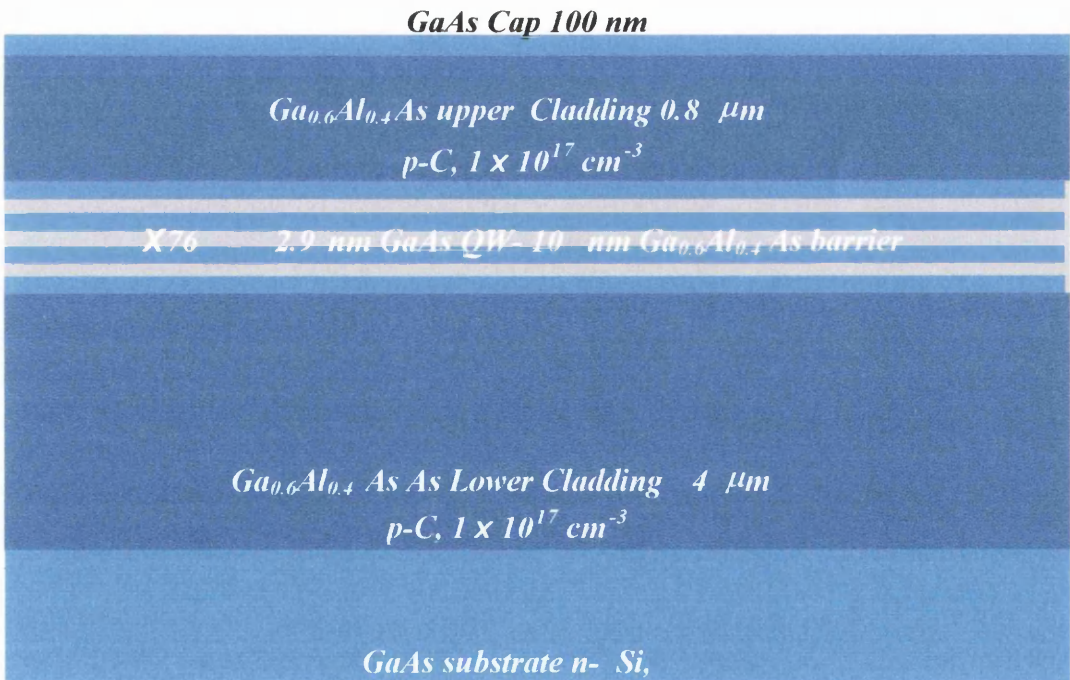
Wafer Structures

In this work there has been a few wafers used during the investigations of intermixing. They can broadly be categorised into two groups, the p-i-n laser structures and the undoped waveguide structures. In this Appendix, we shall list the layer structures used through out this work. All of the laser wafers and some of the waveguide wafers used were grown by metal organic vapour chemical phase epitaxy technique, MOVPE, while the rest of the waveguide wafers were grown by molecular beam epitaxy technique, MBE.



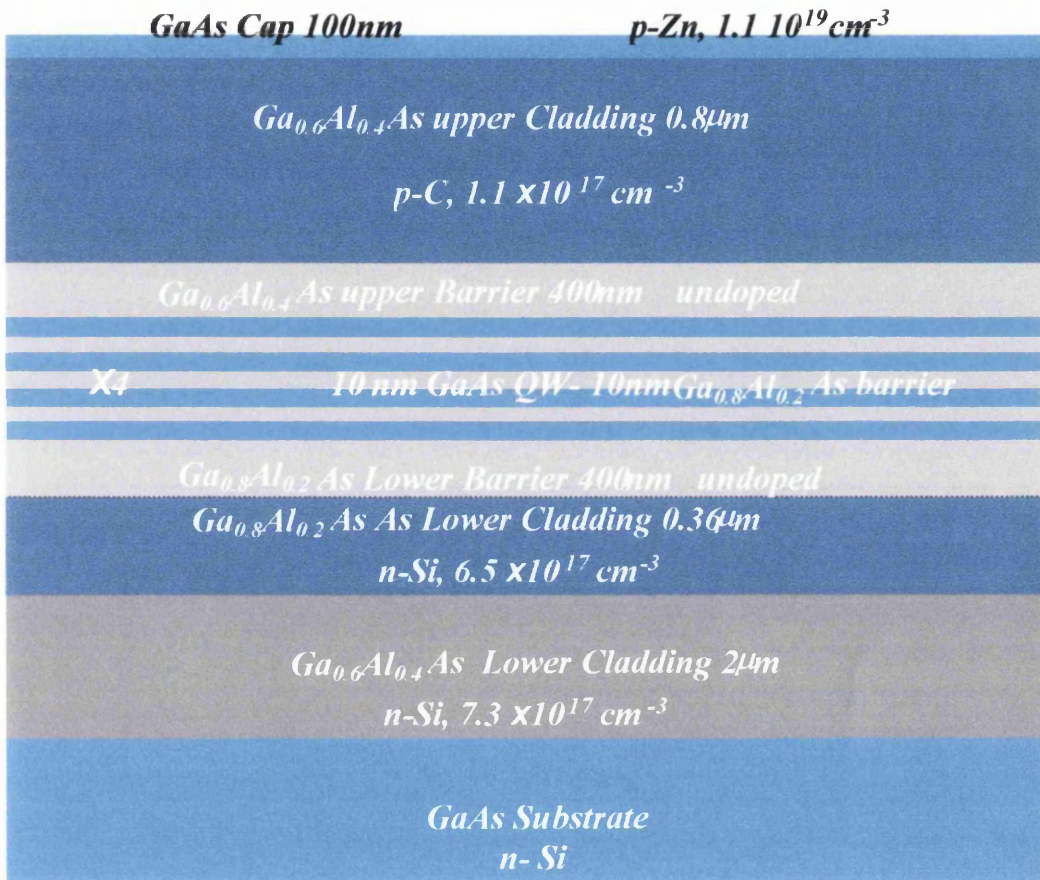
Shallow QW p-i-n structure for quantum well intermixing experiments.

The wafer was used in determining the diffusion coefficient for the plasma induced defect layer intermixing process in chapter 3.



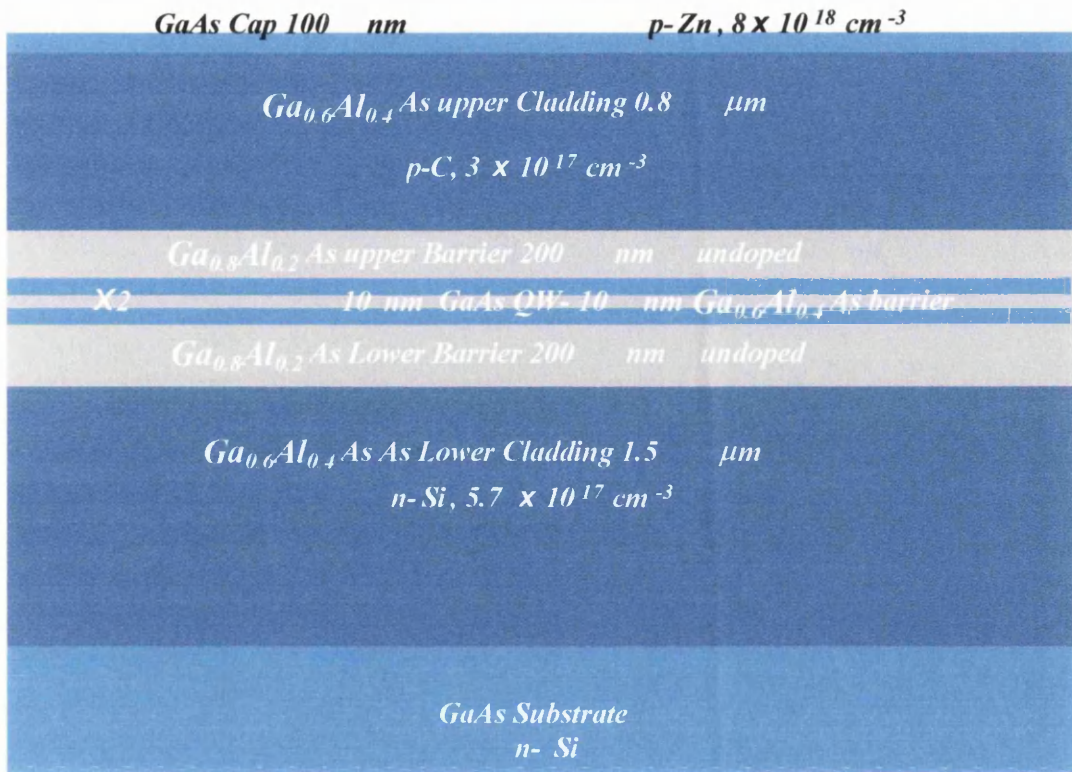
MQW un-doped waveguide structure.

The wafer was used in characterising various intermixing processes in chapters 4 & 5.



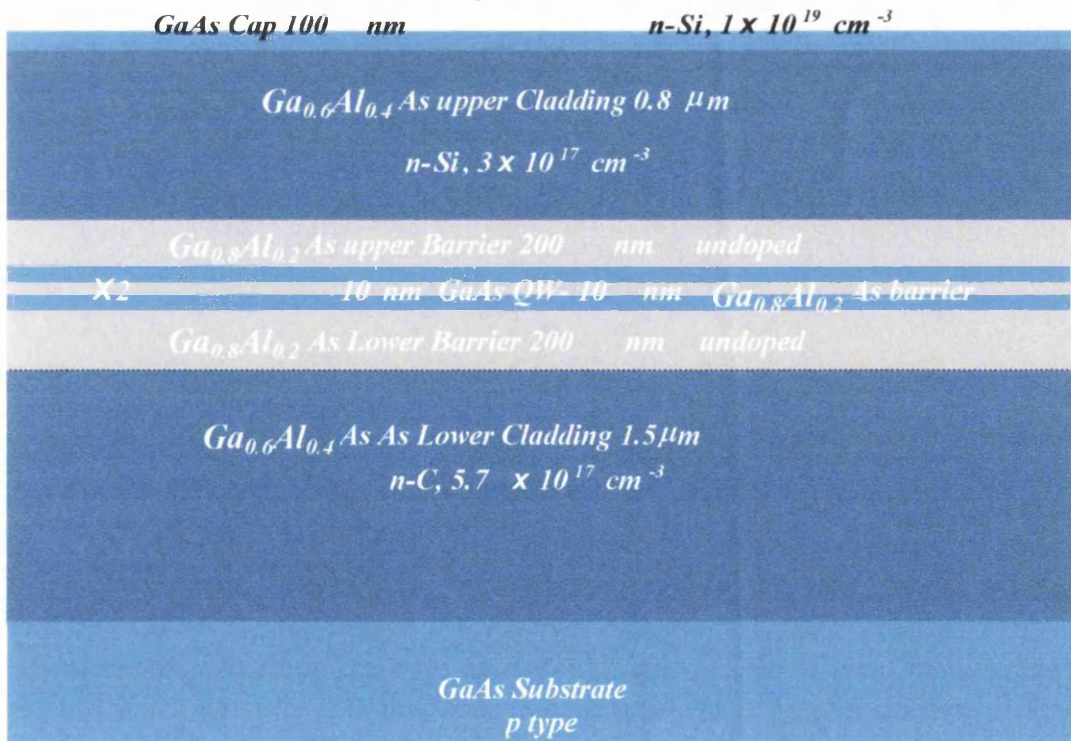
4QW p-i-n laser structure.

The wafer was used in characterising various intermixing processes in chapters 4 & 5.



DQW p-i-n laser structure.

The wafer was used in characterising various intermixing processes in chapters 4 & 5.



DQW n-i-p laser structure.

The wafer was used in characterising the intermixing performance of the SiO₂:P cap in chapter 4.

APPENDIX 2

Experimental Design Techniques

The process of treating silica films with Oxygen plasma has a large parameter space to optimise with a wide range of values for each parameter. Therefore any optimisation attempts undertaken by covering the entire parameter space will be impractical since the number of experiments needed is proportional to the power of number of parameters. In this Appendix we shall describe the basic merits and motivations behind using experimental design. Also the optimisation of the plasma exposure process to suppress intermixing will be presented. It was carried out using the fractional factorial technique

I. USING STATISTICAL DESIGN METHODS FOR PROCESS OPTIMISATION

In the next few points we shall highlight the main obstacles in optimising the fabrication processes:

- In the general case if we have M different levels and n factors then the total number of possible experimental combinations is M^n . We can see, therefore, that the number of experimental runs required increases rapidly as the number of factors and levels increases.
- If we use only two different levels, it means that we cannot identify any curvature in the response. However more levels mean more runs.
- Because a large number of runs cannot be conducted in one process batch, subtle changes in the processing sequence will affect the results.
- At first sight, the logical means of conducting the experiment is to change sequentially the parameters to all the possible levels they can take then to study all the permutations with all the other parameters changed. Even so, there might be effects on the machines which process the samples. Issues such as the chamber conditions in plasma machines are a good example.
- If various parameters are tested independently, the effects of parameter interactions will not be characterised, and these will often have a profound impact on optimisation the reproducibility and of the process.

These are some of the reasons why experimental design tools should be used for such optimisation problems. The statistical nature of such techniques can cover a wide range of parameter space with the minimal number of experiments. They also provide sufficient information about the process, not only for its optimisation and desensitisation, but also about the effect of the cross correlation between various parameters on the process response. They have been used widely in the semiconductor fabrication and growth industries,^{1,2} within which dry etch process optimisation,³ and plasma deposition,⁴ were among the most processes studied using these techniques. A fundamental aspect of such techniques is the choice of the experimental plan, which tells us how to build a map of the experimental space. This then is what allows us to determine which factors interact, in contrast to the one-factor-at-a-time approach to experimentation. If an experiment is properly planned from the beginning, then the analysis part (i.e. where statistics are encountered) is normally relatively straightforward. It is therefore important to select a design, which maximises the statistical information. In our experiment we identified five main factors which we chose to investigate:

Table A3.1 An example set of experiments for a 2 level $2^{(4-1)}$ fractional factorial experiment design.

Parameter Run	A	B	C	ABC ⇒D	AB	AC	AD	BC	BD	CD
1	1	1	1	1	1	1	1	1	1	1
2	1	-1	-1	1	-1	-1	-1	1	-1	-1
3	-1	1	-1	1	-1	1	1	-1	1	-1
4	1	1	-1	-1	1	-1	-1	-1	-1	1
5	-1	-1	1	1	1	-1	-1	-1	-1	1
6	1	-1	1	-1	-1	1	1	-1	1	-1
7	-1	1	1	-1	-1	-1	-1	1	-1	-1
8	1	1	1	1	1	1	1	1	1	1

- A. Silica Film Thickness.
- B. Oxygen Flow Rate.
- C. Plasma RF Power.
- D. Plasma Pressure.
- E. Exposure Time.

In general, the conventional means of conducting 2 level designs would be to conduct a full factorial design. Consider the case of a process with 2 factors to optimise, each at two different levels: there are $2^2 = 4$ different experimental combinations to be carried out. This experimental design is known as a 2-level full factorial design: It is a full factorial because it includes all possible experimental combinations. Fractional factorials, in contrast, are a class of design, which allow us to minimise the resources required in an experiment. Fractional factorial designs can be summarised by:⁵

- As the name suggests, the models generated for processes studied are originally derived from the full factorial designs and differ from them in that some of the information generated by the full factorial models are thought to have insignificant effects on the process response and are disregarded.
- In practice, for most of the processes studied, the disregarded information can be tolerated and fractional factorials can still allow us to build models involving all main effects as well as two-factor interactions.
- Let us consider the situation where we have 4 factors but can only afford 8 runs of the experiment. We first start with the 2^3 full factorial which allows us to determine the *A*, *B*, *C*, *AB*, *AC*, *BC* and *ABC* terms. The design array can be expanded to include the interaction terms by multiplying together array elements, which lie on the same rows.
- In the example shown in Table A3.1; the first row of the *AB* column (+1) is obtained by multiplying the first rows of the *A* column (-1) and the *B* column (-1), and so on. To build

Table A3.2 A set of experiments designed using 1/2 fractional design. Also shown are the PL shifts measured after annealing the samples at 925 °C for 60 s.

Parameter Run	Thickness A	Flow rate B	RF Power C	Pressure D	Time E	Response (PL Shift)
1	50	5	25	10	60	35
2	350	5	25	10	10	39
3	50	50	25	10	10	35
4	350	50	25	10	60	53
5	50	5	275	10	10	51
6	350	5	275	10	60	6.5
7	50	50	275	10	60	17
8	350	50	275	10	10	44
9	50	5	25	150	10	35
10	350	5	25	150	60	35
11	50	50	25	150	60	13
12	350	50	25	150	10	49
13	50	5	275	150	60	50
14	350	5	275	150	10	23
15	50	50	275	150	10	36
16	350	50	275	150	60	31
17	200	27.5	150	80	35	43
18	200	27.5	150	80	35	38
19	200	27.5	150	80	35	52
20	200	27.5	150	80	35	33

a $2^{(4-1)}$ fractional factorial the 4th factor (*D*) is assigned to the *ABC* column. This is the favoured assignment since, in most practical systems, 3-factor interactions are relatively rare. The $2^{(4-1)}$ fractional factorial is therefore composed of the first four columns shown in Table A3.1.

- Using the knowledge and physical principles one has about the process under investigation, it is often possible to reduce the information disregarded by careful allocation of the factors to columns. This is done on the basis of the expectation of the likelihood of interaction between certain factors.

II. PROCESS OPTIMISATION USING FRACTIONAL FACTORIAL DESIGN

Within the course of the research on dielectric caps, our experience showed that electron beam evaporated SiO₂ is the one with the most reproducible results as compared to other types, such as sputtered or PECVD SiO₂. For this reason the cap used for optimisation was the electron beam evaporated SiO₂. The semiconductor structure used in the optimisation

was the DQW laser structure.⁶ Samples were covered with various thicknesses of electron beam evaporated SiO₂ and were then exposed to the oxygen plasma under different conditions. The set of experiments presented in Table A3.2 were designed with the following considerations:

- i. Because of the large number of experiments needed for our process for using a full factorial design, 32 experiments, fractional factorial design was used to reduce the number of runs. This was carried out assuming that interactions between the first 3 parameters, the film thickness, the oxygen flow rate and the plasma RF power are insignificant. This reduces the number of experiments by half, from 32 to 16 runs.
- ii. Although 2-level designs were used for initial investigation, in many circumstances they provide a perfectly adequate description of the process within the range of factor settings explored. In other words, the process can be described by a model which does not involve any quadratic terms. However, in our case, we know, as can be seen in Fig. 4.10 that there is a quadratic dependence on some of the parameters used. 2 level factorials are therefore insufficient and centre runs were added to the 2-level design to be able to characterise such quadratic effects. Centre runs are experiments carried out with parameters within the middle of the range of the 2 levels, and they serve as means by which one can probe any curvature in the response.

Table A3.3 The set of experiment parameters and their combinations to show the interactions.

	Contrasts	Effects
A	8.5	1.0625
B	3.5	0.4375
C	-35.5	-4.4375
D	-8.5	-1.0625
E	-71.5	-8.9375
AB	143.5	17.9375
AC	-107.5	-13.4375
AD	-0.5	-0.0625
AE	12.5	1.5625
BC	-8.5	-1.0625
BD	-31.5	-3.9375
BE	-28.5	-3.5625
CD	51.5	6.4375
CE	-27.5	-3.4375
DE	43.5	5.4375

Table A3.4 The coefficients of the equation generated using the experiments parameters and their combinations to show the interactions.

Terms	Coeffs	StdErr
Constant	47.65761	15.07291
A	-0.02284	0.046043
B	-0.28259	0.31295
C	0.048933	0.056533
D	-0.08217	0.101845
E	-0.17512	0.272741
AB	0.002657	0.000763
AC	-0.00036	0.000137
AD	-2.98E-06	0.000245
AE	0.000208	0.000686
BC	-0.00019	0.000915
BD	-0.00125	0.001634
BE	-0.00317	0.004576
CD	0.000368	0.000294
CE	-0.00055	0.000824
DE	0.001554	0.001471

iii. A common limitation encountered in experimentation is the inability to complete all of the treatments within a single homogeneous unit. For example, it might be that we can only run half of the experiment in one day, and must complete it the following day. However, it is very probable that conditions will change from one day to the next, and this will accordingly affect the results. In such situations it is crucial that the experiment is split in a structured way, if the disregarded information is to be minimised. This splitting of the experiment is known as design blocking. Assume that we can only run 4 treatments in one day and that the experiment is therefore to be spread over a number of days equal to the number of experiments divided by 4. Blocking of a full factorial design can be achieved by confounding the ABC interaction term with "days". The term "days" means the day when a given batch of samples was carried out. Hence, we can regard "days" as a blocking factor and we therefore lose any information on the ABC interaction term. The key is to

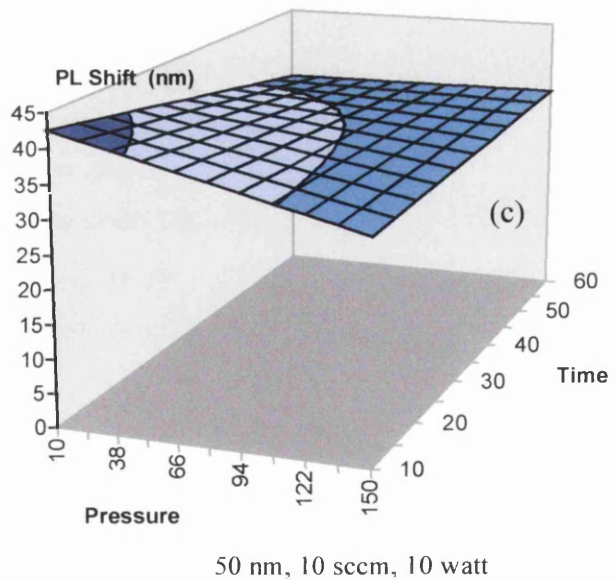
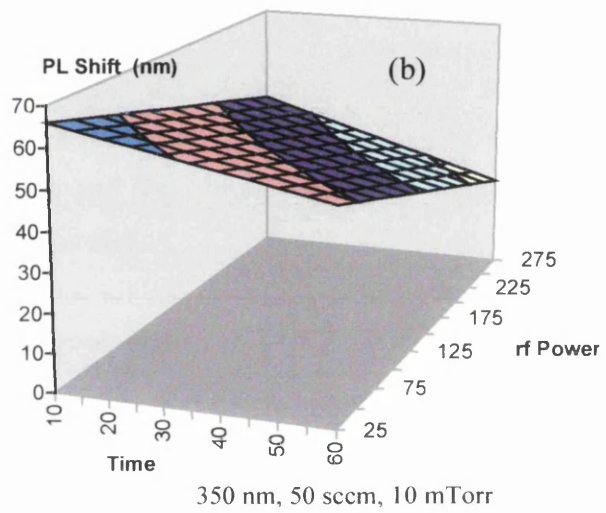
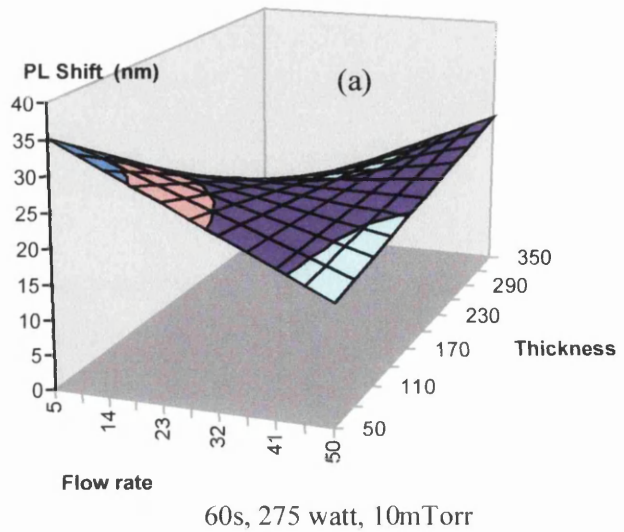


Figure A3.1 The effect of various parameters on the process response. Figures (a), (b), and (c) show the response for different parameter for given settings.

ensure that the block factor is confounded with the effects which are likely to be least important. This is an area where it is important to pay attention to factor/column allocations. From the operating conditions, we found that we can conduct five plasma runs per day, so the experiment was divided into 4 blocks, with a centre run in each block.

- iv. Due to the subtle effects that might arise from running experiments with a sequential change in parameters such as plasma pressure or oxygen flow rate, MATREX software was used to randomise the experiment, as seen in Table A3.2 so as to eliminate these effects.
- v. Since this is an experiment for a dielectric cap, which suppresses intermixing, the process response was chosen to be the PL shift, and it is desired to have the response minimised.
- vi. After carrying out the experiment, the impact of individual parameters on the process response was assessed using two parameters, the *Contrast* and the *Effect*.⁵ These parameters convey similar information, and are only different by a constant factor. They give an indication about the significance of the impact a given parameter has on the process response.⁵
 - For a given parameter, the *Contrast* factor is calculated by subtracting the summation of the process responses at the higher and lower parameter levels from each other.
 - The *Effect* for a given parameter is obtained by subtracting the average process response, (i.e. the average between the PL shift when the lower and higher parameter values are used) at each parameter level instead of subtracting the summation as for contrast calculations.
- vii. The design software will also generate an equation to model the process. The equation describes the response of the process. The model function takes the form,

$$PL\ shift = G + a_1A + a_2B + a_3C... + a_iAB + a_{i+1}AC + a_{i+2}BC....., \quad (A3.1)$$
 where G is a constant factor and the a_i 's will be evaluated using the process response as will be seen further on in the Appendix.

The experiments were carried out in a reactive ion etching machine, BP 80. Each group of experiments, according to the blocking carried out by MATREX, was conducted in one day, with samples annealed together at 925 °C for 60 s with a rise and fall time of 15 s. The results of the runs are shown in Table A3.3. In Table A3.3 the effects and the contrast of the separate and the interaction process parameters are shown. The major single response contribution comes from the time of exposure followed by the RF power of the plasma, which shows less significant yet non trivial impact on the response. The film thickness, chamber

pressure, and oxygen flow rate have little impact on the response. As for the correlated effects, the factors have the thickness-flow rate and thickness-RF power factors have highest impact on the results, while the rest have a less significant, but more or less similar effect. A graphical representation of the effect of certain parameters on the process response is shown in Fig. A3.1. The effects of the time and power are shown to be fairly linear with no curvature, however the effect on the magnitude of process response is quite profound, and is confirmed by the contrast value. There is some curvature in the process response as a function of the film thickness and the flow rate, as can be seen in Fig. A3.1 (b), however this curvature varies depending on the value of the other parameters used. The graph in Fig A3.1 (c) also shows an interesting result where the time of exposure is shown to have little effect, although seen to be very significant for the parameters represented in the Fig A3.1 (a). Similar observations were

made for the pressure at the low end of the parameter range. The information obtained from this graphical representation is by no means exhaustive, which really proves the point about the usefulness of using experimental design to characterise experiments. A lot more can be learned through this graphical representation of the data, however the optimum operating conditions can be easily identified by using the software, as will be explained below.

MATREX, the design package was then used to generate a model for the process with the coefficients of each individual parameter, as well as the correlated factors, being listed in Table A3.4. These coefficients were extracted from the experiments and could, in principle, be used to predict the outcome of a process for a given set of parameters lying within the parameter space used. The model can also be used to extrapolate responses for process parameters outside the range of parameters used, however by how much depends on how accurate the experiments were and also on the nature of the process. Various physical phenomena can have certain domains of validity, beyond which effects of other phenomena set in. Since the software design package is written in Excel, the Excel solver function was

Table A3.5 Results obtained from the model generated for the experiment predicting a decrease intermixing as time of exposure is increased, agreeing with experiment.

Factor	Physical Value	Response Value
a	350.0000	6.499998
b	5.0000	
c	275.0000	
d	10.0000	
e	60.0000	

Factor	Physical Value	Response Value
a	350.0000	3.962498
b	5.0000	
c	275.0000	
d	10.0000	
e	70.0000	

Factor	Physical Value	Response Value
a	350.0000	1.424998
b	5.0000	
c	275.0000	
d	10.0000	
e	80.0000	

used to obtain the predicted response for an extended exposure time for the set of parameters which resulted in minimum intermixing (6.5 nm at 950 °C for 60 s). Indeed, the model predicted a further decrease in intermixing as the exposure time increases, as can be seen in Table A3.5. However operating the RF generator of the RIE at 275 W for more than an hour degrade the power supply performance. It is, however shown in section IV.C. of chapter 4, that increasing the exposure time to 70 minutes indeed decreased the amount of intermixing to approximately 5 nm using the same annealing conditions. This proved model was validated outside the tested parameter space, however further investigation of the optimised parameters was not possible due to limitations in the RIE machine.

VI. REFERENCES

- ¹ K. K. Lin, C. J. Spanos, *IEEE Trans. Semicond. Manufac.*, vol. 3, P 216, 1992.
- ² R. S. Guo, E. Sachs, *IEEE Trans. Semicond. Manufac.*, vol. 6, P 41, 1993.
- ³ G. S. May, J. Haung, C. J. Spanos, *IEEE Trans. Semicond. Manufac.*, vol. 2, P 83, 1991.
- ⁴ D. J. Collins, A. J. Strojaws, D. D. White, Jr., *IEEE Trans. Semicond. Manufac.*, vol. 7, P 176, 1994.
- ⁵ RSD Associates, MATREX LT Design of Experiments Add-In, The Caledonian Suite, St. Andrew House, 141 West Nile St., Glasgow G1, 2RN, 1996.
- ⁶ A.C. Bryce, F. Camacho, P. Cusumano, and J. H. Marsh, *IEEE Journal of Selected Topics in Quantum Electronics*, vol. 3, P 885, 1997.

